Photoinduced Material Transport in Amorphous Azobenzene Polymer Films

Habilitationsschrift zur Erlangung des akademischen Grades

doctor rerum naturalium habilitatus
(Dr. rer. nat. habil.)

der Mathematisch – Naturwissenschaftlichen Fakultät
der Universität Potsdam

vorgelegt von

Marina Grenzer, geb. Saphiannikova

Radeberg, Februar 2007

To my father
in honor of his dreams

Foreword

The role played by azobenzene polymers in the modern photonic, electronic and opto-mechanical applications cannot be underestimated. These polymers are successfully used to produce alignment layers for liquid crystalline fluorescent polymers in the display and semiconductor technology,[1,2] to build waveguides and waveguide couplers,[3,4] as data storage media[5-8] and as labels in quality product protection.[9] A very hot topic in modern research are light-driven artificial muscles based on azobenzene elastomers.[10-12] First attempts are made to use azobenzene polymers as structured templates for production of 3D photonic crystals.[13-16]

The incorporation of azobenzene chromophores into polymer systems via covalent bonding[17,18] or even by blending[19-21] gives rise to a number of unusual effects under visible and ultraviolet irradiation. While light-induced reorientation of azobenzene chromophores in the polymer matrix is now considered to be a well-understood process, the light-induced changes of the matrix itself have been a puzzling phenomenon since the discovery in 1995.[22,23] A satisfying explanation represents a great challenge for the azobenzene community and upon solving will definitely become a milestone in development of the modern polymer physics.

The most astonishing effect is the inscription of surface relief gratings (SRGs) onto thin azobenzene polymer films.[22-25] It is usually performed by exposing the sample to periodic intensity or polarization pattern resulting from the interference of two polarized laser beams. The absorption of light at a wavelength of about 480 nm induces material flow even at room temperature, several tens of Kelvin below the glass transition temperature, T_G, of the polymers.

Another interesting effect is the photoinduced deformation of azobenzene polymer films floating on a water surface.[26] It is shown that different types of azobenzene side-chain polyesters undergo an opposite change of shape under illumination with linear polarized light. Amorphous polyesters elongate along the direction of the electric field vector, while liquid-crystalline polyesters contract in the same direction. This result is in agreement with the observation that the phase of the SRGs, relative to that of the optical grating, strongly depends on the chemical architecture of the particular azobenzene polymer.[3,27]

Several models[28-37] have been proposed to explain the origin of the inscribing force (for review see Ref. 38) but none of them describes satisfactorily the light induced motion of the azobenzene polymers at a molecular level.[39] In most models, to explain the mass transport over micrometer distances during irradiation at room temperature, it is necessary to assume a considerable degree of photoinduced softening, at least comparable with that at the glass transition. However, only very weak softening has been found in mechanical experiments performed recently[40,41] that led to the conclusion that illumination of an azobenzene polymer layer with actinic light cannot induce a transition into a macroscopic low-viscosity melt.

In this study, we shall provide convincing evidence that light induced softening is a very weak accompanying effect rather than a necessary condition for the formation of SRGs. This key finding implies that a light induced stress should lie above the yield point of the azobenzene polymer in order to cause the macroscopic transport well below the glass transition temperature. Consequently, the proper material model for the description of the light induced polymer transport has to be a viscoplastic one.

The first aim of this thesis is to propose a semi-quantitative approach based on the kinetics of the photoisomerization process in azobenzene polymers and giving insight into intrinsic changes of the azobenzene polymer layers under homogeneous illumination with visible and ultraviolet light. It is shown that transient mechanical and dielectric behavior can be readily understood in terms of a two-phase model that considers an azobenzene polymer layer to be consisted of the polymer matrix and the free volume (the latter can be visualized as nanoscopic voids embedded into the polymer matrix[42,43]).

The second aim of this thesis is to provide a viscoplastic modeling of SRG formation to explain a number of visual scattering and X-ray findings on amorphous azobenzene polymer films including the appearance of density gratings buried under the sample surface. It is demonstrated that slight compressibility of the polymer material leads to the density increase in the hill regions of the SRGs. This theoretical prediction is fully confirmed by pulse-force AFM studies. Thus, we show that formation of the surface relief and density gratings can be described in the absence of photoinduced softening using formalism of the viscoplastic theory.

The ultimate aim of this thesis is the development of a new thermodynamic theory explaining the light-induced deformation of free standing films and the formation of surface relief gratings for the main inscription geometries. The basic idea of this theory is that under homogeneous illumination an initially isotropic sample should stretch itself along the polarization direction to compensate the entropy decrease produced by the photoinduced reorientation of azobenzene chromophores. The light induced stress provided by our approach is orders of magnitude higher than that given by the previous theories, being only slightly below a value of the yield stress expected for conventional polymers. The mechanism itself is presently varyfied by molecular dynamics simulations on a number of model azobenzene systems.

This presentation of original results is mainly based on the papers included in the Appendix.

Acknowledgements

Most results presented in this thesis were obtained during my work at the Chair of Structural Analysis and later at the Chair of Soft Matter Physics, University of Potsdam, whereas the first molecular dynamics simulations on azobenzene polymers were started in the group of "Multifunctional Polymeric Micro- and Nanosized Capsules" of Max-Plank Institute of Colloid and Interface Studies in Golm.

I still vividly remember the sunny day of August 1999 when Ullrich Pietsch and Thomas Geue introduced me into the beautiful world of azobenzene polymers. Only working side by side with them, Oliver Henneberg and Knut Morawetz, I could later reach a critical level of understanding at which it was realized that reorientation of azobenzenes should play a main role in the mystery of photoinduced material transport. The four months spent in the group of Gleb Sukhorukov in 2003 gave me an excellent opportunity to learn the other side of the story, namely aggregation properties of azobenzene molecules. Fortunately, this stay also secured my future collaboration with Jaroslav Ilnytskyi, whose profound knowledge in molecular dynamics simulations of complex polymer systems will hopefully provide an ultimate answer about the microscopic mechanism of the light induced material transport. My and Burkhard Stiller's move to the group of Dieter Neher in 2004 led to a synergetic effect when the knowledge previously scattered between three chairs of Potsdam University have been suddenly accumulated and became easily accessible to all involved researchers. It was these two golden years full of numerous discussions and mutual experiments that catapulted the Potsdam University onto the leading place in the world research of azobenzene polymers. Of course, this position could not be ever reached without wonderful experiments carried by Norman Mechau during his PhD studies that clearly demonstrated the absence of light induced softening and light-induced diffusion in amorphous azobenzene films.

Shortly, I am greatly indebted to all of my colleagues-friends mentioned above. Without their warm attitude and everyday readiness to share the knowledge and ideas, this thesis will not be ever published.

Further, I would like to express my deep gratitude to many other colleagues with whom I have worked and taught students the past five years: Andreas Pucher, Jav Davasambuu, Yves Bodenthin, Tobias Panzner, Beate Reinhold, Souren Grigorian, Semen Gorfman from the Chair of Structural Analysis; Elka Derlig, Anke Ebert, Achmad Zen, Frank Jaiser, Thomas Kietzke, Lazar Kulikovsky, Chunhong Yin (Debby) and Elizabeth Lekha Paul from the Chair of Soft Matter Physics. Their mere existence produced an informal and friendly atmosphere in the groups and along with a friendly support helped me to overcome numerous perils of the everyday scientific life.

I am very grateful to my *new* colleagues at the Leibniz Institute of Polymer Research: Prof. Gert Heinrich who put the very idea of habilitation into my mind and then supported me through all stages of this tiresome process; Thomas Horst for his all-round help and enlightening discussions; our invaluable team-assistant Katja Tampe always happy to help; Fedor Semeriyanov, Volodia Toshchevikov and Sven Richter for being good listeners during a rehearsal.

Not to forget my dear friends Lida Oskinova, Wolf-Rainer Hamann, Lisa Feklistova and Fluffy who gave me shelter in Potsdam during the last two years.

Finally, my special thanks go to my faithful knight Jörg whose patient love and nasty scientific critics helped me to bring the whole habilitation adventure to a blissful end.

Contents

Chapter 1

Structure and properties of azobenzene polymers

The class of azobenzene polymers is represented nowadays by a wide variety of chemical structures (for review see Refs. 3 and 38): starting from guest-host systems in which an azobenzene dye is doped into the polymer matrix and thus is prone to agglomeration at higher concentrations,[44-46] through functionalized homo- and co-polymers with side-chain azobenzene chromophores, and finally reaching a complexity of such supramolecular structures as azobenzene polymer networks which can be considered as a cross-linked modification of the two first types. While the scientific interest to uncrosslinked azobenzene polymers is gradually waning, the networks systems has been recently receiving a great and constantly growing attention as very promising templates for production of artificial muscles (attenuators).[10,11,47] The main-chain azobenzene polymers have been also synthesized in the beginning of azobenzene era but it was very soon realized that these systems do not exhibit pronounced orientational and deformational effects, as the mobility of azobenzenes is considerably restricted by their inclusion into the polymer backbone.[3] An attempt was also made to use branched and even dendritic polymer structures[48,49] but again the effects observed were considerably smaller than those in linear azobenzene polymers.

a **b**

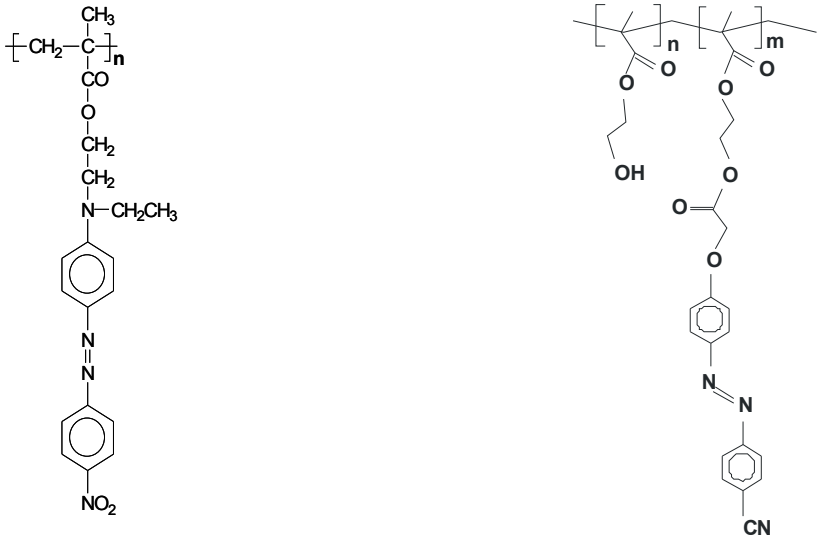

Figure 1.1. The chemical structure of amorphous azobenzene polymers used in this study: (a) homopolymer pDR1M, $T_G = 130^\circ C$; (b) statistical copolymer pCM1, $T_G = 90^\circ C$.

Depending on the length of the spacer, the side-chain azobenzene polymers can be roughly subdivided into amorphous polymers with a short spacer (2-3 methylene groups) and liquid crystalline polymers[48,50] with a long spacer (6-10 methylene groups). The original experimental results discussed in this study were obtained with two types of amorphous

polymers (Fig. 1.1). One is a well-known homopolymer pDR1M [poly((4-nitrophenyl) [4-[[2-(methacryloyloxy)-ethyl] ethylamino] phenyl] diazene)] originally synthesized in the group of Prof. Almeria Natansohn (Kingston College, Canada) and later reproduced in the group of Dr. Burkhard Schulz (Institute of Thin Film Technology and Microsensorics e.V. Teltow). Another is a statistical copolymer pCM1 poly(2-hydroxyethyl)methacrylate-co-(2-(4-(4-cyanophenylazo) phenoxy)acetyl)methacrylate) synthesized in the group of Prof. Henning Menzel (University of Braunschweig).[49]

Although optical properties of these systems as well as transient dipole moments of the isomers are quite different,[51] both polymers have been successfully used for inscription of the SRGs with a similar efficiency at the conventional illumination conditions (10 minutes, 100 mW/cm^2, 488 nm). The amine-substituted azobenzene derivative in pDR1M appears to be rather unstable under prolonged irradiation (30 minutes) at this wavelength due to oxidative degradation.[52,53] It may thereby form other chemical products which presumably secure density changes that were found solely in PDR1M upon heating the polymer above the glass transition temperature (see Section 3.3).[54,55]

There is controversial information about the influence of the molecular weight on the efficiency of the SRG formation in the literature. First, the Natansohn's group reported on significant reduction of the inscription rate with the increasing molecular weight and even on total inhibition of the grating growth at molecular weights of 25 kg/mol and higher.[28] However, this result was obtained with the 1:1 blended films of PDR1A (PDR1M with the backbone methyl group substituted on hydrogen) and PMMA, the molecular weight of which was varied.[24] Thus, these data simply show that increasing number of entanglements in the host PMMA suppresses the grating growth. Later, the group of Tripathy managed to inscribe the SRGs in amorphous azobenzene polymers having very high molecular weight of more than 500 kg/mol, although the inscription was less efficient than for low molecular weight polymers.[3] Also, the systematic variation of the molecular weight of pCM1 (Fig. 1.1b, n=35% and m=65%) up to 200 kg/mol only slowed down the grating inscription, but did not inhibit it completely.[56] Concerning the influence of azobenzene content on the grating formation, here different groups agree that the inscription rate increases with the degree of functionalization in the statistical copolymers up to a certain threshold value that is above 40% and depends on the particular polymer.[49,57,58] After this threshold, the insciption rate is found to be either independent of the degree of functionalization[57] or shows a tendency to a small decrease.[49,58]

Presently, there is no doubt that multiple trans-cis and cis-trans photoisomerizations of the azobenzene moieties are the trigger of the inscription process. Though, it is not clear at all, what kind of microscopic mechanism is responsible for the inscription. Over the years, some of the proposed mechanisms, for example pressure gradients due to volume changes[24] or thermal gradients,[59] had been rejected as they cannot explain some of the essential features of the SRG formation. Also, we showed that the electric force gradients, for some years the most favored model amongst experimentalists,[29,30,34,35] are too small to be seriously taken into account.[39] What stays? Is it simply the mechanical switching between two isomerization states, the impulse of which, due to unknown reasons, pushes the chains to reptate in a particular direction defined by the light polarization (the model of anisotropic diffusion proposed by Lefin et al.[31,32] in 1998 and revived by an unawared group of French scientists[60] in 2006 as the random-walk model of molecular motors). Or maybe, it is the orientation of chromophores that leads to the change in the intermolecular interactions of azobenzenes? In any case, only detailed consideration of the photoisomerization process and its consequences, shall deliver a first insight into the puzzle of the grating inscription in the azobenzene polymers.

1.1. Hole-burning model

Many optoelectronic applications of dye-containing polymers need some aligning of anisotropic or polar active molecules. The reversible trans-cis isomerization (E-Z isomerization[61]) of azobenzenes induced by resonant excitation with a polarized laser beam is by far the mostly used mechanism due to its efficiency and of the good stability of azo-dyes. The polarized light imposes on anisotropic dye molecules an angular selective optical pumping that results in a macroscopic alignment perpendicularly to the light polarization.[62,63] Only in the case of such orientation further absorption of photons is prevented and, hence, a steady state is reached.[64,65] M. Dumont and E. Osman have introduced a theoretical "hole-burning" model for the simulation of photoinduced reorientation of azo-dyes in amorphous polymers.[66,67]

From a steric point of view, the azobenzene moiety in the trans state can be considered as a rigid rod of a length ~ 15 Å and a width ~ 5 Å.[68] The axis of one rod is labeled by the unit vector $\mathbf{e}$, and the rod is assumed to have complete cylindrical symmetry about $\mathbf{e}$. Under illumination with visible or ultraviolet light the photoisomerization takes place, and the angular distribution of trans isomers, $n_T(\theta,t)$, and that of cis isomers, $n_C(\theta,t)$, are described by the following set of differential equations:

$$\frac{\partial n_T(\theta,t)}{\partial t} = -\Phi_{TC} P_T(\theta) n_T(\theta,t) + \Phi_{CT} \int P_{CT}^{ph}(\theta',\theta) P_C(\theta') n_C(\theta',t) d\Omega' + \gamma \int P_{CT}^{th}(\theta',\theta) n_C(\theta',t) d\Omega' + \left(\frac{\partial n_T(\theta,t)}{\partial t} \right)_{Diff} \tag{1.1}$$

$$\frac{\partial n_C(\theta,t)}{\partial t} = -\Phi_{CT} P_C(\theta) n_C(\theta,t) + \Phi_{TC} \int P_{TC}^{ph}(\theta',\theta) P_T(\theta') n_T(\theta',t) d\Omega' - \gamma n_C(\theta,t) + \left(\frac{\partial n_C(\theta,t)}{\partial t} \right)_{Diff} \tag{1.2}$$

with the normalization condition

$$\int \left[n_T(\theta,t) + n_C(\theta,t) \right] d\Omega = N \tag{1.3}$$

Here N is the total molecular density of chromophores, $d\Omega = \sin\theta d\theta$ and θ is the angle between $\mathbf{e}$ and the electric field vector of the electromagnetic wave, $\mathbf{E}$. Φ_{TC} and Φ_{CT} are the quantum yields of the direct trans-cis and reverse cis-trans isomerization, respectively, P_T and P_C are the probabilities of the absorption of a photon by a molecule in the trans and cis state, respectively , and $\gamma = \tau_c^{-1}$ is the rate of the cis-trans thermal back relaxation. $P_{JK}^{ph}(\theta',\theta)$ and $P_{JK}^{th}(\theta',\theta)$ are the probability of rotation from θ' to θ during photoinduced (thermal) *J-K* isomerization (*J(K)=C* or *T*). The last term in each equation is the thermal orientational diffusion.

It is a tremendously difficult task to find a general solution of Eqs. (1.1) and (1.2). M. Dumont and E. Osman supposed that the molecular axis of cis (trans) isomers is distributed around that of trans (cis) isomers before the photoisomerization, with an angular distribution only dependent of the polar angle, α, between two isomers:[67]

$$P_{JK}^{ph}(\alpha) \equiv F(\alpha) = \frac{1}{2}\sum_{p}(2p+1)F_p P_p(\cos\alpha) \tag{1.4}$$

where $P_p(\cos\alpha)$ are Legendre polynomials. The angular distributions of trans and cis isomers were also developed in Legendre polynomials. Then, a set of differential equations (1.1) and (1.2) can be rewritten as a system of two matrix equations, which can further be solved numerically using a number of experimental parameters.

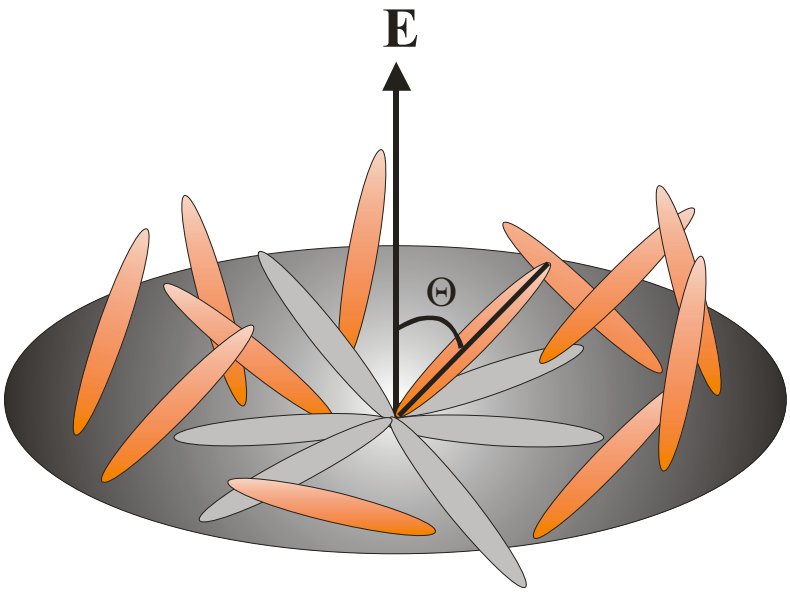

Figure 1.2. Azobenzenes with the long axis laying perpendicular to the electric field vector **E** represented here as gray rods cannot be excited.

We do not want to go here into more details and refer an interested reader to the original work of M. Dumont and E. Osman.[67] The mechanism of angular hole-burning model can be understood intuitively if one considers the probability of absorption. It is given by

$$P_J(\theta) = I_P\sigma_J\left[1+\varepsilon a_J P_2(\cos\theta)\right] \tag{1.5}$$

where I_p is the pumping intensity in W/cm^2, σ_J and a_J are the average absorption cross section and the molecular anisotropy of trans (J=T) and cis (J=C) isomers, respectively. $\varepsilon = 2$ for linear polarized light, and $\varepsilon = -1$ for circular polarized light.[67] Let us consider the irradiation with linear polarized light and assume for simplicity that $a_T = a_C = 1$:

$$P_J(\theta) = 3I_P\sigma_J\cos^2\theta \tag{1.6}$$

Hence, the probability of excitation by the linear polarized light is proportional to $\cos^2\theta$. Therefore, starting from a sample with an isotropic angular distribution of the chromophores, multiple *trans-cis-trans* photoizomerization with linearly polarized light will result in a preferential orientation of the long axis of the chromophores. After some time, a dynamic steady state will be established which is characterized by a rather small fraction of chromophores pointing in the polarization direction and thus a small photoizomerization rate (Fig. 1.2).

1.2. Photoisomerization kinetics

A simplified description of the hole-burning model was proposed by Buffeteau et al.[69]:

$$\frac{\partial n_T(\theta,t)}{\partial t} = -\Phi_{TC} P_T(\theta) n_T(\theta,t) + \Phi_{CT} P_C(\theta) n_C(\theta,t) + \gamma n_C(\theta,t) \tag{1.7}$$

The authors neglected the thermal orientational diffusion and assumed that isomers do not change their orientation during the photoisomerization event. Another questionable approximation made by Buffeteau et al.[69] is that the number of chromophores found at a particular polar angle θ does not change with time (compare with the normalization condition (1.3)):

$$n_T(\theta,t) + n_C(\theta,t) = \frac{N}{2} \tag{1.8}$$

We wrote "questionable" because if for instance the angular distribution of trans isomers has a maximum around $\theta = 90^0$ than the angular distribution of cis isomers should have a maximum around $\theta = 0^0 (180^0)$, and vice versa. One expects however that these two distributions strongly correlate with one another, at least in the amorphous polymer matrix. The stationary angular distribution of trans isomers is given by:

$$n_T(\theta) = \frac{N}{2} \frac{\Phi_{CT} P_C(\theta) + \gamma}{\Phi_{TC} P_T(\theta) + \Phi_{CT} P_C(\theta) + \gamma} \tag{1.9}$$

This function is only suitable for description of very weak orientational effects: in the case when thermal relaxation can be neglected, i.e. $\gamma = 0$ and $a_T = a_C = 1$, one even receives the random distribution of trans isomers. Therefore, to describe strong orientational effects, we recently proposed to use the following model function[70] (it is similar to that used in Onsager's approach[71,72]):

$$n_T(\theta) = norma \cdot \cosh(\alpha \sin\theta) \tag{1.10}$$

where $\alpha \sim I_p$ is the strength of light induced alignment and *norma* is the normalization constant. This function has a peak at $\theta = 90^\circ$ (Fig. 1.3), i.e. azobenzenes align preferentially perpendicular to $\mathbf{E}$.

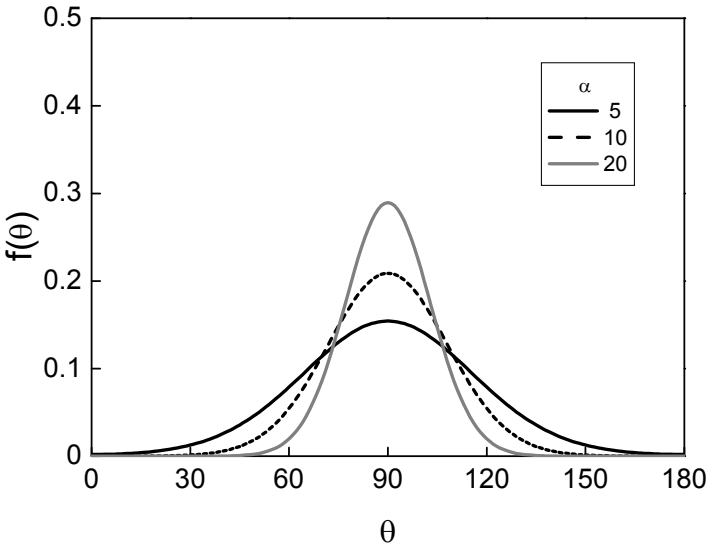

Figure 1.3. Orientational distribution function $f(\theta) \equiv n_T(\theta)$ at different strengths of light induced alignment: $\alpha = 5$, 10 and 20.

In some experiments considered in this thesis, for example when the film is illuminated by unpolarized light[73] or by a sequence of very short pulses followed by longer relaxation pauses,[74] light induced reorientation of the chromophores is proved to be negligible. In this case we are only interested to find the change of cis isomers with time. Upon integrating Eq. (1.5) over θ the probability of absorption can be expressed as follows

$$P_J = 2I_p\sigma_J \quad \text{since} \quad \int_0^{\pi} P_2(\cos\theta)\sin\theta d\theta = 0 \tag{1.11}$$

and Eq. (1.2) can be transformed into

$$\frac{\partial n_C(t)}{\partial t} = -\left(k_{TC}I_p + k_{CT}I_p + \gamma\right)n_C(t) + k_{TC}I_pN \tag{1.12}$$

Here, $k_{TC} = \Phi_{TC}\sigma_T$ is the rate constant of the trans–cis photoisomerization and $k_{CT} = \Phi_{CT}\sigma_C$ is the rate constant of the reverse cis–trans photoisomerization. If we define the cis fraction as $f_C(t) = n_C(t)/N$, then Eq. (1.12) can be rewritten for the cis fraction as

$$\frac{df_C(t)}{dt} = -\tau_p^{-1}f_C(t) + k_{TC}I_p \tag{1.13}$$

Here, we have introduced $\tau_p = \left[(k_{TC} + k_{CT})I_p + \gamma\right]^{-1}$ as the characteristic time of the isomerization process. For the situation where light is switched on at $t = 0$, Eq. (1.13) can be easily solved resulting

$$f_C(t) = k_{TC}I_p\tau_p(1 - \exp(-t/\tau_p)). \tag{1.14}$$

On the other hand, the isomerization rate, $\dot{f}_{iso} \equiv df_{iso}/dt$, is given by

$$\dot{f}_{iso}(t) = \left[(k_{CT} - k_{TC})I_p + \gamma\right] f_C(t) + k_{TC} I_p \tag{1.15}$$

Thus, we define $\dot{f}_{iso}$ as the number of all isomerization events per unit of time, accounting for both trans-cis and cis-trans isomerizations. When the photostationary state is reached ($t = \infty$), the following two relations are obtained

$$f_{C,\infty} = k_{TC} I_p \tau_p$$

and (1.16)

$$\dot{f}_{iso,\infty} = 2 f_{C,\infty} \tau_C^{-1}$$

where $\tau_C = \left[k_{CT} I_p + \gamma\right]^{-1}$ is the effective lifetime of cis isomers under illumination.

Both trans-cis and cis-trans photoisomerization processes stop immediately when the inscribing laser is switched off. The only process that is still continuing in the absence of irradiation is a much slower cis-trans thermal relaxation. The rate of thermal relaxation depends mostly on the type of chromophore and the type of its attachment to the polymer backbone.[75] It is usually a multi-exponential decay on a very short time scale (1 s) followed by a mono-exponential decay for which relaxation times between 10 s and 12 hours have been estimated for a variety of azobenzene polymers.[69,75,76] The rate of thermal relaxation differs considerably between the two polymers used in this study: for amine-substituted azobenzene derivative in PDR1M it is about 10 s, while the cyane-substituted derivative in pCM1 returns into the trans-state during 10 hours.[73]

Chapter 2

Light induced softening and diffusion in azobenzene polymer layers

In most models, to explain the mass transport over micrometer distances during irradiation at room temperature, it is necessary to assume a considerable degree of photoinduced softening, at least comparable with that at the glass transition. In other models,[29,34,36] only the mechanism of SRG inscription is proposed without giving a force estimate. In this chapter we shall provide convincing evidence that there is no considerable softening of the azobenzene layers under illumination. This evidence was obtained using three different techniques operating at totally different time scales: electromechanical spectroscopy (~ 10^{-3} s), atomic force microscopy (~ 1 s) and fluorescence recovery after photobleaching (~10^{3} s).

It is well known that the Young's storage modulus increases exponentially with the frequency in dynamic mechanical measurements.[77] The sample goes through the glass transition in much the same way as when the temperature is lowered. The quartz crystal resonance experiments from Srikhirin et al.[40] were carried out at very high frequencies of several GHz when predicted softening of the azobenzene polymer film under illumination with visible light would probably stay unnoticed. Electromechanical experiments described in the next section were done at a much lower frequency of 2.5 kHz. Still only negligible changes in the plate compliance and in the dielectric constant were observed (10% under illumination against 1000% upon heating till T_G). With the force-distance mode of atomic force microscopy, in which a stress is applied quasi-statically at about 1 Hz, only a 50% decrease in the Young's modulus has been found under illumination with visible light. In the last section, we'll show that there is no change in the viscosity of illuminated films that could allow the diffusion of small molecules as it is observed in thin polymer films around the glass transition temperature.[78-80]

2.1. Electromechanical spectroscopy

2.1.1. Experiment and results

The photoinduced changes in the plate compliance and in the dielectric constant of the thin azobenzene polymer films were measured by means of electromechanical spectroscopy.[81] This method utilizes the electrostriction effect, i.e. the change in thickness, Δh, of a thin polymer layer sandwiched between two electrodes upon application of the alternating electric field. Details of the method are described elsewhere.[73]

The plate compliance is defined by the relative change in layer thickness, $\delta h \equiv \Delta h / h$, upon application of a stress σ_{zz} normal to the layer plane

$$\delta h = \beta_{zz} \sigma_{zz} . \qquad (2.1)$$

Since, in the ideal case, the polymer layer cannot expand parallel to the substrate, β_{zz} differs from the bulk compliance β_{bulk} [82, 83]

$$\beta_{zz} = \frac{1+\nu}{3(1-\nu)}\beta_{bulk} \tag{2.2}$$

with ν being Poisson's ratio. If ν does not change under illumination, the relative light-induced change of bulk compliance is equal to the relative change of β_{zz}

$$\delta\beta_{zz} = \frac{\beta_{zz}(t) - \beta_{zz}(0)}{\beta_{zz}(0)} = \delta\beta_{bulk} \tag{2.3}$$

Here $\beta_{zz}(0)$ is the plate compliance in the dark, before the light is turned on. The value of the plate compliance was calculated from the electrostriction coefficient, Q, according to:

$$Q = -\frac{\varepsilon_{vac}\cdot\beta_{zz}}{6}\left(3\varepsilon' + (\varepsilon'-1)\cdot(\varepsilon'+2)\right) \tag{2.4}$$

where ε_{vac} is the vacuum susceptibility and ε' is the real part of the dielectric constant. Only slow mechanical changes can be followed by measuring the plate compliance, for it takes about 2 minutes to obtain one value. Also, the data are very noisy as we record changes in the film thickness that are less than 10 pm.

The relative change of the dielectric constant is defined as follows

$$\delta\varepsilon'(t) = \frac{\varepsilon'(t) - \varepsilon'(0)}{\varepsilon'(0) - \varepsilon_\infty} \tag{2.5}$$

where $\varepsilon'(0)$ is the initial value of dielectric constant in the dark and ε_∞ is the susceptibility at an infinitely high frequency. ε_∞ can be approximated by n^2, where n is the refractive index of polymer. The dielectric constant can be measured with a very high accuracy and with a time resolution of about 10 seconds.

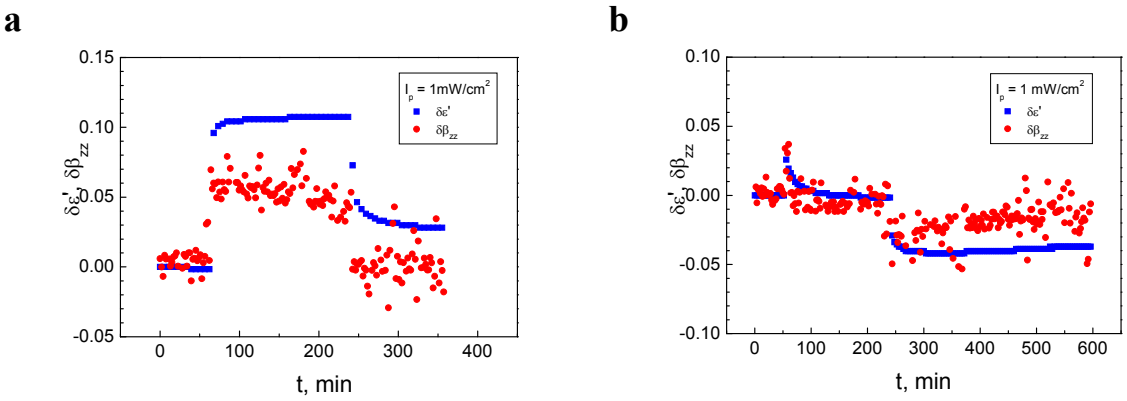

Figure 2.1. Time dependencies of the relative dielectric constant $\delta\varepsilon'$ and the relative plate compliance $\delta\beta_{zz}$ under VIS (a) and UV (b) irradiation with 1 mW/cm^2.

We have found a strong correlation between the time dependent behavior of the plate compliance and the dielectric constant under visible (VIS, $\lambda_{VIS} = 488$ nm) as well as under ultraviolet (UV, $\lambda_{UV} = 365$ nm) irradiation (Fig. 2.1). When VIS light with an intensity of 1 mW/cm^2 is switched on, $\delta\beta_{zz}$ ($\delta\varepsilon'$) increases to a value of 0.06 (0.1) and stays at this level during further irradiation. After switching off the light, $\delta\beta_{zz}$ quickly and $\delta\varepsilon'$ slowly return to their initial values in the dark. If UV light with an intensity of 1 mW/cm^2 is switched on, both quantities first increase rapidly but then start to decrease, approaching their values in the dark. After switching off the light, one observes an initial abrupt drop of $\delta\beta_{zz}$ and $\delta\varepsilon'$, followed by their gradual increase to the initial value in the dark. An essential difference in the time dependent behavior of the dielectric constant and the plate compliance can be observed after the light is switched off: the dielectric constant returns to its initial value much slower than the plate compliance. Such slow relaxation of the dielectric constant is probably caused by orientational effects,[73] even though we tried to avoid these effects by illuminating the sample with unpolarized light.

2.1.2. Two-component mechanical model

To explain the time dependent behavior of the plate compliance and the dielectric constant we propose to consider an azobenzene polymer layer as a two-component system, consisting of the polymer matrix and free volume. Then the bulk modulus of the layer, K, can be approximated by

$$K = K_0(1 - a\phi) \tag{2.6}$$

where K_0 is the mechanical modulus of the polymer matrix at room temperature in the dark, ϕ is the amount of the free volume generated by light-induced molecular motion (Fig. 2.2) and a is the positive coefficient of proportionality. Any free volume present in the layer in the dark is included into K_0.

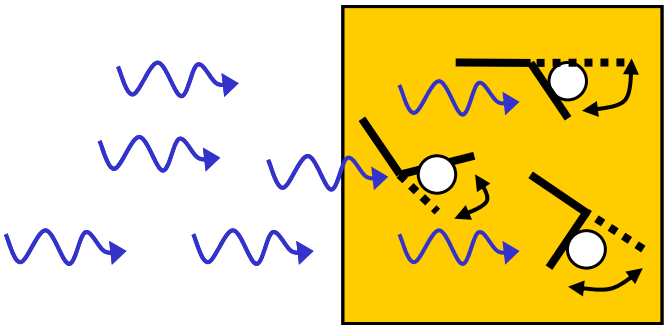

Figure 2.2. Generation of the free volume due to multiple trans-cis-trans isomerization cycles.

Taking into account that $a\phi << 1$, the relative change of the bulk compliance, $\beta = 1/K$, (and hence, according to Eq. (2.3), of the plate compliance) will be proportional to the free volume[51]

$$\delta\beta_{bulk}(t) = a\phi(t) \tag{2.7}$$

When the light is switched off, photoisomerization stops immediately, the free volume gradually disappears and $\delta\beta_{zz}$ returns to its initial value in the dark. Therefore, it is meaningful to correlate ϕ with the rate of trans-cis isomerization $\dot{f}_{iso}$:

$$\delta\beta_{bulk}(t) = a'\dot{f}_{iso}(t) \tag{2.8}$$

a' is the positive coefficient of proportionality.

To explain the complicated response of the azobenzene polymer layer to UV irradiation, we have to consider an additional phenomenon. As it was noticed previously by Srikhirin et al.,[40] hardening of the polymer layer apparently correlates with the increase of the cis concentration. This can be explained if we assume that interactions of azobenzene chromophores in the cis state with their nearest environment are stronger than those in the trans state.[37] Therefore, the modulus of the polymer matrix is expected to increase with the concentration of cis isomers. Thus, in the first linear approximation, Eq. (2.6) can be rewritten as

$$K = K_0(1 + bf_C)(1 - a\phi) \tag{2.9}$$

Here, b is a coefficient of proportionality, which is positive. Taking into account that $bf_C << 1$, the relative change of the bulk compliance is given by

$$\delta\beta_{bulk}(t) = a\phi(t) - bf_C(t) \tag{2.10}$$

and if we again assume that $\phi = a'\dot{f}_{iso}$

$$\delta\beta_{bulk}(t) = a'\dot{f}_{iso}(t) - bf_C(t) \tag{2.11}$$

In the linear approximations (2.8) and (2.11), the light-induced change in the plate compliance is simply proportional to the rate of photoisomerization and the cis fraction. Both can be determined experimentally. Before addressing this point in more detail, we would like to discuss briefly the change in the dielectric constant.

2.1.3. Light-induced changes of the dielectric constant

The real part of the dielectric constant for a system with a single relaxation time, τ, is given by

$$\varepsilon' = \varepsilon_\infty + \frac{\varepsilon_0 - \varepsilon_\infty}{1 + (\omega\tau)^2} \tag{2.12}$$

Here, ε_0 is the static susceptibility, ε_∞ is the susceptibility at an infinitely high frequency and ω is the angular frequency. In the Kirkwood-Fröhlich approach,[84] that take into account intermolecular interactions and hindered rotation,

$$\varepsilon_0 - \varepsilon_\infty = \frac{4\pi}{3k_B T}\frac{3\varepsilon_0}{2\varepsilon_0 + \varepsilon_\infty}\left(\frac{\varepsilon_\infty + 2}{3}\right)^2 \left\langle \delta M^2 \right\rangle \tag{2.13}$$

where k_B is the Boltzmann constant and T is the absolute temperature. In this equation $\left\langle \delta M^2 \right\rangle$ represents fluctuations of the total dipole moment, M, which for a real chain is equal to[85]

$$\left\langle \delta M^2 \right\rangle = gN\mu^2 \tag{2.14}$$

For a system composed from freely rotating dipole units, $\left\langle \delta M^2 \right\rangle$ is equal to $N\mu^2$, with N being the number of dipole groups per unit volume and μ being the dipole moment of a given group. g is the so-called correlation factor which depends on the strength of statistical correlations between dipoles and on their interactions with the polymer matrix. To understand the meaning of the correlation factor, it is instructive to consider two limiting cases:

1) $g = 1$, dipoles rotate freely and $\left\langle \delta M^2 \right\rangle = N\mu^2$.

2) $g = 0$, dipoles are totally frozen in the polymer matrix and, thus, can not rotate at all.

It was reported previously that the increase of ε' under VIS irradiation could be explained by the increase of the dipole moment of azobenzene when it isomerizes from the trans- to the cis state.[86] However, this change would be only detectable, if fluctuations of the long axis or rotation of the azobenzene dye around this axis were possible at (or faster than) the measurement frequency of 2.5 kHz at room temperature. Recent dielectric spectroscopy studies[87] on different azobenzene side chain polymers revealed that the relaxation frequency of the azobenzene moieties is significantly lower being about 1-10 Hz at room temperature. This allows us to argue that ε' changes under irradiation mainly due to the change in g rather than due to the change in the dipole moment of azobenzene.

Consequently, keeping μ constant and using Eqs. (2.12) – (2.14), it is easy to show that the relative change of the dielectric constant is equal to the relative change of the correlation factor

$$\delta\varepsilon'(t) = \frac{\varepsilon'(t) - \varepsilon'(0)}{\varepsilon'(0) - \varepsilon_\infty} = \delta g(t) \tag{2.15}$$

Furthermore, in the absence of statistical correlations between dipoles the relative change of the correlation factor is also given by Eqs. (2.8) and (2.11) (the coefficients can of course take other values). First, it is clear that the presence of the free volume increases the rotational freedom of the dipoles. Second, the presence of cis isomers leads to an increase of the strength of intramolecular interactions in the polymer matrix which results in decrease of rotational freedom of dipoles. This means, that whenever the azobenzene polymer film undergoes changes of its mechanical properties – softens or hardens – this is reflected by an appropriate change in ε'.

Let us now show that our model is able to reproduce the time dependent behavior of the dielectric constant under irradiation with visible light. In our model, $\delta\varepsilon'$ is equal to the

relative change in the correlation factor and, therefore is proportional to the amount of the free volume accumulated in the azobenzene polymer layer from the moment $t = 0$, at which the light is switched on, till the moment t

$$\delta g_{VIS}(t) = c\int_0^t \dot{\phi}(t')\exp[-(t-t')/\tau_m]dt'. \tag{2.16}$$

Here c is the coefficient of proportionality and $\dot{\phi}(t')$ is the additional free volume produced per one unit at time t' due to multiple photoisomerization cycles. Relaxation of ϕ after this moment is described by the exponential decay with the characteristic time τ_m.

The experimentally measured $\delta\varepsilon'$ curve increases with the light intensity nonlinearly.[73] The nonlinear behavior can be understood as follows: when the light intensity reaches a critical value, chromophores can reutilize free volume which has been generated by an earlier isomerization event.[41] As result, the additional free volume is not anymore proportional to the isomerization rate. This has been taken into account by introducing a nonlinear dependence of $\dot{\phi}$ on the isomerization rate

$$\dot{\phi}(t') \sim \left[\dot{f}_{iso}(t')\right]^{a_2} \tag{2.17}$$

with $a_2 < 1$.

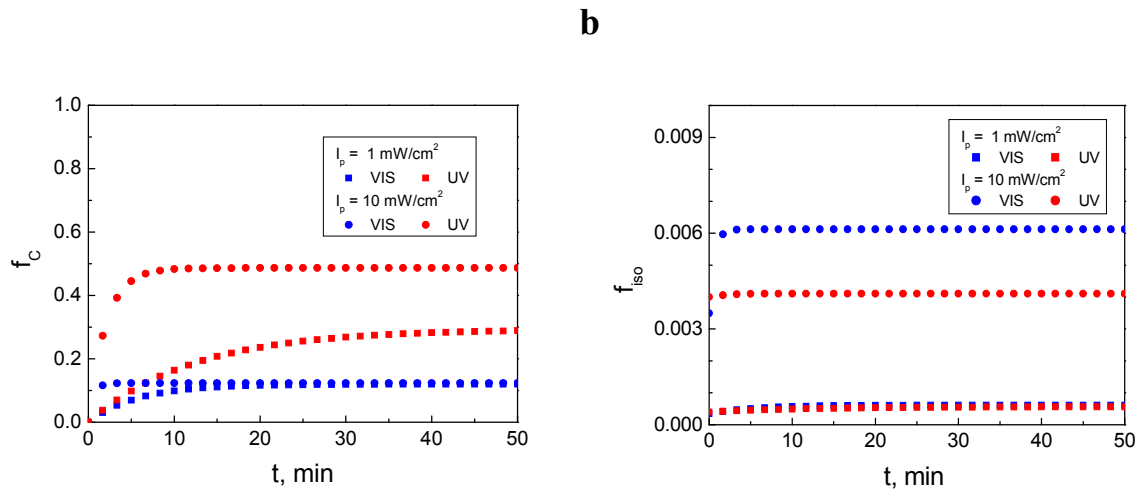

Figure 2.3. Time dependencies of the cis fraction f_C (a) and the isomerization rate $\dot{f}_{iso}$ (b) under VIS and UV irradiation with the different pumping intensities I_p. The curves are calculated using Eqs. (1.14) and (1.15).

This gives

$$\delta g_{VIS}(t) = \delta g_{VIS,\infty} \begin{cases} 1-\exp(-t/\tau_m) & \text{light is on at } \quad t=0 \\ \exp[-(t-t_{off})/\tau_m] & \text{light is off at } \quad t=t_{off} \end{cases} \tag{2.18}$$

where

$$\delta g_{VIS,\infty}(I_p) = a_1 I_p^{a_2} \qquad [I_p] = 1 \text{ W/m}^2 \tag{2.19}$$

with $a_1 = 0.050 \pm 0.004$ and $a_2 = 0.32 \pm 0.03$ taken from the fit of $\delta\varepsilon'(I_p)$.[73] The actual value of $\tau_m = 200\,\text{s}$ was determined from the initial exponential decrease of the relative dielectric constant after switching the light off. It was found to be independent on I_p.

From transient absorption measurements it is possible to determine the rate constants k_{TC}, k_{CT} and γ and calculate $f_C(t)$ and $\dot{f}_{iso}(t)$ for a given light intensity for VIS and UV irradiation (Fig. 2.3).[73] Using $\dot{f}_{iso}(t)$ dependence, we can reasonably well reproduce transient behavior of the relative dielectric constant at different intensities of visible light (Fig. 2.4a). However, when the light is switched off, $\delta\varepsilon'$ relaxes much slower than δg as predicted by Eq. (2.18). We already mentioned that orientational effects (neglected in our model) might be a reason for this discrepancy between the experimental data and the model prediction.

a **b**

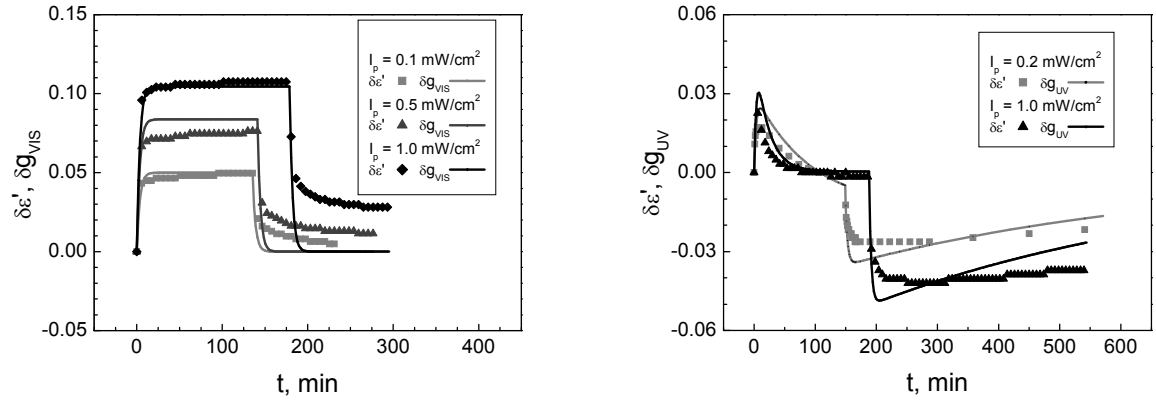

Figure 2.4. Time dependencies of the relative dielectric constant $\delta\varepsilon'$ under VIS (a) and UV (b) at different intensities. Lines show the relative correlation factor δg as predicted by Eqs. (2.16) and (2.20).

In order to describe the time dependent behavior of the dielectric constant under irradiation with ultraviolet light we introduce an additional term in Eq. (2.16)

$$\delta g_{UV}(t) = c\int_0^t \dot{\phi}(t')\exp[-(t-t')/\tau_m]dt' - bf_C(t) \tag{2.20}$$

Here b is a free parameter that correlates the relative hardening to the fraction of cis isomers. This equation, with $\tau_m = 200\,\mathrm{s}$ and $b = 0.1$ satisfactorily describes transient experiments under irradiation with UV light (Fig. 2.4b). When UV radiation is switched off, the cyclic photoisomerization immediately stops, i.e. the first term in Eq. (2.20) disappears, and one observes a sharp drop in the dielectric constant. Interestingly, we could use the same power law to describe the response at different intensities of UV light, although there is a noticeable discrepancy between the model predictions and the measured data at longer times after the UV light is switched off, presumably due to orientational effects.

2.1.4. Light-induced changes of the plate compliance

In contrast to the dielectric constant, the bulk compliance should not (or only weakly) depend on orientational effects. This explains why using the same equations (2.16) and (2.20) (but with different values of the fitting parameters) we managed to describe satisfactorily the time dependence of $\delta\beta_{zz}$ not only under irradiation but also at longer times after the VIS or UV light has been switched off (Fig. 2.5). In spite of significant noise in the data, one can clearly see that, in the case of UV irradiation, the gradual recovery of the bulk compliance to its initial value in the dark is reproduced much better than that of the dielectric constant (Fig. 2.4a). In the case of VIS irradiation, both the model predictions and the measured data exhibit an immediate drop of $\delta\beta_{zz}$ to zero after the light is switched off (Fig. 2.5b).

The coefficient of proportionality c in Eq. (2.16) can be estimated from the dependence of the relative dielectric constant on temperature. We have determined $c \approx 215$ by measuring $\delta\varepsilon'$ at the glass transition temperature ($\delta\varepsilon' \approx 5.4$) and using a literature value of $\phi \approx 0.025$.[84] Clearly, the fraction of free volume created under irradiation with visible light at room temperature is considerably smaller than that at the glass transition temperature. At a pumping intensity of 100 mW/cm^2, typically used for the inscription of SRGs, $\delta\varepsilon' \approx 0.1$. This gives us a value of free volume ca. 50 times smaller than that at T_G.

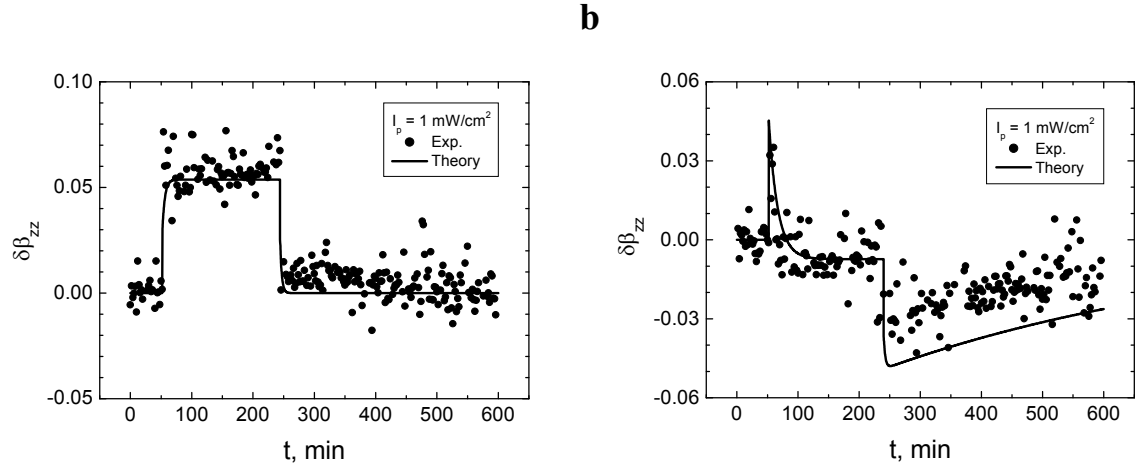

Figure 2.5. Time dependencies of the relative plate compliance under VIS (a) and UV (b) irradiation with 1 mW/cm^2. Lines show model predictions described by Eqs. (2.16) and (2.20).

At closer consideration, such a low value appears to be quite reasonable. Indeed, at the same intensity of 100 mW/cm^2 one isomerization event per one azobenzene moiety is very rare, as it happens only once during 1 s.[41] To notice such an event, for example in the molecular dynamics (MD) simulations, one should observe a system with at least 10^9 side-chains during 1-10 ns. Such system would occupy the MD box with the edge of about 1 μm! It is unclear how a local disturbance, that occurs on the scale of 1 nm during 1 ps, can lead to the softening of the microscopic box. Also, from our point of view, the scenario of anisotropic diffusion proposed by Lefin et al.[31,32] is very unlikely: one side-chain changes its position (= a caterpiller makes the first step) due to isomerization event and waits microseconds till another side-chain in the same macromolecule, the most probably attached to the backbone some 100 nm away, makes the next step. It is difficult to consider such a frozen motion to be a cooperative movement of the chain ensemble, independently on its direction.

2.2. Atomic force microscopy

Scanning probe microscopy experiments were carried out with the help of the commercial atomic force microscope (AFM) with its linearized 100 μm scanner (autoprobe CP, Veeco Instruments, USA). Two different measuring modes were used to gather information on the mechanical properties: the pulsed force mode and conventional force-distance curves.

2.2.1. Pulsed force mode

The pulsed force mode (PFM) extends the capabilities of an atomic force microscopy beyond simply measuring the sample topography. PFM allows one to determine surface properties such as local stiffness and adhesion in form of highly resolved material contrast images.[88,89] This method has been used to measure the local distribution of stiffness in the azobenzene polymer films before und under long-term irradiation with visible light.[90, 91]

A special piezoelectric system introduces on the AFM tip a sinusoidal modulation with the amplitude of 0 ÷ 500 nm at a user-selectable frequency between 100 Hz and 2 kHz. The experiments shown here are done at ~ 1 kHz. The modulation amplitude is adjusted in such a way that the measuring tip briefly but periodically touches the sample surface. At the beginning of every PFM cycle the AFM tip gradually approaches the surface (Fig. 2.6, AB).

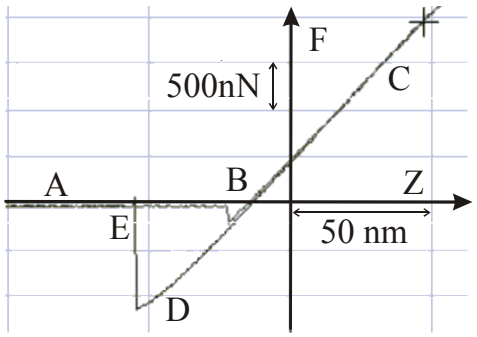

Figure 2.6. Example of the force-distance curve F(z) taken on the pDR1M film.

At close approximation the tip suddenly snaps into contact due to attractive interactions with the film surface. The piezoelectric system pushes the tip further towards the surface, before the force reaches a certain maximal value (Fig. 2.6, BC). As the system pulls the tip back (Fig. 2.6, CD), the latter suddenly looses contact (Fig. 2.6, DE) and snaps away from the surface (Fig. 2.6, E). The force in point D is a measure for the adhesion between the tip and the surface, and its value is fed as an additional signal into an analogue input channel of the AFM to form the adhesion image of the sample. The difference between the maximal force and the force occurring at a time which is determined by a special stiffness trigger is related to the local stiffness of the sample. On hard parts of the sample this difference is larger than on soft ones. This force difference is recorded as a relative value and forms the stiffness image. Changing the tip position with the help of the scanner, it is possible to take force-distance curves along the whole sample area. Thus, PFM provides three simultaneously measured images which contain the information about topography, adhesion and stiffness of the sample surface.

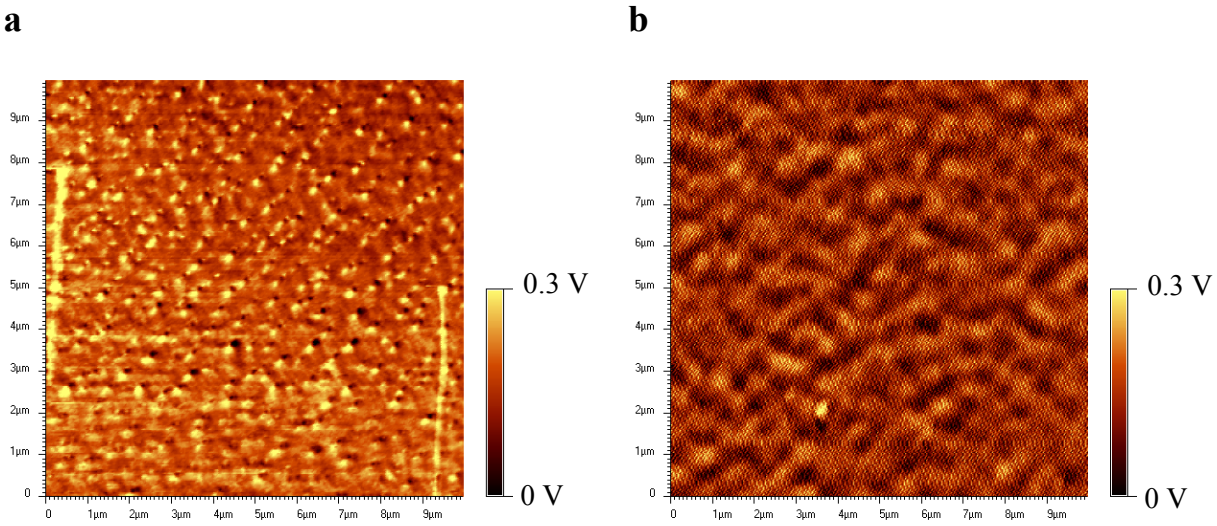

Figure 2.7. Stiffness images measured by pulse force microscopy: a freshly prepared film (a) and the same film after heating above the glass transition temperature (b).

It has been found that freshly prepared films are not homogeneous. On the stiffness map (10μm×10μm) one observes a number of sharp peaks on an otherwise flat background (Fig. 2.7a). The apparent size of the stiffness clusters is about 100 nm. We suppose that due to the fast evaporation of solvent there are more and less dense regions in the film; the latter are enriched by channels through which the solvent evaporates during spin-coating and subsequent tempering at 70 ºC. After heating above T_G (average heating rate ~ 1 grad/min) the grain boundaries considerably smoothen and the films become more homogeneous (Fig. 2.7b). In addition, it is found that the thickness of the film decreases on about 4.5% upon heating above T_G. This finding suggests a significant decrease of the free volume in the film due to closing of the solvent-evaporation-channels.

2.2.2. Force-distance mode

Force–distance measurements have been performed on the sample surface before and under irradiation with visible light. The only difference as compared with the PFM measurements (see Section 2.2.1) is that now the curves are taken at the locations chosen and this is done much more slowly, over a period of 1 s (i.e. at the frequency of 1 Hz). The slope of the force–distance curve (Fig. 2.6) is defined by a superposition of the spring constants of the lever and the elastic film. As the lever properties do not change during measurements, different slopes of the curves taken at different places reflect local changes in the film stiffness.

An abnormal change of stiffness was demonstrated under illumination with visible light ($\lambda = 532$ nm, $I \approx 100$ mW/cm^2). Most of the freshly prepared samples first soften abruptly (10% stiffness decrease after 15 seconds of illumination) and then gradually harden (during 2 min). However, a few samples, in which the measurements are presumably done on stiff spots (see Fig. 2.7a), do not exhibit the first fast process. In all subsequent cycles a reproducible behavior is observed: films are slightly softer under VIS illumination and stiffer when the light is switched off (Fig. 2.8).

An attempt was made to estimate the degree of film softening from the force-distance curves using a parallel mechanical model. In this model the measured stiffness, S, can be expressed as

$$S^{-1} = S_F^{-1} + S_K^{-1} \tag{2.21}$$

where S_F is the film stiffness and S_K is the stiffness of cantilever. As the stiffness of glass is many orders of magnitude higher than the stiffness of cantilever, measuring the stiffness directly on the glass substrate gives a value of S_K. Measurements performed on the layer show that the stiffness of the azobenzene polymer decreases app. twice under illumination. As S_F directly correlates with the elastic modulus of the film, E, we expect an only 50% decrease in E under illumination with visible light.

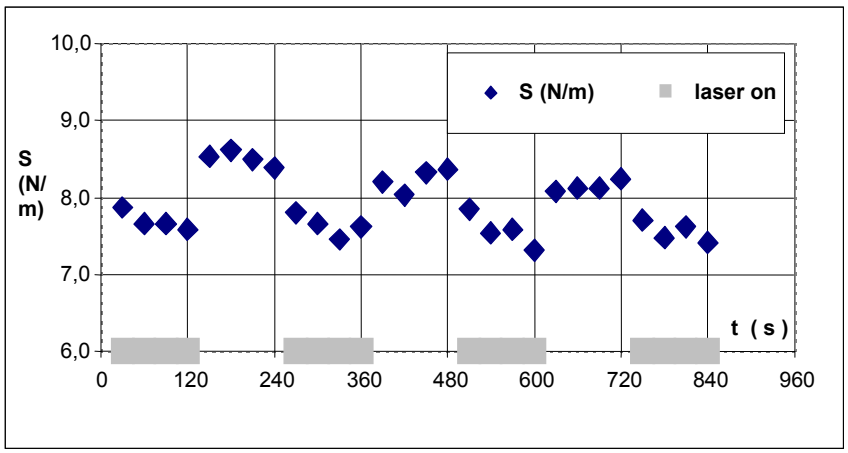

Figure 2.8. Stiffness changes under illumination with visible light ($\lambda = 532$ nm, $I \approx 100$ mW/cm^2) measured on the pDR1M film using the AFM force-distance curves.

It is worth to note that aged pDR1M films, held at least two months after preparation in darkness, do not show any softening under illumination with visible light. Nevertheless, they can be used for inscription of surface relief gratings with the same efficiency as that of SRGs produced on freshly prepared films. We can conclude that light induced softening is a very weak accompanying effect rather than a necessary condition for the formation of SRGs.*

2.3. Fluorescence recovery after photo-bleaching

The force-distance mode of atomic force microscopy operates at a frequency of about 1 Hz. As the polymer response strongly depends on the excitation frequency, it is worth to utilize another method performing at much lower frequencies. Here, we have chosen a fluorescence recovery after photobleaching (FRAP) that operates at the range of minutes.

The FRAP technique has been successfully used to measure the translational motion of tracer molecules in thin polymer films around the glass transition temperature.[78-80] The principle idea of this method is that small dye molecules are mixed to the polymer layer and then destroyed in some area by a burst of light. The photobleached area can then be scanned using a narrow beam of an appropriate wavelength that excites the undestroyed dye molecules which start to emit light. If with time undestroyed molecules diffuse into the photobleached area, the process of diffusion will manifest itself as a gradual increase in the fluorescent intensity.

In this study, the FRAP method was used to follow changes in the viscosity of azobenzene layers at different temperatures and under illumination. According to the free volume theory, the diffusivity of small molecules depends exponentially on the free volume fraction as a result of an exponential increase in the viscosity.[77] Therefore, already a minor increase in the free volume (< 5%),[93] e.g. induced by an increase in temperature above the glass transition temperature, is expected to cause a significant increase in the diffusivity.

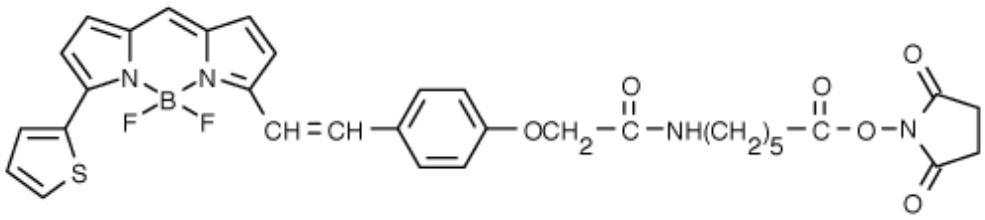

Figure 2.9. Chemical structure of the red-fluorescent dye D10000.

The material investigated is pCM1 with a molecular weight of 8.6 kg/mol, an azobenzene content of 62% and $T_G = 90\,°C$ (Fig. 1.1b). A commercial red-fluorescent dye, D10000 from "Molecular Probes", was used as the tracer molecules (Fig. 2.9). This dye exhibits an absorption maximum at 632 nm, well beyond the absorption of the azobenzene film. The emission of the dye in the polymer matrix is at 650 nm. To avoid aggregation of the

* Yager and Barrett just reported on AFM indentation experiments in which they found "no significant change in elastic modulus with laser illumination, indicating that photosoftening can be neglected in these systems".[92]

dye molecules, only 0.01 wt% D10000 was mixed to the azobenzene polymer. Under these conditions, the fluorescence intensity of the dye was found to be only two times lower within azobenzene-containing layers compared to its value in an inert layer such as PMMA. Investigations of solutions containing both the dye and the azobenzene polymer showed a strong decrease in the fluorescence with increase of the azobenzene concentration. This indicates a certain degree of photoinduced charge transfer to the azobenzene as has been observed for other dye-doped azobenzene layers.[94]

The translational diffusion of the dye molecules within the azobenzene layers was measured by the FRAP-technique. An initial "writing" step with high intensity light of a focused HeNe-laser (~10^8 mW/cm^2) creates a spatial variation of the fluorescent dye concentration in the layer by local photo-bleaching. A second "reading" cycle creates a fluorescence intensity image by scanning the sample with an attenuated reading intensity of the same HeNe laser at a reduced intensity of ~10^4 mW/cm^2 across an area of ca. 40x40 µm^2. The scanning and the fluorescence detection was done with a modified confocal Raman Spectrometer (Dilor).

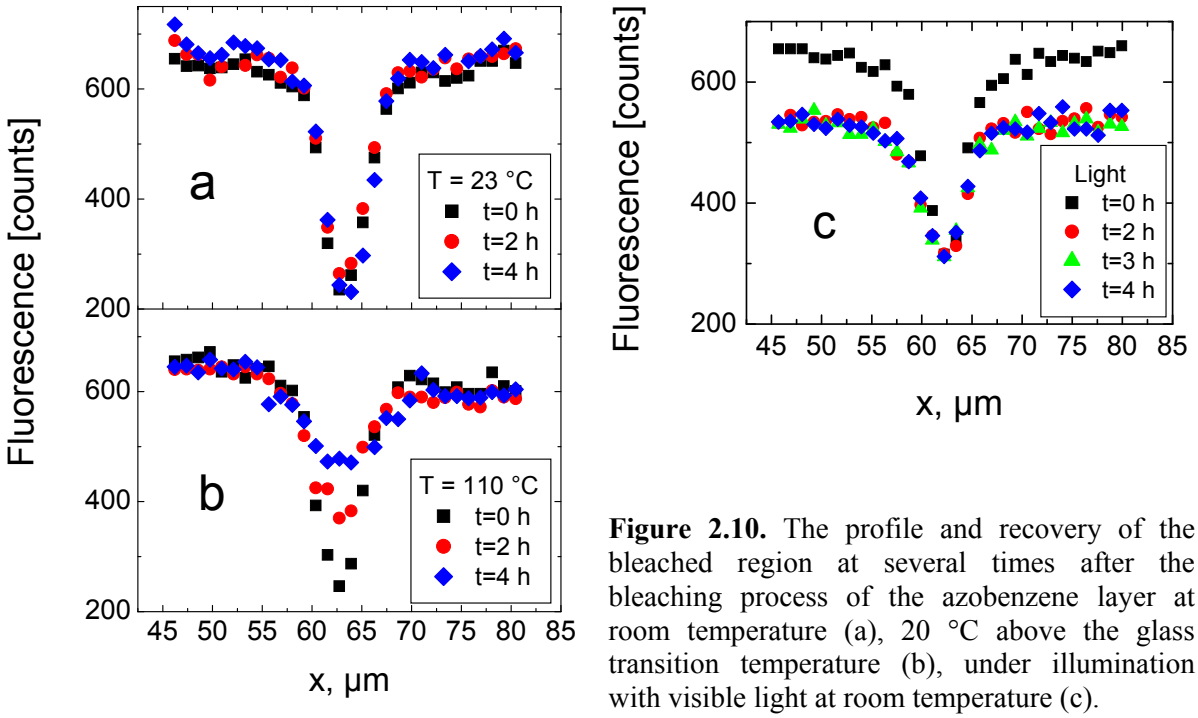

Figure 2.10. The profile and recovery of the bleached region at several times after the bleaching process of the azobenzene layer at room temperature (a), 20 °C above the glass transition temperature (b), under illumination with visible light at room temperature (c).

Translation diffusion of the dyes can then be followed by measuring the fluorescence intensity profiles across the bleached region at successive times at temperatures below and above T_G. At room temperature (23 °C), ca. 70 °C below T_G, the spatial fluorescence intensity of the bleached area did not change within hours (Fig. 2.10a). On the other hand, diffusion of dye molecules could be observed at a temperature of 110 °C, 20 °C above T_G (Fig. 2.10b). The diffusion coefficient, D, in the two-dimensional case can be calculated by using the Einstein relation: $D = a^2/(4\tau)$, where a^2 is the area of the bleached region, and τ is the time constant of the fluorescence recovery of the bleached region. The time constant

was determined from the time dependence of the measured fluorescence recovery (Fig. 2.10b). With $\tau \approx 100$ min at 110 °C and a diameter of the bleached area of 4 μm the diffusion coefficient is calculated to be $7 \cdot 10^{-11}$ cm^2/s. This compares well with values for the diffusion coefficient of small tracer molecules in a PMMA matrix above the glass transition temprature.[95]

To test if tracer-diffusion can be caused by light well below T_G, similar experiments were performed while illuminating a large area of the layer, including the photo-bleached spot, with circular polarized light of an Ar^+ laser at a wavelength of 488 nm and a moderate intensity of 100 mW/cm^2. These parameters are usually used for the inscription of SRGs. Consequently, if an active light-induced change in the viscosity takes place at room temperature, it should be detectable by the initiation of the diffusion. However, the data in Fig. 2.9c clearly show that light-induced diffusion of the dye molecules within the polymer layer is absent under the above-mentioned conditions.

Interestingly, we found a distinct reduction of the fluorescence intensity if the homogenous illumination of the Ar^+ laser at 488 nm wavelength is switched on (Fig. 2.10c). We presume that this reduction is caused by an additional fluorescence quenching in the presence of cis-isomers of the azobenzene dye, which forms upon photo-isomerization. For a constant cis fraction during the illumination at 488 nm, the measured spatial fluorescence intensity remains constant (Fig. 2.10c). The absence of appreciable changes in the fluorescence intensity in the subsequent scanning cycles in Fig. 2.10c proves that the illumination with moderate intensities of 488 nm wavelength does not induce any dye diffusion within the azobenzene layers.

Additionally, we found that an illumination with linear polarized light does not lead to any demonstrable dye diffusion in any particular direction. The independence of the diffusion on the polarization conditions is in contradiction to the concept of photo-induced translational diffusion as proposed by Lefin et al.[31,32] and of an anisotropic photo-fluidity as proposed later by Karageorgiev et al.[96] Based on the observation that the width of a scratch in an azobenzene layer was gradually reduced only when the light polarization was perpendicular to the scratch, the latter authors concluded that an azobenzene layer under illumination behaves like a fluid in the direction perpendicular to the light polarization and like a solid in the parallel direction. Contrary to this interpretation, our recent experimental and theoretical results provide a convincing evidence that it is dealt with a light induced anisotropic stress rather than with light induced anisotropic material properties.[51,70]

In conclusion, we showed that photoisomerization of azobenzene at light intensities typically used for the SRG writing does not cause a softening of the polymer layers from the glassy to the melt state. Moreover, an illumination at several polarization conditions did not reveal any detectable change in the viscosity of azobenzene layers. This leads us again to the conclusion that a light-induced stress should lie above the yield point of the azobenzene polymer to be able to cause the macroscopic transport.

Chapter 3

Viscoelastic modeling of the formation and relaxation of surface relief and density gratings

Thin films of azobenzene-containing polymers have been originally used to inscribe reversible birefringence gratings by inducing an alignment of the azo chromophores with an interference pattern of linearly polarized light.[19] Both amorphous[97,98] and liquid-crystalline[17,18] azobenzene polymers have been proved to be suitable materials for this holographic inscription. Ten years later, it was unexpectedly found that appearance of the birefringence grating is accompanied by a sinusoidal modification of the films surface, correlating with the light interference pattern.[22,23] Again, the surface relief gratings were observed in the amorphous[24,25] as well as in the liquid crystalline[99,100] azobenzene polymers.

The process of grating inscription is strongly dependent on the polarization state of the writing beams. Most groups report that two circular counter-polarized beams (circ-circ geometry) inscribe gratings of maximal diffraction efficiency, followed by two p-p polarized beams (p-p geometry), while two s-s polarized beams (s-s geometry) produce minimal surface changes.[3,101] However, on one particular functionalized copolymer system the p-p geometry is observed to be twice as efficient as the circ-circ geometry at long time scale.[102]

In this study, the surface relief gratings were inscribed using two circular counter-polarized beams from an Ar^+ laser operating at the wavelength of 488 nm and at the pumping intensity of 100 mW/cm^2 (Fig. 3.1a). The angle between the beams was chosen to be 30°. At this angle intensity modulations and a slight ellipticity of the resulting polarization in the interference pattern can be neglected.[103] Thus, the pattern can be considered as a linear polarization pattern with a resulting vector of the electric field rotating along the grating vector.

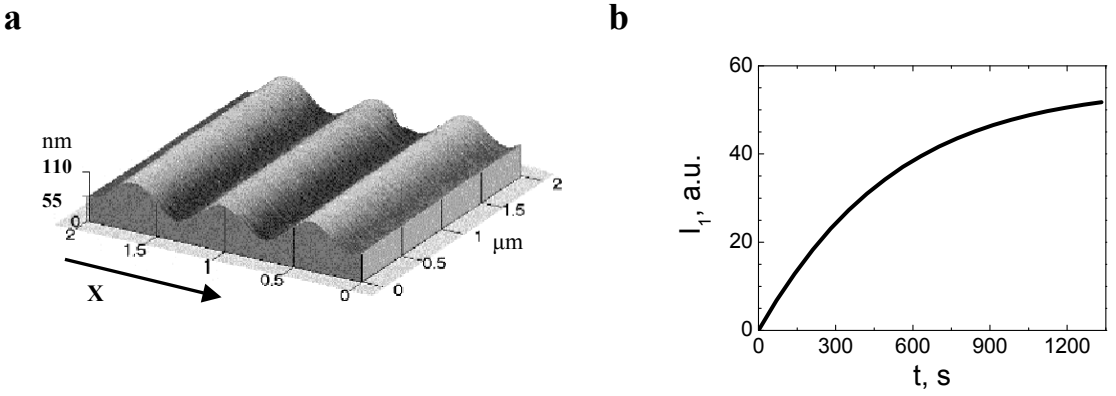

Figure 3.1. AFM topography of the surface relief grating with 880 nm period; the grating vector is parallel to the x axis (a). Time dependence of the 1st order scattering intensity under continuous grating inscription with a linear polarization pattern (b).

The gradual development of the surface relief grating under continuous illumination can be probed *in situ* by a He-Ne laser ($\lambda_{red} = 633\,\text{nm}$) operating outside the absorption band of the azobenzene. The scattering intensity of the 1st order peak increases with inscription time (Fig. 3.1b) and can be used to determine the grating deformation:[74]

$$\varepsilon(t) = 2(I_1 / I_0)^{0.5} \frac{\lambda_{red}}{\pi n_p L}. \tag{3.1}$$

Here I_0 is the specular intensity, $n_p = 1.66$ is the refractive index of the azobenzene polymer and L is the sample thickness.

3.1. The incompressible flow model

When two polarized beams interfere at a certain angle, the resultant intensity or polarization field has sinusoidal variation along the grating vector direction. Therefore, the force acting on the polymer material should also vary sinusoidally along the same direction. This force law together with the assumption of an incompressible viscous material behavior was used by Barrett et al.[28] to calculate the rate of grating inscription. It was shown that the inscription rate increases linearly with the intensity and with the third power of the initial film thickness. This calculation is in good agreement with the experimental data for thin films. Furthermore, when absorption effects are taken into account the above model can explain the film thickness dependence in the range of large thicknesses.[104] In both studies the Navier-Stokes equation was used, i.e. the material model was that of a viscous fluid without any intrinsic relaxation time.

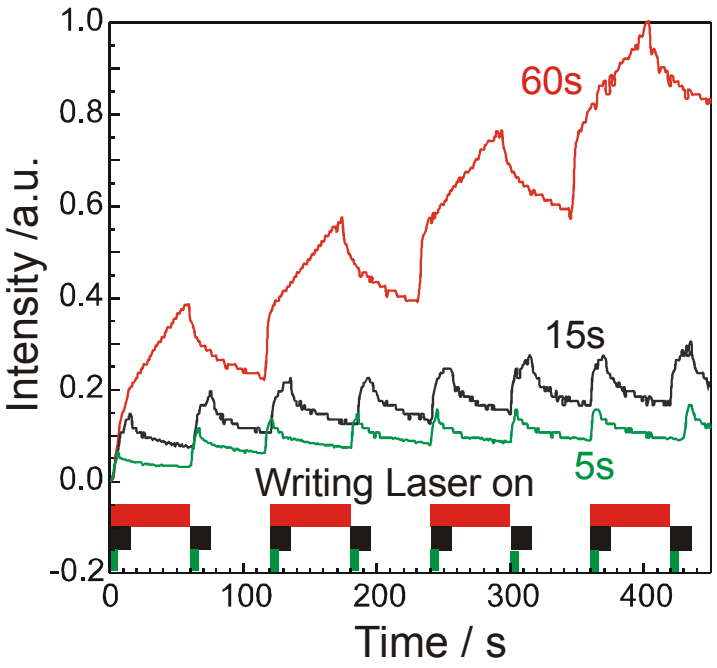

Figure 3.2. Time dependent inscription of the surface relief grating. The pulse length is 5 s (green curve), 15s (black curve) and 60 s (red curve).Time period is 60 s.

This incompressible flow model is not able to describe the time dependent visible light (VIS) scattering experiments performed during the formation of the SRG.[105-107] A typical set of curves is shown on Fig. 3.2. Here the inscribing beam was interrupted by a shutter to produce a sequence of pulses. The development of the surface relief grating under time dependent illumination has been again probed by the He-Ne laser. For every pulse one observes first an elastic response, then a viscous response followed by relaxation in the dark. With increase of the pulse length, the scattering intensity grows faster with time which means that the grating is highest for the red curve in the Fig. 3.2.

3.2. The viscoelastic flow model

In order to reproduce these VIS scattering data we modeled the inscription process under the assumption of the polymer being an isotropic viscoleastic (VE) material with finite compressibility. The particular choice of this model deserves some explanation. It is well-known that a polymer response to an external deformation is not purely viscous but rather viscoelastic. This is true even in the melt state, where the elastic modulus can be as small as few tens of kPa. Such reduction of the modulus accompanied by the corresponding decrease of the viscosity is caused by heating the sample some tens degrees above the glass transition temperature. Slightly above T_G, the viscoelastic behavior is much more pronounced than in the melt state: the elastic modulus is about 1 MPa, only three orders of magnitude smaller than at the glass state. The problem however is that we found only minute softening of the polymer layers under homogeneous visible illumination, using a number of experimental techniques (see Chapter 2).* Thus, in that chapter we inevitably arrived to the conclusion that a yet-unknown inscribing force should be above the yield point of the illuminated azobenzene polymers.

There are no data on the yield stress, σ_Y, of amorphous azobenzene polymers. Our expectation is that in the absence of illumination, it should not be higher than that of conventional polymers uniaxially stretched at small strain rates. For example, for PMMA, from which a number of azobenzene polymers including pDR1M and pCM1 are derived, the yield stress is about 50 MPa at a deformation rate of $10^{-5}\ s^{-1}$ (this rate is comparable with the rate of grating inscription).[108] Under visible illumination the yield stress is probably slightly reduced, following the 50% reduction of the Young's modulus, as it was reported recently.[96]

The proper material model will be then a viscoplastic one (= rate-dependent model with the yield stress): [109]

$$\begin{cases} \sigma = E\varepsilon & \sigma \le \sigma_Y \\ \sigma = \sigma_Y + \sigma_{VE} & \sigma > \sigma_Y \end{cases} \tag{3.2}$$

* Also, if one assumes a considerable softening under illumination, it becomes difficult to understand how a sinusoidal grating can be inscribed by two p-polarized interfering beams. Let us consider a sinusoidal stress in the direction of the grating vector and assume a linear relationship between the stress and the strain. Let us further assume that the Young's modulus decreases many orders of magnitudes at the intensity maxima while at the intensity minima it stays unaffected. Then, elongation in the region of high light intensity will not be accompanied by a contraction of similar magnitude in the region of low light intensity. As a consequence, two peaks will grow on both sides of the illuminated region. This is not observed experimentally.

For stresses below σ_Y, the polymer response is pure elastic, whereby the maximal elastic deformation, $\varepsilon_Y \equiv \sigma_Y / E$, does not exceed 2% for PMMA ($\sigma_Y = 50\ MPa$, $E = 3-4\ GPa$). Above the yield stress, the external stress can be considered as a sum of yield stress, σ_Y, and the viscoelastic stress, σ_{VE}. The time-dependent viscoelastic strain ε_{VE} considerably exceeds the yield strain ε_Y, except the moment when the light is switched on. In the following, we neglect the contribution from the yield stress and omit in σ_{VE} and ε_{VE} the subscript "VE". Hence, we reduce the viscoplastic material model to the viscoelastic one (= rate-dependent model without yield stress).

For the sake of simplicity, we shall consider the case when the light-induced stress does not change with time. Certainly this assumption is not anymore valid for very short inscription pulses (< 1 s). To describe such short pulse inscription, we proposed a modified linear viscoelastic model with the transient stress.[74]

3.3. Linear viscoelastic analysis

The stress-strain equations in the viscoelastic analysis depend not only on the current stress and strain states, but also on the entire history of the development of these states. This constitutive behavior is most readily expressed in terms of hereditary integrals:

$$\sigma(t) = \int_0^t G(t-t') \frac{d\varepsilon(t')}{dt'} dt' \tag{3.3}$$

where $\sigma(t)$ is the current stress and $\varepsilon(t')$ is the strain at a past moment of time t'. The time dependent relaxation modulus, $G(t)$, for materials with a fading memory such as polymers can be described as an exponential series:[110]

$$G(t) = \sum_{k=1}^{N} G_k \exp(-t/\tau_k) \qquad \text{and} \qquad G_0 = G(0) = \frac{E}{2(1+\nu)} \tag{3.4}$$

where E is the Young's modulus, ν is the Poisson's ratio and τ_k are the particular relaxation times of the system.

Under application of a constant stress, σ_0, a time-dependent polymer deformation could be obtained from Eq. (3.3) using the Fourier-Laplace transformation[111]

$$\varepsilon(t) = \sigma_0 \int \frac{d\varpi}{2\pi\omega} \frac{e^{i\omega t}}{G^*(\omega)} \tag{3.5}$$

where integration is performed in the complex plane and $G^*(\omega)$ is the complex shear modulus

$$G^*(\omega) = i\omega \int_0^\infty e^{-i\omega t} G(t) dt\,. \tag{3.6}$$

Using Eq. (3.4) $G^*(\omega)$ can be rewritten as follows

$$G^*(\omega) = \sum_{k=1}^{N} G_k \frac{i\omega\tau_k}{1+i\omega\tau_k} \tag{3.7}$$

Substitution of Eq. (3.7) into Eq. (3.5) gives the creep compliance of the material

$$J(t) = \frac{\varepsilon(t)}{\sigma_0} = \frac{t}{g_0} + \frac{g_1}{g_0^2} + \sum_{k=1}^{N-1} C_k \exp(-\omega_k t) \tag{3.8}$$

where $G_0 = \sum_{k=1}^{N} G_k$, $g_0 = \sum_{k=1}^{N} G_k\tau_k$, $g_1 = \sum_{k=1}^{N} G_k\tau_k^2$, C_k and ω_k are complex functions of G_k and τ_k.[39] The term g_0 can be identified with the stationary viscosity as $\sigma_0 = g_0 d\varepsilon(t)/dt$ at large t.[111]

Our approach to model the SRG inscription utilizes a sinusoidal force varying in the x direction, parallel to the grating vector, and decaying exponentially inside the film to account for the light absorption

$$f_x = AV \exp\left(\frac{z-[h(x)+h_0]}{\mu}\right)\sin\left(\frac{2\pi x}{D}\right). \tag{3.9}$$

Here A is the force density which should be proportional to the laser power in the linear regime, $h(x)$ is the height of the SRG, h_0 is the initial film thickness, μ is the light penetration depth and D is the grating period. The simulated sample volume, V, is set equal to h_0D^2 by choosing the third dimension equal to D. The force is applied in a self-consistent manner starting from $h(x) = 0$. A cleavage plane (x,z- plane, D = 1 μm) was calculated using the finite element method implemented by the commercial computer software Mentat/MARC (Fig. 3.3). The area was divided into a number of quadrilateral plain strain elements. Periodic boundary conditions were applied along the x-direction. As a constraint, no displacement of the sample was allowed at the polymer-substrate interface. We will show below that the force of gravitation can always be neglected in comparison with the inscribing force f_x.

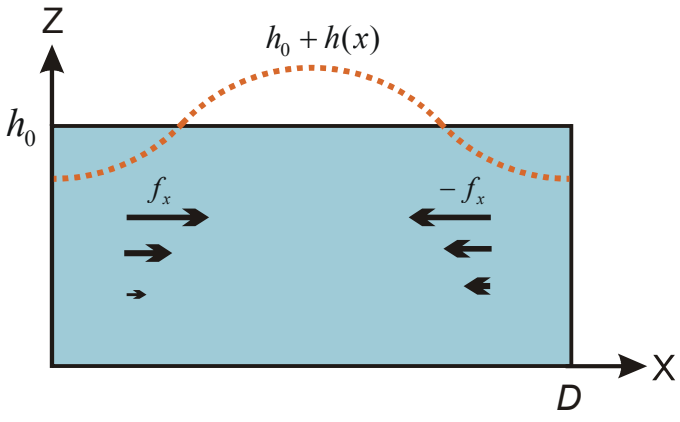

Figure 3.3. Scheme of finite element modeling: h_0 is the initial film thickness, $h(x)$ is the height of the SRG. The inscribing force f_x decays exponentially inside the film to account for the light absorption.

In order to perform a finite element analysis we have to define some material constants. Therefore, we restricted our examination to one particular azobenzene polymer, pDR1M, derived from poly (methyl methacrylate) (PMMA). Molecular weight in the studied samples varied in the range from 7.6 to 11.5 kg/mol (from 20 to 30 monomers). For this low molecular weight azobenzene polymer we expect a Young's modulus of about 1 GPa.[112] The calculated initial density for pDR1M is about 1250 kg/m^3 (ACD/ChemSketch, Version 5.08). Further we have chosen ρ_0=10^3 kg/m^3. While Poisson's ratio for pDR1M is unfortunately unknown, we took the value that is typical for PMMA: ν=0.4.[113] The light penetration depth, μ, of pDR1M was estimated from measurements of the extinction coefficient for different film thicknesses and was found to be about 0.1 μm at λ=488 nm.

3.3.1. Grating formation under continuous illumination

The grating amplitude can be probed in situ by the He-Ne laser (see Eq. 3.1) or directly inspected after inscription using atomic force microscope. We found that the finite element modeling (FEM) can well reproduce the growth of the SRG with only two terms in Eq. (3.8) (*N=2*). The following parameters were used: *E*=1 GPa, $G_1 = 0.9G_0$, $G_2 = 0.1G_0$, τ_1=1 s and τ_2=50 s. The force density, *A*, in Eq. (3.9) was chosen in such a way that substantial material transport could be observed after a few minutes of force application. Force densities of about 10^{14} N/m^3 were necessary to reproduce the growth of the SRG. Comparison of this value with the density of gravitation force (10^4 N/m^3) shows that the latter does not play any role during the inscription process.

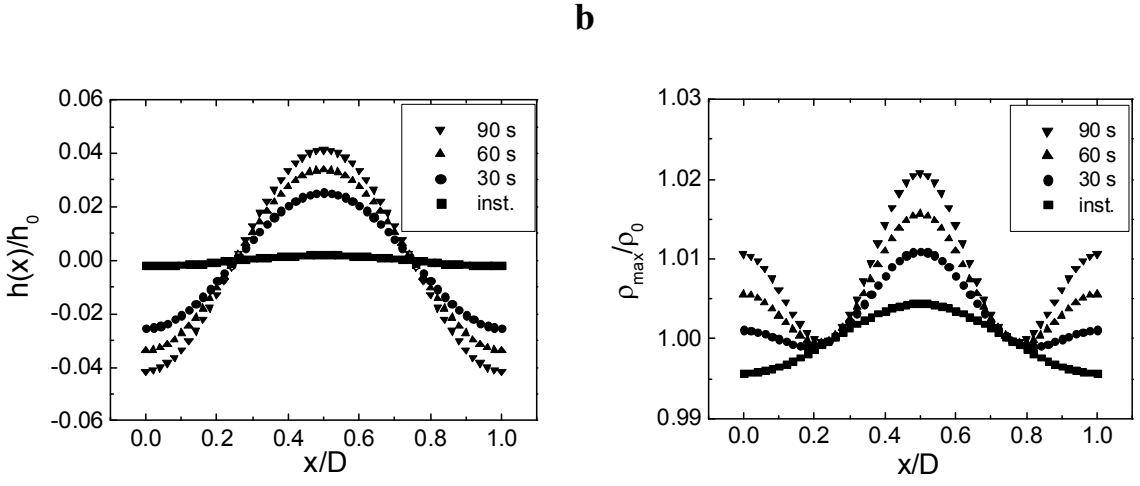

Figure 3.4. Time development of the surface relief grating (a) and the density modulation (b) obtained with FEM just in the beginning and after 30, 60 and 90 s of light exposure. $h_0 = 1$ μm.

The surface relief grating as well as the accompanying density distribution appears from the very beginning of the force application (instantaneous response on Fig. 3.4). During the first seconds of illumination both profiles can be described by a sinusoidal function of equal periods D (Fig. 3.4). Initially, the polymer material is mildly compressed in the regions of the surface relief peaks and slightly expanded between the peaks (Fig. 3.4b). As time

increases the compressed regions extend toward the substrate. At the same time the polymer material in the region of the relief trough is also compressed but this second "type" of compressed region is much smaller in volume and remains located close to the surface (Fig. 3.5). Thus, FEM predicts density increase in the region to which the azobenzene polymer chains have migrated. This prediction is in agreement with phase imaging AFM measurements that have revealed changes in density on the surface of the azobenzene polymer film induced by an optical near field.[114,115] Using second harmonic generation SNOM, it was shown recently that the mobility of chromophores is reduced in the region of grating hills which was attributed to an increase in density in these areas.[116]

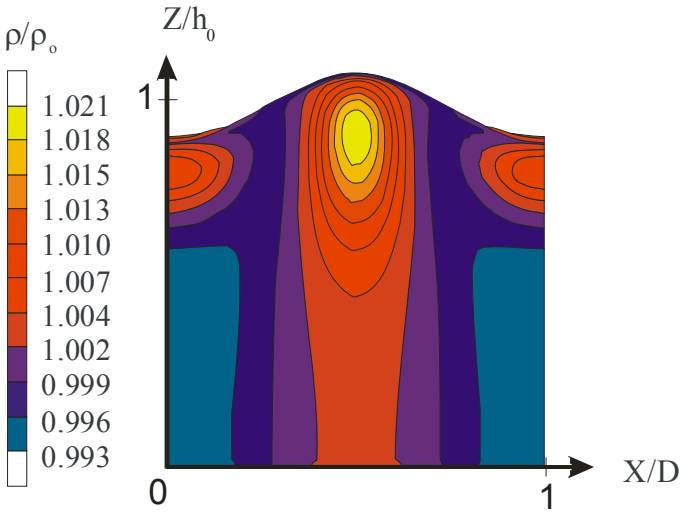

Figure 3.5. FEM of the grating formation after continuous exposure of 90 seconds. $h_0 = 1$ μm.

In this study we consider polymer films with ν=0.4. We have also shown that with an increase of the sample compressibility (the Poisson's ratio was varied in the range of 0.35 to 0.45) the amplitude of the SRG decreases and the density grating becomes more pronounced. This results in a comparable density change in the peaks and valleys of the SRG.[107] Thus, we always expect the appearance of a density grating as far as the studied materials are compressible. First indirect indications of its existence were found in X-ray studies of pDR1M films.[54,55] Here, the 1st order scattering peak was still preserved after thermal erasure of the surface profile (proved by AFM inspection). The presence of a sinusoidal density grating would naturally explain these observations. Later, the density grating formation under continuous illumination has been verified in situ using two different low power probe lasers operating at 514 nm and 670 nm wavelength.[117]

To visualize mechanical properties of an optically modified film, two-dimensional surface relief gratings were inspected with the help of pulsed force microscopy (see Section 2.2.1).[9,118] Figure 3.6 shows topography and stiffness images of the cross grating. Here, we intentionally chose a part of the sample with a defect in a middle, to demonstrate that we always study exactly the same area. These two images reveal a strong correlation between mechanical properties and topography of the cross grating. Cross-sections taken from the PFM images unambiguously demonstrate that at the hills of SRG the polymer material becomes stiffer. As the stiffness is expected to increase with the increase in polymer density, this result fully confirms the FEM predictions.

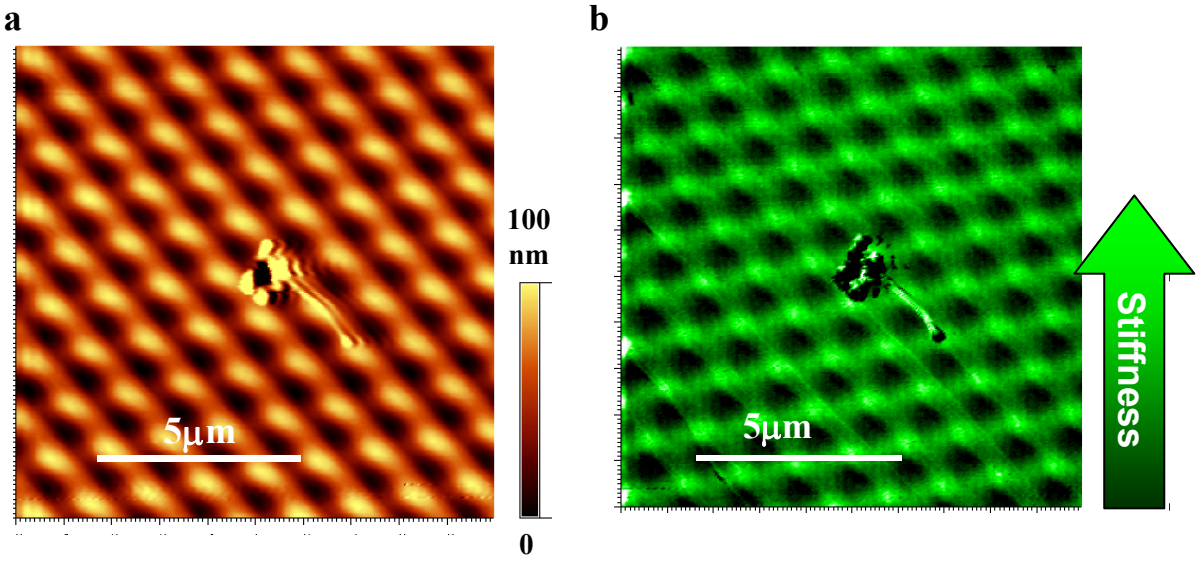

Figure 3.6. Topography (a) and stiffness (b) images measured by pulse force microscopy. The two-dimensional cross grating was produced by two-step inscription procedure, whereby the second step was made after rotating the sample on 60° around its normal.

3.3.2. Grating formation under time-dependent illumination

The development of a surface relief grating under pulse-like exposure was reproduced using a cyclic external force applied as follows

$$f = \begin{cases} f_x; & 0 \le t \le t_1 \\ 0; & t_1 < t \le T \end{cases} \tag{3.10}$$

where f_x is given by Eq. (3.9), t_1 is the pulse length and T is the cycle length. The response to this complex loading history can be calculated using the Boltzmann superposition principle

$$\varepsilon(t) = \sum_i \Delta\sigma_i J(t - t_i), \tag{3.11}$$

where

$$\begin{matrix} \Delta\sigma_{2i-1} \sim f_x \\ \Delta\sigma_{2i} \sim -f_x \end{matrix} \quad \text{and} \quad \begin{matrix} t_{2i-1} = (i-1)T \\ t_{2i} = (i-1)T + t_1 \end{matrix} \tag{3.12}$$

and i is the cycle number.

Although the density distribution was found to relax immediately after releasing the load, the surface profile can be accumulated even for pulse-like exposure if the pulse length exceeds some critical value. The FEM based on the two-terms-material model (Eq. (3.8), N=2) matches the functional behavior as found previously by the VIS experiment. However, it overestimates density and surface relaxation after the light is switched off. This results in prediction of large deformational jumps that are especially pronounced for very short pulses.

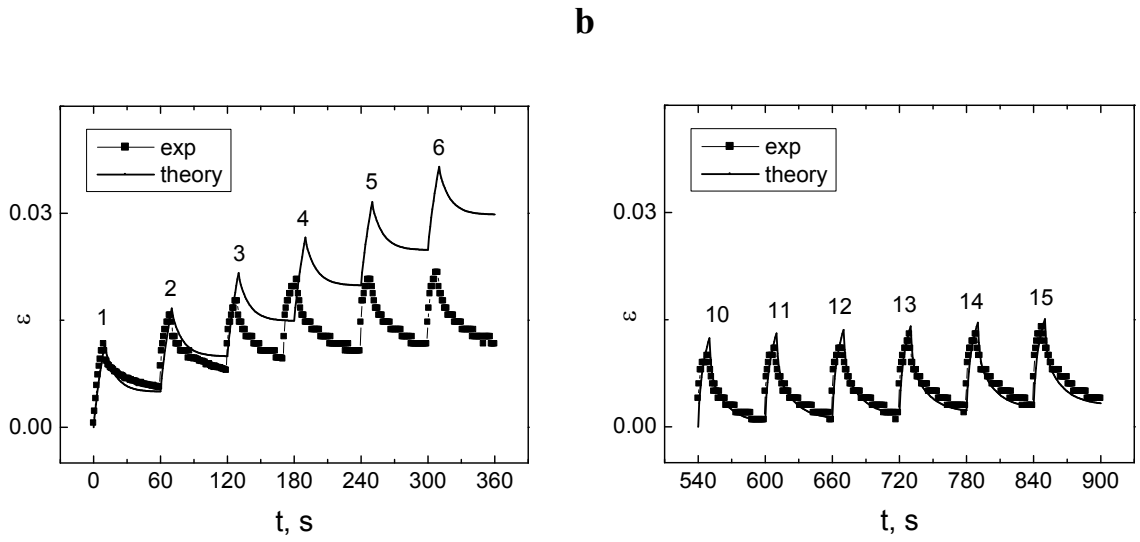

Figure 3.7. Development of the surface deformation during the first six pulses of light exposure (a) and the last pulses in the series (b).The pulse length $t_1 = 10\,s$. Experiment and one-dimensional theory based on the three-terms-material model. The right curves are shifted vertically starting again from zero deformation.

The time-resolved VIS scattering experiments[107,105] can be well reproduced in the frame of the one-dimensional viscoelastic theory by adding one more term (Eq. (3.8), N=3). Fig. 3.7 shows the experimental results and the theoretical prediction for $t_1 = 10$ s and $T = 60$ s. The first cycle of exposure is fitted with the following material parameters: G_0=1 GPa, $G_1 = 0.999G_0$, $G_2 = 0.0008G_0$, $G_3 = 0.0002G_0$, τ_1=0.002 s, τ_2=1 s and τ_3=30 s (Fig. 3.7a). Thus, the shear modulus decreases from 1 GPa to 1 MPa within 0.002 s after switching on the laser light and increases from 1 MPa to 1 GPa within the same 0.002 s when the light is switched off. This choice of parameters deserves a historical comment. At the time when this study was done everybody in the azobenzene community including ourselves still believed in a pronounced light-induced softening comparable with that taking place above the glass transition, i.e. amounting at least three orders of magnitude. In recent years we have, however, learned that the light-induced softening is a minor effect (see Chapter 2). In the light of this finding the decrease of modulus can be interpreted as a polymer yielding under light-induced stress.

The three-terms-material model describes particularly well the relaxation after the light is switched off. The fitting procedure reveals that G_0 gradually decreases from cycle to cycle until reaching a saturation value of 0.6 GPa (Fig. 3.7b). This result shows that an actual light-induced softening could take place during the subsequent light pulses, in spite of the transient nature of the applied force. The magnitude of light-induced softening as revealed by FEM is comparable with that found in the AFM studies (see Section 2.2.2) Relaxation times τ_2 and τ_3 also gradually increase and reach saturation values of 5 s and 400 s, correspondingly, for the last cycles. This may be an indication of gradual unfreezing of co-operative motions of polymer molecules in the film, i.e. the addressing of an increased number of azobenzene side groups by the light. The latter hypothesis is supported by ex-situ AFM inspections performed after inscription with a single short pulse.[119]

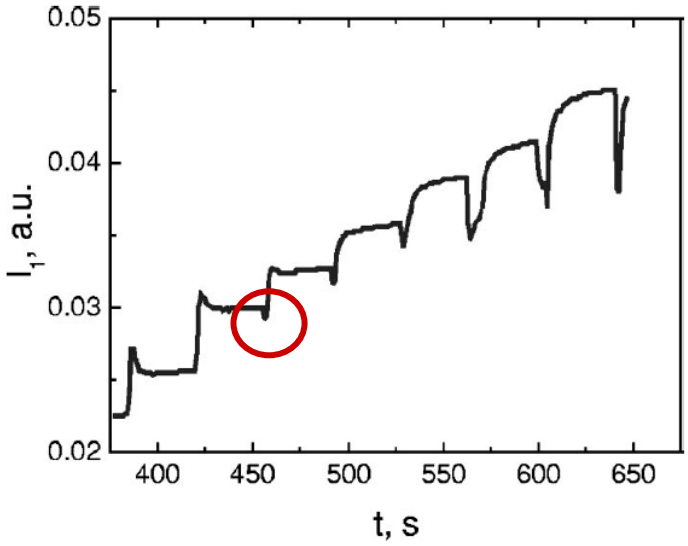

Figure 3.8. First order VIS grating peak intensity during short pulse exposure. The change in the sign of the response is indicated by the red circle.

An unexpected behavior has been observed in the VIS scattering measurements when the film was exposed to a long sequence of short pulses ($\leq$ 1s).[39] After 400 s of inscription the materials response suddenly changes its sign: VIS scattering intensity is now higher when the light is off (Fig. 3.8). A similar effect was reported in Ref. 106: the diffraction efficiency has slightly increased after the pumping laser was turned off in case of long irradiation. This change of behavior can be explained in the frame of scattering theory proposed by Pietsch.[120] The theory shows that the scattering amplitude of the first order VIS grating peak is a complex difference of two Bessel functions. The first function is varying with the amplitude of the SRG and the second one with the amplitude of density grating. Depending on the film thickness these gratings can be in-phase or out-of-phase (when $h_0 \sim 0.5$ μm). In the latter case the density slightly increases with every subsequent pulse leading at some moment to a change in the sign of the response.

To conclude, surface grating development under pulse-like exposure cannot be explained in the frame of an incompressible fluid model. However, it is easily reproduced using the viscoelastic model with finite compressibility.

Chapter 4

Light induced reorientation of azobenzene chromophores as a driving force of material transport

In Chapter 2 we provided convincing evidence that photoisomerization of azobenzene at light intensities typically used for the SRG writing does not cause a softening of the polymer layers from the glassy to the melt state. This evidence contradicts to the assumption of significant photoinduced softening made in the model of isomerization pressure[24,28] and the model of anisotropic diffusion.[31,32] The theories of electric force gradients[29,30,34,35] can be also eliminated as we showed recently that the force density predicted by these theories is negligibly small.[39] Presently, the mechanism based on the light-induced reorientation of azobenzene moieties looks the most promising explanation. This reorientation arises statistically, after a number of isomerization cycles, when the long axis of chromophores is mainly found to be perpendicular to the polarization direction.[62,63]

The idea that the force inscribing the SRGs may originate from the light-induced orientation of azobenzene moieties belongs to Pedersen et al.[33] The authors were able to explain the grating inscription with the help of the Maier-Saupe theory,[121] which is valid for nematic liquid-crystals: Under illumination with linearly polarized light, the azobenzene chromophores will orient parallel to each other and, therefore, their mutual attraction will increase. Due to this attraction, the sample should contract in the illuminated regions and the peaks of the SRG are predicted to form in the bright areas. Indeed, this prediction is consistent with results obtained for liquid-crystalline (LC) azobenzene polymers.[3] In another approach proposed by Bublitz et al.[36] it is postulated that the orientation of chromophores along the grating vector leads to a deformation of the polymer film in this direction. Without providing a detailed microscopic picture, the authors correctly explain the inscription of SRGs as well as deformation of azobenzene polymer films floating on a water surface.[26]

With every year, more and more evidence appears that chromophore reorientation must be the primary source for the inscription of SRGs and the film deformation under homogeneous illumination. Here, we like to mention studies carried out recently in the groups of Finkelmann and Ikeda on liquid-crystalline elastomers, in which preferential orientation of liquid crystalline moieties was imposed during a crosslinking process.[122] These monodomain samples exhibit a substantial thermally induced contraction upon the nematic-isotropic phase transition.[123-125] This effect was explained by the strong coupling between LC ordering and the elastic properties of the polymer network.[126-128] Moreover, a reversible elongation-contraction[10] as well as bending-unbending behaviour[11,47] of similar LC systems containing azobenzene moieties was observed upon alternating illumination with ultraviolet and visible light. The driving force for the large shape changes is suggested to arise from a variation in alignment order of the liquid-crystalline groups, caused by the *trans-cis* photoisomerization of the azobenzene chromophores.[129]

Following the spirit of these studies, we propose a new approach based on free energy and symmetry considerations for amorphous azobenzene polymer films. The basic idea is that under homogeneous polarized illumination an initially isotropic unconstrained sample is

allowed to stretch itself along the polarization direction. The stretching compensates the entropy decrease produced by the photoinduced reorientation of azobenzene chromophores. This approach readily explains uniaxial elongation of free-standing amorphous films as well as bending of the films on a flexible substrate under homogeneous illumination. Moreover, our model can correctly predict the formation of SRGs for the main inscription geometries as well as the orientational distribution of chromophores at any grating position. Last but not the least – this approach allows us to estimate the light-induced elastic stress imposed by the light-induced reorientation of chromophores within the polymer matrix.

4.1. Deformation of free-standing amorphous films under homogeneous illumination

The probability that a chromophore, oriented at an angle θ with respect to the polarization direction, will be excited by the polarized light, is proportional to $\cos^2\theta$ (see Eq. (1.6)). Therefore, starting from a sample with an isotropic angular distribution of the chromophores, multiple *trans-cis-trans* photoizomerizations with linearly polarized light will result in a preferential orientation of the long axis of the chromophores.[62,63] After some time, a dynamic steady state will be established which is characterized by a rather small fraction of chromophores pointing in the polarization direction and thus a small photoizomerization rate.

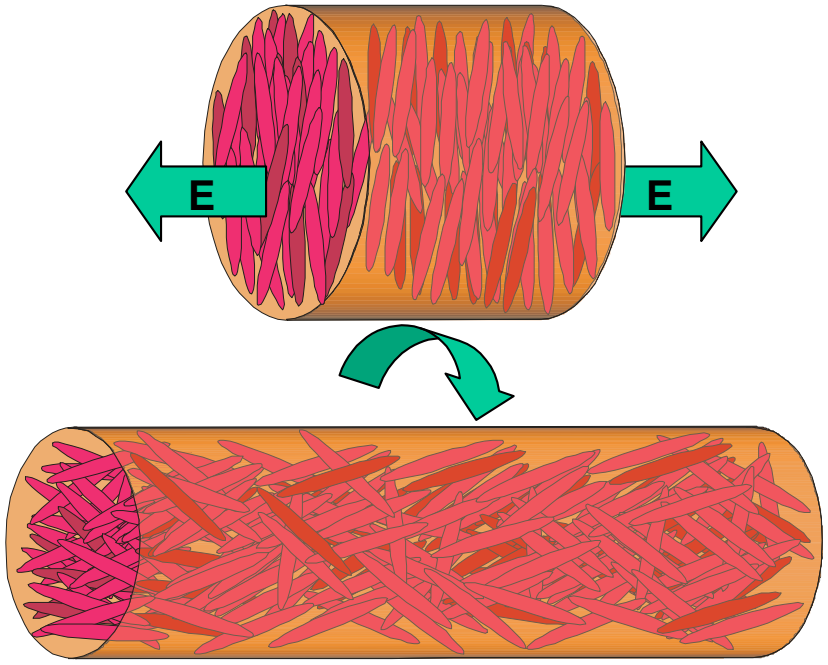

Figure 4.1. Change of the orientational distribution of chromophores due to sample stretching. Here $\mathbf{E}$ is the homogeneous light field used to orient the chromophores perpendicular to $\mathbf{E}$.

The entropy decrease per one azobenzene moiety due to the preferential reorientation of chromophores is given by[72]

$$S_{azo} = -k_B \iint f(\theta_{\mathbf{E}}) \ln[4\pi f(\theta_{\mathbf{E}})] d\Omega \tag{4.1}$$

where k_B is the Boltzmann constant, $\theta_{\mathbf{E}}$ is the angle between the long axis of chromophore and the electric field vector $\mathbf{E}$ and $d\Omega = \sin\theta_{\mathbf{E}} d\theta_{\mathbf{E}} d\varphi$ with $0 \le \theta_{\mathbf{E}} \le \pi$ and $0 \le \varphi \le 2\pi$. Here $f(\theta_{\mathbf{E}})$ is the orientational distribution of chromophores given for example by Eq. (1.10):

$$f(\theta_{\mathbf{E}}) = norma \cdot \cosh(\alpha \sin\theta_{\mathbf{E}})$$

where α is the strength of light induced alignment and $norma$ is the normalization constant.

Further, we shall assume that anisotropic interactions between azobenzene moieties can be neglected in the case of amorphous polymers because of the high steric hindrance imposed on the chromophores by a short spacer connecting the azobenzenes to the polymer backbone. Another factor that will be neglected in our approach is the change of the main chain entropy under illumination. With these two simplifications, the free energy per one azobenzene has only the entropy term $F_{azo} = -TS_{azo}$ with T the absolute temperature.

We now consider a sample which had been exposed to linearly polarized light, resulting in a preferential orientation of the azobenzene chromophores (Fig. 4.1, above). In order to minimize the free energy, the system under consideration needs to maximize its orientational entropy. In the case of free-standing films this can be achieved if the sample stretches itself along the direction of the electric field vector (Fig. 4.1, below). This has been indeed observed experimentally by Bublitz et al. in the case of amorphous polymers.[26]

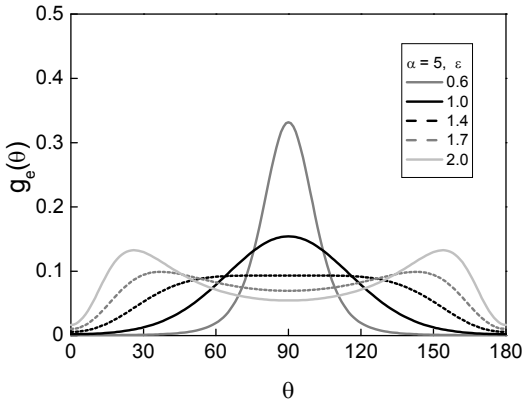

Figure 4.2 a. Orientational distribution function at different strains. The initial strength of light induced alignment was $\alpha = 5$.

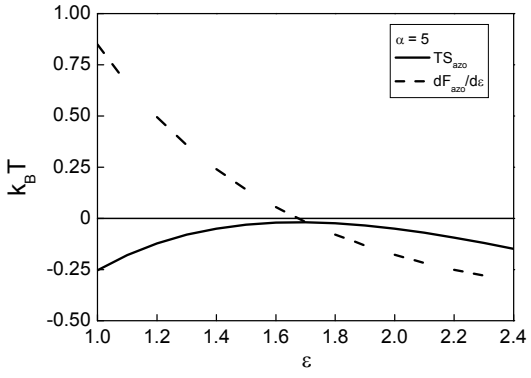

Figure 4.2 b. Dependence of the orientational entropy per one azobenzene S_{azo}, multiplied by the absolute temperature T, on the elongation for $\alpha = 5$. Also is shown the derivative of the free energy over deformation $\partial F_{azo}(\varepsilon)/\partial\varepsilon$.

Let us assume an affine deformation and incompressibility of the sample. Under this assumption, the stretching along the direction of the electric field vector will reorient the chromophores parallel to this direction. Knowing the initial light-induced distribution $f(\theta_{\mathbf{E}})$, it is possible to calculate a new orientational distribution function, $g(\varepsilon,\theta)$, for particular values of strain ε.[70] Figure 4.2a shows an example when the initial strength of light induced alignment is equal to 5 (black curve with $\varepsilon = 1$). With the increase of strain the peak around $90°$ gradually disappears, $g(\varepsilon,\theta)$ flattens ($\varepsilon = 1.4$) and two new peaks at $30°$ and $150°$ start to grow. At higher deformations these peaks sharpen and shift towards $0°$ and $180°$, i.e. azobenzenes are reoriented by the elongation field and most of them are now aligned along the direction of the electric field vector. Correspondingly, with the increase of strain the orientational entropy per one azobenzene goes through a maximum (Fig. 4.2b). Hence, our approach predicts that after reaching this turning point, $\varepsilon_{\max}(\alpha)$, the film should not furthermore change its shape. In reality, because the polarized light constantly reorients the chromophores back, perpendicular to $\mathbf{E}$, higher deformations than $\varepsilon_{\max}$ should be possible.

The magnitude of elastic stress can be estimated by taking the derivative of the free energy over deformation[82]

$$\sigma(\varepsilon) = n\frac{\partial F_{azo}(\varepsilon)}{\partial \varepsilon} \tag{4.2}$$

where n is the number density of chromophores. For relatively weak reorientation with $\alpha = 5$ we receive $\left.\frac{\partial F_{azo}(\varepsilon)}{\partial \varepsilon}\right|_{\varepsilon=1} = 0.85\ k_B T$ (Fig. 4.2b); and with n of about $1.5\cdot10^{21}$ cm^{-3},[41,130] the elastic stress should be about 5 MPa at the beginning of deformation. This value is comparable with the magnitude of elastic stress that should be applied to unsoftened polymer films (elastic modulus of 1 GPa) in finite element simulations in order to mimic the inscription of SRGs.[39]

4.2. Surface relief gratings

For further understanding, it is important to consider the changes in an initially isotropic sample under uniaxial deformation. Such situation corresponds to the elongation (compression) in the non-illuminated areas of the SRG. It is clear that the initially flat orientational distribution should transform into a peaked function: if the sample contracts ($\varepsilon < 1$), the maximum of $g(\varepsilon,\theta)$ grows at $90°$; if the sample elongates ($\varepsilon > 1$) two maxima grow at $0°$ and $180°$ (Fig. 4.3a). In both cases, an entropy decrease leads to the appearance of a restoring elastic force (the elongational branch of solution is shown in Fig. 4.3b).

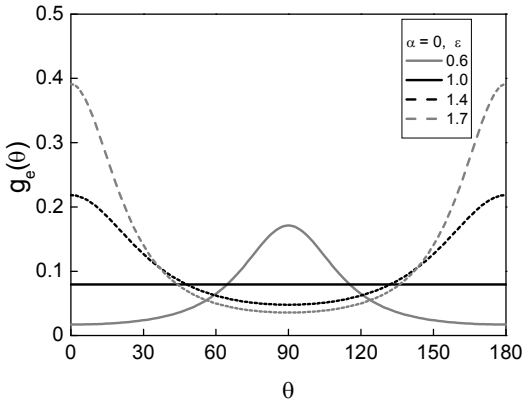

Figure 4.3 a. Orientational distribution function at different strains: $\varepsilon = 0.6$, 1.0, 1.4 and 1.7 for an initially isotropic sample ($\alpha = 0$).

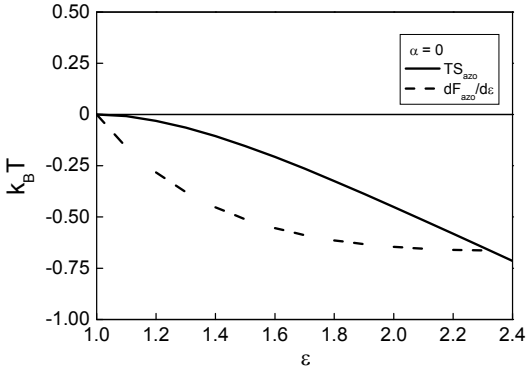

Figure 4.3 b. Dependence of the orientational entropy per one azobenzene S_{azo}, multiplied by the absolute temperature T, on the elongation for an initially isotropic sample ($\alpha = 0$). Also is shown the derivative of the free energy over deformation $\partial F_{azo}(\varepsilon)/\partial\varepsilon$.

4.2.1. Example - p-p inscription geometry

The process of grating inscription is strongly dependent on the polarization state of the writing beams (see introduction to Chapter 3). Let us now consider in detail the simplest case, namely the p-p geometry. First, one needs to calculate $\theta_{\mathbf{E}}$ in the laboratory frame. Let us take the direction of the grating vector as the *x*-axis, the direction along the grating grooves (in the sample plane) as the *y*-axis and the direction perpendicular to the substrate as the *z*-axis. In this frame, $\mathbf{e} = (e_x, e_y, e_z)$ with $e_x = \cos\theta_0$, $e_y = \sin\theta_0 \cos\varphi_0$ and $e_z = \sin\theta_0 \sin\varphi_0$. Here θ_0 is the angle between $\mathbf{e}$ and the *x*-axis and φ_0 is the angle between $\mathbf{e}$ and the *y*-axis. Further, $\cos\theta_{\mathbf{E}} = \dfrac{(\mathbf{E}\cdot\mathbf{e})}{|\mathbf{E}|\cdot|\mathbf{e}|}$.

For a grating with the period D, the electric field vector $\mathbf{E}$, the light intensity I and the angle $\theta_{\mathbf{E}}$ are given by the following functions of x

$$\mathbf{E} = E_0 \cos\left(\frac{\pi x}{D}\right)\mathbf{i}, \qquad I(x) = I_0 \cos^2\left(\frac{\pi x}{D}\right) \quad \text{and} \quad \sin\theta_{\mathbf{E}} = (1 - e_x^2)^{0.5}. \tag{4.3}$$

Here, we have followed the assignment of Lagugne-Labarthet et al.,[131] whereby the intensity maxima appear at $x = 0$ or $x = D$ and the intensity minimum at $x = D/2$. The strength of alignment should be proportional to the intensity of light, therefore, we have introduced

$$\alpha(x) = \alpha_0 \cos^2\left(\frac{\pi x}{D}\right). \tag{4.4}$$

The orientational distribution function for p-p geometry is then

$$f(\theta_0, x) = norma \cdot \cosh\left\{\alpha_0 \cos^2\left(\frac{\pi x}{D}\right)\left(1 - e_x^2\right)^{0.5}\right\}. \tag{4.5}$$

The orientational entropy per one azobenzene at the position x along the grating vector can be calculated as

$$S_{azo}(x) = -k_B \iint f(\theta_0, \varphi_0, x) \ln\left[4\pi f(\theta_0, \varphi_0, x)\right] d\Omega \tag{4.6}$$

and, hence, the drop of orientational entropy per one grating period D due to the preferential reorientation of chromophores can be expressed as

$$S_0 = -k_B n h_0 D \int_0^D S_{azo}(x) dx \tag{4.7}$$

where h_0 is the thickness of the active layer. Here, for simplicity, the sample width along the y-axis is taken to be D. Further, a dimensionless quantity

$$\hat{S}_0 = \frac{S_0}{2k_B n h_0 D^2} = \int_0^{1/2} S_{azo}(\hat{x}) d\hat{x} \qquad \text{with} \qquad \hat{x} = x / D \tag{4.8}$$

will be considered. Due to symmetry of solution the dimensionless entropy $\hat{S}_0$ is calculated for half of the grating period.

In order to maximize its orientational entropy, the film can undergo an appropriate deformation $\varepsilon(x)$ at every position along the grating vector. Due to translational symmetry along the y-axis the sample can only deform itself in two other directions. Again, if we assume an incompressible material, elongation (contraction) along the grating vector has to be accompanied by contraction (elongation) in the direction perpendicular to the sample surface. Further, since the polarization pattern is a sinusoidal function with periodicity D, it is meaningful to assume $\varepsilon(x)$ to be of the same form:

$$\varepsilon(x) = 1 + \varepsilon_0 \cos(2\pi x / D + \phi). \tag{4.9}$$

Here ϕ is the phase of the surface relief grating: $\phi = 0$ (case I) corresponds to the mass transport into non-illuminated regions for the p-p geometry, while $\phi = \pi$ (case II) describes the mass transport into non-illuminated regions for the s-s geometry. Further we shall consider only these two cases as other phases lead to asymmetrical solutions.

At small deformations, $\varepsilon_0 < 0.2$, the deformation law given by Eq. (4.9) results in a nearly sinusoidal grating. At higher deformations, the grating deviates from a sinusoidal one because the finite element with the initial coordinate x_0 shifts towards

$$x(x_0) = \int_0^{x_0} \varepsilon(x)dx = x_0 \mp \varepsilon_0 \frac{D}{2\pi}\sin(2\pi x_0 / D) \tag{4.10}$$

where the sign "-" corresponds to case I and the sign "+" to case II. However, the grating period is preserved: $D^{-1}\int_0^D \varepsilon(x)dx = 1$. The grating relief height at coordinate x is defined by $h(x) = h_0 / \varepsilon(x_0(x))$, which insures the incompressibility of the sample: $D^{-1}\int_0^D h(x)dx = h_0$.

If we again assume an affine deformation and take into account that the film is confined along the y-axis, it is possible to calculate a new orientational distribution function, $g(\varepsilon, \theta_1, \varphi_1)$, at any position x for the value of strain $\varepsilon(x)$. The dimensionless entropy per a half of grating period after deformation is given by

$$\hat{S}(\varepsilon_0) = \frac{1}{2k_B n h_0 D^2}\int_0^{1/2} \frac{S_{azo}(\varepsilon(\hat{x}))}{\varepsilon(\hat{x}_0(\hat{x}))}d\hat{x} \tag{4.11}$$

where

$$S_{azo}(\varepsilon) = -k_B \iint g(\varepsilon, \theta_0, \varphi_0)\ln[4\pi g(\varepsilon, \theta_0, \varphi_0)]d\Omega \tag{4.12}$$

and the absolute change of dimensionless entropy per one half of the grating period is equal to $\Delta\hat{S} = \hat{S}(\varepsilon_0) - \hat{S}_0$.

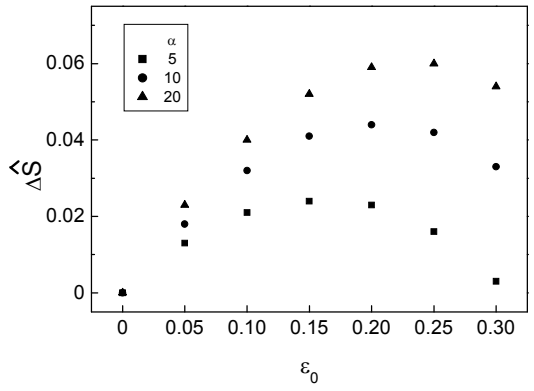

Figure 4.4 a. Dependence of the absolute change of the dimensionless entropy on strain for different strengths of the initial light-induced alignment: $\alpha = 5$, 10 and 20.

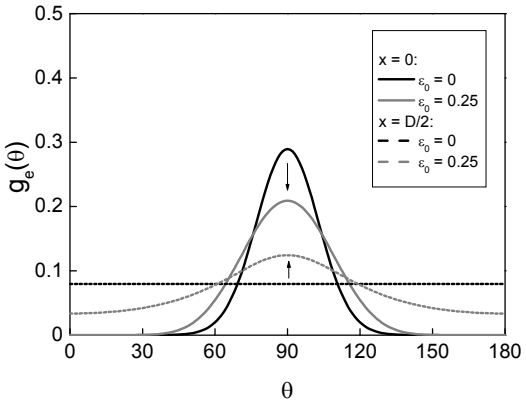

Figure 4.4 b. Orientational distribution function at different positions of the grating for $\varepsilon_0 = 0.25$. Black arrows show the direction of transformation of the distribution function. $\alpha = 20$.

Elongation in the region of low intensity ($x = D/2$), Case II, results in the further decrease of entropy and thus we should rule out this possibility. Contrary, as it can be seen from Figure 4.4a, elongation in the region of high intensity ($x = 0$ or $x = D$), Case I, effectively increases the entropy. Thus, our model predicts that polymer chains move from the

regions with high light intensity into the non-illuminated regions. This is indeed observed experimentally for most amorphous polymers. Depending on the strength of light induced alignment, different maximum deformations are predicted: from 0.15 for $\alpha = 5$ to 0.25 for $\alpha = 20$. If one considers a 500 nm thick polymer layer, the height of SRG will be in the range of 150-250 nm.

Our approach allows us further to calculate the orientational distribution function at any position of SRG. Figure 4.4b represents this function for case I at the valleys (intensity maximum, $x = 0$ or $x = D$) and at the peak (intensity minimum, $x = D/2$) before and after deformation. Due to elongation, chromophores situated at the valleys of the SRG become less oriented. Therefore, local entropy is considerably increased upon deformation. Due to the compressive deformation at the peak (situated in the dark area), the initially randomly oriented chromophores align perpendicular to the grating vector. This leads to a slight decrease of the local entropy, the value of which nevertheless stays higher than that at the valley. On the whole, the total entropy, integrated over one grating period, is effectively increased due to favorable redistribution of mass: polymer chains move in the direction of local entropy increase.

4.2.2. Discussion of main results

Application of the thermodynamic approach to other inscription geometries has been demonstrated in ref. 70. Here we briefly discuss the main results.

In agreement with experimental findings, we predict that polymer chains should move into the non-illuminated regions in the case of the s-s and p-p inscription geometries. For the circ-circ geometry, we expect the same direction of the chain transport as for the p-p geometry (from the regions where $\mathbf{E}$ is parallel to the grating vector), similar to prediction by Bublitz et al.[36] and contrary to some of the experimental reports.[24,132] Presently, we cannot propose any reason why during inscription with two circularly polarized beams the chains should move in the direction opposite to that found for the p-p geometry. The electric field in the circ-circ geometry is a linear superposition of the electric fields in the p-p and in the s-s geometries. Since the p-p geometry is found to induce a stronger force than the s-s geometry, it is not surprising that our calculations predict chain transport to occur in the same direction as in the p-p geometry. Interestingly, the discrepancy in the shape of the orientational distribution functions determined from Raman spectrometry results for the circ-circ geometry[132] and of those obtained by the thermodynamic approach[70] can be eliminated if the chain transport occurs in the same direction as for the p-p geometry. Indeed, Lagugne-Labarthet et al. have recognized that their first Raman results concerning the peak and valley positions were in error.[133] Thus, our prediction for direction of the chain transport in the circ-circ geometry corresponds to this later finding of the French group.

In agreement with experiment, the maximum deformations predicted by our model for the s-s geometry are noticeably smaller than those for the circ-circ and p-p geometries. On the other hand, our calculations predict an intermediate efficiency for the circ-circ geometry in comparison to the s-s and p-p geometries.[70] Only one functionalized copolymer system has so far been reported to exhibit the highest surface grating efficiency in the p-p inscription geometry,[134] whereas a number of the other experiments[3,101,135] unambiguously show that the circ-circ geometry is the most effective one (Fig. 4.5). It is worth to mention here that several authors were using a Lloyd mirror setup causing a substantial deviation from the circ-circ geometry.[103]

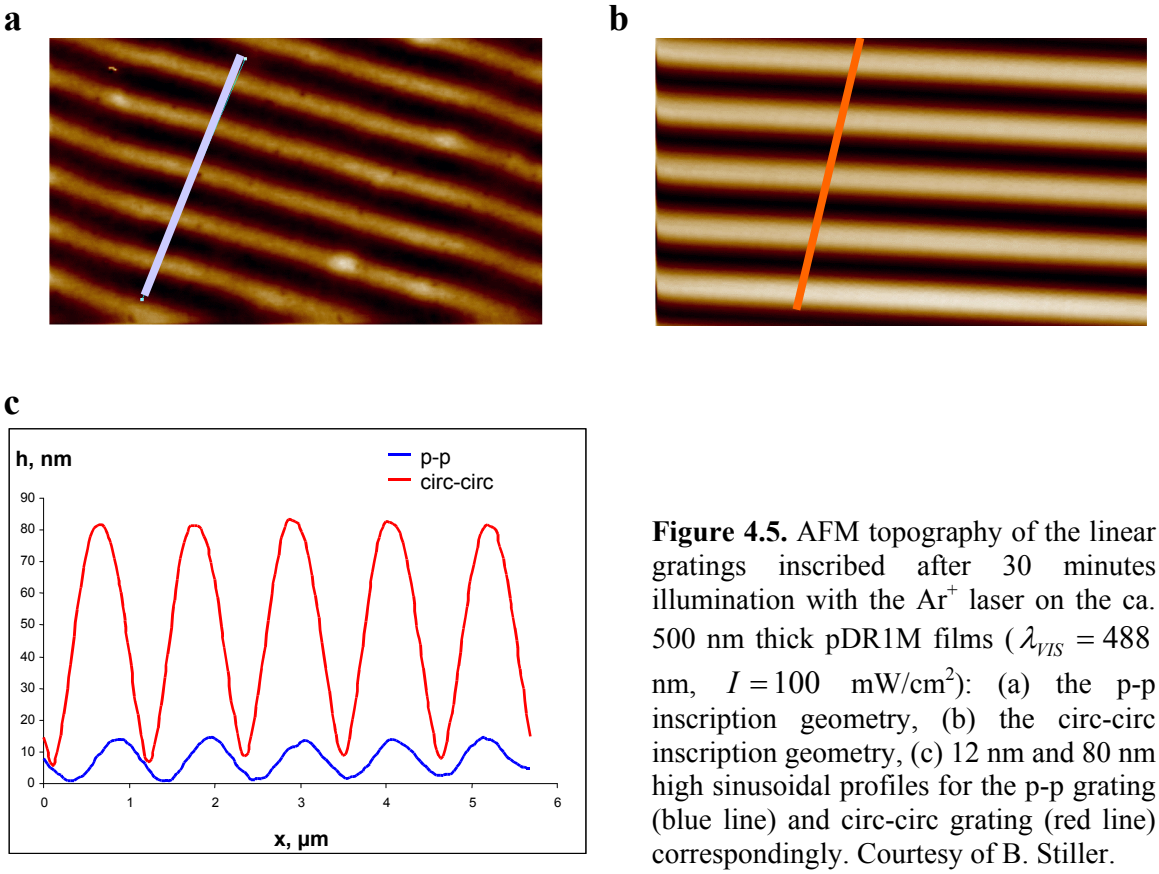

Figure 4.5. AFM topography of the linear gratings inscribed after 30 minutes illumination with the Ar^+ laser on the ca. 500 nm thick pDR1M films ($\lambda_{VIS} = 488$ nm, $I = 100$ mW/cm^2): (a) the p-p inscription geometry, (b) the circ-circ inscription geometry, (c) 12 nm and 80 nm high sinusoidal profiles for the p-p grating (blue line) and circ-circ grating (red line) correspondingly. Courtesy of B. Stiller.

Also, a possible reason of the discrepancy between most experimental studies and our prediction can be a slight light-induced softening of the polymer film. Obviously, this softening is expected to be less pronounced in the p-p and s-s geometries due to the presence of non-illuminated regions. Further, it should be noted that presently we do not consider the dynamic reorientation of chromophores that takes place in the circ-circ geometry when polymer material is moving between two grating positions with slightly different polarization directions. One may expect that this reorientation can be also responsible for the higher effectiveness of the circ-circ geometry in comparison with the p-p geometry. Also, we neglect any intermolecular interactions between azobenzene chromophores, although these interactions may play a role at high laser intensities. With the increase of light intensity, the strength of chromophore reorientation increases which in its turn should lead to an increase of attractive side-side interactions between chromophores. If the attractive contribution to the free energy overcomes the entropy term, the mass transport will change its direction, as it is found in ref. 30. The same is true in the case of liquid crystalline systems which have non-negligible intermolecular interactions between the chromophores.[3]

Another interesting prediction of our theory is that an azobenzene polymer film coated on a flexible substrate should bend when illuminated homogeneously with polarized light. The behavior of this composite sample is similar to that of a bilayer strip consisting of a polymer layer attached to an inert elastic backing and swollen due to water absorption.[136]

Conclusions

1a. It is shown that the transient mechanical and dielectric behavior of azobenzene polymer layers under homogeneous illumination with visible light can be readily understood in terms of a two-component mechanical model. This model assumes that an azobenzene polymer layer is composed from the polymer matrix and the free volume; the latter slightly increases under illumination with visible light.

1b. The complex mechanical and dielectric behavior under homogeneous illumination with ultraviolet light can be also explained in the frame of a two-component mechanical model if one assumes that a high fraction of cis-isomers is able to harden the polymer layer.

2a. It is demonstrated that softening of azobenzene layers does not exceed 50 % under homogeneous illumination with visible light. This evidence was obtained using two different techniques operating at totally different time scales: electromechanical spectroscopy and atomic force miscoscopy.

2b. Therefore, the light-induced stress should be above the yield stress of the (illuminated) azobenzene polymer layer in order to induce the transport of polymer chains over micrometer distances.

2c. The method of fluorescence recovery after photobleaching reveals that there is no light-induced diffusion under homogeneous illumination, neither isotropic with unpolarized visible light nor anisotropic with polarized visible light.

3a. It is shown that the proper material model for the description of the light-induced polymer transport should be based on viscoplastic deformation. This model can be reduced to a viscoelastic model that reproduces very well formation and relaxation of the surface relief gratings as found by visible scattering experiments.

3b. Finite element calculations in the frame of the viscoelastic model reveal the presence of density grating buried under the sample surface. Simultaneous formation of surface and density gratings explains a number of unusual effects observed in visual and X-ray scattering experiments. The presence of density grating is directly confirmed by recent pulsed force AFM studies.

4. Finally, a new thermodynamic approach is proposed that explains the origin of the light-induced stress. This approach can readily describe the light-induced deformation of free standing films and the formation of surface relief gratings for the main inscription geometries. The basic assumption of the theory is that under homogeneous polarized illumination an initially isotropic sample should stretch itself along the polarization direction to compensate the entropy decrease produced by the photoinduced reorientation of azobenzene chromophores.

Outlook

Until recently, formation of the surface relief gratings has been mainly studied on the macroscopic level which inevitably lead to less or more severe speculations in the existing theoretical models including the thermodynamic approach presented here. It is however clear that further progress in understanding of this puzzling phenomenon cannot be achieved without studies on the nanoscopic level. Here, computer simulation methods offer a number of advantages in comparison with the conventional experimental methods.[137,138]

The first simulation of photoinduced reorientation of azobenzene side-chain polymers was done already in 1998 when the influence of matrix rigidity and cooperative interactions between the chromophores was studied.[139] However, the matrix in these Monte Carlo simulations was virtual. The most important question to answer is: How does the molecular architecture of azobenzene polymers influence the formation of surface relief gratings? Realizing this, we launched in 2005 robust molecular dynamics (MD) simulations utilizing the program that was developed for liquid crystalline polymers with arbitrary topology.[140,141]

Presently, we try to reproduce the key experiment of Bublitz et al.[26] assuming that the chromophore reorientation is the primary source for the film deformation under homogeneous illumination. The azobenzene moieties are represented in the MD simulation by the Gay-Berne rods.[142] Their rotational diffusion is caused by an effective potential $U(\theta_{\mathbf{E}}) = U_0 \cos^2 \theta_{\mathbf{E}}$ created by the light field.[143] Two different molecular architectures have been used. The first one has a flexible main chain and a long spacer in the side chains, i.e. the elastic connection between the polymer matrix and the chromophore is weak.[144] The second model has a stiff main chain and a short spacer, i.e. the elastic connection is strong. Both models demonstrate deformation under homogeneous illumination with the visible light, but the sign of deformation is different depending on the molecular architecture. It seems that the experiment of Bublitz et al.[26] can be reproduced in the computer simulations without assuming dipole-dipole forces[37] or the anisotropic steps performed by molecular motors.[31,60] Though, these non-polymer models may explain formation of the weak surface relief gratings in a number of glass-forming low molecular weight compounds with incorporated azobenzene groups.[145,60]

The MD simulations are a powerful tool but as every method it has a number of limitations. The main one is the use of simplified molecular models and generalized potentials that do not allow the estimation of real temperatures and stresses in the system under investigation. In this study we have shown that it is very desirable to estimate the yield stress of the thin azobenzene polymer film illuminated with visible light. In principle, this can be done using the method of bending cantilever,[136] however the first attempts undertaken in the group of Soft Matter Physics did not provide quantitative results.[51, 96]

Another limitation of MD simulations is that it is impossible to implement one full grating period and thus to study different inscription geometries. Here, we believe, the future is by a combined approach in which a microscopic mechanism gained from the MD simulations will serve as an input of an elaborated version of the analytical approach presented in this study. Only when a new theory will be able to explain dependence of the inscription efficiency on the polarization conditions, the mystery of surface relief gratings will be truly solved.

Bibliography

1. Sainova, D.; Zen, A.; Nothofer, H.-G.; Asawapirom, U.; Scherf, U.; Hagen, R.; Bieringer, T.; Kostromine, S.; Neher, D. *Adv. Funct. Mat.* **2002,** 12, 49-57.
2. Zen, A.; Neher, D.; Bauer, C.; Asawapirom, U.; Scherf, U.; Hagen, R.; Kostromine, S.; Mahrt, R. F. *Appl. Phys. Lett.* **2002,** 80, 4699-4701.
3. Viswanathan, N. K.; Kim, D. Y.; Bian, S.; Williams, J.; Liu, W.; Li, L.; Samuelson, L.; Kumar, J.; Tripathy, S. K. *J. Mater. Chem.* **1999,** 9, 1941- 1955.
4. Natansohn, A.; Rochon, P. *Adv. Mater.* **1999,** 11, 1387-1391.
5. Berg, R. H.; Hvilsted, S.; Ramanujam, P. S. *Nature* **1996,** 383, 505-508.
6. Rasmussen, P. H.; Ramanujam, P. S.; Hvilsted, S.; Berg, R. H. *J. Am. Chem. Society* **1999,** 121, 4738-4743.
7. Zilker, S. J.; Bieringer, T.; Haarer, D.; Stein, R. S.; van Egmond, J. W.; Kostromine, S. G. *Adv. Mater.* **1998,** 10, 855-859.
8. Stracke, A.; Wendorff, J. H.; Goldmann, D.; Janietz, D.; Stiller, B. *Adv. Mater.* **2000**, 282-285.
9. Stiller, B.; Geue, T.; Morawetz, K.; Saphiannikova, M. *J. Micros.* **2005,** 219, 109-114.
10. Finkelmann, H.; Nishikawa, E.; Pereira, G. G.; Warner, M. *Phys. Rev. Lett.* **2001,** 87, 015501, 1-4.
11. Camacho-Lopez, M.; Finkelmann, H.; Palffy-Muhoray, P.; Shelly, M. *Nature Mater.* **2004,** 3, 307-310.
12. Yu, Y. L.; Nakano, M.; Ikeda, T. *Nature* **2003,** 425, 145-145.
13. Reinhold, B.; Geue, T. M.; Morawetz, K.; Saphiannikova, M.; Grenzer, J.; Panzner, T.; Pietsch, U. *HASYLAB annual report, Hamburg* **2002**.
14. Reinhold, B. In-situ Untersuchungen zur Abscheidung kolloidaler Schichten auf vorstrukturierten Substraten. Diplomarbeit, Universität Potsdam, Potsdam, 2006.
15. Yi, D. K.; Kim, M. J.; Kim, D.-Y. *Langumir* **2002,** 18, 2019-2023.
16. Henneberg, O.; Morawetz, K.; Schulz, B.; Dietzel, B.; Saphiannikova, M.; Roth, M.; Pietsch, U. *Proc. SPIE* **2006,** 6343, 634337, 1-12.
17. Eich, M.; Wendorff, J. H.; Reck, B.; Ringsdorf, H. *Makromol. Chem. Rapid Commun.* **1987,** 8, 59-63.
18. Eich, M.; Wendorff, J. H. *Makromol. Chem. Rapid Commun.* **1987,** 8, 467-471.
19. Todorov, T.; Nikolova, L.; Tomova, N. *Appl. Opt.* **1984,** 23, 4309-4312.
20. Todorov, T.; Nikolova, L.; Tomova, N. *Appl. Opt.* **1984,** 23, 4588-4591.
21. Todorov, T.; Nikolova, L.; Stoyanova, K.; Tomova, N. *Appl. Opt.* **1985,** 24, 785-788.
22. Rochon, P.; Batalla, E.; Natansohn, A. *Appl. Phys. Lett.* **1995,** 66, 136-138.
23. Kim, D. Y.; Tripathy, S. K.; Li, L.; Kumar, J. *Appl. Phys. Lett.* **1995,** 66, 1166-1168.
24. Barrett, C.; Rochon, P.; Natansohn, A. *J. Phys. Chem.* **1996,** 100, 8836-8842.
25. Kim, D. Y.; Li, L.; Jiang, X. L.; Shivshankar, V.; Kumar, J.; Tripathy, S. K. *Macromolecules* **1995,** 28, (26), 8835-8839.
26. Bublitz, D.; Helgert, M.; Fleck, B.; Wenke, L.; Hvilstedt, S.; Ramanujam, P. S. *Appl. Phys. B* **2000,** 70, 863-865.
27. Holme, N. C. R.; Nikolova, L.; Hvilsted, S.; Rasmussen, P. H.; Berg, R. H.; Ramanujam, P. S. *Appl. Phys. Lett.* **1999,** 74, 519-521.
28. Barrett, C. J.; Rochon, P. L.; Natansohn, A. L. *J. Chem. Phys.* **1998,** 109, 1505-1516.
29. Kumar, J.; Li, L.; Jiang, X. L.; Kim, D.-Y.; Lee, T. S.; Tripathy, S. *Appl. Phys. Lett.* **1998,** 72, 2096-2098.

30. Bian, S.; Williams, J. M.; Kim, D. Y.; Li, L.; Balasubramanian, S.; Kumar, J.; Tripathy, S. *J. Appl. Phys.* **1999,** 86, 4498-4508.
31. Lefin, P.; Fiorini, C.; Nunzi, J.-M. *Pure Appl. Opt.* **1998,** 7, 71-82.
32. Lefin, P.; Fiorini, C.; Nunzi, J. M. *Opt. Mater.* **1998,** 9, 323-328.
33. Pedersen, T. G.; Johansen, P. M.; Holme, N. C. R.; Ramanujam, P. S.; Hvilsted, S. *Phys. Rev. Lett.* **1998,** 80, 89-92.
34. Baldus, O.; Leopold, A.; Hagen, R.; Bieringer, T.; Zilker, S. J. *J. Chem. Phys.* **2001,** 114, 1344-1349.
35. Baldus, O.; Zilker, S. J. *Appl. Phys. B* **2001,** 72, 425-427.
36. Bublitz, D.; Fleck, B.; Wenke, L. *Appl. Phys. B* **2001,** 72, 931-936.
37. Gaididei, Y. B.; Christiansen, P. L.; Ramanujam, P. S. *Appl. Phys. B* **2002,** 74, 139-146.
38. Oliveira Jr., O. N.; Kumar, J.; Li, L.; Tripathy, S. K., Surface-relief gratings on azobenzene-containing films. In *Photoreactive Organic Thin Films*, Sekkat, Z.; Knoll, W., Eds. Elsevier Science: 2002; p 560.
39. Saphiannikova, M.; Geue, T. M.; Henneberg, O.; Morawetz, K.; Pietsch, U. *J. Chem. Phys.* **2004,** 120, 4039-4045.
40. Srikhirin, T.; Laschitsch, A.; Neher, D.; Johannsmann, D. *Appl. Phys. Lett.* **2000,** 77, 963-965.
41. Mechau, N.; Neher, D.; Börger, V.; Menzel, H.; Urajama, K. *Appl. Phys. Lett.* **2002,** 81, 4715-4717.
42. Cohen, M. H.; Turnbull, D. *J. Chem. Phys.* **1959,** 31, 1164-1169.
43. Turnbull, D.; Cohen, M. H. *J. Chem. Phys.* **1961,** 34, 120-125.
44. Whitten, D. G.; Chen, L. H.; Geiger, H. C.; Perlstein, J.; Song, X. D. *J. Phys. Chem. B* **1998,** 102, 10098-10111.
45. Kim, B. J.; Park, S. Y.; Choi, D. H. *Bull. Korean Chem. Soc.* **2001,** 22, 271-275.
46. Hoeben, F. J. M.; Jonkheijm, P.; Meijer, E. W.; Schenning, A. P. H. J. *Chem. Rev.* **2005,** 105, 1491-1546.
47. Yu, Y. L.; Nakano, M.; Shishido, A.; Shiono, T.; Ikeda, T. *Chem. Mater.* **2004,** 16, 1637-1643.
48. Hvilsted, S.; Ramanujam, P. S. *Monatshefte für Chemie* **2001,** 132, 43-51.
49. Börger, V. Maßgeschneiderte azobenzolhaltige Polymere für Untersuchungen zum photoinduzierten Massetransport. PhD Thesis, Braunschweig University, Braunschweig, 2004.
50. Freiberg, S.; Lagugne-Labarthet, F.; Rochon, P.; Natansohn, A. *Macromolecules* **2003,** 36, 2680-2688.
51. Mechau, N. Lichtinduziertes Erweichen azobenzolhaltiger Polymerfilme. PhD Thesis, Potsdam University, Potsdam, 2005.
52. Galvan-Gonzalez, A.; Belfield, K. D.; Stegeman, G. I.; Canva, M.; Chan, K.-P.; Park, K.; Sukhomlinova, L.; Twieg, R. J. *Appl. Phys. Lett.* **2000,** 77, 2083-2085.
53. Srikhirin, T.; Cimrova, V.; Schiewe, B.; Tzolov, M.; Hagen, R.; Kostromine, S.; Bieringer, T.; Neher, D. *Chem. Phys. Chem.* **2002,** 3, 335-342.
54. Geue, T.; Schultz, M.; Grenzer, J.; Pietsch, U.; Natansohn, A.; Rochon, P. *J. Appl. Phys.* **2000,** 87, 7712-7719.
55. Pietsch, U.; Rochon, P.; Natansohn, A. *Adv. Mater.* **2000,** 12, 1129-1132.
56. Börger, V.; Menzel, H.; Huber, M. R. *Mol. Cryst. Liq. Cryst.* **2005,** 430, 89-97.
57. Fukuda, T.; Matsuda, H.; Shiraga, T.; Kimura, T.; Kato, M.; Viswanathan, N. K.; Kumar, J.; Tripathy, S. K. *Macromolecules* **2000,** 33, 4220-4225.

58. Andruzzi, L.; Altomare, A.; Ciardelli, F.; Solaro, R.; Hvilsted, S.; Ramanujam, P. S. *Macromolecules* **1999,** 32, 448-454.
59. Yager, K. G.; Barrett, C. J. *J. Chem. Phys.* **2004,** 120, 1089-1096.
60. Bellini, B.; Ackermann, J.; Klein, H.; Grave, C.; Dumas, P.; Safarov, V. *J. Phys.:Condens. Matter* **2006,** 18, 1817-1835.
61. Geue, T. Lichtinduzierte Eigenschaftsänderungen in ultradünnen organischen Filmsystemen. PhD thesis, Humboldt University, Berlin, 1995.
62. Geue, T.; Ziegler, A.; Stumpe, J. *Macromolecules* **1997,** 30, 5729-5738.
63. Jung, C. C.; Rosenhauer, R.; Rutloh, M.; Kempe, C.; Stumpe, J. *Macromolecules* **2005,** 38, 4324-4330.
64. Kulinna, C.; Hvilsted, S.; Hendann, C.; Siesler, H. W.; Ramanujam, P. S. *Macromolecules* **1998,** 31, 2141-2151.
65. Yaroschuk, O.; Sergan, T.; Lindau, J.; Lee, S. N.; Kelly, J.; Chien, L. C. *J. Chem. Phys.* **2001,** 114, 5330-5337.
66. Sekkat, Z.; Dumont, M. *Synth. Met.* **1993,** 54, 373-381.
67. Dumont, M.; Osman, A. E. *Chem.Phys.* **1999,** 245, 437-462.
68. Saphiannikova, M.; Radtchenko, I.; Sukhorukov, G.; Shchukin, D.; Yakimansky, A.; Ilnytskyi, J. *J. Chem. Phys.* **2003,** 118, 9007-9014.
69. Buffeteau, T.; Lagugne-Labarthet, F.; Pezolet, M.; Sourisseau, C. *Macromolecules* **2001,** 34, 7514-7521.
70. Saphiannikova, M.; Neher, D. *J. Phys. Chem. B* **2005,** 109, 19428-19436.
71. Onsager, L. *Ann. NY Acad. Sci.* **1949,** 51, 627-659.
72. de Gennes, P. G.; Prost, J., *The Physics of Liquid Crystals*. 2nd ed.; Clarendon press: Oxford, 1995; p 597.
73. Mechau, N.; Saphiannikova, M.; Neher, D. *Macromolecules* **2005,** 38, 3894-3902.
74. Saphiannikova, M.; Henneberg, O.; Geue, T. M.; Pietsch, U.; Rochon, P. *J. Phys. Chem. B* **2004,** 108, 15084-15089.
75. Barrett, C.; Natansohn, A.; Rochon, P. *Chem. Mater.* **1995,** 7, 899-903.
76. Ramanujam, P. S.; Hvilsted, S.; Zebger, I.; Siesler, H. W. *Macromol. Rapid Commun.* **1995,** 16, 455-461.
77. Strobl, G. R., *The physics of polymers*. 2nd ed.; Springer: Berlin, 1995.
78. Cicerone, M. T.; Blackburn, F. R.; Ediger, M. D. *Macromolecules* **1995,** 28, 8224-8232.
79. Tseng, K. C.; Turro, N. J.; During, C. J. *Polymer* **2000,** 41, 4751-4755.
80. van Keuren, E.; Schrof, W. *Macromolecules* **2003,** 36, 5002-5007.
81. Winkelhahn, H. J.; Pakula, T.; Neher, D. *Macromolecules* **1996,** 29, 6865-6871.
82. Landau, L. D.; Lifshitz, E. M., *Theory of Elasticity*. 2 ed.; Elsevier Science Ltd.: 1981; p 176.
83. Ferry, J. D., *Viscoelastic Properties of Polymers*. John Wiley & Sons: New York, 1980.
84. McCrum, N. G.; Read, B. E.; Williams, G., *Anelastic and Dielectric Effects in Polymeric Solids*. Dover Publications, Inc. New York: 1967.
85. Saphiannikova, M. G.; Lukasheva, N. V.; Darinskii, A. A.; Gotlib, Y. Y.; Brickmann, J. *Macromolecules* **2000,** 33, 606-612.
86. Fritz, A., *Korrelation optischer und dielektrischer Untersuchungen an photochromen Copolymeren mit Azobenzolderivaten in der Seitengruppe*. Mensch & Buch Verlag: Berlin, 2000; p 150.
87. Fritz, A.; Schönhals, A.; Sapich, B.; Stumpe, J. *Macromol. Chem. Phys.* **1999,** 200, 2213-2220.

88. Schieferdecker, H. Bestimmung der Adhäsionseigenschaften von Oberflächen mit dem Rasterkraftmikroskop. Diplomarbeit, Ulm University, Ulm, 1999.
89. Friedbacher, G.; Fuchs, H. *Angew. Chem.* **2003,** 115, 5804-5820.
90. Stiller, B.; Mechau, N.; Saphiannikova, M.; Neher, D. *Poster presented at the 69. Jahrestagung der DPG* **4-9 March 2005**, 124-124.
91. Morawetz, K.; Stiller, B.; Ilnytskyi, J.; Neher, D.; Katholy, S.; Ries, R.; Richter, A. *Europhys. Conf. Abst.* **2006,** 30A, 111-111.
92. Yager, K. G.; Barrett, C. J. *Macromolecules* **2006,** 39, 9320-9326.
93. Sperling, L. H., *Introduction to Physical Polymer Science*. Third Edition ed.; Wiley-Interscience: 2001.
94. Gimenez, R.; Millaruelo, M.; Pinol, M.; J.L., S.; A., V.; R., R.; T., F.; Stumpe, J. *Polymer* **2005,** 46, 9230-9242.
95. Neogie, P., *Diffusion in Polymers*. Dekker, New York: 1996.
96. Karageorgiev, P.; Neher, D.; Schulz, B.; Stiller, B.; Pietsch, U.; Giersig, M.; Brehmer, L. *Nature Mater.* **2005,** 4, 699-703.
97. Ivanov, M.; Todorov, T.; Nikolova, L.; Tomova, N.; Dragostinova, V. *Appl. Phys. Lett.* **1995,** 66, 2174-2176.
98. Fleck, B.; Dowling, D. A.; Wenke, L. *J. Mod. Opt.* **1996,** 43, 1485-1493.
99. Ramanujam, P. S.; Holme, N. C. R.; Hvilsted, S. *Appl. Phys. Lett.* **1996,** 68, 1329-1331.
100. Holme, N. C. R.; Nikolova, L.; Ramanujam, P. S.; Hvilsted, S. *Appl. Phys. Lett.* **1997,** 70, 1518-1520.
101. Henneberg, O.; Panzner, T.; Pietsch, U.; Geue, T.; Saphiannikova, M.; Rochon, P.; Finkelstein, K. *Z. Kristallogr.* **2004,** 219, 218-223.
102. Lagugne-Labarthet, F.; Buffeteau, T.; Sourisseau, C. *J. Phys. Chem. B* **1999,** 103, 6690-6699.
103. Lagugne-Labarthet, F.; Buffeteau, T.; Sourisseau, C. *Appl. Phys. B* **2002,** 74, 129-137.
104. Sumaru, K.; Yamanaka, T.; Fukuda, T.; Matsuda, H. *Appl. Phys. Lett.* **1999,** 75, 1878-1880.
105. Geue, T. M.; Saphiannikova, M. G.; Henneberg, O.; Pietsch, U.; Rochon, P. L.; Natansohn, A. L. *Phys. Rev. E* **2002,** 65, 052801,1-4.
106. Lagugne-Labarthet, F.; Buffeteau, T.; Sourisseau, C. *J. Phys. Chem. B* **1998,** 102, 2654-2662.
107. Henneberg, O.; Geue, T.; Saphiannikova, M.; Pietsch, U.; Rochon, P.; Natansohn, A. *Appl. Surf. Sci.* **2001,** 182, 272-279.
108. Janssen, P. R. M.; van Breemen, L. C. A.; Pelletier, C. P. In 13th International conference on deformation, yield and of polymers, Rolduc Abbey, Kerkrade, the Netherlands, 2006; Rolduc Abbey, Kerkrade, the Netherlands, 2006.
109. Göldner, H., *Höhere Festigkeitslehre*. 1992; Vol. 2.
110. Bird, R. B.; Curtiss, C.; Armstrong, R. C.; Hassager, O., *Dynamics of polymeric liquids*. Wiley-Interscience: New York, 1987.
111. Doi, M.; Edwards, S. F., *The Theory of Polymer Dynamics*. Clarendon Press: Oxford, 1986.
112. Boyd, R. H.; Phillips, P. J., *The Science of Polymer Molecules*. University Press: Cambridge, 1993.
113. Sane, S. B.; Knauss, W. G. *Mech. Time-Depend. Mater.* **2001,** 5, 325-343.
114. Ikawa, T.; Mitsuoka, T.; Hasegawa, M.; Tsuchimori, M.; Watanabe, O.; Kawata, Y.; Egami, C.; Sugihara, O.; Okamoto, N. *J. Phys. Chem. B* **2000,** 104, 9055-9058.

115. Keum, C.-D.; Ikawa, T.; Tsuchimori, M.; Watanabe, O. *Macromolecules* **2003,** 36, 4916-4923.
116. Lagugne-Labarthet, F.; Sourisseau, C.; Schaller, R. D.; Saykally, R. J.; Rochon, P. *J. Phys. Chem. B* **2004,** 108, 17509-17608.
117. Pietsch, U.; Rochon, P. *J. Appl. Phys.* **2003,** 94, 963-967.
118. Stiller, B.; Karageorgiev, P.; Geue, T.; Morawetz, K.; Saphiannikova, M.; Mechau, N.; Neher, D. *Phys. Low - Dim. Struct.* **2004,** 1/2, 129-138.
119. Henneberg, O.; Geue, T.; Saphiannikova, M.; Pietsch, U.; Chi, L. F.; Rochon, P.; Natansohn, A. L. *Appl. Phys. Lett.* **2001,** 79, 2357-2359.
120. Pietsch, U. *Phys. Rev. B* **2002,** 66, 155430, 1-9.
121. Maier, W.; Saupe, A. *Z. Naturforsch.* **1959,** 14, 882-889.
122. Küpfer, J.; Finkelmann, H. *Macromol. Chem., Rapid Commun.* **1991,** 12, 717-726.
123. Wermter, H.; Finkelmann, H. *e-Polymers* **2001,** 13, 1-13.
124. Clarke, S. M.; Hotta, A.; Tajbakhsh, A. R.; Terentjev, E. M. *Phys. Rev. E.* **2001,** 64, 061702.
125. Tajbakhsh, A. R.; Terentjev, E. M. *Eur. Phys. J. E* **2001,** 6, 181-188.
126. Warner, M.; Terentjev, E. M. *Prog. Polym. Sci.* **1996,** 21, 853-891.
127. de Gennes, P. G.; Hebert, M.; Kant, R. *Macromol. Symp.* **1997,** 113, 39-49.
128. Warner, M.; Terentjev, E. M., *Liquid Crystal Elastomers*. Clarendon: Oxford, 2003.
129. Sung, J.-H.; Hirano, S.; Tsutsumi, O.; Kanazawa, A.; Shiono, T.; Ikeda, T. *Chem. Mater.* **2002,** 2002, 385-391.
130. Henneberg, O. In-situ Untersuchungen zur Entstehung von Oberflächengittern in Polymeren. PhD thesis, Potsdam University, Potsdam, 2004.
131. Lagugne-Labarthet, F.; Bruneel, J. L.; Rodriguez, V.; Sourisseau, C. *J.Phys. Chem. B* **2004,** 108, 1267-1278.
132. Lagugne-Labarthet, F.; Buffeteau, T.; Sourisseau, C. *J.Phys. Chem. B* **1998,** 102, 5754-5765.
133. Lagugne-Labarthet, F.; Buffeteau, T.; Sourisseau, C. *Macromol. Symp.* **1999,** 137, 75-82.
134. Lagugne-Labarthet, F.; Buffeteau, T.; Sourisseau, C. *J. Phys. Chem. B* **1999,** 103, 6690.
135. Jiang, X. L.; Kumar, J.; Kim, D. Y.; Shivshankar, V.; Tripathy, S. K. *Appl. Phys. Lett.* **1996,** 68, 2618-2620.
136. Berry, B. S.; Pritchet, W. C. *IBM J. Res. Develop.* **1984,** 28, 662-667.
137. Heermann, D. W., *Computer Simulation Methods in Theoretical Physics*. Springer: Berlin Heidelberg New York, 1990.
138. Rubinstein, M.; Colby, R. H., *Polymer Physics*. Oxford University Press: Oxford, 2003.
139. Fuhrmann, T.; Kunze, M.; Wendorff, J. H. *Macromol. Theory Simul.* **1998,** 7, 421-429.
140. Ilnytskyi, J.; Wilson, M. R. *Comput. Phys. Commun.* **2001,** 134, 23-32.
141. Ilnytskyi, J.; Wilson, M. R. *Comput. Phys. Commun.* **2002,** 148, 43-58.
142. Gay, J. G.; Berne, B. J. *J. Chem. Phys.* **1981,** 74, 3316-3319.
143. Kwok, H.-S.; Chigrinov, V. G.; Takada, H.; Takatsu, H. *IEEE/OSA J. Display Technology* **2005,** 1, 41-50.
144. Ilnytskyi, J.; Saphiannikova, M.; Neher, D. *Cond. Matter Phys.* **2006,** 9, 87-94.
145. Fuhrmann, T.; Tsutsui, T. *Chem. Mater.* **1999,** 11, 2226-2232.

Appendix

The following articles represent considerable contribution to the field of photoinduced material transport in amorphous azobenzene polymers:

T.M. Geue, M.G. Saphiannikova, O. Henneberg, U. Pietsch, P.L. Rochon and A.L. Natansohn. *Formation mechanism and dynamics in polymer surface gratings.* Phys. Rev. E 65, 052801/1-052801/4 (2002)

M. Saphiannikova, I. Radtchenko, G. Sukhorukov, D. Shchukin, A. Yakimansky and J. Illnytskyi. *Molecular-dynamics simulations and x-ray analysis of dye precipitates in the polyelectrolyte microcapsules.* J. Chem. Phys. 118, 9007-9014 (2003)

M. Saphiannikova, T.M. Geue, O. Henneberg, K. Morawetz and U. Pietsch. *Linear viscoelastic analysis of formation and relaxation of azobenzene polymer gratings.* J. Chem. Phys. 120, 4039-4045 (2004)

M. Saphiannikova, O. Henneberg , T.M. Geue, U. Pietsch and P. Rochon. *Nonlinear effects during inscription of azobenzene surface relief gratings.* J. Phys. Chem. B. 108, 15084-15089 (2004)

N. Mechau, M. Saphiannikova and D. Neher. *Dielectric and mechanical properties of azobenzene polymer layers under visual and ultraviolet irradiation.* Macromolecules 38, 3894-3902 (2005).

B. Stiller, T. Geue, K. Morawetz and M. Saphiannikova. *Optical patterning in azobenzene polymer films.* Journal of Microscopy 219, 109-114 (2005)

M. Saphiannikova and D. Neher. *Thermodynamic theory of light-induced material transport in amorphous azobenzene polymer films***.** J. Phys. Chem. B. 109, 19428-19436 (2005)

J. Ilnytskyi, M. Saphiannikova and D. Neher. *Photo-induced deformations in azobenzene-containing side-chain polymers: molecular dynamics study.* Condensed Matter Physics 9, 87-94 (2006).

N. Mechau, M. Saphiannikova and D. Neher. *Molecular tracer diffusion in thin azobenzene polymer layers.* Appl. Phys. Lett. 89, 251902/1-251902/3 (2006).

Formation mechanism and dynamics in polymer surface gratings

T. M. Geue, M. G. Saphiannikova, O. Henneberg, and U. Pietsch
Institute of Physics, University of Potsdam, P.O.B. 601553, Potsdam, D-14415 Germany

P. L. Rochon
Department of Physics, Royal Military College, Kingston, Ontario, Canada K7K 5L0

A. L. Natansohn
Department of Chemistry, Queen's University, Kingston, Ontario, Canada K7L 3N6

(Received 10 October 2001; published 8 May 2002)

We present the results of time-dependent x-ray and visible light (VIS) scattering measurements during formation of surface relief grating (SRG). These gratings are formed on polymer films containing azobenzene side groups during pulselike exposure with a holographic pattern of circularly polarized light at 488 nm. The SRG formation is accompanied by a density grating just below the film surface. Assuming viscoelastic flow, a change in polymer's elastic properties upon light exposure can explain the massive material transport. Finite element calculations reveal a dynamic model of grating formation characterized by different relaxation times. The simultaneous formation of a surface relief grating and of a density grating explains quantitatively the findings of the VIS experiment, but only qualitatively the findings of the x-ray measurements.

DOI: 10.1103/PhysRevE.65.052801 PACS number(s): 61.41.+e, 61.10.Kw, 68.35.Rh, 68.65.−k

It is well known that a surface relief pattern can be inscribed on polymer films containing azobenzene moieties [1–5]. This is done by exposing the sample to a periodic polarization pattern obtained when two contracircularly polarized light beams interfere. The absorption of this light induces material flow even at temperatures as low as 100 K below the glass transition temperature T_g of the polymers. The resultant surface relief has an approximately sinusoidal cross section. Depending on the power of illumination and on the state of light polarization, the grating depths may approach several hundreds of nanometers. A number of mechanisms had been proposed to explain the massive material displacement [6–8] but they do not describe the dynamics of surface relief grating (SRG) formation. Bian *et al.* and Kumar *et al.* [9,10] developed an optical gradient field force model for low-laser powers to describe the surface deformations during SRG formation. Unfortunately, this model is not able to describe the changes in the very initial stages of SRG development as well as all findings from x-ray investigations [11,12]. Thus, it is of particular interest to learn more about the nature of this light-induced material transport in polymers. In a previous experiment, we have shown that simultaneous probe by x-ray and visible light (VIS) can give additional information because these methods probe the sample at different length scales [11]. Both methods are now applied to study the time development of the grating formation process.

The sample investigated is a side-chain azobenzene polymer, poly{(4-nitrophenyl)[4-{[2-(methacryloyl-oxy)-ethyl]ethylamino}phenyl]diazene} (pDR1M), which has a glass transition temperature of $T_g = 129\,^{\circ}\mathrm{C}$ [3,11]. A 400 nm thick film was deposited on a glass substrate by spin coating. Surface relief gratings with a period of $D \approx 1000$ nm were inscribed onto the polymer films using the interference pattern of two plane waves produced by counter-circularly polarized beams obtained from an argon-ion laser with a power density of 50 mW/cm^2. The x-ray experiments were performed at CHESS (Cornell University Ithaca, N.Y; $\lambda = 0.1238$ nm) using an incidence angle $\alpha_i = 0.5°$ with respect to the average surface and a charge-coupled device (CCD) camera (ADSC Quantum CCD, 1152×1152 pixels) as a two-dimensional detector. In addition, normal incidence laser scattering ($\lambda = 633$ nm) was performed at RMC Kingston using the same setup. *Ex situ* AFM inspection of several sample surfaces after short-time exposure has been performed using a Nanoscope IIIa (Digital Instruments) in tapping mode [12].

Figure 1 shows the time development of the first-order x-ray grating peak during the pulse-like exposure with blue light. It was detected simultaneously with the specular reflection and higher-order grating peaks (see inset) after exposure to a series of 5, 10, 15, and 60 s pulses. Each pulse was

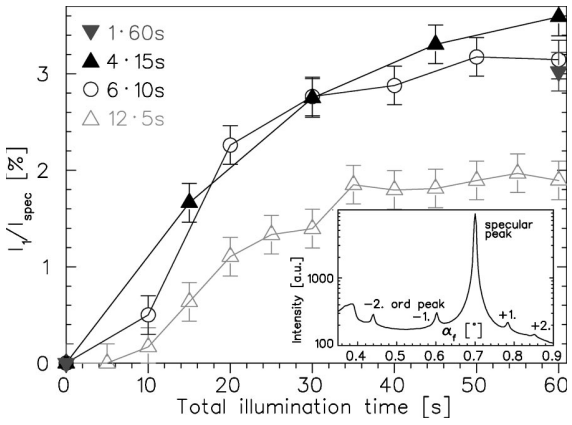

FIG. 1. Development of first-order x-ray grating peak intensity after exposure during 5, 10, 15, and 60 s with a holographic light pattern at 488 nm. The inset shows a line scan through the CCD frame.

followed by a 60 s delay in the dark and then the CCD was exposed to the x-ray signal for 30 s, the readout took 10 s. The peak intensity initially increases after each laser pulse and finally saturates. As clearly seen in Fig. 1, the maximum intensity, I_{x-max}, depends on the pulse length. For the same total exposure time, the series of 10, 15, and 60 s pulses approach almost equal $I_{x-max} \approx 3\%$, whereas the 5 s pulses gave much lower efficiency (2%) of the grating formation. Obviously, the 5 s is below a critical time of the formation process at the chosen illumination power. Unfortunately, we could not determine the critical time more precisely, as the time resolution of the x-ray experiment was limited.

Therefore, further experiments were performed outside the x-ray beamline using the VIS scattering only. The time resolution in this case was of the order of 1s. The samples were exposed to the blue light every 60 s with pulses of 5, 10, 15, and 60 s and held in the dark in between. Unlike in the x-ray experiment, the intensity of the first-order grating peak was detected continuously. A multistep development mechanism was observed and consisted of at least three different processes. (1) A very fast increase of the grating intensity in the beginning ($t<1$s); (2) A further increase at a rate that is up to 20 times smaller than the first one (Fig. 2); (3) An exponential decay of the intensity in the absence of illumination, indicating partial relaxation of the polymer. The remnant grating intensity also depends on the pulse duration. The first steep slope is the same for all pulse lengths and can be associated with an elastic process. Pulses shorter than about 1 s do not produce a grating [12]. Only the second inelastic process produces a permanent grating and its diffraction efficiency depends on the duration of the process. This qualitatively explains the findings of the x-ray measurements during the relaxation process.

Let us introduce a model that, we believe, describes the findings of coherent light scattering as well as the x-ray reflectivity data. We consider a two-dimensional problem with the x axis chosen to be parallel and the z axis perpendicular to the polymer surface, $z=0$ corresponds to the "polymer-substrate" interface. We assume that the holographic light pattern initiates trans-cis and cis-trans isomerizations of the azobenzene moieties and that this produces a periodic lateral force parallel to the sample surface. The model utilizes a sinusoidal force f_x varying in the x direction [5,9,14]. In keeping with the Lambert-Beer law, the force f_x decays exponentially with the distance from the film surface z

$$f = A \exp\left[\frac{z-[h(x)+h_0]}{\mu}\sin\left(\frac{2\pi x}{D}\right)\right], \tag{1}$$

where A is the force density, $h(x)$ is the surface relief grating, h_0 is the initial film thickness, μ is the light penetration depth, and D is the grating period. We apply the force in a self-consistent manner starting from $h(x)=0$.

In the present paper, we describe the polymer as an isotropic viscoelastic (VE) material. A simple linear VE approach with time-dependent shear modulus G was found to be sufficient to mimic the multiple inscriptions of gratings

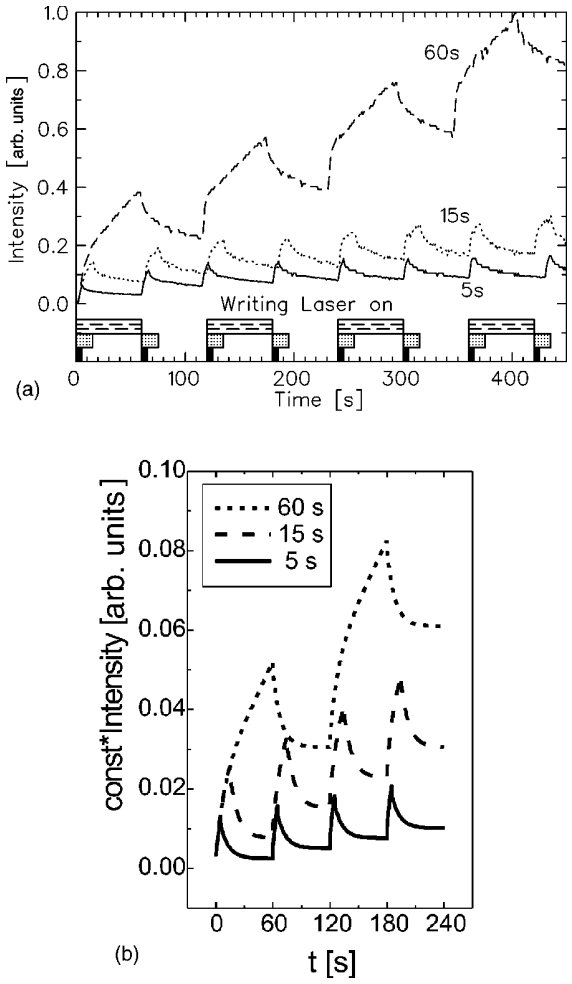

FIG. 2. Time development of the first-order VIS grating peak intensity during short pulse exposure: measurement (a), simulation (b).

$$G(t) = \sum_{k=1}^{N} G_k \exp\left(\frac{-t}{\tau_k}\right) \quad \text{and} \quad G_0 = G(0) = \frac{E}{2(1+\nu)} \tag{2}$$

where E is Young's modulus, ν is the Poisson's ratio, and τ_k are particular relaxation times of the system. As the key point of our paper, we assume that due to the photoinduced cis-trans isomerization of azobenzene chromophores, the polymer film undergoes considerable plasticization, which reduces its original Young's modulus by at least three orders of magnitude. Thus, the value of Young's modulus falls into the range for a polymer around its glass transition temperature.

A finite element modeling (FEM) can reproduce the development of the surface profile, density distribution, and the ensuing scattering signal. A cleavage plane (x,z plane, $h_0 = D = 1$ μm) was calculated using the commercial software Mentat 3.2.0. The area was divided into 2500 square finite elements. Periodic boundary conditions were applied along the x direction. As a constraint, no displacement of sample was allowed at the polymer substrate interface.

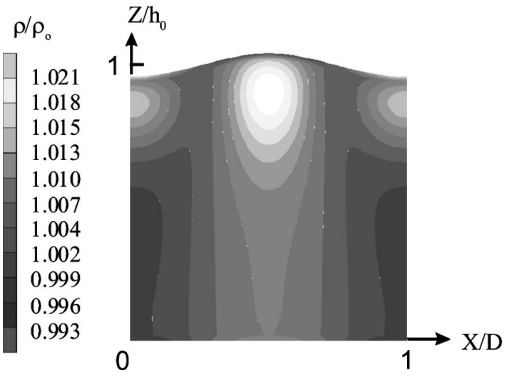

FIG. 3. FEM of the grating formation after continuous exposure of 90 s.

Figure 3 shows the results of the FEM for a constant load of $A=100$ N/cm^3 and using the following material parameters: initial density $\rho_0=10^3$ kg/m^3, $E=1$ MPa, $\nu=0.40$, $G_1=0.9G_0$, $G_2=0.1G_0$, $\tau_1=2$ s, $\tau_2=50$ s. Already the use of two different shear moduli and time constants produces not only a sinusoidal relief at the surface, but a periodic density difference below the surface as well.

The application of a constant load produces an instantaneous elastic deformation followed by a continuous deformation with time (delayed elastic and viscous effects). In contrast to [7], the observed SRG formation appears to be not only a ''surface initiated'' process. The surface relief grating, as well as the lateral density variation below the surface, appears from the very beginning of the force application (instantaneous effect). During the first seconds of illumination, both profiles can be described by sinusoidal functions of equal period D (see Fig. 4). The polymer material is slightly compressed at the region of surface relief peaks and slightly expanded in between. As time increases this compressed region extends toward the substrate. At the same time the polymer material in the region of relief troughs (see Fig. 3) becomes compressed but this compressed region remains concentrated close to the surface. These results were obtained for $\mu=h_0=1.0$ μm, which means that the light penetrates down to the substrate. When the penetration depth is decreased, the amplitude of the surface relief also decreases. For sufficiently small μ ($\mu=0.1$ μm) the relief height reaches about 20 nm after 2 min of illumination and is accompanied with a plastification of 2 and 1% at the ridge and valley regions, respectively. The height is similar to the value measured by AFM.

To simulate a transient behavior we applied a cyclic external force in the same manner as was done in the VIS experiment. Generally, VIS probes the grating formation via phase contrast, described by Bessel functions

$$I_{\mathrm{VIS}}=I_0\left|\sum_i J_m[\phi_i(t)]\right|^2, \quad \phi_i(t)=\frac{2\pi}{\lambda_{VIS}}(\Delta n\Delta d), \quad (3)$$

and depends on total index of refraction which includes density-induced difference Δn and on the relief height Δd index m is the grating order. Since Δd does not exceed 2% [see Fig. 3(b)] the scattered light intensity is a measure of the

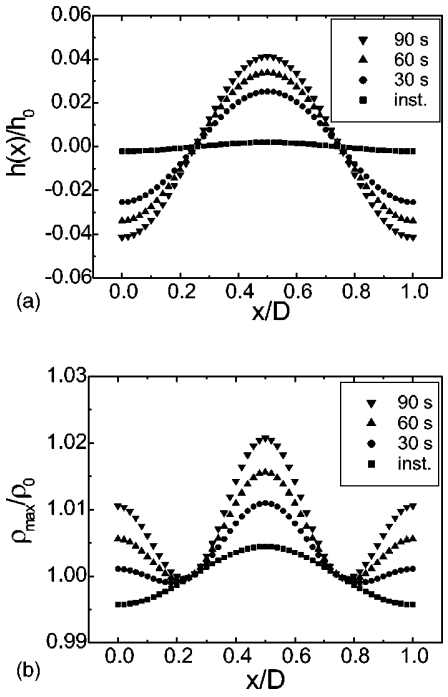

FIG. 4. Time development of the surface relief grating, $h(x)$, (a) and the density modulation, $r(x)$, (b) obtained by FEM just in the beginning and after 30, 60, and 90 s of light exposure.

relief amplitude. The FE simulation does match the right functional behavior as found by the VIS experiment [Fig. 2(a)].

In principle, the FE program cannot describe processes if one of the relaxation times is considerably smaller than an optimal time step chosen to cover the time scale of the experiment. Therefore, we developed an analytical solution for the one-dimensional transient problem with three relaxation times. As shown in Fig. 2(b), the elastic and inelastic response of the material is well described. The first cycle of exposure could be mostly fitted with the following material parameters: $G_0=1$ GPa, $G_1=0.999G_0$, $G_2=0.0008G_0$, $G_3=0.0002G_0$, $\tau_1=0.002$ s, $\tau_2=2$ s, and $\tau_3=50$ s. It means that after switching on the laser light the shear modulus falls from 1 GPa to 1 MPa within 0.002 s. Then, G_0 gradually decreases from cycle to cycle until reaching a saturation at about 0.5 GPa.

This result shows that further plastification takes place during the following light pulses, in spite of the transient nature of the applied force. Also, we found that τ_2 and τ_3 increase from cycle to cycle, reaching 5 and 400 s, correspondingly. This may be an indication of gradual unfreezing of cooperative motions of polymer molecules in the film, i.e., the addressing of an increased number of azobenzene side groups by the light.

The latter hypothesis is supported by *ex situ* AFM inspections performed after single short pulse inscription [12]. Up to an exposure time of 2 s there is no surface relief formation at all. The material response is entirely elastic. After 5 s of illumination, a speckled surface modification starts rising with an average height of 13 nm. Longer exposure time will

saturate the relief height at about 22 nm, and the surface relief becomes rather uniform. This may be explained by the larger number of cis-trans photoisomerizations taking place at the material modification. Here again, some sort of "critical time constant" plays an important part in the process, but these times should strongly depend on the extent of isomerization, i.e., the illumination power.

Our simulation results also explain the x-ray results shown in Fig. 1. Assuming sinusoidal modulation, the time dependence of the intensity of the mth-order scattering grating peak is proportional to the square of the induced density difference $\Delta\delta$ parallel and perpendicular to the average sample surface [13]

$$I^m_{x\text{-}ray}(q_x,q_z,t) \approx I_0 \left| \int \int \Delta\delta(x,z,t) \sin\left(\frac{2\pi m}{\lambda} x\right) \times \exp\{-i(q_x x + q_z z)\} dx\, dz \right|^2 . \quad (4)$$

I^m x-ray is expressed in terms of the reciprocal space coordinates $q_z = 2\pi/\lambda(\alpha_i + \alpha_f)$ and $q_x = \pi/\lambda(\alpha_i^2 - \alpha_f^2)$. The x-ray experiment probes the density differences between surface relief and air as well as the light-induced density differences below the sample surface. Considering the time regime used for measurement, the x-ray grating intensity always represents the accumulated plasticization induced by each light pulse. Using Figs. 3 and 2(b) we can qualitatively understand why 5 s exposure gives much lower intensity compared with those given by longer pulses. If the elastic regime takes the first 2–4 s, the induced plasticization is small at 5 s but larger for longer pulses. Unfortunately, our model does not reproduce the saturation of intensity observed in Fig. 1. The Fourier transform of FEM pictures calculated for subsequent time steps always shows increasing intensity. Taking the surface tension into account the saturation of intensity might be expected due to the saturation of the surface profile growth.

In summary, the time-resolved x-ray and VIS scattering experiments can be explained by the simultaneous formation of a density grating below the film surface and a surface relief grating on top of the film. This obviously proves that the SRG formation is not solely a surface controlled process. Using the viscoelastic flow model we can understand that the response of the polymer material to the light-induced lateral force is entirely elastic during the first 2–4 s but plasticization takes place later on. The key assumption of our model is the light-induced reduction of the shear modulus during exposure down to values typical for polymers close to their glass transition temperatures.

Our experiments have been performed at low-laser power and on one azobenzene polymer material. To understand how high-laser powers, as well as changes in the material structure affect the formation of gratings, further experiments have to be performed and the modeling has to be improved as well. Several more experiments are under way to clarify the origin of the lateral force causing the material transport, which is still an unsolved question.

This work was supported by the DFG under Grant Nos. Pi217/17-1 and 436RUS17/18/01. M.S. acknowledges support from The Russian Foundation for Fundamental Research (Grant No. 99-03-33314). The authors thank CHESS for allocating beam time and K. Finkelstein for supporting the x-ray experiment.

[1] P. Rochon, E. Batalla, and A. Natansohn, Appl. Phys. Lett. **66**, 136 (1995).

[2] D. Y. Kim, S. K. Tripathy, L. Li, and J. Kumar, Appl. Phys. Lett. **66**, 1166 (1995).

[3] C. J. Barrett, A. L. Natansohn, and P. L. Rochon, J. Phys. Chem. **100**, 8836 (1996).

[4] D. Y. Kim, T. S. Lee, X. Wang, X. L. Jiang, L. Li, J. Kumar, and S. K. Tripathy, Proc. SPIE **195**, 2298 (1995).

[5] C. L. Barrett, P. L. Rochon, and A. L. Natansohn, J. Chem. Phys. **109**, 1505 (1998).

[6] T. G. Pedersen, P. M. Johansen, N. C. R. Holme, P. S. Ramanujam, and S. Hvilsted, Phys. Rev. Lett. **80**, 89 (1998).

[7] N. K. Viswanathan, S. Balasubramanian, L. Li, J. Kumar, and S. K. Tripathy, J. Phys. Chem. **B102**, 6064 (1998).

[8] P. Lefin, C. Fiorini, and J.-M. Nunzi, Pure Appl. Opt. **7**, 71 (1998).

[9] S. Bian, L. Li, J. Kumar, D. Y. Kim, J. Williams, and S. K. Tripathy, Appl. Phys. Lett. **73**, 1817 (1998).

[10] J. Kumar, L. Li, X. L. Jiang, D.-Y. Kim, T. S. Lee, and S. K. Tripathy, Appl. Phys. Lett. **72**(17), 2096 (1998).

[11] Th. Geue, M. Schultz, J. Grenzer, U. Pietsch, A. Natansohn, and P. Rochon, J. Appl. Phys. **87**(11), 7712 (2000).

[12] O. Henneberg, Th. Gene, M. Saphiannikova, U. Pietsch, P. Rochon, and A. Natansohn, Appl. Surf. Sci. (to be published).

[13] V. Holy, U. Pietsch, and T. Baumbach, *High Resolution X-Ray Scattering from Thin Films and Multilayers*, Springer Tracts in Modern Physics Vol. 149 (Springer, Berlin, 1999).

[14] K. Sumaru, T. Yamanaka, T. Fukuda, and H. Matsuda, Appl. Phys. Lett. **75**, 1878 (1999).

Molecular-dynamics simulations and x-ray analysis of dye precipitates in the polyelectrolyte microcapsules

Marina Saphiannikova,[a] Igor Radtchenko, and Gleb Sukhorukov
Max Planck Institute of Colloid and Interfaces, 14424 Potsdam/Golm, Germany

Dmitri Shchukin
Institute for Physico-Chemical Problems, 220054 Minsk, Belarus

Alexander Yakimansky
Institute of Macromolecular Compounds of Russian Academy Sciences, Bolshoi pr. 31, 199004 St. Petersburg, Russia

Jaroslav Ilnytskyi
University of Durham, DH1 3HP Durham, United Kingdom

(Received 18 October 2002; accepted 19 February 2003)

The precipitate of the Disperse Red-1 dye in bulk and in confined microsized volumes was investigated by x-ray powder diffraction and molecular-dynamics simulations. The diffraction patterns exhibited two different precipitation regimes: In bulk when dye molecules form a distinct crystallite structure and inside polyelectrolyte capsules with a diameter up to 8 μm when the precipitate presumably represents a very fine polycrystalline powder. The latter result was further supported by molecular-dynamics simulations carried out for up to 640 dye molecules in the NVT ensemble. Calculations have also shown that effects of confined geometry and steric restrictions arising due to encapsulated polyelectrolyte molecules can not prohibit dye nucleation and subsequent crystallization. However, nonspecific interactions between Disperse Red-1 and encapsulated polyelectrolyte could cause the onset of heterogeneous nucleation resulting in formation of a fine polycrystalline powder. The formation process was directly observed building configuration snapshots and calculating the Gay–Berne orientational order parameter and radial distribution function resolved parallel and perpendicular to the director. Comparison of powder diagrams derived from simulation data indicates that it is nearly impossible to distinguish a fine polycrystalline powder from the isotropic system. © *2003 American Institute of Physics.*
[DOI: 10.1063/1.1566732]

I. INTRODUCTION

The development of functional colloidal particles gains interest in different areas such as biosensing, catalysis, biotechnology, medicine, ecology, and others. A novel approach to fabricate micro- and nanocapsules has been recently introduced. The method consists in layer-by-layer adsorption[1] of oppositely charged macromolecules onto colloidal particles.[2,3] Different templates with size ranged from 50 nm to tens of microns, such as organic and inorganic colloid particles, protein aggregates, emulsion droplets, biological cells and drug nanocrystals can be coated by multilayer film. Various materials have been used as layer constituents to fabricate the shell (for review see Ref. 4). The possibility to use various materials as layer constituents to fabricate the shell makes it possible to design the capsules with required stability, biocompatibility, and affinity properties. Some colloidal templates can be decomposed at conditions where the polymer shell is stable, what leads to the formation of hollow capsules. The permeability through the capsule wall and release of the encapsulated materials depend on the shell wall thickness and composition and can be regulated afterwards by pH, ionic strength, or solvent exchange.[5–7] The hollow capsules can be used as templates for the controlled precipitation of dyes from bulk solution.[8]

The presence of polyelectrolyte only on one side of the capsule wall leads to establish a polarity or pH-gradient across the capsule wall.[9,10] As described in Ref. 11 the presence of hydrophilic polymers inside the capsules shifts the polarity toward aqueous media in a water–aceton mixture. It has been utilized for precipitation of dyes with solvent dependent solubility in the capsule interior. A similar effect have been observed for pH-dependent dye precipitation.[4] Small molecules (dyes, drugs) can permeate into the restricted volume of capsule and precipitate inside due to low solubility. The crystalline structure of precipitates is one of the important features of precipitating dyes. It is formed in a confined geometry and can differ from that formed in the bulk, which opens up new possibilities to design chromophores for nonlinear optical applications. Moreover, in the field of photorefractive materials low molecular weight noncrystalline chromophores with glass forming properties are required.[12,13] Precipitation of dyes in the restricted volume of the capsules could also help to obtain such substances.

In this paper we have applied the method of x-ray powder diffraction and molecular-dynamics (MD) simulations to

[a]On leave from Institute of Macromolecular Compounds of Russian Academy Sciences, Bolshoi pr. 31, 199004 St. Petersburg, Russia. Electronic mail: mary@gadir.physik.uni-potsdam.de

explore the precipitate nature of an azo dye—Disperse Red-1 (DR-1). MD simulations were performed with the help of a parallel program GBMOLDD[14,15] that uses the domain decomposition algorithm and is targeted at large-scale simulations of molecular systems with complex architecture. The main feature of this program is the use of both spherical Lennard-Jones (LJ) particles and anisotropic particles that can be of either Gay–Berne[16] (GB) or soft repulsive spherocylinders[17] type. In our study the former have been used to build encapsulated polymer chains and the latter to represent dye molecules.

Section II describes materials, their characterization with the x-ray powder diffraction method and the MD techniques used to study the nucleation behavior. X-ray powder diffraction data and simulation results are presented in Sec. III. In Sec. IV applicability of MD simulations to investigation of crystallization from solution is discussed. Finally, in Sec. V some conclusions are drawn.

II. MATERIALS AND METHODS

A. Materials

Disperse Red-1 was purchased from Sigma. Its chemical structure is presented on Fig. 1(a). Dispersions of monodispersed weakly cross-linked melamine formaldehyde particles with a diameter 5.6 μm were purchased from Microparticles GmbH (Berlin, Germany). These particles have been used as templates for the production of hollow polyelectrolyte capsules by means of layer-by-layer adsorption of oppositely charged polyelectrolytes.[3,18] Sodium poly(styrene sulfonate) (PSS, $M_W \sim 7 \cdot 10^4$ g/mol) and poly(allylamine hydrochloride) (PAH, $M_W \sim 5 \cdot 10^4$ g/mol) were obtained from Aldrich.

The approach used to encapsulate high molecular weight PSS ($M_W \sim 10^6$ g/mol) into the polyelectrolyte capsules consists in formation of the double shell structure. The inner shell containing PSS is made by the surface controlled precipitation method requiring for best results M_W about 10^6 g/mol.[19] It can be later decomposed releasing polymer component into the capsule interior. The outer shell remains stable and provides PSS capturing.[9] Monomer concentration of encapsulated polyelectrolyte was 0.1 M.

Exposed to nonpolar solution (aceton) capsules loaded with PSS show ability to provide a polarity gradient across their walls.[11] Presence of the polar hydrophilic groups only inside them results in higher water content in their interior. This gradient between capsule inner volume and bulk solution allows to precipitate poorly water-soluble materials exclusively inside the capsules. The encapsulation procedure consists in exposition the capsules and DR-1 to a water–aceton mixture with subsequent evaporation of the aceton from solution, which leads to complete precipitation of the DR-1 inside the capsules (Fig. 2). Concentration of the DR-1 inside the capsules was estimated to be ~7 molecules of DR-1 per one sulfonate group of PSS. For details of DR-1 precipitation inside the capsules see Ref. 11.

B. X-ray powder diffraction

X-ray powder diffraction analysis was carried out using a Nonius PDS120 diffractometer. The monochromatic radiation was supplied by the Nonius FR 590 generator ($CuK\alpha_1\alpha_2$ doublet, $\lambda = 1.542$ Å) equipped with a monochromator. Powder patterns were registered by the Nonius CPS 120 detector. All recordings were accumulated during 18 hours. Diffraction from the mount stage was accumulated during four hours and after normalization subtracted from the sample recordings. Sample preparation for x-ray analysis was as follows: 0.5 ml of water solution containing 3% v/v DR-1 loaded polyelectrolyte capsules was dropped onto the surface of a quartz mount stage and dried at room temperature under vacuum. For comparison as-received DR-1 without further purification was taken.

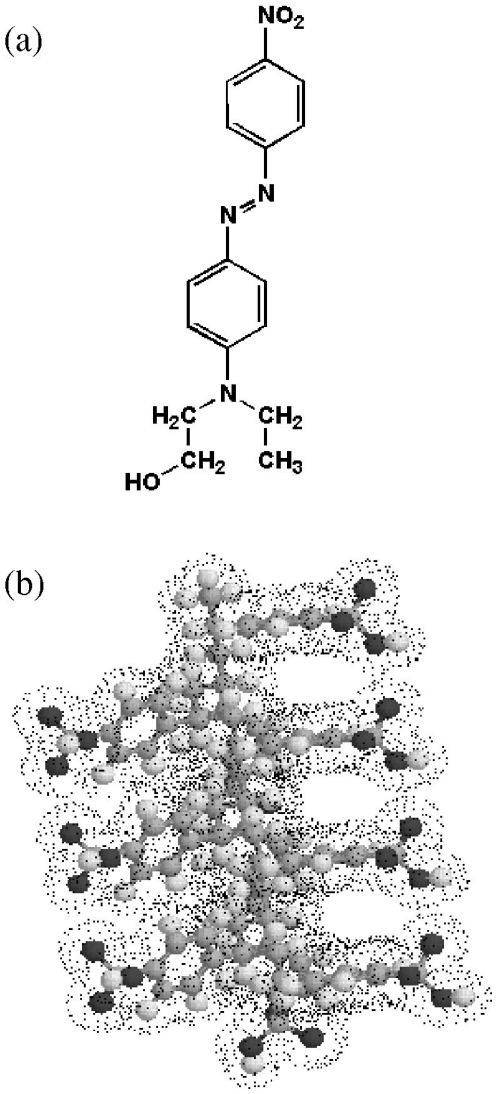

FIG. 1. (a) Chemical structure of Disperse Red-1 (DR-1); (b) side view of the trigonal arranged sulfonate groups of isotactic PSS.

C. Molecular-dynamics simulation

The dye molecules used in the current study have essentially nonspherical shape [Fig. 1(a)]. In first approximation, DR-1 could be considered as a rodlike molecule. As a simulation model we chose the GB particle which is a sort of anisotropic LJ potential including both repulsive and attrac-

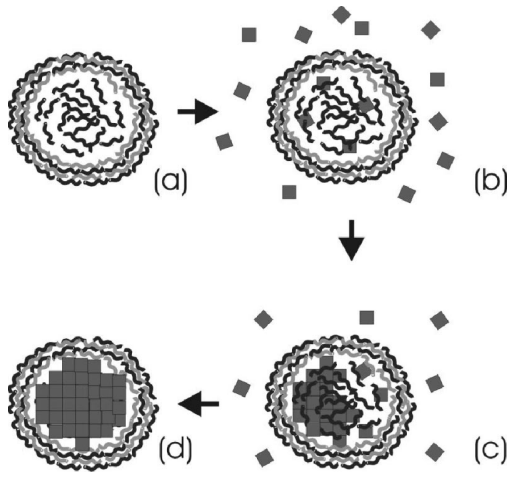

FIG. 2. Schematic representation of preparation of capsules filled with dyes. (a) Capsules loaded with polyelectrolytes; (b) and (c) capsules and dye suspension in a water–acetone solvent: (b) A high acetone content, (c) a low acetone content; (d) suspension of capsules with precipitated dye in water.

tive contributions. The latter can not be neglected in our study as we would like to simulate dye nucleation.

The anisotropic interaction energy between two GB particles i and j with orientations given by unit vectors $\mathbf{u}_i$ and $\mathbf{u}_j$ and with centers separated by the intermolecular vector $\mathbf{r}$ can be written as[16]

$$U_{ij}=4\epsilon_0\epsilon_1^{\nu}(\mathbf{u}_i,\mathbf{u}_j)\epsilon_2^{\mu}(\mathbf{u}_i,\mathbf{u}_j,\hat{\mathbf{r}})\left\{\left[\frac{\sigma_0}{r-\sigma(\mathbf{u}_i,\mathbf{u}_j,\hat{\mathbf{r}})+\sigma_0}\right]^{12}-\left[\frac{\sigma_0}{r-\sigma(\mathbf{u}_i,\mathbf{u}_j,\hat{\mathbf{r}})+\sigma_0}\right]^{6}\right\}, \tag{1}$$

where $\hat{\mathbf{r}}=\mathbf{r}/r$. The information about the particle shape is contained in the orientation dependent distance of separation σ and $\epsilon_0\epsilon_1^{\nu}\epsilon_2^{\mu}$ is the orientation dependent well depth. σ, ϵ_1^{ν} and ϵ_2^{μ} are given by Eqs. (2)–(7) of Ref. 20, $\sigma_0=4.721$ Å, $\epsilon_0\cong 0.56\,\mathrm{kg\cdot Å^2\,s^{-2}}$. The strength anisotropy is described by the parameter $\kappa'=\epsilon_s/\epsilon_e$, where ϵ_s and ϵ_e are the well depths for the side-by-side and end-to-end configurations.

A useful feature of the GB potential is that it can be easily tuned to alter molecular shape and the strength of interactions. The molecular weight of DR-1 is 314 g/mol, its calculated molecular length is ~15 Å and the breadth is ~2.8 Å. Hence, to represent the DR-1 molecule we chose a rodlike particle with the mass, m_{GB}, equal to 300 g/mol and the shape anisotropy (length to breadth ratio), κ, equal to 5; the particle length: $l_{\mathrm{GB}}=\kappa\sigma_0$.

Supersaturated water solutions of DR-1 have a concentration of about 10^{-3} mol/l. This gives less than two molecules in the simulation box with the edge, A, equal to 10 particle lengths. To find the regime of nucleation we have studied a much higher density—128 molecules in the box with $A=4l_{\mathrm{GB}}$. This corresponds to the reduced number density, $\rho^*=\kappa(\sigma_0)^3\rho$, of 0.08. It is worth to note that for rodlike hard ellipsoids of revolution with $k=5$ the isotropic–nematic transition occurs at a much higher density, $\rho^*=0.71$, in accordance with the molecular-dynamics simulations.[21] To adjust the strength of interactions one should choose appropriate strength parameters κ', μ, and ν. In the original paper of Gay and Berne[16] these constants were fixed to the values $k'=5$, $\mu=2$, and $\nu=1$. Taking these values we found an orientationally disordered (isotropic) state expected for such low densities[21] as ours. Berardi *et al.*[20] reported enhancement of the side-by-side and end-to-end interactions between particles using $k'=5$, $\mu=1$, and $\nu=3$. Indeed, we observed a fast crystallite growth (0.8 ns) accompanied by enormous release of latent heat. Using expressions for the orientation dependent well depth we estimated that in-layer (side-by-side) interactions, ϵ_s, for this crystallite are equal to 9.9 $\mathrm{kg\cdot Å^2\,s^{-2}}$ which is far away from the realistic situation. Organic crystals have in-layer interactions around the strength of a typical hydrogen bond[22] (20 kJ/mol≈3.3 $\mathrm{kg\cdot Å^2\,s^{-2}}$). Luckhurst *et al.*[23] have used the values $k'=5$, $\mu=1$, and $\nu=2$. This set of parameters also allows to observe the nucleation process: A crystallite with $\epsilon_s=3.6\,\mathrm{kg\cdot Å^2\,s^{-2}}$ was grown in 1.6 ns. To increase intra-layer (end-to-end) interactions $k'=4$ was chosen that gives $\epsilon_e=0.9\,\mathrm{kg\cdot Å^2\,s^{-2}}$. The final choice of parameters is as follows: $k=5$, $k'=4$, $\mu=1$, and $\nu=2$.

Heterogeneous systems containing these GB rodlike particles and usual LJ spherical sites based on parameters for a CH_2 united-atom[24] have been also simulated. Full details of the interaction potentials between two LJ particles and between un-like particles have been given elsewhere.[25]

All simulations were performed at room temperature that was kept constant throughout the simulation by rescaling the velocities[26] every 100 time steps, $\Delta t=2\cdot 10^{-15}$ s. The more sophisticated Nose–Hoover extended system strategy[27,28] was checked for a pure GB system and found to give twice higher temperature oscillations after the onset of nucleation for any chosen thermostat mass. It is impossible to choose an appropriate thermostat mass by comparison with simulations in the NVE ensemble due to a large amount of latent heat exposed during nucleation.

III. RESULTS

A. X-ray powder diffraction

Diffraction recording of commercially purchased DR-1 shows a number of sharp peaks [Fig. 3(a)]. The size of crystals was calculated from the angular width, $\Delta(2\theta)$, at half maximum of three highest peaks according to the Scherrer formula[29]

$$\Delta(2\theta)=\frac{\lambda}{S\cos\theta_0}. \tag{2}$$

Here S is the thickness of the crystal and θ_0 is the angular position of the observed line. S is found to be about 60 nm.

The diffraction pattern of DR-1 precipitates found inside the capsules reveals three very broad peaks [Fig. 3(a)]. We checked that empty microcapsules exhibit one peak around $2\theta_0=20°$ [Fig. 3(b)]. Therefore, the diffraction pattern of DR-1 precipitates indicates the presence of a polycrystalline powder. Considering the very low intensity of the peaks one can not neglect the possibility that some amount of dye is in the isotropic state.

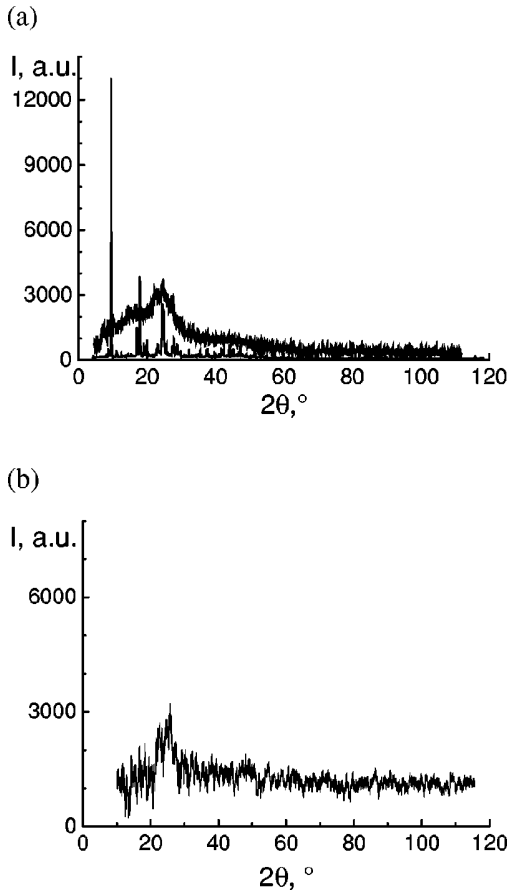

FIG. 3. X-ray powder diffraction patterns. (a) As-received DR-1 (thin line, a signal is divided by 50 for the better comparison) and the capsules filled with DR-1 (thick line); (b) empty capsules.

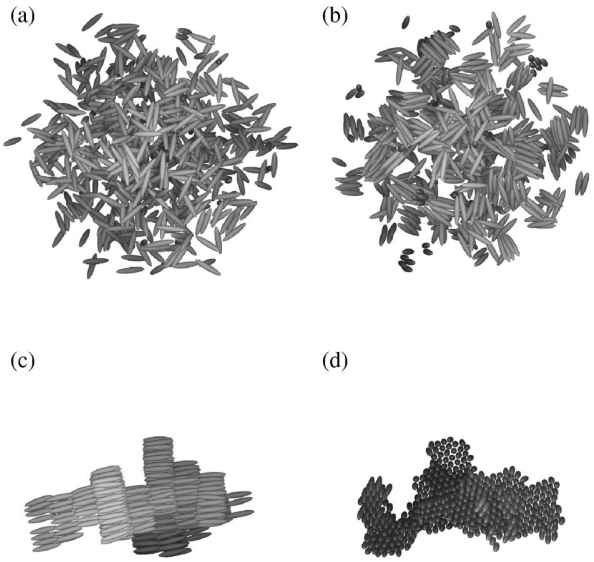

FIG. 4. Snapshots from simulations showing the growth of crystallite in bulk. (a) Initial isotopic state; (b) onset of nucleation at $t=0.04$ ns; final crystalline state at $t=4$ ns: (c) longitudinal view, (d) transverse view.

B. Molecular-dynamics simulation

1. Homogeneous nucleation in bulk

We started by studying precipitation in the absence of polyelectrolyte capsules when only dye molecules are present in the solvent. Further this case will be addressed as homogeneous nucleation in bulk. We could not of course follow the gradual change in the quality of solvent, which takes in reality three days. Instead, we assumed that a state of supersaturation is already achieved. The effective GB potential chosen in Sec. II describes a situation when attractive interactions between two dye molecules are much stronger than their interactions with solvent. Thus, we do not explicitly consider the solvent in this paper.

To overcome the long-time scales characteristic of the process of crystallization from solution, we have increased the solute density by approximately three orders of magnitude in comparison to that of supersaturated solvent. According to Avrami equation[30,31] the volume fraction, f, of transformed material is

$$f=1-\exp\left(-\frac{\pi}{3}\dot{N}U^3t^4\right)\approx\frac{\pi}{3}\dot{N}U^3t^4. \tag{3}$$

Here $\dot{N}$ is the nucleation rate and U is the linear growth rate. $\dot{N}$ is proportional to the density of nucleation sites, which in our case can be considered to be equal to the solute density, ρ. $U\sim\gamma a_0$, where $\gamma=(kT/3\pi\eta)\rho$ is the frequency factor, η is the viscosity and a_0 is the molecular size. Thus, $f\sim\rho^4t^4$ and increasing ρ three orders of magnitude we can grow the crystallite of the same size 1000 times faster. As will be shown below, in 10 ns we managed to grow a crystallite built from about 1000 molecules. In practice, DR-1 crystals grown in bulk could reach 1 μm length that corresponds to 10^9 molecules and takes about 1 ms at realistic concentrations. However, as we study the very onset of the crystallization process, the MD simulations technique proves to be a suitable method.

To simulate homogeneous nucleation in bulk we took the box with the edge $A=6.1l_{\mathrm{GB}}$ and 640 dye molecules ($\rho^*=0.1$) randomly inserted into it. We were able to follow the nucleation process producing configuration snapshots every 0.01 ns. In the beginning a totally isotropic state was observed [Fig. 4(a)]. But after 0.04 ns a number of clusters built from two or three molecules appeared in the box [Fig. 4(b)]. With time the average size of clusters increases as result of two processes: (1) Aggregation of clusters; (2) competition between bigger and smaller clusters when bigger clusters pull out molecules from the smaller ones which sometimes totally disappear. After 4 ns a crystallite was grown [Fig. 4(c)] and as can be seen from Fig. 4(d) molecules in one layer are organized in a hexagonal pattern as expected in a crystalline layer structure. Such pattern arises due to rotational symmetry of our model molecule. Real organic molecules do not possess so high symmetry and, therefore, exhibit a wide variety of possible crystal packings.

To characterize the system quantitatively, at the end of every run orientational and translational ordering of the GB particles was defined; the former through the calculation of the orientational order parameter and the latter through the radial distribution function

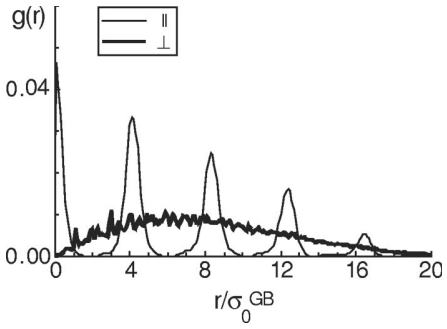

FIG. 5. Radial distribution functions $g_{\parallel}(r)$ and $g_{\perp}(r)$ for dye molecules forming the crystallite.

$$g(r)=\frac{2}{N_{\mathrm{dye}}(N-1_{\mathrm{dye}})}\sum_{i=1}^{N_{\mathrm{dye}}}\sum_{j\neq i}^{N_{\mathrm{dye}}}\delta(\mathbf{r}-\mathbf{r}_{ij}). \tag{4}$$

In the GBMOLDD program,[14] S_2 is associated with the largest eigenvalue λ_+ obtained through the diagonalization of the ordering tensor

$$Q_{\alpha\beta}=\frac{1}{N_{\mathrm{dye}}}\sum_{i=1}^{N_{\mathrm{dye}}}\frac{3}{2}u_{i\alpha}u_{i\beta}-\frac{1}{2}\delta_{\alpha\beta}\quad \alpha,\beta=x,y,z. \tag{5}$$

The eigenvector associated with λ_+ provides the director describing the average direction of alignment for rodlike particles. The radial distribution function could be resolved into two components $g_{\parallel}(r)$ and $g_{\perp}(r)$ describing translational order parallel (intra-layer) and perpendicular (in-layer) to the director.

Indeed, GB particles in the crystallite are perfectly oriented: $S_2=0.99$. $g_{\parallel}(r)$ indicates the presence of five layers with a layer spacing of $\sim 4\sigma_0$ (Fig. 5). This value is less than the molecule length because molecules of the next layer pack into the holes between molecules of the previous layer. If we move transversally to the director a lot of well defined peaks appear indicating a high degree of structure in the layer. The double structure of the second peak confirms a hexagonal ordering of the crystallite.

2. Geometry restrictions

X-ray powder diffraction of the dye precipitate inside the polyelectrolyte capsules revealed that the high crystalline order typical for that precipitate in bulk is considerably suppressed. To understand the possible reason of disordering we checked different scenarios.

Let us first consider the capsule interior. PSS molecules of $M_W\sim 7\cdot 10^4$ g/mol which were used to build the first capsule layer are protruding from the inner wall. Free PSS molecules of $M_W\sim 10^6$ g/mol are encapsulated in concentration of 0.1 monoM.[11] At such concentration it is very plausible that PSS molecules organize themselves in a kind of physical network. If we assume the cubic one and take into account that the length of a PSS monomer is 2.6 Å[26] then an estimated distance between two subsequent knots, L_{knot}, is equal to 10 dye lengths. The physical network divides the capsule interior in tiny similar subvolumes. Thus, we do not need to simulate a whole capsule volume (an unreachable length scale from the point of view of MD simulations) but instead we can follow the crystallization process inside these subvolumes.

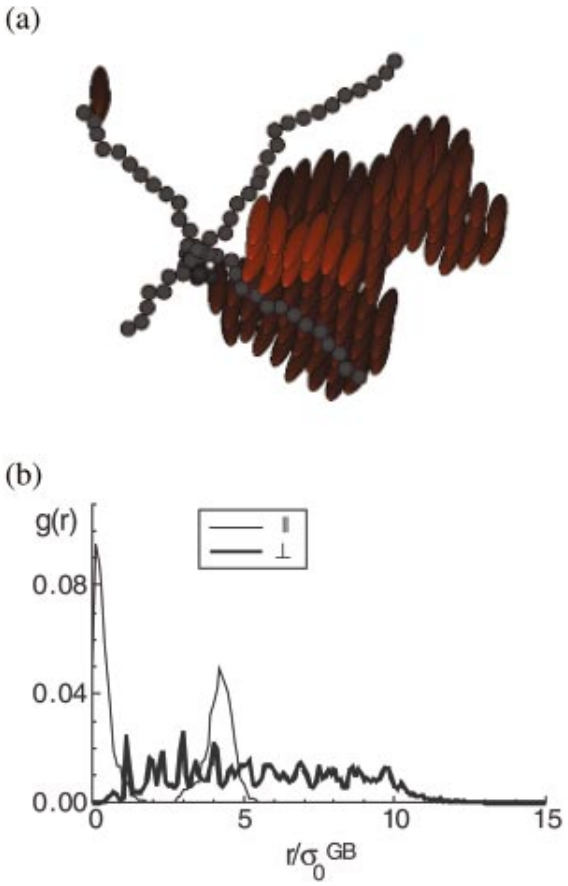

FIG. 6. (Color) (a) Snapshot from simulations showing the crystallite grown in the presence of a cubic polymer network. Dye molecules are denoted by brick ellipsoids; Lennard-Jones sites are denoted by black spheres. (b) Radial distribution functions $g_{\parallel}(r)$ and $g_{\perp}(r)$ for dye molecules forming the crystallite.

Thus, the first hypothesis to check: Could geometrical restrictions alone suppress the growth of crystallite. Two cubic networks with $L_{\mathrm{knot}}=4l_{\mathrm{GB}}$ and $L_{\mathrm{knot}}=2.3l_{\mathrm{GB}}$ were built from LJ particles. Totally stretched subchains are not stable and can be easily broken in the process of simulation. Therefore, LJ particles in an initial configuration were aligned along zigzag with angle between two subsequent bonds equal to 60°. After building a network 128 GB particles were randomly inserted into the box. Attractive interactions between polymer network and dye molecules could be neglected for they are four times lower than dye–dye interactions.

In the case of a polymer network with $L_{\mathrm{knot}}=4l_{\mathrm{GB}}$ a flat crystallite has been grown during 0.52 ns [Fig. 6(a)]. It consists from only two hexagonal packed layers [Fig. 6(b)] but still possesses a perfectly oriented structure, $S_2=0.99$. Twice higher time was needed to build a crystallite in the case of a polymer network with $L_{\mathrm{knot}}=2.3l_{\mathrm{GB}}$. In spite of severe geometrical restrictions we again observed a two-layer crystallite with $S_2=0.78$.

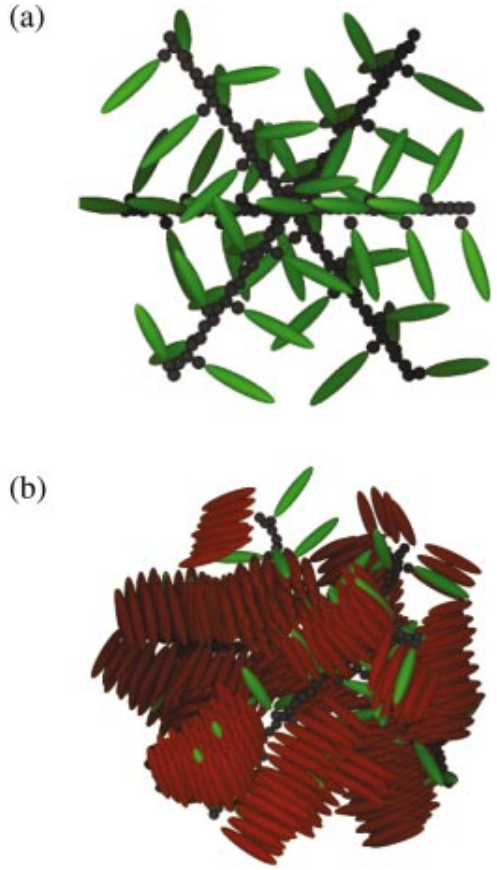

FIG. 7. (Color) (a) Model structure for the PSS cubic network. (b) Polycrystalline powder grown in the presence of the PSS cubic network. Nucleation centers are denoted by green ellipsoids.

3. Crystalline powder

As the geometrical restrictions alone are not enough to prohibit the dye crystallization we checked the second hypothesis: Heterogeneous nucleation due to interactions with PSS molecules. Fig. 1(b) provides a graphical representation of isotactic PSS as constructed using molecular modeling.[32] Sulfonate groups are trigonal and the distance between the groups oriented in one direction is 0.62 nm. We assumed that in the regime of heterogeneous nucleation PSS monomer units may serve as nucleation centers (NC) for dye molecules: Both contain aromatic rings which could interact via π-interactions.

A cubic network with $L_{\mathrm{knot}}=6.1l_{\mathrm{GB}}$ is now built from LJ particles and 54 NCs which are attached to every second subchain atom via a LJ spacer [Fig. 7(a)]. As a NC we chose the same GB rodlike particle. The trigonal pattern is preserved in the course of simulation due to addition of artificial bonds between the first and the second NC neighbors. In the same time, interactions between them are excluded to prohibit self-crystallization of NCs. 128 dye molecules have been added to the system every 0.2 ns. Hereby we tried to mimic the gradual entering of dye into the capsule. The final state with $N_{\mathrm{dye}}=640(\rho^*=0.1)$ is represented on Fig. 7(b). It looks like a very fine polycrystalline powder. Indeed, the orientational order parameter, $S_2=0.07$, is nearly as low as that for the isotropic sample and only few diffuse peaks could be seen on the $g_\perp(r)$ curve (Fig. 8). These peaks found at low separation distances are due to the nearest neighbor correlations which are the only one survived in the system. $g_\parallel(r)$ is very similar to that of the isotropic system and demonstrates no intra-layer peaks.

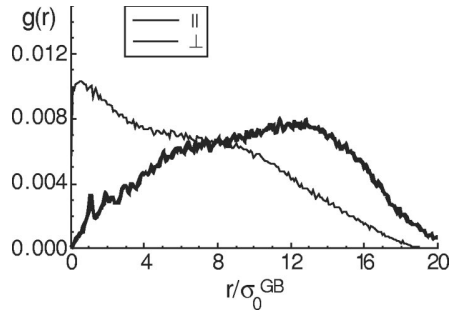

FIG. 8. Radial distribution functions $g_\parallel(r)$ and $g_\perp(r)$ for dye molecules forming the crystalline powder.

The third and the last hypothesis that has been checked is nonspecific dye interactions with the PSS molecule. This time, instead of freezing NCs in some regular pattern we allowed them to rotate freely and to interact with each other. This model assumes that in a bad solvent which is the case, dye–polymer interactions are more preferable than dye–solvent interactions. The first molecules entering the capsule in a negligible concentration can not find another DR-1 molecule and are forced to precipitate on the polymer backbone similar to heterogeneous nucleation on the wall. These first molecules serve for the newly coming dye as NCs. We took 36 NCs and attached them to every third subchain atom of the cubic network with $L_{\mathrm{knot}}=6.1l_{\mathrm{GB}}$. This system is more ordered than the previous one: $S_2=0.29$ and very diffuse first and second intra-layer peaks could be seen on the $g_\parallel(r)$ curve. However, one finds no difference between the two systems considering their x-ray powder diffraction patterns.

The powder diagram could be easily calculated knowing the lengths r_{ij} of all the interatomic vectors; it does not depend on their mutual orientations. Usually results are presented in the terms of an interference function[29]

$$\Phi(q)=\frac{I_{N_{\mathrm{dye}}}(q)}{N_{\mathrm{dye}}f^2}=1+\frac{2}{N_{\mathrm{dye}}}\sum_{i=1}^{N_{\mathrm{dye}}}\sum_{j\neq i}^{N_{\mathrm{dye}}}\frac{\sin(qr_{ij})}{qr_{ij}}, \tag{6}$$

where $I_{N_{\mathrm{dye}}}(q)$ is the observed intensity, f is the structure factor of the dye molecule and q is the scattering vector. As can be seen from Fig. 9, although the crystallite is built only from 640 dye molecules it exhibits in the diffraction pattern three well-pronounced peaks which could be assigned to the intra-layer ordering. Smaller peaks correspond to the crystallite dimensions. No observable pattern has been demonstrated by both crystalline powders produced using frozen NCs (powder I on Fig. 9) as well as freely rotating NCs (powder II on Fig. 9). We can conclude that so fine powders will be classified by x-ray measurements as amorphous samples which is not really the case.

IV. DISCUSSION

The complexity of the phenomenon and the long time scales involved have been a serious obstacle to computer simulations of crystallization from solution. This study dem-

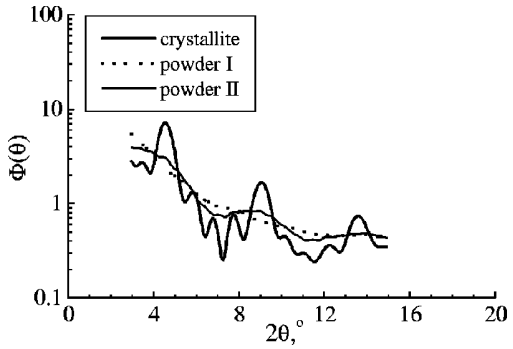

FIG. 9. X-ray interference function $\Phi(\theta)$ for the crystallite grown in bulk (thick line) and two crystalline powders. Powder I (dotted line) was grown from dye molecules interacting with PSS sulfonate groups; powder II (thin line) was grown using nonspecific interaction between dye molecules and the PSS.

onstrates that some tendencies of homogeneous and heterogeneous nucleation can in fact be simulated using the method of molecular dynamics for a model system consisting of both anisotropic Gay–Berne particles and isotropic Lennard-Jones sites. The former represent dye molecules (and nucleation centers), the latter are used to build alkyl chains modeling polyelectrolyte molecules encapsulated inside the capsules.

Long time scales arise due to negligible (from the point of view of MD simulations) solute density and could be eliminated increasing it three to four orders of magnitude. As far as one works far below the isotropic-nematic transition such ''densification'' does not affect the physical behavior of the system. As was mentioned above, it is impossible to simulate the crystallization process in a whole interior for the capsules with diameter of about 10 μm. Fortunately, it is sufficient to do this for much smaller subvolumes separated by encapsulated PSS macromolecules, the length scale of these subvolumes being covered by MD simulations.

In this study the effect of supersaturation is achieved by changing the solubility of dye molecules, through the strength parameters of the Gay–Berne potential, rather than by increasing their concentration. Thus, solvent molecules are not present in our simulations explicitly but are described via the properly adjusted effective potentials.

We did not report much on the very process of nucleation (formation and aggregation of clusters, their size distribution etc.) as we were interested in the final product of crystallization. Our observations, however, are very similar to those obtained recently by molecular-dynamics simulations of a model solute–solvent system consisting only from different Lennard-Jones sites.[33] At this point, it is worth to mention that we have found the GBMOLDD program[14,15] initially used to simulate liquid crystals and liquid crystalline polymers to be very flexible and quite powerful to simulate nearly any imaginable complex organic architecture. As far as we know, our study is the first attempt in the field addressing nucleation of organic molecules in bulk and in the presence of polymer chains.

Concerning different ways of dye precipitation in bulk and inside the polyelectrolyte capsules, we are quite sure it is not the confined volume that is responsible for dye amorphization. Our simulations of steric restrictions caused by a quite dense polymer network proved that they are not strong enough to suppress the growth of a big crystal (as big as to be seen in the x-ray powder diffraction pattern). Therefore, it seems quite unlikely that walls of the capsule separated by micron distances could impose some geometric or energetic restrictions leading to amorphization. Such effects are expected for the pure liquid crystalline solvents[34] but not in solutions where dye is present in a minor concentration. The most probable source of amorphization is polymer molecules contained in the capsule interior. We have shown that nonspecific interactions with these molecules result in formation of a very fine polycrystalline powder barely seen on diffraction patterns. Thus, already the effect of particle size broadening alone could result in seemingly amorphous x-ray data. One should not forget about other kinds of imperfection (strains, faulting) and instrumental broadening which all together could totally hide the coherent signal under the noise level.

V. CONCLUSIONS

We can conclude that both methods utilized in this study—x-ray powder diffraction and MD simulations—indicate strong amorphization of the DR-1 precipitate inside the capsules in comparison with the dye precipitated in bulk. The lateral size of crystallites found in the capsules is at least one order of magnitude smaller than that of as purchased crystals. Interactions between DR-1 and PSS molecules contained inside the capsules as well as building its inner wall should cause the amorphization. Considering a very general rodlike model used in this study, our simulation results have to be valid for a whole class of organic dyes with the structure similar to that of DR-1.

The amorphization of the dye structure is rather desirable for potential use of dyes as photorefractive media without polymer host matrices.[12,13] It is also important to emphasize that one should be able to affect the degree of crystallinity (amorphicity) of the precipitates by varying the chemical structure and ionization degree of polyelectrolytes, which constitute the shells of the capsules and interact with substances precipitating inside the capsules. This tuning of the supramolecular structure could have favorable consequences for applications of the precipitates not only in nonlinear optics but also in biotechnologies.

ACKNOWLEDGMENTS

This work was supported by Sofia Kovalevskaya Program funded by the Alexander von Humboldt Foundation and the German Ministry of Education and Research. Professor Dr. Möhwald is gratefully acknowledged for continuous support and stimulating discussions. One of the authors (M.S.) would like to thank MPI-KG for providing computer time on its parallel SGI R10000 machine. She also acknowledges support from the Russian Foundation for Fundamental Research (Grant No. 02-03-33135) and from INTAS Grant No. 99-1114.

[1] G. Decher, Science **277**, 1232 (1997).
[2] G. B. Sukhorukov, E. Donath, H. Lichtenfeld, E. Knippel, M. Knippel, A. Budde, and H. Möhwald, Colloids Surf., A **137**, 253 (1998).

[3] E. Donath, G. B. Sukhorukov, F. Caruso, S. Davis, and H. Möhwald, Angew. Chem. Int. Ed. Engl. **37**, 2021 (1998).
[4] G. B. Sukhorukov, in *Novel Methods to Study Interfacial Layers*, edited by D. Möbius and R. Miller (Elsevier Science B.V. 201a), p. 384.
[5] G. B. Sukhorukov, A. A. Antipov, A. Voigt, E. Donath, and H. Möhwald, Macromol. Rapid Commun. **22**, 44 (2001).
[6] Y. Lvov, A. A. Antipov, A. Mamedov, H. Möhwald, and G. B. Sukhorukov, Nanoletters **1**, 125 (2001).
[7] G. Ibarz, L. Dähne, E. Donath, and H. Möhwald, Macromol. Rapid Commun. **23**, 474 (2002).
[8] G. Sukhorukov, L. Dähne, J. Hartmann, E. Donath, and H. Möhwald, Adv. Mater. **12**, 112 (2000).
[9] I. L. Radtchenko, G. B. Sukhorukov, and H. Möhwald, Colloids Surf., A **202**, 127 (2002).
[10] I. L. Radtchenko, G. B. Sukhorukov, and H. Möhwald, Int. J. Pharm. **242**, 219 (2002).
[11] G. B. Sukhorukov, M. Brumen, E. Donath, and H. Möhwald, J. Phys. Chem. B **103**, 6434 (1999).
[12] P. M. Lundquist, R. Wortmann, C. Geletneky, R. J. Twieg, M. Jurich, V. Y. Lee, and C. R. Moylan, Science **274**, 1182 (1996).
[13] R. Wortmann, C. Poga, R. J. Twieg *et al.*, J. Chem. Phys. **105**, 10637 (1996).
[14] J. M. Ilnytskyi and M. R. Wilson, Comput. Phys. Commun. **134**, 23 (2001).
[15] J. M. Ilnytskyi and M. R. Wilson, Comput. Phys. Commun. **148**, 43 (2002).
[16] J. G. Gay and B. J. Berne, J. Chem. Phys. **74**, 3316 (1981).
[17] T. Kihara, Adv. Chem. Phys. **5**, 147 (1963).
[18] G. B. Sukhorukov, E. Donath, S. Davis, H. Lichtenfeld, F. Caruso, V. I. Popov, and H. Möhwald, Polym. Adv. Technol. **9**, 759 (1998).
[19] V. Dudnik, G. B. Sukhorukov, I. L. Radtechenko, and H. Möhwald, Macromolecules **34**, 2329 (2001).
[20] R. Berardi, A. P. J. Emerson, and C. Zannnoni, J. Chem. Soc., Faraday Trans. **89**, 4069 (1993).
[21] M. P. Allen, Phys. Rev. Lett. **65**, 2881 (1990).
[22] R. Yu, A. Yakimansky, I. G. Voigt-Martin, M. Fetten, C. Schnorpfeil, D. Schollmeyer, and H. Meier, J. Chem. Soc., Perkin Trans. 2 **1999**, 1881.
[23] G. R. Luckhurst, R. A. Stephens, and R. W. Phippen, Liq. Cryst. **8**, 451 (1990).
[24] S. Leggetter and D. J. Tildesley, Mol. Phys. **68**, 519 (1989).
[25] M. R. Wilson, J. Chem. Phys. **107**, 8654 (1997).
[26] M. P. Allen and D. J. Tildesley, *Computer Simulations of Liquids* (Clarendon, Oxford, 1987).
[27] S. Nose, J. Chem. Phys. **81**, 511 (1984).
[28] W. G. Hoover, Phys. Rev. A **31**, 1695 (1985).
[29] A. Guinier, *X-ray Diffraction* (Dover, New York, 1994).
[30] M. Avrami, J. Chem. Phys. **9**, 177 (1941).
[31] D. Uhlmann, in *Advances in Ceramics*, edited by J. Simmons, D. Uhlmann, and G. Beall (Amer. Ceram. Soc., Columbus, Ohio, 1982), Vol. 4, p. 80.
[32] E. Donath, D. Walther, V. N. Shilov, E. Knippel, A. Budde, K. Lowack, C. A. Helm, and H. Möhwald, Langmuir **13**, 5294 (1997).
[33] J. Anwar and P. K. Boateng, J. Am. Chem. Soc. **62**, 9600 (1998).
[34] G. P. Crawford and S. Zumer, *Liquid Crystals in Complex Geometries Formed by Polymer and Porous Networks* (Taylor and Francis, London, 1996).

JOURNAL OF CHEMICAL PHYSICS VOLUME 120, NUMBER 8 22 FEBRUARY 2004

Linear viscoelastic analysis of formation and relaxation of azobenzene polymer gratings

Marina Saphiannikova,[a] Thomas M. Geue, Oliver Henneberg, Knut Morawetz, and Ullrich Pietsch
Institute of Physics, University of Potsdam, P.O. Box 601553, D-14415 Germany

(Received 23 July 2003; accepted 24 November 2003)

Surface relief gratings on azobenzene containing polymer films were prepared under irradiation by actinic light. Finite element modeling of the inscription process was carried out using linear viscoelastic analysis. It was assumed that under illumination the polymer film undergoes considerable plastification, which reduces its original Young's modulus by at least three orders of magnitude. Force densities of about 10^{11} N/m^3 were necessary to reproduce the growth of the surface relief grating. It was shown that at large deformations the force of surface tension becomes comparable to the inscription force and therefore plays an essential role in the retardation of the inscription process. In addition to surface profiling the gradual development of an accompanying density grating was predicted for the regime of continuous exposure. Surface grating development under pulselike exposure cannot be explained in the frame of an incompressible fluid model. However, it was easily reproduced using the viscoelastic model with finite compressibility.
 [DOI: 10.1063/1.1642606]

I. INTRODUCTION

In the last decade a lot of publications have been devoted to the inscription of surface relief gratings (SRGs) on azobenzene polymer films.[1–4] These films show very unusual properties, namely, huge material transport under irradiation of actinic light, strong polarization dependence of the inscription rate, and pronounced birefringence after the first minutes of illumination. These properties make the investigated polymer materials very attractive for applications, in particularly for high-density optical storage. Inscription is done by exposing the sample to a periodic intensity or polarization pattern that results from the interference of two polarized laser beams. The wavelength of the laser should be near the absorption maximum associated with the *trans-cis* and *cis-trans* isomerization of the azobenzene moieties. The absorption of this light induces material flow even at room temperature, which is at least 100 K below the glass transition temperature T_G of the polymers. The process of inscription is strongly dependent on the polarization state of the writing beams: two circular counterpolarized beams inscribe gratings of maximal diffraction efficiency, while two *s*-polarized beams produce negligible surface changes.[4,5]

A number of theories have been proposed to explain the mass material transport.[5–9] One of the first hypotheses[5] suggests light induced pressure gradients that depend on the intensity and polarization pattern produced by the writing beams. These pressure gradients would arise from the increase of *cis* population with intensity and ellipticity of the polarized light, due to the large free volume requirement of the *cis* isomers. The theory predicts the highest pressure gradients for two *s*-polarized beams. This is in contradiction with experimental data, which demonstrate negligible diffraction efficiency for this geometry. Two other theories which exploit the forces acting on induced electric dipoles in an inhomogeneous electric field[6,7] describe satisfactorily all the important aspects of experimental findings. Unfortunately, the force density estimated for conventional lasers is two orders of magnitude smaller than that of the gravitational force (10^4 N/m^3), and thus is too small to be of influential importance (see the Appendix). Some authors[8] consider anisotropic diffusion of chromophores along the polarization direction. Nevertheless, this scenario is not supported by the main microscopic observation: the chromophores illuminated by polarized light tend to be oriented perpendicular to the polarization state. Only in the case of such orientation is further absorption of photons prevented and, hence, a steady state is reached.[10,11] Another approach[9] bases its predictions on this preferential orientation, but assumes that the electric field resulting from interference of two contracircularly polarized beams is linearly polarized. However, this field is elliptically polarized. Therefore, in spite of enormous experimental and theoretical efforts none of the groups working in the field can explain satisfactorily the mass polymer transport at a molecular level.

When two polarized beams interfere at a certain angle the resultant intensity or polarization field has sinusoidal variation along the grating vector direction. Therefore, the force acting on the polymer material should also vary sinusoidally along the same direction. This force law (together with the assumption of incompressible viscous material behavior) was used to calculate the rate of grating inscription.[1] It was shown that the inscription rate increases linearly with the intensity and with the third power of the initial film thickness. This calculation is in good agreement with the experimental data for thin films. Furthermore, when absorption effects are taken into account the above model can explain the

[a]Electronic mail: mary@gadir.physik.uni-potsdam.de

film thickness dependence in the range of large thicknesses.[12]

Recent studies[13] on thermal erasure of the SRGs show that upon heating the sample toward the glass transition temperature T_G the SRG disappears, but some weak periodic density modulation is still preserved. On the other hand, the density variation in the case of the polar polymer pDR1M [poly{(4-nitrophenyl)(4-{[2-(methacryloyloxy)-ethyl]ethylamino}phenyl)diazene}] keeps growing further when the sample is heated above T_G.[14] The appearance of density changes during the process of grating inscription cannot be explained in the framework of an incompressible flow model.[3,12] Moreover, this model is not able to describe the time-dependent visible light (VIS) scattering experiments performed during the formation of the SRG.[15–17]

II. MODELING

In order to reproduce recent VIS scattering data, we modeled the inscription process under the assumption of the polymer being an isotropic viscoleastic material with finite compressibility. The stress-strain equations in the viscoelastic analysis depend not only on the current stress and strain states, but also on the entire history of the development of these states. This constitutive behavior is most readily expressed in terms of hereditary integrals:

$$\sigma(t)=\int_0^t G(t-t')\frac{d\varepsilon(t')}{dt'}dt', \tag{1}$$

where σ is the current stress and ε is the current strain.

Furthermore, the time-dependent shear modulus $G(t)$ for materials with a fading memory can be described as an exponential series:

$$G(t)=\sum_{k=1}^{N} G_k\exp(-t/\tau_k) \quad \text{and} \quad G_0=G(0)=\frac{E}{2(1+\nu)}, \tag{2}$$

where E is Young's modulus, ν is Poisson's ratio, and τ_k are the particular relaxation times of the system. As the key point of our model, we assume that, due to the photoinduced *cis-trans* isomerization of the azobenzene chromophores, the polymer film undergoes considerable plastification, which reduces its original Young's modulus by at least three orders of magnitude. Thus, the value of the Young's modulus falls into the range of values characteristic for polymers around their glass transition temperatures. Another widely accepted approach is that when the dynamics of photoinduced SRG formation is studied using an incompressible flow model.[5,12,18] This model assumes that under holographic inscription the azobenzene polymer not only undergoes a glass-rubbery transition but reaches a fluid state which is characterized by zero values of the Young's modulus.

Under application of a constant stress σ_0, time-dependent polymer deformation could be obtained from Eq. (1) using a Fourier–Laplace transformation[19]

$$\varepsilon(t)=\sigma_0\int\frac{d\omega}{2\pi\omega}\frac{e^{i\omega t}}{G^*(\omega)}, \tag{3}$$

where integration is performed in the complex plane and $G^*(\omega)$ is the complex shear modulus

$$G^*(\omega)=i\omega\int_0^\infty e^{-i\omega t}G(t)dt. \tag{4}$$

Using Eq. (2) $G^*(\omega)$ can be rewritten as follows:

$$G^*(\omega)=i\omega\sum_{k=1}^{N}\frac{G_k}{(i\omega+1/\tau_k)}. \tag{5}$$

Substitution of Eq. (5) into Eq. (3) gives the creep compliance of the material,

$$J(t)=\frac{\varepsilon(t)}{\sigma_0}=\frac{1}{G_0}\left[\frac{t}{g_0}+\frac{g_1}{g_0}+\sum_{k=1}^{N-1}C_k\exp(-\omega_k t)\right], \tag{6}$$

where $G_0=\Sigma_{k=1}^{N}G_k$, $g_0=\Sigma_{k=1}^{N}G_k\tau_k$, $g_1=\Sigma_{k=1}^{N}G_k\tau_k^2$, and C_k and ω_k are constants depending on G_k and τ_k. In the present work we consider material models that are characterized by two ($N=2$) or three ($N=3$) relaxation modes.

Our model utilizes a sinusoidal force varying in the x direction parallel to the grating vector and decaying exponentially with the distance z from the film surface,

$$f_x=AV\exp\left(\frac{z-[h(x)+h_0]}{\mu}\right)\sin\left(\frac{2\pi x}{D}\right). \tag{7}$$

Here A is the force density, which should be proportional to the laser power in a linear regime, $h(x)$ is the height of the SRG, h_0 is the initial film thickness, μ is the light penetration depth, and D is the grating period. The sample volume V is equal to h_0D^2. The force is applied in a self-consistent manner starting from $h(x)=0$. A cleavage plane (x,z plane, $D=1\ \mu$m) was calculated using the finite element method implemented by the commercial computer software MENTAT/MARC. The area was divided into a number of quadrilateral plane strain elements. Periodic boundary conditions were applied along the x direction. As a constraint, no displacement of the sample was allowed at the polymer-substrate interface.

For short inscription times the influence of the surface tension on the inscription process can be neglected. However, the saturation of the SRG growth observed at long inscription times[5] can be explained only if the surface tension force is taken into account. This force increases proportionally to the second derivative of the surface profile (in linear approximation) and acts in the direction perpendicular to the substrate surface,

$$f_z=\Omega D\frac{\partial h^2(x)}{\partial x^2}\delta x, \tag{8}$$

where Ω is the value of the surface tension. This vertical force acts on a strip of polymer surface between two frontiers, D is the length of a frontier, and δx is the distance between them. We will show below that the force of gravitation can always be neglected in comparison with the inscribing force f_x.

In order to simulate a pulselike inscription process the cyclic external force was applied as follows:

$$f=\begin{cases} f_x, & 0\leqslant t\leqslant t_1,\\ 0, & t_1<t\leqslant T,\end{cases} \tag{9}$$

where f_x is given by Eq. (7), t_1 is the pulse length, and T is the cycle length. The response to this complex loading history can be calculated using the Boltzmann superposition principle

$$\varepsilon(t)=\sum_i \Delta\sigma_i J(t-t_i), \tag{10}$$

where

$$\begin{aligned}&\Delta\sigma_{2i-1}\sim f_x, \quad t_{2i-1}=(i-1)T,\\ &\Delta\sigma_{2i}\sim -f_x, \quad t_{2i}=(i-1)T+t_1,\end{aligned} \tag{11}$$

and i is the cycle number.

In order to perform finite element analysis we have to define some material constants. Therefore, we restricted our examination to one particular azobenzene polymer, pDR1M, derived from poly (methyl methacrylate) (PMMA). Molecular weight in the studied samples varied in the range of 7.6 to 11.5 kg/mol (from 20 to 30 monomers). The elastic properties of glassy polymers become independent of molecular weight as the latter increases. When the chain length is sufficient to form a solid material at room temperature, the Young's modulus does not vary greatly. For example, the Young's modulus of low molecular weight polyethylene (built from 20–30 monomers) is about 25–40% of the Young's modulus of high molecular weight polyethylene.[20] Experimental data on the mechanical properties of glassy azobenzene polymers are very rare. The plate compliance of thin layers was determined by electromechanical spectroscopy for the derivative of PMMA with a molecular weight of 86 kg/mol (about 2000 monomers) and an azo content of 65%.[21] The Young's modulus calculated[22] from this plate compliance was found to be 2.5 GPa, which is in the range of values typical for PMMA. Thus, we expect for the low molecular weight azobenzene polymers derived from PMMA a Young's modulus of about 1 GPa. The bulk modulus for the low molecular weight azobenzene polymer pMEA, a derivative of PMMA, was determined by mechanical methods to be 2 GPa.[3,5] This leads again to a value of the Young's modulus of about 1 GPa. The calculated initial density for pDR1M is about 1250 kg/m^3 (ACD/CHEMSKETCH, version 5.08) and we have chosen $\rho_0=10^3$ kg/m^3. While Poisson's ratio for pDR1M is unfortunately unknown, we took the value that is typical for PMMA from which it was derived: $\nu=0.4$.[23] The light penetration depth μ of pDR1M was estimated from measurements of the extinction coefficient for different film thicknesses and was found to be about 0.1 μm at $\lambda=488$ nm.

III. RESULTS

A. Grating formation under continuous illumination

The gradual development of the surface relief grating under continuous light exposure can be observed *in situ* by measuring the ensuing VIS scattering signal. After grating inscription its amplitude can be directly inspected using atomic force microscope (AFM). As expected a finite element modeling (FEM) can easily reproduce the growth of SRGs. Unfortunately, there is no straightforward way to prove another FEM prediction: the gradual development of density changes in the polymer film. However, indirect indications of their existence were found in our recent x-ray studies of pDR1M:[13,14] the first order scattering peak was still preserved after thermal erasure of the surface profile (proved by AFM inspection). The presence of a sinusoidal density grating explains these observations naturally.

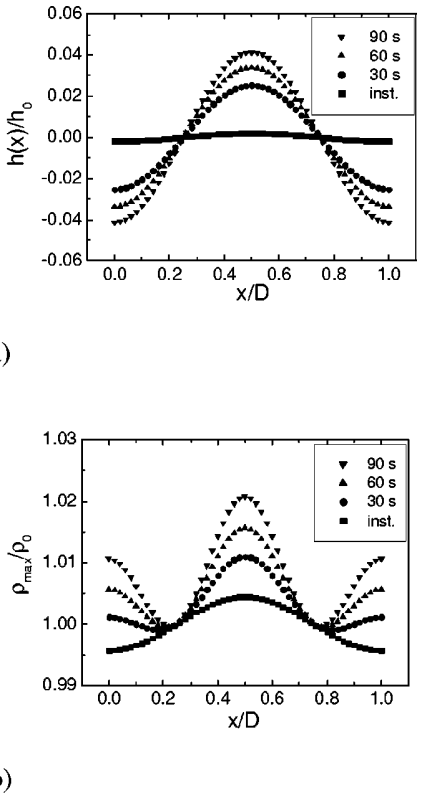

FIG. 1. Time development of the surface relief grating (a) and the density modulation (b) obtained by FEM just in the beginning and after 30, 60, and 90 s of light exposure. $h_0=1$ μm.

For FEM we used the two-term-material model [Eq. (6), $N=2$] with the following parameters: $E=1$ MPa, $G_1=0.9G_0$, $G_2=0.1G_0$, $\tau_1=1$ s, and $\tau_2=50$ s. The force density A in Eq. (7) was chosen in such a way that substantial material transport could be observed after a few minutes of force application. Force densities of about 10^{11} N/m^3 were necessary to reproduce the growth of the SRG. Comparison of this value with the density of gravitation force (10^4 N/m^3) shows that the latter does not play any role during the inscription process. It is worth noting that in the linear viscoelastic analysis both initial and time-dependent deformations depend on the ratio of the external force to the Young's modulus. Therefore, if we do not consider initial photoinduced plastification ($E=1$ GPa) we would need to apply force densities of about 10^{14} N/m^3 in order to reproduce the growth of the SRG.

The surface relief grating as well as the accompanying density distribution appears from the very beginning of the force application (instantaneous response on Fig. 1). During the first seconds of illumination both profiles can be described by a sinusoidal function of equal periods D (Fig. 1). Initially, the polymer material is mildly compressed in the

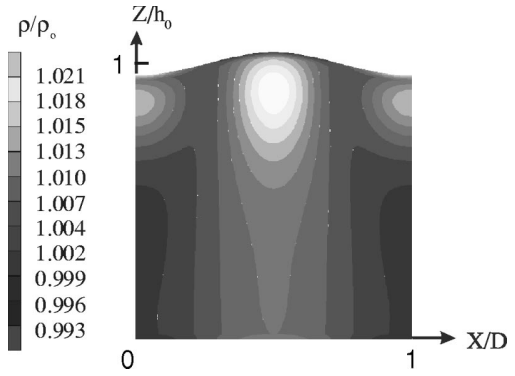

FIG. 2. FEM of the grating formation after continuous exposure of 90 s. $h_0=1\ \mu$m.

regions of the surface relief peaks and slightly expanded between the peaks [Fig. 1(b)]. As time increases the compressed regions extend toward the substrate. At the same time the polymer material in the regions of relief troughs is also compressed, but this second type of compressed region is much smaller and remains concentrated close to the surface (Fig. 2). Thus, the FEM predicts the density increase in the region where the azobenzene polymer chains have migrated. This prediction is in agreement with phase imaging AFM measurements, which have revealed changes in density on the surface of the azobenzene polymer film induced by an optical near field.[24]

In this study we consider polymer films with $\nu=0.4$. Recently, we showed that with an increase of the sample compressibility (the Poisson's ratio was varied in the range of 0.35 to 0.45) the amplitude of the SRG decreases and the density grating becomes more pronounced resulting in comparable density changes in the peaks and valleys of the SRG.[15] Thus, we always expect the appearance of a density grating as long as the studied materials are compressible.

The fast growth of the surface relief grating becomes saturated at long inscription times. This corresponds to the saturation of the first order VIS grating peak intensity I_1 [Fig. 3(a)]. The most likely restoring force is that of surface tension. It is equal to zero when the surface is flat and increases proportionally to the second derivative of the surface profile. In order to mimic the process of saturation we incorporated the force of surface tension with $\Omega=0.1$ N/m into the FE model (the calculated value of Ω is about 0.05 N/m; ACD/CHEMSKETCH, version 5.08). The process of saturation depends on the counterbalance between the inscription force and the force of surface tension. This balance can be shifted in favor of the surface tension force by increasing Ω. We intentionally used a value of Ω larger than calculated to speed up the FEM, since it is a time-consuming technique that covers only a few minutes scale. For a sinusoidal profile with $h(x)=B\sin(2\pi x/D)$ the value of the surface tension force per period could be estimated using Eq. (8):

$$f_z=8\pi B\Omega. \tag{12}$$

When the grating amplitude B reaches 20 nm the density of the surface tension force f_z/V piles up to 10^{11} N/m^3 ($h_0=0.5\ \mu$m) and becomes comparable to the density of the

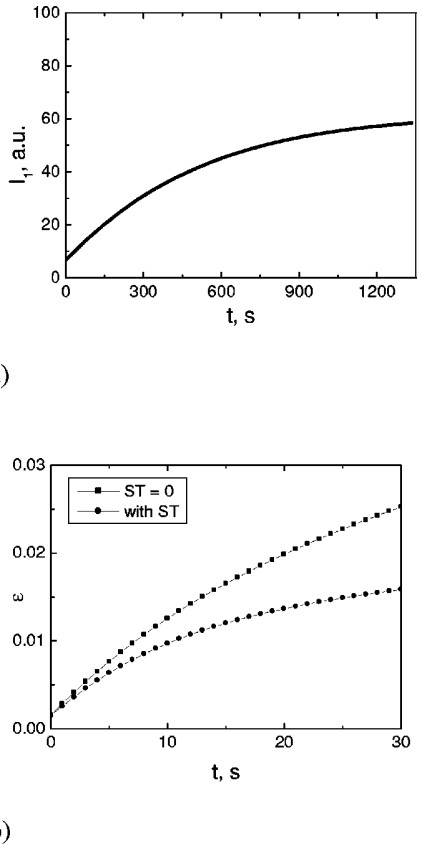

FIG. 3. Development of the surface profile amplitude during continuous light exposure: (a) the first order VIS grating peak intensity I_1 (power density of 100 mW/cm^2) and (b) FEM with and without surface tension (ST) force. $h_0=0.5\ \mu$m.

inscribing force. The FEM predicts saturation of the growth just after 30 s when B reaches approximately 10 nm [Fig. 3(b)]. This value is less than estimated because we did not account for the exponential attenuation of the inscribing force due to light absorption. In VIS scattering measurements saturation of the growth was observed later, after 900 s, when B reaches approximately 90 nm [Fig. 3(a)]. As was mentioned above, the FEM predicts earlier saturation and hence smaller B values due to overestimation of the surface tension force.

It is known that the initial film thickness could affect the inscription process in case of relatively thin films, $h_0<500$ nm.[5] Thus, we compared final states of two films with $h_0=50$ and 250 nm, after an identical inscription time of 10 min. Our simulation predicts that thicker films should undergo more pronounced changes than thinner ones. For the sample with $h_0=250$ the relative deformation $\varepsilon=h_{\max}(x)/h_0$ is found to be equal to 0.15, approximately three times higher than the relative deformation for the thin film [Fig. 4(a)]. Relative density changes $(\rho-\rho_0)/\rho_0$ in the region of surface relief peaks reach 6%, six times higher than those for the thin film [Fig. 4(b)]. This difference could be explained by the fact that much higher forces are working on thicker samples in comparison with thinner ones. When the film thickness is bigger than a light penetration depth, the force saturates and hence no difference should be observed

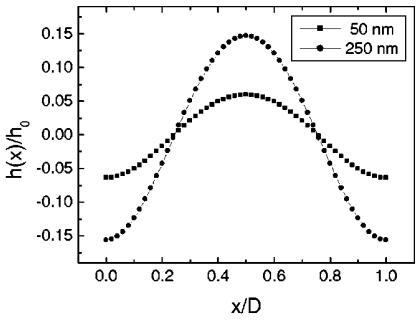

(a)

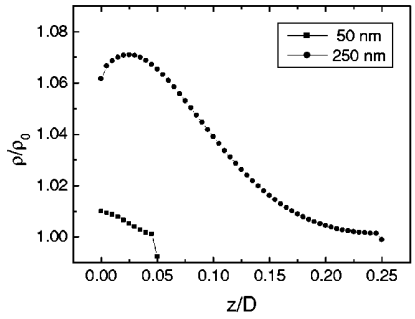

(b)

FIG. 4. Film thickness influence on the surface profile (a) and the density profile (b) at $x/D=0.5$ after continuous exposure of 10 min.

for such "bulk" samples. For example, the pDR1M films are characterized by a light penetration depth of about 0.1 μm at $\lambda=488$ nm. This means that the inscribing force should be the same for all pDR1M films thicker than 800 nm due to exponential decay of the light amplitude [see Eq. (7)].

To check the predictions of the FEM we have prepared and tested two series of samples. The first series of gratings was inscribed on a film with a thickness of about 226 nm, while for the second one a film of about 45 nm thickness was used. In all cases inscription was performed with the same laser power of 100 mW/cm^2 and with the same inscription time of 10 min. The amplitude of gratings thus inscribed was measured by AFM. It was found that in the first series B varies between 60 and 80 nm (the FEM predicts 38 nm). In the second series of samples the surface changes after inscription were negligible ($B\approx 0$ nm). This can be easily understood if we consider the absolute deformation predicted by the FEM for 50 nm thick samples. It reaches about 3 nm after 10 min of inscription and is lower than the original sample roughness. The latter increases with the decrease of the film thickness, namely, from about 1–2 nm for thick samples to at least 5 nm for thin ones (the thinner the sample the more it is affected by air humidity).

B. Grating formation under time-dependent illumination

Development of the surface relief grating under pulselike exposure was investigated using a cyclic external force. Although the density distribution was found to relax immediately after releasing the load, the surface profile can be accumulated even for pulselike exposure if the pulse length exceeds some critical value (Fig. 5). The FEM based on the two-term-material model [Eq. (6), $N=2$] matches the functional behavior as found previously by the VIS experiment.[15] However, it overestimates density and surface relaxation due to neglecting the polymer hardening after the light is switched off. This results in deformational jumps that are especially pronounced for very short pulses (Fig. 5).

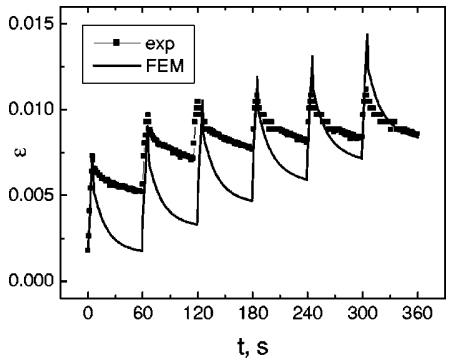

FIG. 5. Development of the surface deformation during pulselike exposure: experiment (see Ref. 15) and FEM (using $N=2$ and $h_0=0.25\,\mu$m). $t_1=5$ s.

The hardening process was taken into consideration in the one-dimensional viscoelastic theory that enabled us to reproduce the time-resolved VIS scattering.[15] We used the three-term-material model [Eq. (6), $N=3$]. Typical results are presented in Fig. 6. The pulse length t_1 is equal to 10 s. The first cycle of exposure is fitted with the following material parameters: $G_0=1$ GPa, $G_1=0.999G_0$, $G_2=0.0008G_0$, $G_2=0.0002G_0$, $\tau_1=0.002$ s, $\tau_2=1$ s, and $\tau_3=30$ s [Fig. 6(a)]. Thus, the shear modulus decreases from 1 GPa to 1 MPa within 0.002 s after switching on the laser light and increases from 1 MPa to 1 GPa within the same 0.002 s when the light is switched off. From comparison of Figs. 5 and 6 it is clearly seen that the three-term-material model much better describes the relaxation process after the light is switched off.

G_0 gradually decreases from cycle to cycle until reaching a saturation value of 0.6 GPa [Fig. 6(b)]. This result shows that further plastification could take place during the subsequent light pulses, in spite of the transient nature of the applied force. The relaxation times τ_2 and τ_3 also gradually increase and reach saturation values of 5 and 400 s, respectively, for the last cycles. This may be an indication of gradual unfreezing of cooperative motions of polymer molecules in the film, i.e., the addressing of an increased number of azobenzene side groups by the light. The latter hypothesis is supported by *ex situ* AFM inspections performed after inscription with a single short pulse.[25]

An unexpected behavior was observed in our recent VIS scattering measurements when the film was exposed to a long sequence of short pulses ($\leqslant 1$ s). After 400 s of inscription the material response suddenly changes its sign (Fig. 7): VIS scattering intensity is now higher when the light is off. A similar effect was reported in Ref. 17: the diffraction effi-

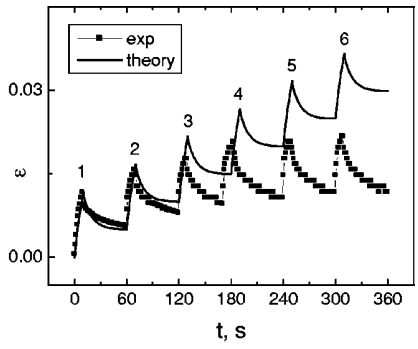

(a)

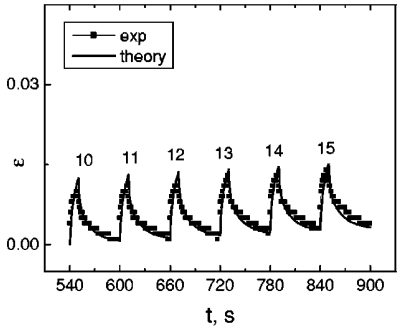

(b)

FIG. 6. Development of the surface deformation during the first six pulses of light exposure (a) and the last pulses in the series (b): experiment (see Ref. 15) and one-dimensional theory (using $N=3$). $t_1=10$ s.

ciency slightly increased after the pump laser was turned off in the case of long irradiation. This change of behavior can be explained in the frame of scattering theory proposed by Pietsch.[26] This theory shows that the scattering amplitude of the first order VIS grating peak is a complex difference of two Bessel functions. The first function varies with the amplitude of the SRG and the second one with the amplitude of density grating. Depending on the film thickness these gratings can be in phase or out of phase (when $h_0 \sim 0.5\ \mu$m). In the latter case the density jumps increase slightly with every subsequent pulse, leading to a change in the sign of response at some moment.

IV. OUTLOOK

Our modeling was carried out using the linear viscoelastic model, which describes only small deformations adequately. When deformations become comparable with the initial film thickness the model produces an unphysical increase of density, especially in the region of relief troughs. Moreover, the linear analysis predicts no difference in the inscription processes performed at small and large laser powers, which is in contradiction with the observations.[27] To overcome these drawbacks we propose to carry out the FEM using a slightly compressible nonlinear Ogden model.

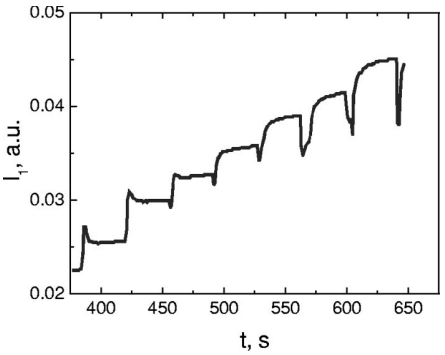

FIG. 7. First order VIS grating peak intensity during short pulse exposure.

ACKNOWLEDGMENTS

This work was supported by the DFG under Grants No. Pi217/17-3 and No. 436 RUS 17/16/03. M.S. acknowledges support from Russian Foundation for Fundamental Research (Grant No. 02-03-33135). The authors are very thankful to Dr. Paul Rochon for supporting the VIS scattering experiment (Fig. 7).

APPENDIX: FORCE DENSITY OF INHOMOGENEOUS ELECTRIC FIELD

The optically induced gradient force density (averaged over time) is given by[6,27]

$$f(r)=\langle [P(r,t)\cdot\nabla]E(r,t)\rangle, \tag{A1}$$

where $P(r,t)=\varepsilon_0\chi E(r,t)$ is the medium polarization, $\varepsilon_0=8.854\times10^{-12}\ \mathrm{C^2/(N\,m^2)}$ is the permittivity of vacuum, and $|\chi|\sim1$ is the medium susceptibility. Let us consider the case of two circularly counterpolarized beams. It is easy to show that the resulting force acts in the direction x parallel to the grating vector, and its density is equal to

$$f=-k\varepsilon_0\chi E_0^2\sin\theta(1+\cos^2\theta)\sin(kx\sin\theta), \tag{A2}$$

where 2θ is the angle between two beams and the term $k=2\pi/\lambda$ appears due to the ∇ derivative in Eq. (A1). Taking into account that $E_0^2=2Iz_0$ (I is the laser intensity and $z_0=377\ \Omega$ is the vacuum impedance) the upper estimate of f will be

$$f_{\max}=\frac{4\pi}{\lambda}\varepsilon_0 z_0\chi I. \tag{A3}$$

Typically $I=100\ \mathrm{mW/cm^2}$ and $\lambda=488$ nm. This gives a force density about $100\ \mathrm{N/m^3}$, which is two orders of magnitude smaller than the density of the gravitational force.

[1] P. Rochon, E. Batalla, and A. Natansohn, Appl. Phys. Lett. **66**, 136 (1995).
[2] D. Y. Kim, S. K. Tripathy, L. Li, and J. Kumar, Appl. Phys. Lett. **66**, 1166 (1995).
[3] C. J. Barrett, A. L. Natansohn, and P. L. Rochon, J. Phys. Chem. **100**, 8836 (1996).
[4] X. L. Jiang, L. Li, J. Kumar, D. Y. Kim, V. Shivshankar, and S. K. Tripathy, Appl. Phys. Lett. **68**, 2618 (1996).
[5] C. L. Barrett, P. L. Rochon, and A. L. Natansohn, J. Chem. Phys. **109**, 1505 (1998).
[6] J. Kumar, L. Li, X. L. Jiang, D. Y. Kim, T. S. Lee, and S. Tripathy, Appl. Phys. Lett. **72**, 2096 (1998).

[7] O. Baldus, A. Leopold, R. Hagen, T. Bieringer, and S. J. Zilker, J. Chem. Phys. **114**, 1344 (2001).
[8] P. Lefin, C. Fiorini, and J.-M. Nunzi, Pure Appl. Opt. **7**, 71 (1998).
[9] T. G. Pedersen, P. M. Johansen, N. C. R. Holme, P. S. Ramanujam, and S. Hvilsted, Phys. Rev. Lett. **80**, 89 (1998).
[10] C. Kulinna, S. Hvilsted, C. Hendann, H. W. Siesler, and P. S. Ramanujam, Macromolecules **31**, 2141 (1998).
[11] O. Yaroschuk, T. Sergan, J. Lindau, S. N. Lee, J. Kelly, and L.-C. Chien, J. Chem. Phys. **114**, 5330 (2001).
[12] K. Sumaru, T. Yamanaka, T. Fukuda, and H. Matsuda, Appl. Phys. Lett. **75**, 1878 (1999).
[13] T. Geue, M. Schulz, J. Grenzer, U. Pietsch, A. Natansohn, and P. Rochon, J. Appl. Phys. **87**, 7712 (2000).
[14] U. Pietsch, A. Natansohn, and P. Rochon, Adv. Mater. (Weinheim, Ger.) **12**, 1129 (2000).
[15] O. Henneberg, Th. Geue, M. Saphiannikova, U. Pietsch, P. Rochon, and A. Natansohn, Appl. Surf. Sci. **182**, 272 (2001).
[16] Th. Geue, M. Saphiannikova, O. Henneberg, U. Pietsch, P. Rochon, and A. Natansohn, Phys. Rev. E **65**, 052801 (2002).
[17] F. L. Labarthet, T. Buffeteau, and C. Sourisseau, J. Chem. Phys. B **1998**, 2655.
[18] T. Fukuda, H. Matsuda, T. Shiraga, T. Kimura, M. Kato, N. K. Viswanathan, J. Kumar, and S. K. Tripathy, Macromolecules **33**, 4220 (2000).
[19] M. Doi and S. F. Edwards, *The Theory of Polymer Dynamics* (Clarendon, Oxford, 1986).
[20] R. H. Boyd and P. J. Phillips, *The Science of Polymer Molecules* (Cambridge University Press, Cambridge, Great Britain, 1993).
[21] N. Mechau, D. Neher, V. Börger, H. Menzel, and K. Urayama, Appl. Phys. Lett. **81**, 4715 (2002).
[22] N. Mechau (private communication).
[23] S. B. Sane and W. G. Knauss, Mech. Time-Depend. Mater. **5**, 325 (2001).
[24] T. Ikawa, T. Mitsuoka, M. Hasegawa, M. Tsuchimori, O. Watanabe, Y. Kawata, C. Egami, O. Sugihara, and N. Okamoto, J. Phys. Chem. B **104**, 9056 (2000); C.-D. Keum, T. Ikawa, M. Tsuchimori, and O. Watanabe, Macromolecules **36**, 4916 (2003).
[25] O. Henneberg, Th. Geue, M. Saphiannikova, U. Pietsch, L. F. Chi, P. Rochon, and A. Natansohn, Appl. Phys. Lett. **79**, 2357 (2001).
[26] U. Pietsch, Phys. Rev. B **66**, 155430 (2002).
[27] S. Bian, J. M. Williams, D. Y. Kim, L. Li, S. Balasubramanian, J. Kumar, and S. Tripathy, J. Appl. Phys. **86**, 4498 (1999).

Nonlinear Effects during Inscription of Azobenzene Surface Relief Gratings

Marina Saphiannikova,* Oliver Henneberg, Thomas M. Geue, and Ullrich Pietsch

Institute of Physics, University of Potsdam, Am Neuen Palais 10, 14469 Potsdam, Germany

Paul Rochon

Department of Physics, Royal Military College, Kingston, Ontario, Canada K7L 3N6

Received: December 16, 2003; In Final Form: July 14, 2004

Surface relief gratings were inscribed on azobenzene polymer films using a pulselike exposure of an Ar^+ laser. The inscription process was initiated by a sequence of short pulses followed by much longer relaxation pauses. The development of the surface relief grating was probed by a He−Ne laser measuring the scattering intensity of the first-order grating peak. The growth time of the surface relief grating was found to be larger than the length of the pulses used. This unusual behavior can be considered as a nonlinear material response associated with the trans−cis isomerization of azobenzene moieties. In this study the polymer stress was assumed to be proportional to the number of cis-isomers. One-dimensional viscoelastic analysis was used to derive the polymer deformation. The rate of trans−cis isomerization increases with the intensity of the inscribing light; in the dark it is equal to the rate of thermal cis−trans isomerization. The respective relaxation times were estimated by fitting theoretical deformation curves to experimental data.

Introduction

The first inscriptions of surface relief gratings (SRGs) on azobenzene polymer films were performed independently in 1995 by Rochon et al.[1] and Kim et al.[2] Several models have been proposed to explain the origin of the inscribing force,[3−8] but none of them describes satisfactory the mass polymer transport at a molecular level. The most promising model is based on the interaction of induced electric dipoles with an inhomogeneous electric field.[4] This model explains the magnitude of SRGs obtained for different combinations of polarization states of the inscribing beams. However, the force density estimated for conventional lasers is 2 orders of magnitude smaller than that of the gravitational force (10^4 N/m^3) and, thus, too small to be of influential importance.[9] Besides, this electric force cannot explain the experiment described in the present study. Here we have chosen a pulselike illumination to resolve the time evolution of SRG formation and found that the grating amplitude continues to grow after switching off the pumping laser. This experiment clearly indicates that the inscribing light provides a momentum that is partially maintained in the dark and is able to push polymer molecules over distances that are comparable with the molecular length.

Presently, there is no doubt that multiple trans−cis and cis−trans photoisomerizations of the azobenzene moieties are the trigger of the inscription process. However, both photoisomerization processes stop immediately when the inscribing laser is switched off. The only process that is still continuing in the absence of irradiation is a much slower cis−trans thermal relaxation. The rate constants depend mostly on the type of chromophore and the type of its attachment to the polymer backbone.[10] Relaxation times between 10 s and 12 h have been estimated for a variety of azobenzene polymers.[10−12] In the present study we explain the maintaining growth process in the dark by this slow cis−trans thermal relaxation and determine its relaxation time by fitting an appropriate model to experimental data. The proposed model is an adaptation of our recent viscoelastic approach[9] to the case of short time exposures.

Experiment

For the present investigations we used an azobenzene side-chain homopolymer pDR1M (poly{(4-nitrophenyl)[4-[[2-(methacryloyloxy)ethyl]ethylamino]phenyl]diazene}). This amorphous polymer was dissolved in tetrahydrofurane (5 mass %) and then spun on a clean glass substrate at spins of 1500−2000 rpm. The film thickness was measured with a Dektak II depth profiler to be about 500 nm.

SRGs were inscribed onto the polymer films using the interference pattern of two plane waves. They were produced by contracircularly polarized beams from an Ar^+ laser operating at the wavelength of 488 nm and at a power density of 0.1−2.5 W/cm^2 on the film surface. The angle between the beams was chosen to be 30°. At this angle intensity, modulations and a slight ellipticity of the resulting polarization in the interference pattern can be neglected.[13] Thus, the pattern can be considered as a linear polarization pattern with a resulting vector of the electric field rotating along the grating vector.

A sequence of short pulses followed by much longer relaxation pauses was utilized for the inscription process (Figure 1). Hereby we do not expect a local heating of our samples. Recent measurements using an electromechanical spectroscopy method[14] have revealed that the softening temperature for a thin azobenzene film reduces only by 12 K under homogeneous illumination with 2.4 W/cm^2. On the other hand, a temperature modeling study[15] predicts a temperature rise of about 1 K during short time irradiation (1 s at 1 W/cm^2). Even if we use this overestimate but consider very long pauses between pulses (10 s at power densities above 1 W/cm^2), it becomes clear that the local heating of samples can be neglected in the present investigations. Also we did not observe photobleaching of the

10.1021/jp0378788 CCC: $27.50
Published on Web 08/28/2004

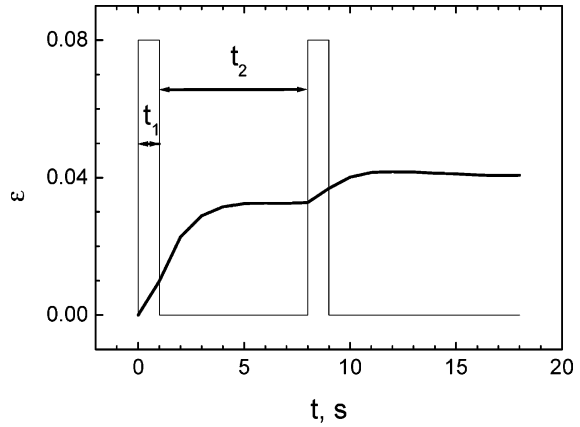

Figure 1. Dependence of the relative deformation $\epsilon(t)$ on the inscription time t: only the first two pulses are shown (thick line). The thin line represents a pulse sequence with the pulse length $t_1 = 1$ s and the pause between pulses $t_2 = 7$ s. $I_p = 1.25$ W/cm^2.

illuminated area at high power densities, because the exposed dose was always very low and did not exceed 25 J/cm^2.

The gradual development of the SRG was probed in situ by a He−Ne laser. After inscription, the film was scanned with an atomic force microscope. This measurement revealed SRGs with a minimum amplitude of about 10 nm. In this study we neglect birefringence effects which were observed for a functionalized polymer in the few first seconds of illumination.[16] These effects are responsible for a strong increase of the diffraction intensity at the very beginning of illumination. However, birefringence only appears under illumination, it cannot explain that the grating amplitude continues to grow after switching the light off. Neglecting the birefringence grating, the first-order scattering intensity is proportional to the Bessel function of the first order

$$I_1 = J_1^2(\Delta\psi) I_0 \tag{1}$$

where I_0 is the specular intensity, $\Delta\psi = \pi n_p A/\lambda_{red}$, $n_p = 1.66$ is the refractive index of the azobenzene polymer, A is the amplitude of the SRG, and $\lambda_{red} = 633$ nm is the wavelength of the probing He−Ne laser. The relative deformation, $\epsilon(t) = A(t)/L$, caused by a sequence of very short pulses is small. Thus, $I_1/I_0 \approx \Delta\psi^2/4$, and relative deformations can be calculated from measured intensities as follows

$$\epsilon(t) = 2(I_1/I_0)^{0.5} \frac{\lambda_{red}}{\pi n_p L} \tag{2}$$

where $L \approx 500$ nm is the sample thickness.

Theoretical Approach

Generally the polymer deformation can be described by[17]

$$\epsilon(t) = \int_0^t J(t-u) \frac{d\sigma(u)}{du} du \tag{3}$$

where $\sigma(t)$ is the stress at the time t and $J(t)$ is the creep compliance of the material obtained from a simple single step loading creep test. It was calculated previously for a model with one, two, and three relaxation times.[9] The choice between two latter models will not affect the outcome of our approach qualitatively. Therefore, to keep the number of fit parameters small we only consider a model with two relaxation times, τ_1 and τ_2. In this model the stress relaxation modulus consists of two components

$$G(t) = G_1 e^{-t/\tau_1} + G_2 e^{-t/\tau_2} \tag{4}$$

and the creep compliance is defined by

$$J(t) = \frac{1}{G_0}\left[\frac{t}{g_0} + \frac{g_1}{g_0} + C\exp(-\omega_0 t)\right] \tag{5}$$

where $G_0 = G_1 + G_2$, $g_0 = G_1\tau_1 + G_2\tau_2$, $g_1 = G_1\tau_1^2 + G_2\tau_2^2$, $\omega_0 = g_0/\tau_1\tau_2$, and $C = (-\omega_0 + \tau_1^{-1})(-\omega_0 + \tau_2^{-1})/\omega_0^2$.

To solve eq 3 we have to define the relation between polymer stress and the pulse sequence used. It was already proposed by Barrett et al.[3] that the origin of the pressure experienced in the material is due to the excess free volume required for isomerization from the compact trans isomer to the bulkier cis isomer. To take into account polarization effects, this model assumes that pressure is proportional not only to the cis isomer population but also to a polarization activity factor which changes along the grating vector. In our one-dimensional approach, we follow a similar hypothesis assuming that the polymer stress, σ, averaged over one grating period is proportional to the molecular density of cis isomers, n.

By use of a hole-burning model[18,19] n can be expressed as follows (see Appendix)

$$\frac{\partial n(t)}{\partial t} = -(5k_T I_p + \tau_c^{-1}) n(t) + k_T I_p N \tag{6}$$

where N is the total density of chromophores, I_p is the intensity of the pumping beam in W/cm^2, and $k_T = \Phi_{TC}\sigma_T$. Here Φ_{TC} is the quantum yield of the direct trans−cis isomerization and σ_T is the average cross section of the trans isomers. τ_c^{-1} is the rate of the cis−trans thermal back relaxation. In the presence of the pumping beam the molecular density changes according to

$$n_1(1,t) = n_{sat}(1 - e^{-t/\tau_p})$$

for the first pumping cycle

$$n_1(i,t) = (n_2(i-1,t_2) - n_{sat})e^{-t/\tau_p} + n_{sat} \tag{7}$$

for the ith pumping cycle, and in absence of the pumping beam it changes to

$$n_2(i,t) = n_1(i,t_1)e^{-t/\tau_c}$$

for the ith pumping cycle. Here $n_{sat} = k_T I_p N \tau_p$ is the molecular density of cis isomers at the saturation limit for a given intensity of the inscribing laser, $\tau_p^{-1} = 5k_T I_p + \tau_c^{-1}$ where τ_p^{-1} is the rate of the trans−cis isomerization, t_1 is the pulse length, and t_2 is the pause between two pulses. It is obvious that in the absence of the pumping beam, the maximum value of τ_p is equal to τ_c and it decreases with the intensity of the pumping beam.

The stress derivative in eq 3 can be expressed as

$$\frac{d\sigma(t)}{dt} = \frac{dn_k(i,t)}{dt} = p_i^k e^{-(t-u_i^k)/\tau_k} \tag{8}$$

where $p_1^1 = n_{sat}/\tau_p$, $p_i^1 = (n_{sat} - n_2(i-1,u_i^1))/\tau_p$, and $p_i^2 = -n_1(i,u_i^2)/\tau_c$. Here $u_i^1 = T(i-1)$ and $u_i^2 = u_i^1 + t_1$, $T = t_1 +$

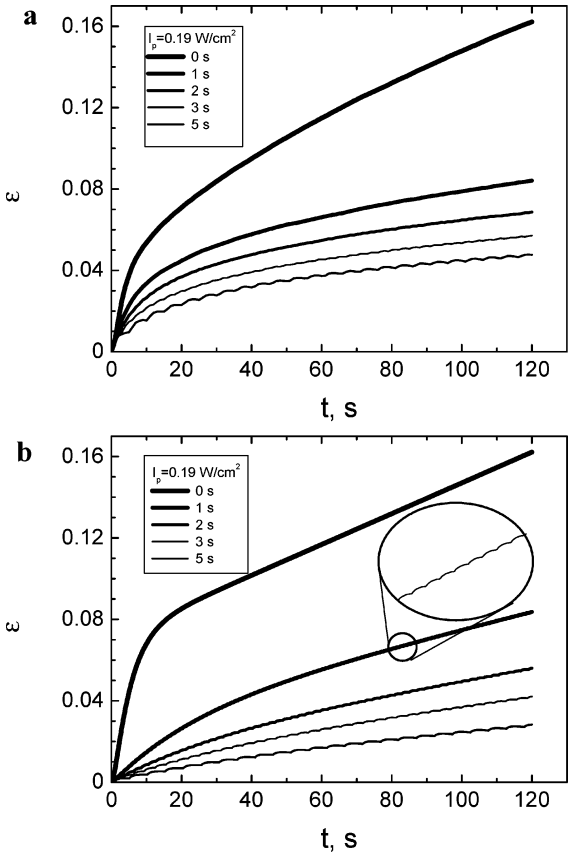

Figure 2. Dependence of the relative deformation $\epsilon(t)$ on the inscription time t: (a) experiment and (b) theory. Pulse length: $t_1 = 0.125$ s. Pause between pulses: $t_2 = 0$ s (continuous exposure), 1, 2, 3, and 5 s. $I_p = 0.19$ W/cm^2.

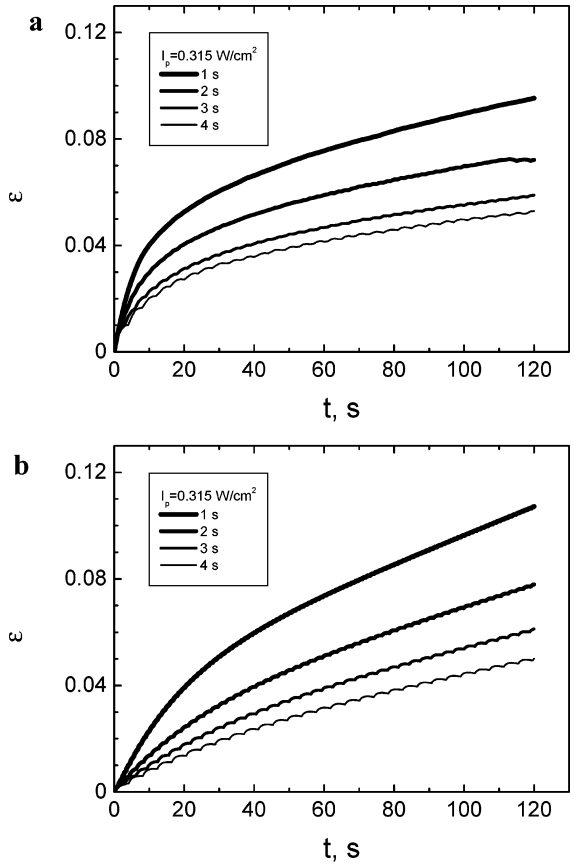

Figure 3. Dependence of the relative deformation $\epsilon(t)$ on the inscription time t: (a) experiment and (b) theory. Pulse length: $t_1 = 0.125$ s. Pause between pulses: $t_2 = 1$ s, 2, 3, and 4 s. $I_p = 0.315$ W/cm^2.

t_2. Together with the Boltzmann superposition principle[17] eq 3 gives

$$\epsilon(t) = \sum_{i=1}^{N} \begin{bmatrix} \int_{T(i-1)}^{T(i-1)+t_1} J(t-u) p_i^1 e^{-u/\tau_p}\, du + \\ \quad \int_{T(i-1)+t_1}^{Ti} J(t-u) p_i^2 e^{-u/\tau_c}\, du + \\ + \int_{Ti}^{t} J(t-u) p_{i+1}^1 e^{-u/\tau_p}\, du, \qquad 0 \le t \le t_1 \\ + \int_{Ti}^{Ti+t_1} J(t-u) p_{i+1}^1 e^{-u/\tau_p}\, du + \\ \quad \int_{Ti+t_1}^{t} J(t-u) p_{i+1}^2 e^{-u/\tau_c}\, du, \qquad t_1 \le t \le t_2 \end{bmatrix} \tag{9}$$

Substitution of eq 5 in eq 9 leads to a final solution which was solved numerically using a recursive Fortran program.

Results

Our experimental data can be divided into two groups.

In the first group the pulse length, t_1, was kept constant but the pause between pulses, t_2, was gradually increased. Experimental data for $t_1 = 0.125$ s and $I_p = 0.19$ W/cm^2 are presented in Figure 2a. For $t_2 = 5$ s moments of time when the inscribing laser is switched on can be recognized as local minima on the $\epsilon(t)$ curve. The SRG grows continuously far beyond the length of the pulse. Therefore, it becomes difficult to distinguish between subsequent pulses if the pause between them is smaller than 3 s. For shorter pauses between pulses (1 and 2 s) the deformation curves are very smooth. They appear to be similar to the curve obtained under continuous inscription. The relative deformations accumulated after a long series of pulses are approximately half of the value achieved under continuous inscription. A qualitatively similar behavior was observed for $t_1 = 0.125$ s and $I_p = 0.315$ W/cm^2 (Figure 3a). Pulses can be usually recognized if the pause between them is 3 or 4 s. Again, shorter pauses provide smooth deformation curves.

In the second group of experiments the pulse length, t_1, was gradually decreased but the pause between pulses, t_2, was kept constant. The typical behavior is shown for $t_2 = 10$ s and $I_p = 1.25$ W/cm^2 (Figure 4a). The lowest curve corresponds to the shortest pulse length, $t_1 = 0.125$ s, and the highest one to the longest pulse length, $t_1 = 1$ s. However, differences in shape between the deformation curves are small. The inscription part is nearly as long as the relaxation part: about 3 s for the shortest pulse and about 5 s for the longest one. This unusual behavior can be considered as a nonlinear material response. In a linear case we would expect that the length of the relaxation part is equal to the length of a pause between pulses. We observed linear behavior at much lower powers of the inscription laser.[9]

The inscription part of the deformation curve can be slightly reduced if pulses become ultrashort. An example of such reduction is presented for $t_2 = 10$ s and $I_p = 2.5$ W/cm^2 (Figure 5a). The lowest curve corresponds to the shortest pulse length, $t_1 = 0.005$ s; the inscription part is about 1 s. The highest curve corresponds to the longest pulse length, $t_1 = 0.125$ s; the inscription part is about 5 s.

The nonlinear behavior of the deformation curves can be reproduced using the theory presented in the Theoretical

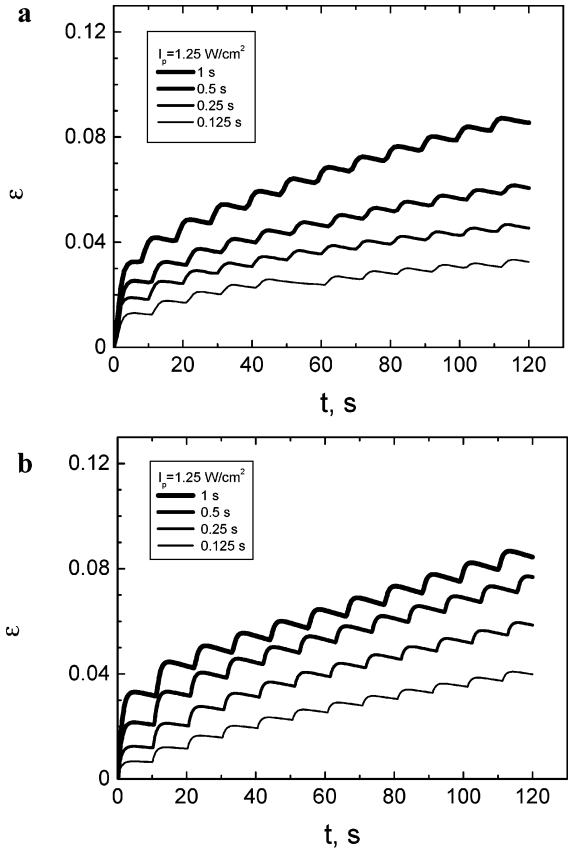

Figure 4. Dependence of the relative deformation $\epsilon(t)$ on the inscription time t: (a) experiment and (b) theory. Pulse length: $t_1 = 1$, 0.5, 0.25, and 0.125 s. Pause between pulses: $t_2 = 10$ s. $I_p = 1.25$ W/cm^2. The longer plateau in the lowest curve of part a of the figure is an experimental error.

Approach. After multiple fitting the following set of parameters was chosen for the description of the experimental data:

$$\tau_c = 50 \text{ s}, \qquad k_T = 0.2 \text{ cm}^2/\text{J}$$
$$G_1/G_0 = 0.9, \qquad G_2/G_0 = 0.1$$
$$\tau_1 = 0.1 \text{ s}, \qquad \tau_2 = 100 \text{ s}$$

Corresponding fitting results are presented in Figures 2−5b. The theory reproduces quite satisfactory the form of the deformation curves for all intensities of the pumping beam. However, it underestimates their initial slopes due to neglect of birefringence effects. On the other hand, it is known that the cis−trans thermal back relaxation is not strictly monoexponential but exhibits an anomalous fast component for the first few seconds.[10] The hole-burning model utilized in this study, however, assumes a monoexponential decay in the absence of irradiation. This can also lead to some discrepancies between experimental and calculated data.

Discussion

In this study we assume that the polymer stress is proportional to the number of cis isomers, $n(t)$. Hence, a saturation value of stress will be achieved when $n(t) = n_{sat}$. The fraction of cis isomers, $f = n_{sat}/N$, increases with the inscription intensity (see also Figure 6)

$$f = \frac{1}{5 + (k_T I_p \tau_c)^{-1}} \tag{10}$$

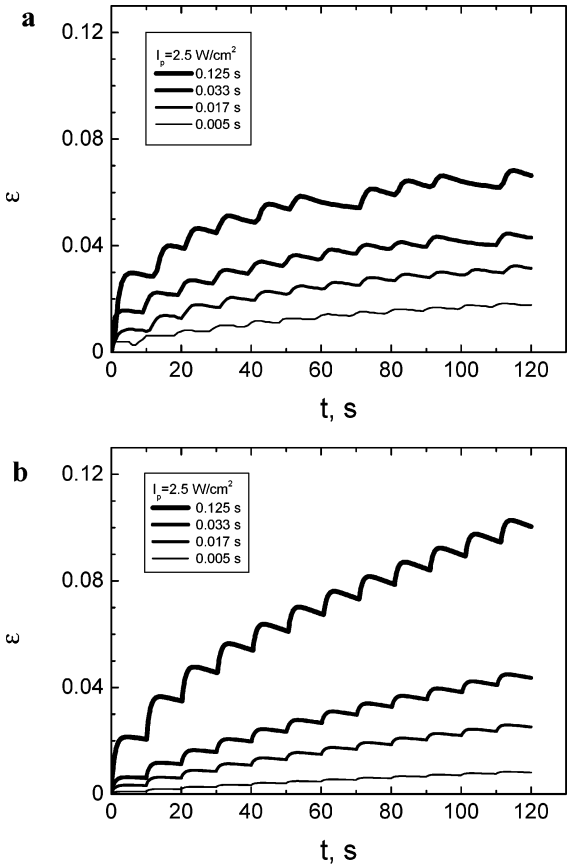

Figure 5. Dependence of the relative deformation $\epsilon(t)$ on the inscription time t: (a) experiment and (b) theory. Pulse length: $t_1 = 0.125$, 0.033, 0.017, and 0.005 s. Pause between pulses: $t_2 = 10$ s. $I_p = 2.5$ W/cm^2. The longer plateaus in the upper curve of part a of the figure are an experimental error.

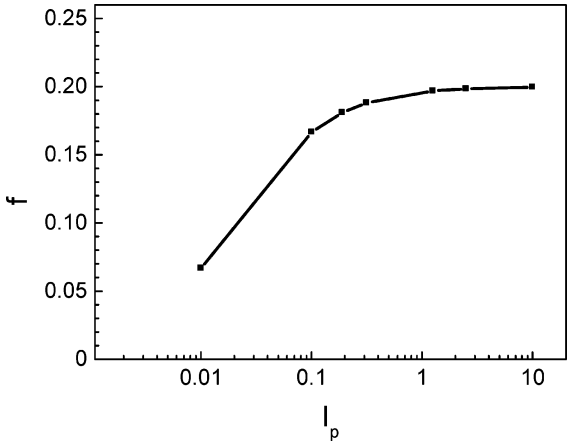

Figure 6. Dependence of the cis isomer fraction f on the inscription intensity I_p.

At high inscription intensities f saturates to about 0.2. This saturation value is entirely defined by the ratio $k_C/k_T = 4$ (see Appendix). A smaller ratio of k_C/k_T will not affect the time dependencies, but the estimated fraction of cis isomers will become larger (for example, $f = 0.25$ follows from $k_C/k_T = 3$). Our saturation value is in fairly good agreement with ref 12 for poly[4-[2-(methacryloyloxy)ethyl]azobenzene], where a saturation value of 0.19 was obtained. The authors also used a hole-burning model but did not consider the cis−trans thermal back relaxation. Therefore, in their study f did not depend on the inscription intensity.

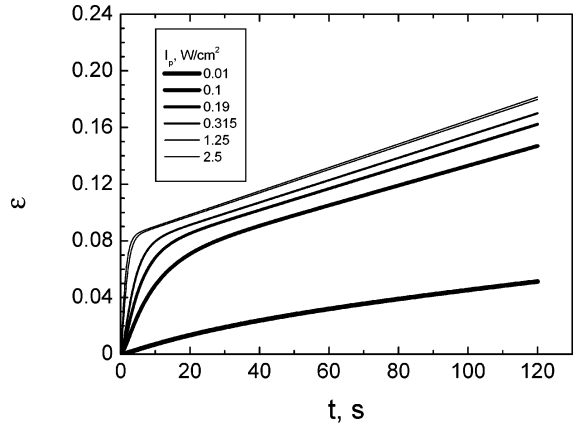

Figure 7. Theoretical dependence of the relative deformation $\epsilon(t)$ on the inscription time t. Continuous exposure. $I_p = 0.01$, 0.1, 0.19, 0.315, 1.25, and 2.5 W/cm^2.

How fast $n(t)$ will reach its saturation value depends on the rate of trans−cis isomerization, $\tau_p^{-1} = 5k_T I_p + \tau_c^{-1}$. Thus, τ_p is also a function of the inscription intensity. In our case it is equal to 4.8 s for $I_p = 0.19$ W/cm^2, 3.0 s for $I_p = 0.315$ W/cm^2, 0.8 s for $I_p = 1.25$ W/cm^2, and 0.4 s for $I_p = 2.5$ W/cm^2.

The theory presented utilizes a nonlinear force model: the force is saturated at high intensities of the inscription laser. For illustration purposes we calculated deformation curves under continuous exposure for different intensities (Figure 7). Polymer deformation (achieved after 120 s) can be significantly enhanced by increasing I_p as far as $I_p < 0.1$ W/cm^2. At higher inscription intensities the number of cis-isomers starts to saturate (see also Figure 6). As a result of increasing I_p from 0.1 to 2.5 W/cm^2, the polymer deformation can be enhanced only by a few percent. The curves for $I_p = 1.25$ W/cm^2 and $I_p = 2.5$ W/cm^2 are nearly undistinguishable. This result correlates with the intensity dependence of SRG formation measured for a number of azobenzene-functionalized polymers.[20] The inscription rate was saturated at a power of about 0.01 W/cm^2 and was found to be independent of either the degree of azo functionalization or chemical structure. In all cases, Disperse Red 1 (DR-1) was used as the chromophore which led the authors to conclusion that only the photoisomerization dynamics of DR-1 defines the saturation intensity. The polymer used in our study is also functionalized with DR-1; however we obtained a higher estimate of the saturation intensity.

To fit the theoretical model to the experimental data, we have used $\tau_c = 50$ s. From absorption measurements for pDR1M τ_c was found to be about 10 s.[10] Thus, our estimation of the cis−trans thermal relaxation time has the same order of magnitude as this experimental value. The remaining quantitative discrepancy can be again assigned to model simplifications discussed above.

Acknowledgment. This work was supported by the DFG under Grant Pi217/17-3 and 436 RUS 17/16/03. We further would like to acknowledge fruitful discussions with Dr. S. Stockhause.

Appendix. Hole-Burning Model

The hole-burning model is described in detail in ref 12. According to this model the number density of trans isomers, $n_T(t)$, is connected with the number density of cis isomers, $n_C(t)$, via the differential equation

$$\frac{\partial n_T(\theta)}{\partial t} = -\Phi_{TC} P_T(\theta) n_T(\theta) + \Phi_{CT} P_C(\theta) n_C(\theta) + \gamma n_C(\theta) \quad \text{(A1)}$$

where Φ_{TC} and Φ_{CT} are the quantum yields of the direct trans−cis and reverse cis−trans isomerization, respectively, P_T and P_C are the probabilities of the absorption of a photon by a molecule in the trans and cis state, respectively, and $\gamma = \tau_c^{-1}$ is the rate of the cis−trans thermal back relaxation.

For linear polarized light the probability of absorption is given by

$$P_J(\theta) = I\sigma_J[1 + 2e_J P_2(\cos\theta)] \quad \text{(A2)}$$

where σ_J and e_J are the average absorption cross section and the molecular anisotropy of trans (J = T) and cis (J = C) isomers, respectively. At the beginning of the inscription process, the number of cis isomers is negligible and trans isomers are distributed randomly in the polymer matrix. Further, we assume that a sequence of very short pulses followed by much longer relaxation pauses does not result in any preferential orientation of the isomers

$$\begin{cases} n_C(\theta,t) = n(t) & t > 0 \\ n(t) = 0 & t = 0 \end{cases}$$

and

$$n_T(\theta,t) = \frac{N}{2} - n(t) \quad \text{(A3)}$$

where N is the total molecular density of chromophores.

Upon integrating eq A2 over θ, the probability of absorption can be expressed

$$P_J(\theta) = 2I\sigma_J \quad \text{(A4)}$$

since

$$\int_0^\pi P_2(\cos\theta)\sin\theta\, d\theta = 0$$

and eq A1 can be transformed into

$$\frac{\partial n(t)}{\partial t} = -(\Phi_{TC}\sigma_T I + \Phi_{CT}\sigma_C I + \gamma)n(t) + \Phi_{TC}\sigma_T IN \quad \text{(A5)}$$

This equation can be further simplified considering values of the average absorption cross section and the quantum yield of the direct and reverse photoisomerization at $\lambda_{blue} = 488$ nm (the wavelength of the Ar inscribing laser)[21]

$$\sigma_C/\sigma_T = 0.51, \quad \Phi_{CT} = 0.7 \pm 0.1, \quad \Phi_{TC} = 0.11 \pm 0.03 \quad \text{(A6)}$$

Introducing $k_T = \Phi_{TC}\sigma_T$ and $k_C = \Phi_{CT}\sigma_C$, one receives $k_C/k_T = 3.3 \pm 1.4$. If we choose $k_C = 4k_T$, then eq A5 can be rewritten as follows

$$\frac{\partial n(t)}{\partial t} = -(5k_T I + \gamma)n(t) + k_T IN \quad \text{(A7)}$$

References and Notes

(1) Rochon, P.; Batalla, E.; Natansohn, A. *Appl. Phys. Lett*. **1995**, *66*, 136.

(2) Kim, D. Y.; Tripathy, S. K.; Li, L.; Kumar, J. *Appl. Phys. Lett.* **1995**, *66*, 1166.

(3) Barrett, C. L.; Rochon, P. L.; Natansohn, A. L. *J. Chem. Phys*. **1998**, *109*, 1505.

(4) Kumar, J.; Li, L.; Jiang, X. L.; Kim, D. Y.; Lee, T. S.; Tripathy, S. *Appl. Phys. Lett*. **1998**, *72*, 2096.

(5) Baldus, O.; Leopold, A.; Hagen, R.; Bieringer, T.; Zilker, S. J. *J. Chem. Phys*. **2001**, *114*, 1344.

(6) Lefin, P.; Fiorini, C.; Nunzi, J.-M. *Pure Appl. Opt*. **1998**, *7*, 71.

(7) Pedersen, T. G.; Johansen, P. M.; Holme, N. C. R.; Ramanujam, P. S.; Hvilsted, S. *Phys. Rev. Lett*. **1998**, *80*, 89.

(8) Bublitz, D.; Fleck, B.; Wenke, L. *Appl. Phys. B* **2001**, *72*, 931.

(9) Saphiannikova, M.; Geue, T. M.; Henneberg, O.; Morawetz, K.; Pietsch, U. J. *Chem. Phys*. **2004**, *120*, 4039.

(10) Barrett, C.; Natansohn, A.; Rochon, P. *Chem. Mater*. **1995**, *7*, 899.

(11) Ramanujam, P. S.; Hvilsted, S.; Zebger, I.; Siesler, H. W. *Macromol. Rapid Commun*. **1995**, *16*, 455.

(12) Buffeteau, T.; Lagugne-Labarthet, F.; Pezolet, M.; Sourisseau, C. *Macromolecules* **2001**, *34*, 7514.

(13) Lagugne-Labarthet, F.; Buffeteau, T.; Sourisseau, C. *Appl. Phys. B* **2002**, *74*, 129.

(14) Mechau, N.; Neher, D.; Börger, V.; Menzel, H.; Urayama, K. *Appl. Phys. Lett.* **2002**, *81*, 4715.

(15) Yager, K. G.; Barrett, C. J. *J. Chem. Phys*. **2004**, *120*, 1089.

(16) Lagugne-Labarthet, F.; Buffeteau, T.; Sourisseau, J. *Phys. Chem. B* **1998**, *102*, 2654.

(17) Ferry, J. D. *Viscoelastic properties of polymers*; John Wiley & Sons: New York, 1980.

(18) Sekkat, Z.; Dumont, M. *Synth. Met*. **1993**, *54*, 373.

(19) Dumont, M.; Osman, A. E. *Chem. Phys*. **1999**, *245*, 437.

(20) Fukuda, T.; Matsuda, H.; Shiraga, T.; Kimura, T.; Kato, M.; Viswanathan, N. K.; Kumar, J.; Tripathy, S. K. *Macromolecules* **2000**, *33*, 4220.

(21) Loucif-Saibi, R.; Nakatani, K.; Delaire, J. A.; Dumont, M.; Sekkat, Z. *Chem. Mater.* **1993**, *5*, 229.

Dielectric and Mechanical Properties of Azobenzene Polymer Layers under Visible and Ultraviolet Irradiation

Norman Mechau, Marina Saphiannikova,* and Dieter Neher

Institute of Physics, University of Potsdam, Am Neuen Palais 10, 14469 Potsdam, Germany

Received October 7, 2004; Revised Manuscript Received February 23, 2005

ABSTRACT: Photoinduced changes in the mechanical and dielectric properties of azobenzene polymer films were measured utilizing the method of electromechanical spectroscopy. The measurements revealed a strong correlation between the time-dependent behavior of the plate compliance and the dielectric constant under irradiation. Actinic light causes a light softening of the film that also manifests itself in the increase of the dielectric constant, whereas ultraviolet irradiation results in an initial plasticization of the film followed by its hardening. The latter is accompanied by decrease of the dielectric constant. A semiquantitative model based on the kinetics of the photoisomerization process in azobenzene polymers is proposed. We assume that both visible and ultraviolet irradiation increase the free volume in the layer due to photoisomerization. Additionally, ultraviolet light increases the modulus of the polymer matrix due to the presence of a high density of azobenzene moieties in the cis state. These assumptions allowed us to reproduce the time-dependent behavior of the bulk compliance as well as the dielectric constant at different irradiation intensities, for both visible and ultraviolet light, with only two adjustable parameters.

Introduction

The first inscriptions of surface relief gratings (SRGs) on azobenzene polymer films were reported independently in 1995 by two research groups.[1,2] Inscription was done by exposing the sample to a periodic intensity or polarization pattern that resulted from the interference of two polarized laser beams. The wavelength of the laser was in the absorption region associated with the cyclic trans−cis−trans isomerizations of the azo dye. Most important, the absorption of light on this wavelength induced material flow over micrometer distances even at room temperature, which is well below the glass transition temperature, T_g, of the investigated polymers.

Several models[3−8] have been proposed to explain the origin of the inscribing force (see review in ref 9), but none of them describe satisfactorily the light-induced motion of the azobenzene polymers at a molecular level.[10] In all models, to explain the mass transport over micrometer distances during irradiation at room temperature, it is necessary to assume a considerable degree of photoinduced plasticization, at least comparable with that at the glass transition. For example, it has been proposed, in a linear viscoelastic analysis of the dynamics of SRG formation, that the Young's modulus of the azobenzene polymer film must be reduced by 3 orders of magnitude under illumination with actinic light.[10,11] However, only very weak plasticization has been found in mechanical experiments performed recently in our group.[12,13] At room temperature, a less than 10% increase of the plate compliance upon homogeneous illumination with actinic light was observed. This is far below the degree of "softening" induced by heating the same layer above T_g. These results suggest that illumination of an azobenzene polymer layer with actinic light cannot induce a transition into a macroscopic low-viscosity melt.

Presently, there is no doubt that multiple trans−cis and cis−trans photoisomerizations of the azobenzene moieties are involved in the light-induced material flow. In many studies the softening effect was attributed to this rapid cycling between two conformations of the azobenzene moieties. Interestingly, using low-intensity ultraviolet light, Srikhirin et al.[12] observed an opposite effect: the film compliance decreased by a few percent. The authors argued that cis isomers somehow harden the material when illuminated with ultraviolet light.

Until now, photoinduced mechanical changes in azobenzene polymers have been explained empirically.[12,13] The reason is that neither photoisomerization rates nor cis fractions were estimated in the polymer film used for particular mechanical experiment. In this study we combine, for the first time, transient absorption data with the results of electromechanical and dielectric spectroscopy to gain insight into the intrinsic relationship between photokinetics and mechanical processes in the layer. Moreover, we propose a model that is capable of describing quantatively the transient behavior of the plate compliance as well as the dielectric constant under illumination at different intensities with actinic and ultraviolet light. This model seems to prove the validity of intuitive assumptions proposed previously by different authors.[12,14]

Experiment

The material investigated was an amorphous azobenzene side chain polymer, poly(2-hydroxyethyl)methacrylate-*co*-(2-(4-(4-cyanophenylazo)phenoxy)acetyl)methacrylate) (see Figure 1), with a molecular weight of 86 000 g/mol, an azo content of 52%, and a glass transition temperature $T_g = 99$ °C. Layers for transient absorption measurements were prepared from a solution of the polymer in tetrahydrofuran (2.5 wt %), which was spun at 1000 rpm onto a glass substrate. The layer thickness was 150 nm in all cases. Films for electromechanical and dielectric experiments were coated on glass slides covered with ca. 100 nm thick transparent indium−tin oxide bottom electrodes. The layer thickness was measured with a Dektak II depth profiler to be about 500 nm. After drying and annealing, several equally spaced 4 mm wide aluminum strip top electrodes (80 nm) were deposited onto the film surface by thermal evaporation.

In the electromechanical and dielectric experiments, the sample was irradiated with visible (VIS) or ultraviolet (UV) light: $\lambda_{VIS} = 488$ nm and $\lambda_{UV} = 365$ nm. In both cases a xenon lamp was used as a light source with an appropriate interfer-

10.1021/ma0479316 CCC: $30.25
Published on Web 04/02/2005

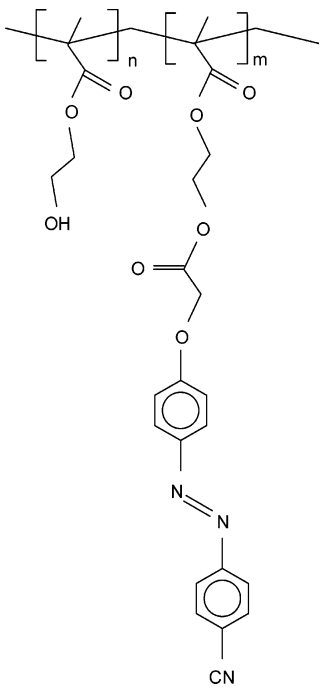

Figure 1. Chemical formula of the statistical copolymer poly-(2-hydroxyethyl)methacrylate-*co*-(2-(4-(4-cyanophenylazo)phenoxy)acetyl)methacrylate). Here $n = 48\%$ and $m = 52\%$.

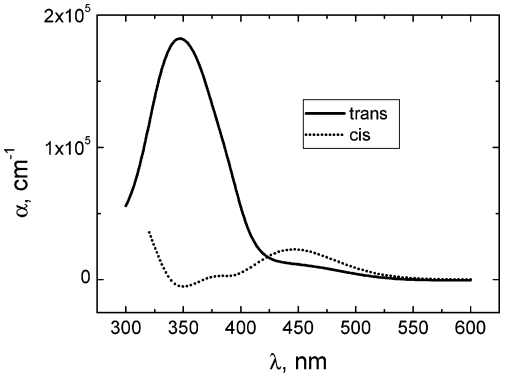

Figure 2. Absorption spectra of the investigated polymer when all chromophores are in the trans or in the cis state. The latter was calculated using the procedure described in ref 15.

ence filter. The light was unpolarized to diminish photoorientational effects. Figure 2 shows absorption spectra of the investigated polymer when all chromophores are in the trans or in the cis state. The latter was calculated from the absorption spectra of a 150 nm thick layer, using the procedure proposed in ref 15. One can see that at $\lambda_{UV} = 365$ nm mainly the trans isomers absorb the light, while at $\lambda_{VIS} = 488$ nm both isomers have comparable absorption coefficients and, thus, a cyclic trans−cis−trans isomerization takes place.

Transient absorption experiments were performed with the help of the lock-in technique. Samples were illuminated with homogeneous light of either $\lambda_{UV} = 365$ nm or $\lambda_{VIS} = 488$. The intensity at the sample was varied from 1 to 10 mW/cm^2 (for UV irradiation) and from 1 mW/cm^2 to 1 W/cm^2 (for VIS irradiation). The absorption of the polymer layer at 365 nm was probed by simultaneously illuminating the sample at $\lambda = 365$ nm with a beam of about 1 μW/cm^2. This intensity was sufficiently small to avoid any influence on the transient absorption experiment. The probing beam was chopped to create a reference signal for the lock-in detection. Its light intensity was measured using a large-area Si diode.

The photoinduced changes in the mechanical and dielectric properties of the thin azobenzene polymer films were measured by means of electromechanical spectroscopy.[16] This method utilizes the electrostriction effect, i.e., the change in thickness, Δh, of a thin polymer layer sandwiched between two electrodes upon application of the alternating electric field

$$\Delta h = Q E_0^2 h \tag{1}$$

Here, h is the initial layer thickness, E_0 is the field amplitude, and Q is the electrostriction coefficient, which is proportional to the plate compliance, β_{zz}

$$Q = -\frac{\epsilon_{vac}\beta_{zz}}{6}(3\epsilon' + (\epsilon' - 1)(\epsilon' + 2)) \tag{2}$$

where ϵ_{vac} is the vacuum susceptibility and ϵ' is the real part of the dielectric constant. The Claussius−Mosotti formula $\partial\epsilon'/\partial h = -(\epsilon' - 1)(\epsilon' + 2)/(3h)$ has been used in the derivation of eq 2.[16] This formula is valid for an isotropic material subjected to hydrostatic pressure,[17] and thus, eq 2 is an approximation for thin polymer layers.

The frequency of the alternating electric field in the electromechanical measurements was 2.5 kHz, which caused a periodic variation in layer thickness of ca. 10 pm at a frequency of 5 kHz. This thickness modulation was measured interferometrically by analyzing the field-induced phase shift of a beam from a He−Ne laser reflected at the aluminum top electrodes. Real and imaginary parts of the dielectric constant were recorded simultaneously at 2.5 kHz with a home-built setup.

Results

Plate Compliance. The plate compliance is defined by the relative change in layer thickness, $\delta h \equiv \Delta h/h$, upon application of a stress σ_{zz} normal to the layer plane

$$\delta h = \beta_{zz}\sigma_{zz} \tag{3}$$

Since, in the ideal case, the polymer layer cannot expand parallel to the substrate, β_{zz} differs from the bulk compliance β_{bulk}[18,19]

$$\beta_{zz} = \frac{1 + \nu}{3(1 - \nu)}\beta_{bulk} \tag{4}$$

with ν being Poisson's ratio. In the following, we assume that ν does not change under illumination, and thus, the relative change of bulk compliance is equal to the relative change of β_{zz}

$$\delta\beta_{zz} = \frac{\beta_{zz}(t) - \beta_{zz}(0)}{\beta_{zz}(0)} = \delta\beta_{bulk} \tag{5}$$

Here $\beta_{zz}(0)$ is the plate compliance in the dark, before the light is turned on. The value of the plate compliance was calculated from the electrostriction coefficient Q according to eq 2 utilizing the in-situ measured real part of the dielectric constant.

Figure 3 shows relative changes of the plate compliance $\delta\beta_{zz}$ under VIS and UV irradiation. When VIS light with an intensity of 1 mW/cm^2 is switched on, $\delta\beta_{zz}$ rapidly increases to a value of 0.06 and stays at this level during further irradiation. After switching off the light, $\delta\beta_{zz}$ quickly returns to its initial value in the dark. As it was already mentioned in the Introduction, UV illumination causes a complicated response. When UV light with an intensity of 1 mW/cm^2 is switched on, $\delta\beta_{zz}$ first increases rapidly but then starts to decrease gradually. After switching off the light, one observes an initial abrupt drop of $\delta\beta_{zz}$, followed by its gradual increase to the initial value in the dark.

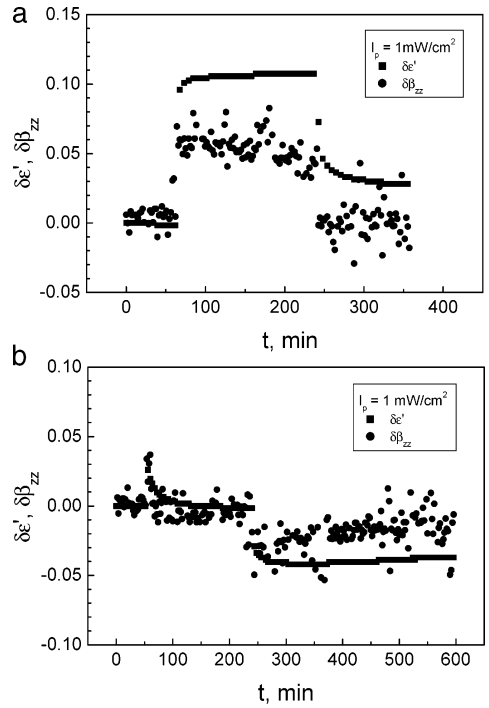

Figure 3. Time dependencies of the relative dielectric constant, $\delta\epsilon'$, and the relative plate compliance, $\delta\beta_{zz}$, under VIS (a) and UV (b) irradiation with 1 mW/cm^2.

Although these measurements of the plate compliance give a characteristic qualitative result, they can be hardly used to develop a quantitative model for two reasons. First, it is impossible to follow very rapid mechanical changes at the moments when the light is switched on or off (it takes about 2 min to measure the plate compliance). Second, the data are usually very noisy when we record changes in the film thickness that are less than 10 pm and thus are very sensitive to any vibrations.

Dielectric Constant. Fortunately, we have found a strong correlation between the time-dependent behavior of the plate compliance and the dielectric constant, under VIS as well as under UV irradiation (Figure 3). Contrary to the plate compliance, the dielectric constant can be measured with a very high accuracy and with a time resolution of about 10 s.

Figure 3 shows relative changes of the dielectric constant

$$\delta\epsilon'(t) = \frac{\epsilon'(t) - \epsilon'(0)}{\epsilon'(0) - \epsilon_\infty} \tag{6}$$

under VIS and UV irradiation. Here $\epsilon'(0)$ is the initial value of dielectric constant in the dark, and ϵ_∞ is the susceptibility at an infinitely high frequency. $\epsilon'(0)$ slightly varies from sample to sample, being about 3.2 $\pm$ 0.1. ϵ_∞ can be approximated by n^2, where n is the refractive index of polymer. In this study, n was determined by means of ellipsometry to be equal to 1.60 at 632 nm, which gives $\epsilon_\infty = 2.56$.

When VIS light with an intensity of 1 mW/cm^2 is switched on, $\delta\epsilon'$ increases within a few minutes to a value of 0.1 and stays at this level during further irradiation. After switching off the light, $\delta\epsilon'$ slowly returns to its initial value in the dark. When UV light with an intensity of 1 mW/cm^2 is switched on, $\delta\epsilon'$ first increases rapidly but then starts to decrease, approaching its value in the dark. After switching off the light, one observes an abrupt drop of the dielectric constant followed by its very slow increase to the initial value in the dark.

As it was already mentioned, relative changes of the dielectric constant and plate compliance demonstrate very similar qualitative behavior under VIS and UV irradiation (Figure 3). We suspect that the reason for these changes is common in both cases and is related to the photoisomerization process in the polymer layer. Direct light-induced heating of the layer can be excluded, since illumination with VIS and UV light causes very different behavior. Light-induced changes in the layer thickness, $\Delta h(t)$, can be also excluded as a possible source for the observed effects. For illumination with either VIS or UV light, we could not detect any change in thickness by atomic force microscopy within the resolution of ca. 1 nm (limited by the layer roughness of ca. 1 nm). Such small light-induced changes in thickness would cause only negligible variations in β and ϵ', in comparison to those found in this study.

An essential difference in the time-dependent behavior of the dielectric constant and the plate compliance can be observed after the light is switched off: the dielectric constant returns to its initial value much slower than the plate compliance. Such slow relaxation of the dielectric constant is probably caused by orientational effects, even though we tried to avoid these effects by illuminating the sample with unpolarized light. However, a certain degree of photoinduced alignment of the azobenzenes molecules in the direction perpendicular to the film surface is still possible. Therefore, when the light is switched off, the chromophores might relax back to an isotropic orientational distribution, which results in a slow change of the dielectric constant.

Theoretical Approach

Photoisomerization Kinetics. To understand transient electromechanical properties, one should first consider configurational changes of the azobenzene chromophore which take place in the polymer film under irradiation. Before the light is turned on, all chromophores are in the trans state. Under illumination with VIS or UV light, photoisomerization takes place, and the number density of trans isomers, $n_T(t)$, decreases according to the following differential equation:

$$\frac{dn_T(t)}{dt} = -k_{TC}I_p n_T(t) + k_{CT}I_p n_C(t) + \gamma n_C(t) \tag{7}$$

Here, $n_C(t)$ is the number density of cis isomers, k_{TC} is the rate constant of the trans−cis photoisomerization, k_{TC} is the rate constant of the reverse cis−trans photoisomerization, I_p is the intensity of the light in W/cm^2, and γ is the rate of the cis−trans thermal back-relaxation. If we define the cis fraction as $f_C(t) = n_C(t)/N$, where N is the total number density of chromophores, then eq 7 can be rewritten for the cis fraction as

$$\frac{df_C(t)}{dt} = -\tau_p^{-1} f_C(t) + k_{TC}I_p \tag{8}$$

Here, we have introduced $\tau_p = [(k_{TC} + k_{CT})I_p + \gamma]^{-1}$ as the characteristic time of the isomerization process. For

Table 1. Rate Constants and Absorption Coefficients for VIS and UV Illumination

	k_{TC}, cm²/J	k_{CT}, cm²/J	γ, s^{-1}	α, cm^{-1}
VIS	0.41 ± 0.05	2.9 ± 0.4	$(3.0 \pm 0.1) \times 10^{-5}$	6.6×10^3
UV	3.2 ± 0.3	2.9 ± 0.3	$(3.0 \pm 0.1) \times 10^{-5}$	1.6×10^5

the situation where light is switched on at $t = 0$, eq 8 can be easily solved, resulting in

$$f_C(t) = k_{TC} I_p \tau_p (1 - \exp(-t/\tau_p)) \quad (9)$$

On the other hand, the isomerization rate, $\dot{f}_{iso} \equiv df_{iso}/dt$, is given by

$$\dot{f}_{iso}(t) = [(k_{CT} - k_{TC})I_p + \gamma] f_C(t) + k_{TC} I_p \quad (10)$$

Thus, we define $\dot{f}_{iso}$ as the number of all isomerization events per unit of time, accounting for both trans−cis and cis−trans isomerizations. When the photostationary state is reached ($t = \infty$), the following two relations are obtained

$$f_{C,\infty} = k_{TC} I_p \tau_p \qquad \dot{f}_{iso,\infty} = 2 f_{C,\infty} \tau_C^{-1} \quad (11)$$

where $\tau_C = [k_{CT} I_p + \gamma]^{-1}$ is the effective lifetime of cis isomer under illumination.

From transient absorption measurements it is possible to determine all rate constants (see Appendix and Table 1) and calculate $f_C(t)$ and $\dot{f}_{iso}(t)$ for a given light intensity for VIS and UV irradiation. Since the studied layers were quite thick (ca. 500 nm), we took into account that the light intensity is not constant throughout the film but decreases with the penetration depth, z, according to the Lambert−Beer law

$$I_p(z) = I_p \exp(-\alpha z) \quad (12)$$

where α is the absorption coefficient at a particular wavelength (shown in Table 1) and z-axis points toward the substrate. Therefore, in eqs 9−11 an average intensity $I_p(1 - \exp(-\alpha h))/\alpha h$ was used instead of I_p. It should be noticed that α does not stay constant during VIS or UV illumination but slightly varies with time. However, in this paper we do not account for this variation because it is the second-order correction and does not affect the outcome of our approach. Comparing $f_C(t)$ and $\dot{f}_{iso}(t)$ curves calculated with the experimental parameters (see Table 1) at the same light intensity (Figure 4), two main differences between photoisomerization at VIS and UV can be noticed: (1) At λ_{VIS}, the cis fraction in the steady state is relatively small, about 0.1, while at λ_{UV}, the cis fraction is relatively high, about 0.3 at $I_p = 1$ mW/cm² and 0.5 at $I_p \geq 10$ mW/cm². (2) At λ_{VIS}, the isomerization rate is significantly higher than at λ_{UV} for $I_p \geq 10$ mW/cm². These two differences motivated us to introduce a two-component mechanical model which is capable of explaining the time dependences of the plate compliance and the dielectric constant under visible and ultraviolet irradiation.

Two-Component Mechanical Model. Let us consider an azobenzene polymer layer as a two-component system, consisting of the polymer matrix and free volume (the latter can be visualized as small voids embedded into the polymer matrix). Then, in the linear approximation, the bulk modulus of the layer, K, can be defined as

$$K = K_0(1 - a\phi) \quad (13)$$

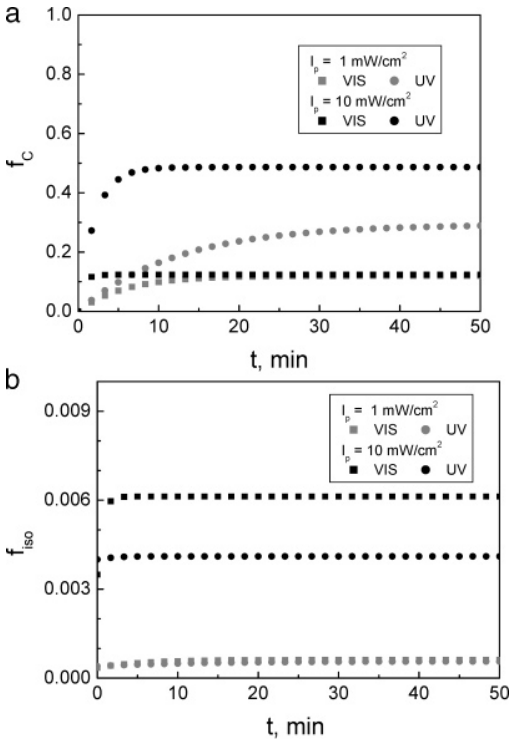

Figure 4. Time dependencies of cis fraction, f_C, (a) and isomerization rate, $\dot{f}_{iso}$, (b) under VIS and UV irradiation with 1 and 10 mW/cm². These dependencies were calculated from eqs 9 and 10, using parameters extracted from transient absorption experiments (see Appendix).

where K_0 is the mechanical modulus of the polymer matrix at room temperature in the dark, ϕ is the amount of the free volume, and a is the positive coefficient of proportionality. Any free volume present in the layer in the dark is included into K_0.

We now assume that photoisomerization of the azobenzene molecules generates a certain number of small voids in the frozen amorphous polymer environment. Therefore, because of irradiation with the VIS light, the bulk modulus of the layer will decrease according to eq 13, and hence, the bulk compliance, $\beta = 1/K$, will increase. Taking into account that $a\phi \ll 1$, relative changes of the bulk compliance (and hence of the plate compliance, see eq 5) will be proportional to the free volume

$$\delta\beta_{bulk}(t) = a\phi(t) \quad (14)$$

It is clear that using eq 14, we can readily explain the qualitative changes of the plate compliance under VIS irradiation (Figure 3a). Multiple photoisomerization cycles create free volume in the azobenzene polymer film which manifests itself as a softening of the layer. When the light is switched off, photoisomerization stops immediately, the free volume gradually disappears, and $\delta\beta_{zz}$ returns to its initial value in the dark.

To explain the complicated response of the azobenzene polymer layer to UV irradiation, we have to consider an additional phenomenon. As it was noticed previously by Srikhirin et al.[12] and confirmed by our own experiment (see Figure 3b), hardening of the polymer layer apparently correlates with the increase of the cis concentration. This can be explained if we assume that interactions of azobenzene chromophores in the cis state with their nearest environment are stronger than those

in the trans state. Therefore, the modulus of the polymer matrix is expected to increase with the concentration of cis isomers. Thus, in the first linear approximation, eq 13 can be rewritten as

$$K = K_0(1 + bf_C)(1 - a\phi) \tag{15}$$

Here, b is a coefficient of proportionality, which is positive. Taking into account that $bf_C \gg 1$, the relative change of the bulk compliance is given by

$$\delta\beta_{bulk}(t) = a\phi(t) - bf_C(t) \tag{16}$$

Interestingly, we did not observe that the layer hardens in the presence of cis isomers in the VIS experiments. This difference in behavior between VIS and UV can be explained if we assume that only a large fraction of cis isomers is able to harden the matrix.

Light-Induced Changes of the Dielectric Constant. The real part of the dielectric constant for a system with a single relaxation time, τ, is given by

$$\epsilon' = \epsilon_\infty + \frac{\epsilon_0 - \epsilon_\infty}{1 + (\omega\tau)^2} \tag{17}$$

Here, ϵ_0 is the static susceptibility, ϵ_∞ is the susceptibility at an infinitely high frequency, and ω is the angular frequency. In the Kirkwood−Fröhlich approach,[20] which takes into account intermolecular interactions and hindered rotation

$$\epsilon_0 - \epsilon_\infty = \frac{4\pi}{3k_BT}\frac{3\epsilon_0}{2\epsilon_0 + \epsilon_\infty}\left(\frac{\epsilon_\infty + 2}{3}\right)^2\langle\delta M^2\rangle \tag{18}$$

where k_B is the Boltzmann constant and T is the absolute temperature. In this equation $\langle\delta M^2\rangle$ represents fluctuations of the total dipole moment, M, which for a real chain is equal to[21]

$$\langle\delta M^2\rangle = gN\mu^2 \tag{19}$$

Here, $N\mu^2$ is the value of $\langle\delta M^2\rangle$ for a system composed from freely rotating dipole units, with N being the number of dipole groups per unit volume and μ being the dipole moment of a given group. g is the so-called correlation factor which depends on the strength of statistical correlations between dipoles and on their interactions with the polymer matrix. To understand the meaning of the correlation factor, it is instructive to consider two limiting cases: (1) $g = 1$, dipoles rotate freely and $\langle\delta M^2\rangle = N\mu^2$; (2) $g = 0$, dipoles are totally frozen in the polymer matrix and, thus, cannot rotate at all.

It was reported previously that the increase of ϵ' under VIS irradiation could be explained by the increase of the dipole moment of azobenzene when it isomerizes from the trans to the cis state.[22] However, this change would be detectable, only if fluctuations of the long axis or rotation of the azobenzene dye around this axis were possible at (or faster than) the measurement frequency of 2.5 kHz at room temperature. Recent dielectric spectroscopy studies[23] on different azobenzene side chain polymers showed that only the γ-relaxation process and the high-frequency tail of the β-relaxation process contribute to the dielectric constant at these conditions. The γ-relaxation process was assigned to the rotational fluctuations of the methyl groups and the β-relaxation process to the local fluctuations of the ester groups. In contrast, the relaxation frequency of the azobenzene moieties was significantly lower (about 1−10 Hz). This allows us to argue that ϵ' changes under irradiation mainly due to the change in g rather than due to the change in the dipole moment of azobenzene. This interpretation is supported by relating the predicted change in dipole moment of our chromophore, which is 5.2 D in the cis state compared to 6.8 D in the trans state (the quantum chemistry calculations were carried out by using a commercial software product "Gaussian 98") to the observed change in dielectric constant. Despite the presence of cis isomers with smaller dipole moment, we observe a well-pronounced increase of ϵ' in the VIS-illuminated sample.

Consequently, keeping μ constant and using eqs 17−19, it is easy to show that the relative change of the dielectric constant is equal to the relative change of the correlation factor

$$\delta\epsilon'(t) = \frac{\epsilon'(t) - \epsilon'(0)}{\epsilon'(0) - \epsilon_\infty} = \delta g(t) \tag{20}$$

Furthermore, one can show that in the absence of statistical correlations between dipoles the relative change of the correlation factor is also given by eqs 14 and 16 (the coefficients can of course take other values). First, it is obvious that the presence of the free volume increases the rotational freedom of the dipoles. Second, the presence of cis isomers leads to an increase of the strength of intramolecular interactions in the polymer matrix which results in decrease of rotational freedom of dipoles. This means that whenever the azobenzene polymer film undergoes changes of its mechanical properties—softens or hardens—this is reflected by an appropriate change in ϵ'.

Let us show that our model is able to reproduce the time-dependent behavior of the dielectric constant under irradiation with visible light. In our model, $\delta\epsilon'$ is equal to the relative change in the correlation factor and, therefore, is proportional to the amount of the free volume accumulated in the azobenzene polymer layer from the moment $t = 0$, at which the light is switched on, until the moment t

$$\delta g_{VIS}(t) = c\int_0^t \dot{\phi}(t')\exp[-(t - t')/\tau_m]\,dt' \tag{21}$$

Here $\dot{\phi}(t')$ is the additional free volume produced per one unit at time t' due to multiple photoisomerization cycles. Relaxation of ϕ after this moment is described by the exponential decay with the characteristic time τ_m. The coefficient of proportionality c can be estimated from the dependence of the relative dielectric constant on temperature. We have determined $c \approx 215$ by measuring $\delta\epsilon'$ at the glass transition temperature ($\delta\epsilon' \approx 5.4$) and using a literature value of $\phi \approx 0.025$.[20]

Let us first assume that $\dot{\phi}$ is strictly proportional to the isomerization rate

$$\dot{\phi}(t') = a_0\dot{f}_{iso}(t') \tag{22}$$

This gives

$$\delta g_{VIS}(t) = \delta g_{VIS,\infty}\begin{cases}[1 - \exp(-t/\tau_m)] & \text{light is on at } t = 0\\ \exp[-(t - t_{off})/\tau_m] & \text{light is off at } t = t_{off}\end{cases} \tag{23}$$

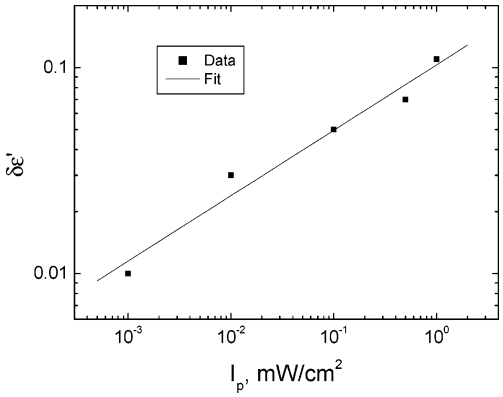

Figure 5. Intensity dependence of the relative dielectric constant, $\delta\epsilon'$, under VIS irradiation.

with

$$\delta g_{\mathrm{VIS},\infty}(I_\mathrm{p}) = a_0 c \dot{f}_{\mathrm{iso},\infty}\tau_\mathrm{m} \approx 2a_0 c\,\frac{k_\mathrm{TC}\,k_\mathrm{CT}}{k_\mathrm{TC}+k_\mathrm{CT}}\,\tau_\mathrm{m} I_\mathrm{p} \qquad (24)$$

By deriving this equation, we took into account that γ is negligibly small compared to $k_\mathrm{TC}I_\mathrm{p}$ and $k_\mathrm{CT}I_\mathrm{p}$. Actual values of τ_m were determined from the initial exponential decrease of the relative dielectric constant after switching the light off. They were found to be independent of I_p, and thus, eq 24 predicts a linear increase of the relative dielectric constant with the light intensity in the stationary state. However, the experimentally measured $\delta\epsilon'$ curve increases with the light intensity nonlinearly, as demonstrated in Figure 5. This curve can be fitted using a power-law dependence

$$\delta g_{\mathrm{VIS},\infty}(I_\mathrm{p}) = a_1 I_\mathrm{p}^{\,a_2} \quad \mathrm{W\ m^{-2}} \qquad (25)$$

with $a_1 = 0.050 \pm 0.004$ and $a_2 = 0.32 \pm 0.03$. The nonlinear behavior can be understood as follows: when the light intensity reaches a critical value, chromophores can reutilize free volume which has been generated by an earlier isomerization event.[13] As result, the additional free volume is not anymore proportional to the isomerization rate. This has been taken into account by introducing a nonlinear dependence of $\dot{\phi}$ on the isomerization rate

$$\dot{\phi}(t') = [a_0\,\dot{f}_\mathrm{iso}(t')]^{a_2} \qquad (26)$$

This assumption does not change the principal form of the time-dependent solution given by eq 23, but $\delta g_{\mathrm{VIS},\infty}$ is now defined by eq 25 with

$$a_1 \approx c(a_0 k_\mathrm{TC})^{a_2}\left[1 + a_2\,\frac{k_\mathrm{CT}-k_\mathrm{TC}}{k_\mathrm{TC}+k_\mathrm{CT}}\right]\tau_\mathrm{m} \qquad (27)$$

Taking $\tau_\mathrm{m} = 200$ s, we can reasonably well reproduce the time dependencies of the relative dielectric constant at different intensities of visible light (Figure 6a). However, when the light is switched off, $\delta\epsilon'$ relaxes much slower than δg as predicted by eq 23. We already mentioned that orientational effects (neglected in our model) might be a reason for this discrepancy between the experimental data and the model prediction.

To describe the time-dependent behavior of the dielectric constant under irradiation with ultraviolet light,

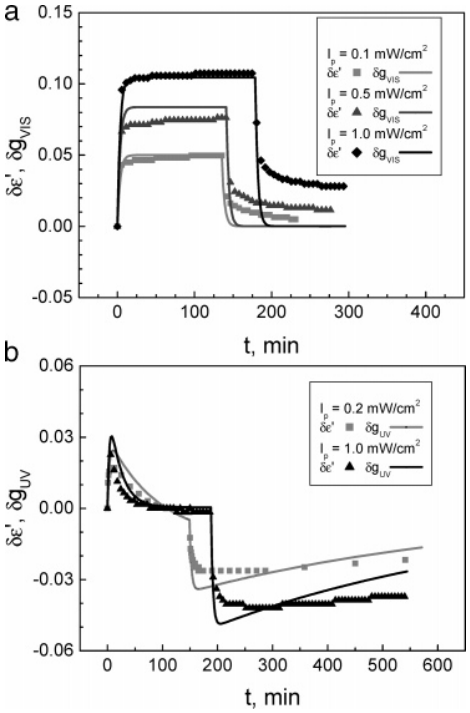

Figure 6. Time dependencies of the relative dielectric constant, $\delta\epsilon'$, under VIS (a) and UV (b) at different intensities. Lines show the relative correlation factor, δg, as predicted by eqs 21 and 28.

we introduce an additional term in eq 21

$$\delta g_\mathrm{UV}(t) = \int_0^t \dot{\phi}(t')\,\exp[-(t-t')/\tau_\mathrm{m}]\,\mathrm{d}t' - b f_\mathrm{C}(t) \qquad (28)$$

Here b is a free parameter which correlates the relative hardening to the fraction of cis isomers. This equation, with $\tau_\mathrm{m} = 200$ s and $b = 0.1$, satisfactorily describes transient experiments under irradiation with UV light (Figure 6b). When UV radiation is switched off, the cyclic photoisomerization immediately stops, i.e., the first term in eq 28 disappears, and one observes a sharp drop in the dielectric constant. Interestingly, we could use the same power law (see eq 25 for VIS light) to describe the response at different intensities of UV light. Note that there is a significant discrepancy between the model predictions and the measured data at longer times after the UV light is switched off.

In contrast to the dielectric constant, the bulk compliance should not (or only weakly) depend on orientational effects. This explains why using the same eqs 21 and 28 (but with different values of the fitting parameters) we managed to describe satisfactorily the time dependence of $\delta\beta_{zz}$ not only under irradiation but also at longer times after the VIS or UV light has been switched off (Figure 7). Despite significant noise in the data, one can clearly see that, in the case of UV irradiation, the gradual recovery of the bulk compliance to its initial value in the dark is reproduced much better than that of the dielectric constant (Figure 7a). In the case of VIS irradiation, both the model predictions and the measured data exhibit an immediate drop of $\delta\beta_{zz}$ to zero after the light is switched off (Figure 7b).

Equipped with the formalism described above, we are also able to reproduce the complicated time dependence of the dielectric constant under multiple illumination with VIS and UV (Figure 8). During the first two cycles

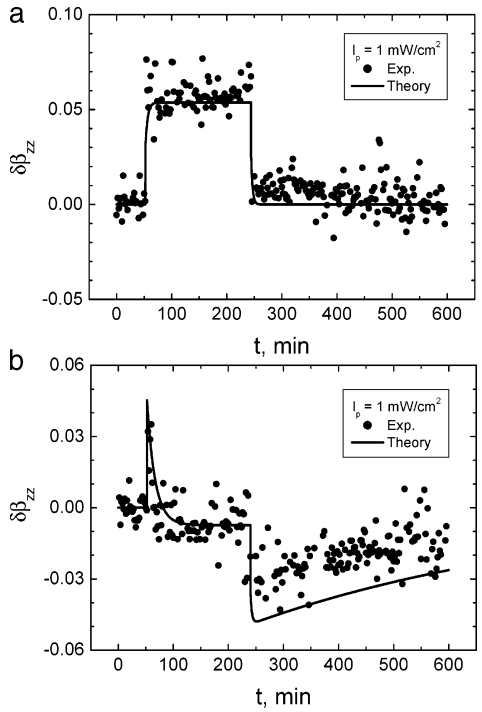

Figure 7. Time dependencies of the relative plate compliance, $\delta\beta_{zz}$, under VIS (a) and UV (b) irradiation with 1 mW/cm^2. Lines show a model prediction as described by eqs 21 and 28.

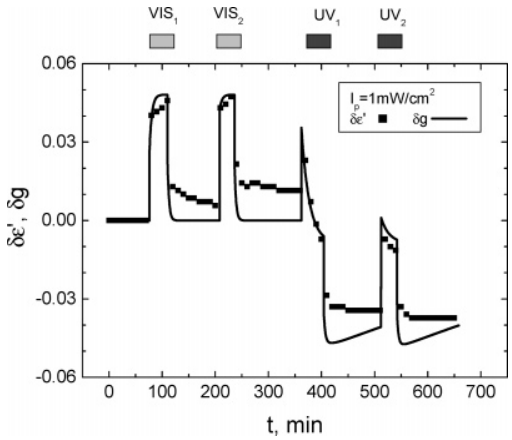

Figure 8. Time dependencies of the relative dielectric constant, $\delta\epsilon'$, under multiple irradiation with VIS and UV light. The relative correlation factor, δg, as predicted by eqs 21 and 28, is also shown.

the film is illuminated with VIS light. Because of the fast cyclic photoisomerization the layer undergoes slight softening, leading to an increase of $\delta\epsilon'$ to a value of 0.05. When the VIS light is switched off, photoisomerization stops immediately and ϵ' slowly relaxes to its initial value in the dark. Note that the height of the plateau in the second VIS illumination step is comparable to that in the first step. In the subsequent two cycles, the film was illuminated with UV light. At the beginning of every illumination cycle, the layer slightly softens due to photoisomerization but then gradually hardens due to the increase of the cis fraction. When the UV light is switched off, photoisomerization abruptly stops, but the remaining cis content leads to the sudden drop of ϵ'. This results in an effective "hardening" of the layer compared to the nonilluminated material, which slowly relaxes back to the initial value in the dark. The characteristic time of the relaxation process is comparable to the lifetime of the cis isomers $1/\gamma \sim 10$ h. This is in agreement to our model prediction that the recovery of ϵ' correlates with the thermal back-relaxation of the cis fraction. Because the dark pause between the two UV illumination steps is less than 2 h, the cis content is still very high at the beginning of the second UV cycle. Therefore, the maximum of $\delta\epsilon'$ in the second UV illumination step is considerably lower than that measured during the earlier illumination cycles.

Discussion and Conclusions

In this study we have developed a semiquantitative model that is capable to describe the time and intensity dependence of the electromechanical and dielectric properties of an azobenzene polymer layer measured at two particular wavelengths: $\lambda_{VIS} = 488$ nm and $\lambda_{UV} = 365$ nm. This two-phase model is based on two assumptions: (1) Cyclic photoisomerization creates additional free volume in the polymer layer that results in a softening of the layer. This process does not change the mechanical modulus of the polymer matrix. (2) In addition, in the case of UV irradiation, a high population of the cis fraction slightly increases the modulus of the polymer matrix. This effect can be explained if cis isomers have stronger interactions with the surrounding matrix than trans isomers.

To support the model presented here, we plan to measure changes in mechanical and dielectric properties of the film when irradiated at intermediate wavelengths. Such measurements will hopefully clarify the question why we do not observe an abrupt hardening after switching the light off in the film previously irradiated with VIS light. Note that only 10% of azobenzene chromophores are in the cis state at $\lambda_{VIS} = 488$ nm. Presently, we assume that the matrix only hardens when the cis fraction reaches some critical value, which is far above 10%. Another possible explanation is that different isomerization mechanisms—inversion at VIS and rotation at UV—could be responsible for the different matrix response when illuminated at 365 and 488 nm.

With respect to the formation of SRG under nonhomogeneous illumination, the data presented here support our earlier interpretation that light-induced changes in the polymer film (either VIS or UV illumination) are very different from those caused by simple heating.[13] Most important, all data can be explained by a model that is continuous with respect to time and intensity. This excludes that illumination under conditions described here induces a phase transition. Nevertheless, the data suggest that a certain fraction of free volume is introduced into the layer by the photoisomerization process and that this additional volume remains within the layer for a considerable amount of time (ca. 5 min). Therefore, the experiments strongly suggest that the light-induced free volume must redistribute itself differently (with time and/or spatially) than the free volume introduced by simple heating, which allows the otherwise still hard material to flow in response to a light-driven force (still unknown). Such a difference is expected since one isomerization event consumes ca. 2 eV in energy in the range of picoseconds, and this energy can be then gradually converted into a considerable molecular rearrangement—reorientation of azobenzene moieties, presumably followed by a change of main chain conformation.

Interestingly, recent studies on the inscription of the surface relief gratings revealed that the diffraction efficiency decreases with increasing temperature.[24] When the temperature exceeded 50 °C, it was impossible to induce any changes of the layer topography. This result appears to be totally unexpected since the bulk compliance of azobenzene polymers slightly increases with temperature. Therefore, any flow of material in response to the external force is expected to be faster at higher temperatures. Our experiments allow us to speculate that the main reason behind such puzzling behavior could be the faster relaxation of the light-induced free volume at higher temperatures, caused by an increase in local chain dynamics. In this case, we indeed expect that the formation of SRGs at higher temperatures is less effective compared to SRGs formed at room temperature.

Acknowledgment. V. Börger and H. Menzel (University of Braunschweig) are gratefully acknowledged for supplying the polymers. We, further, acknowledge Dr. Stumpe (IAP Golm) for many fruitful discussions. We also thank Dr. K. Morawetz for the ellipsometric measurements and B. Stiller for performing the AFM experiments under illumination. This work was financially supported by the DFG under Grant NE410/6-2.

Appendix. Transient Absorption

The time dependence of absorption coefficient was probed at $\lambda_{UV} = 365$ nm with concurrent illumination of the layer at 365 and 488 nm. From these data, the time-dependent normalized absorption was calculated

$$\delta A(t) \equiv \frac{A_\infty - A(t)}{A_\infty - A_0} \tag{A1}$$

where A_0 and A_∞ are the absorbance in the dark and in the photostationary state, respectively. Here, we did not take into account the photoorientation of azobenzene moieties because after switching the light off we have observed a full recovery of the absorbance to its initial value in the dark (this process correlates with the thermal back-relaxation of the cis fraction). In the case if photoorientation effects in the investigated polymer will be pronounced, we would not expect a full recovery of the absorbance value.

Figure 9 shows the time dependencies of $-\ln(\delta A)$ at different intensities of VIS and UV light. The slope of the curves gives $\tau_p^{-1} = (k_{TC} + k_{CT})I_p + \gamma$, which depends linearly on I_p. Plotting the linear dependence of τ_p^{-1} on I_p yields its slope, S, which is equal to the sum of the rate constants k_{TC} and k_{CT}.

Further, the photostationary value of the cis fraction increases with the light intensity as

$$f_{C,\infty} = \frac{k_{TC} I_p}{S I_p + \gamma} \tag{A2}$$

and saturates at high intensities to

$$f_{C,\infty} = \frac{k_{TC}}{S} = 1 - \frac{A_\infty}{A_0} \tag{A3}$$

For our polymer, $f_{C,\infty}$ is 0.12 at VIS and 0.55 under UV illumination. Knowing S and measuring $f_{C,\infty}$, we were able to separate k_{TC} and k_{CT}. Additionally, we have measured the rate of the cis−trans thermal back-relaxation, γ, following recovery of the normalized film absorbance after switching off the light. It is known that the cis−trans thermal back-relaxation is not strictly monoexponential but exhibits an anomalous fast component for the first few seconds.[25] Therefore, the value of γ, relevant to the time scale of our experiments, was estimated after the first 3 min, when a much slower monoexponential decay of absorption was already established.

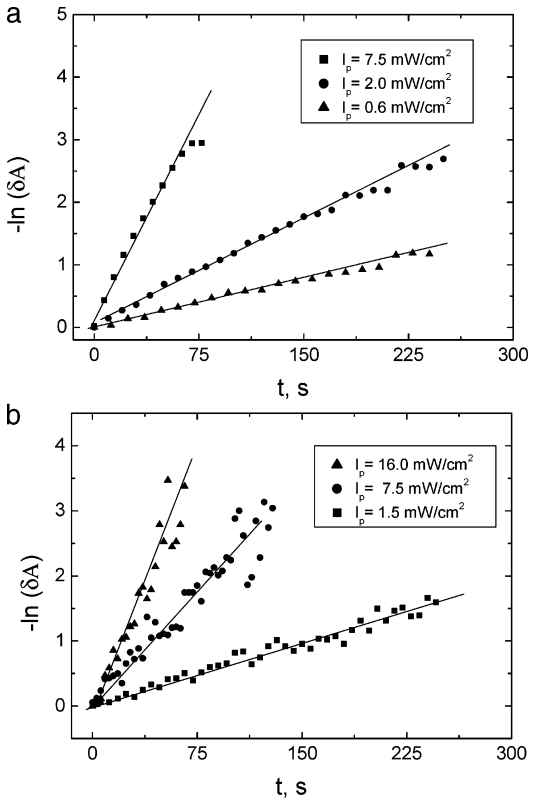

Figure 9. Time dependencies of $-\ln(\delta A)$ measured at different intensities of VIS (a) and UV (b) light.

The values determined from transient absorption experiment, for illumination with VIS and UV, are summarized in Table 1.

References and Notes

(1) Rochon, P.; Batalla, E.; Natansohn, A. *Appl. Phys. Lett.* **1995**, *66*, 136.
(2) Kim, D. Y.; Li, L.; Jiang, X. L.; Shivshankar, V.; Kumar, J.; Tripathy, S. K. *Macromolecules* **1995**, *28*, 8835−8839.
(3) Barrett, C. J.; Rochon, P. L.; Natansohn, A. L. *J. Chem. Phys.* **1998**, *109*, 1505.
(4) Kumar, J.; Li, L.; Jiang, X. L.; Kim, D.-Y.; Lee, T. S.; Tripathy, S. *Appl. Phys. Lett.* **1998**, *72*, 2096.
(5) Baldus, O.; Zilker, S. J. *Appl. Phys. B: Laser Opt.* **2001**, *72*, 425.
(6) Lefin, P.; Fiorini, C.; Nunzi, J.-M. *Pure Appl. Opt.* **1968**, *7*, 71.
(7) Pedersen, T. G.; Johansen, P. M.; Holme, N. C. R.; Ramanujam, P. S.; Hvilsted, S. *Phys. Rev. Lett.* **1998**, *80*, 89.
(8) Bublitz, D.; Fleck, B.; Wenke, L. *Appl. Phys. B: Laser Opt.* **2001**, *72*, 931.
(9) Oliveira, O. N., Jr.; Kumar, J.; Li, L.; Tripathy, S. K. In *Photoreactive Organic Thin Films*; Sekkat, Z., Knoll, W., Eds.; Elsevier Science: Amsterdam, 2002; p 560.
(10) Saphiannikova, M.; Geue, T. M.; Henneberg, O.; Morawetz, K.; Pietsch, U. *J. Chem. Phys.* **2004**, *120*, 4039−4045.
(11) Geue, T.; Saphiannikova, M.; Henneberg, O.; Pietsch, U.; Rochon, P.; Natansohn, A. *Phys. Rev. E.* **2002**, *65*, 052801.
(12) Srikhirin, T.; Laschitsch, A.; Neher, D.; Johannsmann, D. *Appl. Phys. Lett.* **2000**, *77*, 963−965.

(13) Mechau, N.; Neher, D.; Börger, V.; Menzel, H.; Urajama, K. *Appl. Phys. Lett.* **2002**, *81*, 4715−4717.
(14) Viswanathan, N. K.; Kim, D. Y.; Bian, S.; Williams, J.; Liu, W.; Li, L.; Samuelson, L.; Kumar, J.; Tripathy, S. K. *J. Mater. Chem.* **1999**, *9*, 1941−1955.
(15) Fischer, E. *J. Phys. Chem.* **1967**, *71*, 3704.
(16) Winkelhahn, H. J.; Pakula, T.; Neher, D. *Macromolecules* **1996**, *29*, 6865.
(17) Osman, A. E.; Dumont, M. *Opt. Commun.* **1999**, *164*, 277.
(18) Landau, L. D.; Lifshitz, E. M. *Theory of Elasticity*, 2nd ed.; Elsevier Science Ltd.: Amsterdam, 1981.
(19) Ferry, J. D. *Viscoelastic Properties of Polymers*; John Wiley & Sons: New York, 1980.
(20) McCrum, N. G.; Read, B. E.; Williams, G. *Anelastic and Dielectric Effects in Polymeric Solids*; Dover Publications: New York, 1967.
(21) Saphiannikova, M. G.; Lukasheva, N. V.; Darinskii, A. A.; Gotlib, Y. Y.; Brickmann, J. *Macromolecules* **2000**, *33*, 606−612.
(22) Fritz, A. *Korrelation optischer und dielektrischer Untersuchungen an photochromen Copolymeren mit Azobenzolderivaten in der Seitengruppe*; Mensch & Buch Verlag: Berlin, 2000.
(23) Fritz, A.; Schönhals, A.; Sapich, B.; Stumpe, J. *Macromol. Chem. Phys.* **1999**, *200*, 2213−2220.
(24) Henneberg, O. *In-situ Untersuchungen zur Entstehung von Oberflächengittern in Polymeren*; Potsdam University: Potsdam, 2004.
(25) Barrett, C.; Natansohn, A.; Rochon, P. *Chem. Mater.* **1995**, *7*, 899.

MA0479316

Journal of Microscopy, Vol. 219, Pt 3 September 2005, pp. 109–114
Received 15 November 2004; accepted 27 April 2005

Optical patterning in azobenzene polymer films

B. STILLER, T. GEUE*, K. MORAWETZ & M. SAPHIANNIKOVA
Institute of Physics, University of Potsdam, Am Neuen Palais 10, 14469 Potsdam, Germany
**Laboratory for Neutron Scattering (WHGA/110), Paul Scherrer Institute, ETH Zurich, CH-5232 Villigen – PSI, Switzerland*

Key words. AFM, force–distance curve, optically induced material transport, pulse force mode, SNOM, surface relief grating.

Summary

Thin azobenzene polymer films show a very unusual property, namely optically induced material transport. The underlying physics for this phenomenon has not yet been thoroughly explained. Nevertheless, this effect enables one to inscribe different patterns onto film surfaces, including one- and two-dimensional periodic structures. Typical sizes of such structures are of the order of micrometers, i.e. related to the interference pattern made by the laser used for optical excitation. In this study we have measured the mechanical properties of one- and two-dimensional gratings, with a high lateral resolution, using force–distance curves and pulse force mode of the atomic force microscope. We also report on the generation of considerably finer structures, with a typical size of 100 nm, which were inscribed onto the polymer surface by the tip of a scanning near-field optical microscope used as an optical pen. Such inscription not only opens new application possibilities but also gives deeper insight into the fundamentals physics underlying optically induced material transport.

Introduction

Inscription of surface relief gratings (SRGs) can be achieved by exposing an azobenzene polymer film to a periodic intensity or polarization pattern that results from the interference of two polarized laser beams (for a review see Wiswanathan *et al.*, 1999; Yager & Barett, 2001; Natansohn & Rochon, 2002). The wavelength of the laser beam should be near the absorption maximum associated with the $\pi-\pi^*$ transition for *trans* moieties and the $n-\pi^*$ transition for *cis* moieties. As the result, cyclic *trans–cis–trans* isomerization of the azobenzene chromophores takes place. Absorption of this light induces material flow even at room temperature, which is well below the glass transition temperature of the polymers investigated here.

In spite of enormous experimental and theoretical efforts, the optically induced mass transport in azobenzene polymer films has not yet been completely explained. Several models of surface evolution upon illumination have been discussed (Barrett *et al.*, 1998; Kumar *et al.*, 1998; Lefin *et al.*, 1998; Pedersen *et al.*, 1998; Baldus *et al.*, 2001; Bublitz *et al.*, 2001) but none of these provides a satisfactory explanation for the mass transport at a molecular level. Nevertheless, it is widely accepted that multiple *trans–cis* and *cis–trans* photoisomerizations of the chromophores trigger the inscription process. Moreover, growth of the surface relief gratings was found to be continued even after switching the pumping laser off, and this effect was explained by the slow *cis–trans* thermal relaxation in the dark (Saphiannikova *et al.*, 2004a,b). At present, force models based on the light-induced reorientation of azobenzene moieties (Pedersen *et al.*, 1998; Bublitz *et al.*, 2001) look the most promising explanation. This reorientation arises statistically, after a number of isomerization cycles, when the long axis of chromophores is mainly found to be perpendicular to the polarization direction (Dumont & Osman, 1999).

Although scanning probe microscopy itself is not able to visualize the process of molecular isomerization or reorientation, it is often used for visualization and inspection of the inscribed nano- and micro-structures (Stiller *et al.*, 2000, 2001). In this study we have used atomic force microscopy (AFM) not only to visualize the photoinduced structures but also to detect mechanical changes of the optically modulated film surface. The latter could be achieved by utilizing the pulse force mode (PFM), which extends the capabilities of AFM beyond simply measuring the sample topography. Additionally to this option, PFM allows one to determine such surface properties as local stiffness and adhesion, in the form of well-resolved material contrast images. Also, we report on generation and inspection of ultrafine surface reliefs that were produced using a focused light in the optical near-field.

Experimental

Film preparation

The compound investigated was an amorphous azobenzene side-chain homopolymer {poly (4-nitrophenyl)[4-[[2-(methacryloyloxy)-ethyl] ethylamino] phenyl] diazene}

Correspondence to: Dr B. Stiller. Fax: +49 331977 1083; e-mail: busti@rz.uni-potsdam.de

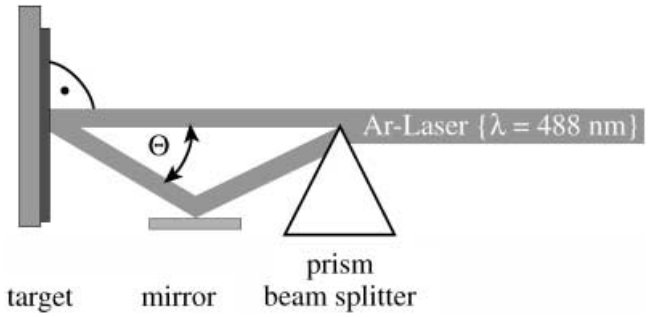

Fig. 1. Geometry for inscription of surface relief gratings.

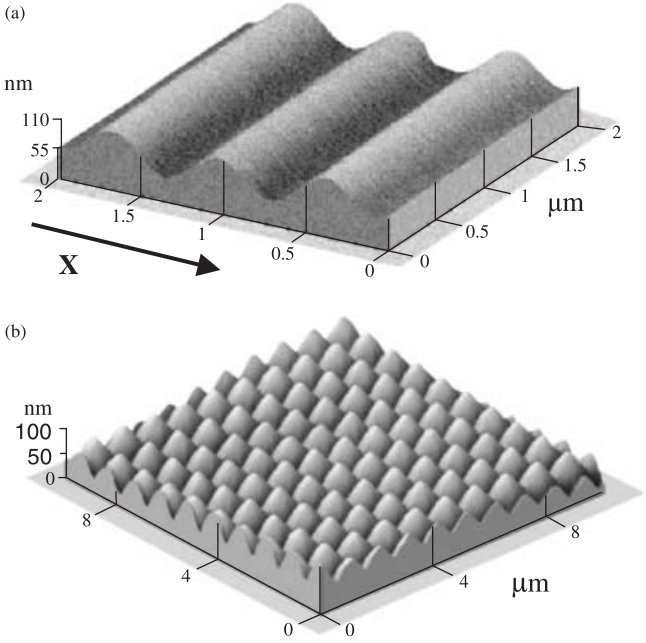

Fig. 2. AFM topography of the linear grating with 880-nm period (a) and the cross grating (b) produced by two-step illumination. The second step of inscribing was performed after rotating the film by 60° about its normal.

(pDR1M), built from 15–30 repeat units. The glass transition temperature, T_g, was measured calorimetrically and found to increase from 105 to 120 °C with the increase in polymer length. For film preparation the polymer was first dissolved in tetrahydrofurane (Merck, 0.5–5.0 wt%), and then the freshly prepared solution was spin coated onto thin glass plates at 1500–2500 r.p.m. (Spin Coater Delta 10TT/BM Süss Microtec, Siegen, Germany). The resulting pinhole-free films were found to be quite flat with an average surface roughness of about 2–5 nm. A constant layer thickness of about 500 nm was determined by AFM and also by two optical methods of extinction and ellipsometry.

Inscription of surface relief gratings

Microscopic surface relief gratings were inscribed onto the polymer films using the holographic interference pattern of two plane waves (Fig. 1). The pattern was produced by two counter-circularly polarized beams of an argon ion laser (LG Laser Technologies, Kleinostheim, Germany) operating at a wavelength of $\lambda = 488$ nm and at a power density of about 15 mW cm^{-2} (target area). The writing time was in the range 10–20 min. It was possible to inscribe one-dimensional (1D) line gratings (Fig. 2a) with the period $D = \lambda/\sin\theta$, varying in the range 800–5000 nm by changing θ, the interference angle between the beams. In some experiments, the second illumination step was added after rotating the sample around its normal at 60° or 90° with respect to the writing beam. Such a two-step inscription procedure resulted in a 2D cross grating with the same period D in both principal directions (Fig. 2b).

Scanning probe microscopy

Scanning probe microscopy experiments were carried out using a commercial atomic force microscope with its linearized 100-μm scanner (autoprobe CP, Veeco Instruments, U.S.A.) and a commercial scanning near-field optical microscope (SNOM), which includes an AFM option (Alpha SNOM, Witec GmbH, Ulm, Germany). We have used commercial contact cantilevers NSC17 (NT-MDT, Russia) with a tip radius of *c.* 35 nm, spring constant of 3 N m^{-1} and resonance frequency of ~75 kHz. These cantilevers were utilized for measuring the AFM topography and conventional force–distance curves, as well as for the PFM measurements. A special SNOM cantilever with an aperture of *c.* 100 nm was used for highly resolved optical excitation of the polymer film. All experiments were carried out at ambient conditions, i.e. at atmospheric pressure and at room temperature.

Pulse force microscopy

Pulse force microscopy is a so-called non-resonant intermediate contact mode. An external hardware unit is added to the AFM system to stimulate the measuring tip and to analyse the force data. A special piezoelectric system introduces on the AFM tip a sinusoidal modulation with amplitude of 0–500 nm at a user-selectable frequency between 100 Hz and 2 kHz. The experiments shown here are performed at ~1 kHz. The modulation amplitude is adjusted in such a way that the measuring tip briefly but periodically touches the sample surface. At the beginning of every PFM cycle, similar to the case when conventional force–distance curves are taken, the AFM tip gradually approaches the surface (see Fig. 3, AB). After some time the tip suddenly snaps into contact owing to attractive interactions with the film surface. The piezoelectric system pushes the tip further towards the surface, before the force reaches a certain maximal value (Fig. 3, BC). As the system pulls the tip back (Fig. 3, CD), the latter again suddenly loses contact with

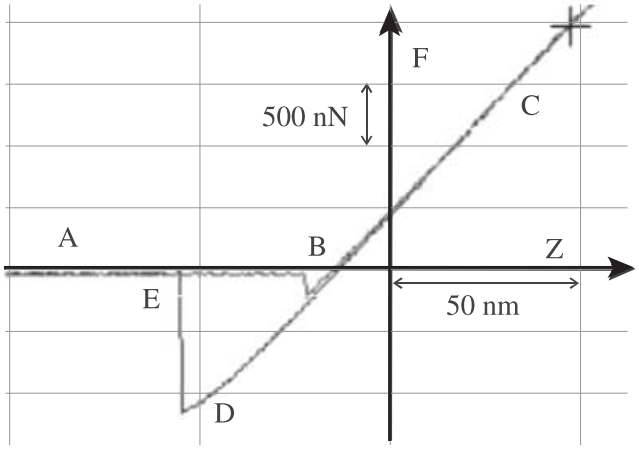

Fig. 3. Example of the force–distance curve $F(z)$ taken on the line grating.

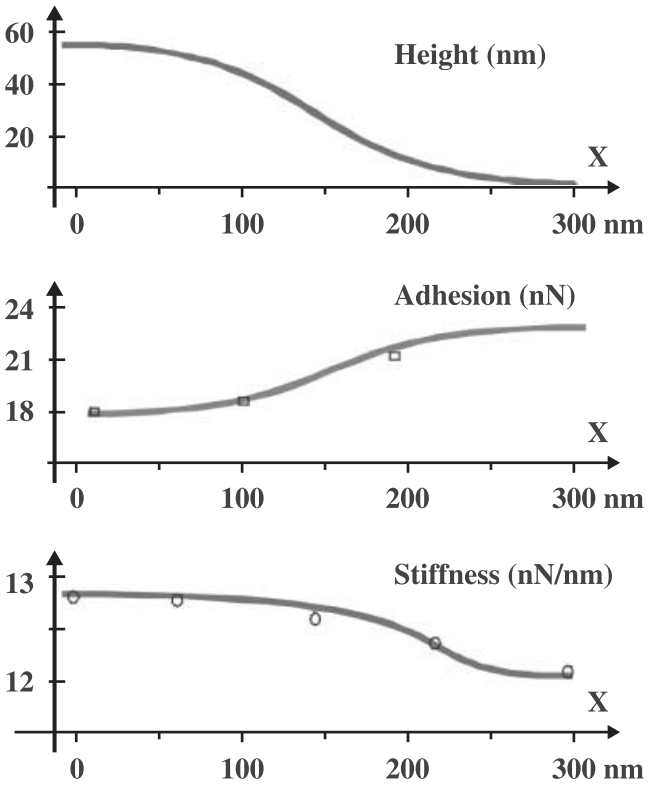

Fig. 4. Height, adhesion and stiffness measured at points along the *x*-direction on the line grating shown on Fig. 2(a).

the surface (Fig. 3, DE). When the tip snaps away from the surface (Fig. 3, E) this so-called adhesion peak is a measure of the adhesion force, and its value is fed as an additional signal into an analog input channel of the AFM to form the adhesion image of the sample. The difference between the maximal force and the force occurring at a time which is determined by a special stiffness trigger is related to the local stiffness of the sample. On hard parts of the sample this difference is larger than on soft parts. This force difference is recorded as a relative value and forms the stiffness image. Changing the tip position with the help of the scanner, it is possible to create force–distance curves along the whole sample area. Thus, PFM provides three simultaneously measured images which contain information about the topography, adhesion and stiffness of the sample surface.

Results and discussion

Characterization of surface reliefs by scanning methods

Recent X-ray studies of linear SRGs, inscribed on pDR1M films and then thermally erased, contain indirect indications of local changes in the polymer density along the grating vector (Pietsch *et al.*, 2000; Geue *et al.*, 2002). These studies were strongly supported by linear viscoelastic analysis of the grating formation, which was shown to result in a sinusoidal density variation with the same period as that of the topography grating (Saphiannikova *et al.*, 2004a,b). Furthermore, it was predicted that the regions of higher density should coincide with the topographical hills to which the azobenzene polymer chains had migrated. The latter prediction is in agreement with the phase imaging AFM measurements, in which hardness changes, induced on the surface of the azobenzene polymer film by the optical near-field of polystyrene microspheres, were inspected (Ikawa *et al.*, 2000; Keum *et al.*, 2003). Using second harmonic generation SNOM, it was shown recently that the mobility of chromophores is reduced in the region of grating hills (Lagugne-Labarthet *et al.*, 2004). This effect was attributed to a density increase in these areas. To confirm these indirect findings, mechanical properties that directly depend on the polymer density should be studied locally, i.e. along the grating vector. This was done in our study by measuring the force–distance curves and using the pulse force mode of AFM.

Force–distance measurements were taken at the hills, valleys and flanks of the linear grating shown on Fig. 2(a). At each location, the tip was gradually moved towards the film surface, snapping on it and then shortly pressing onto the film; the tip was then retracted until snapping off (for a detailed description see the PFM section above). The only difference as compared with the PFM measurements is that now the curves are taken at the locations chosen and this is done much more slowly, over a period of 1 s. The slope of the force–distance curve (Fig. 3) is defined by a superposition of the spring constants of the lever and the elastic film. As the lever properties do not change during measurements, different slopes of the curves taken at different places reflect local changes in the film stiffness. Different values for the ('snapping off') point of release peaks represent local changes in adhesion. Height, adhesion and stiffness measured at chosen points of the line grating along the *x*-direction are shown in Fig. 4. At the hills adhesion is found to be lower than at the valleys, whereas

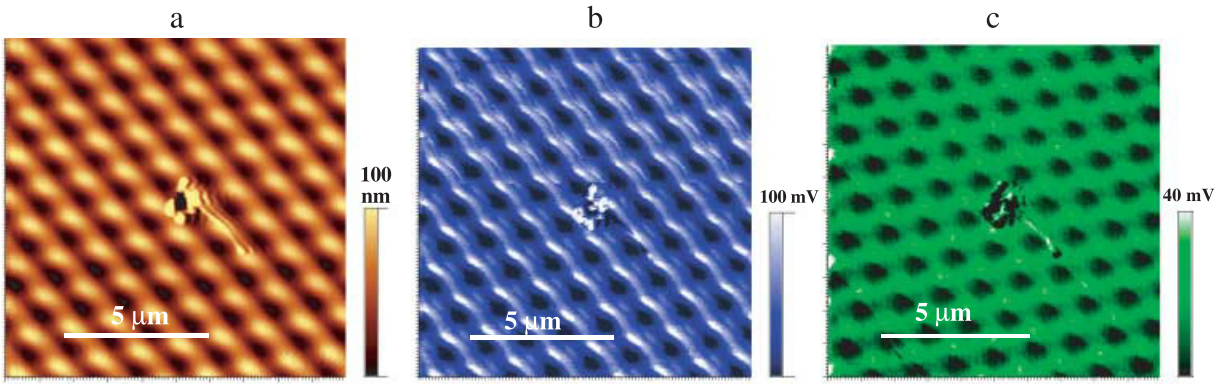

Fig. 5. Topography (a), adhesion (b) and stiffness (c) images measured by pulse force microscopy. The two-dimensional cross grating was produced by a two-step inscription procedure, whereby the second step was made after rotating the sample by 60° about its normal.

stiffness behaves in the opposite manner. As stiffness is expected to increase with an increase in polymer density, the latter result is in accordance with the recent theoretical prediction made by our group (Saphiannikova *et al.*, 2004a,b).

To visualize the mechanical properties of an optically modified film, 2D surface relief gratings were inspected using PFM. Figure 5 shows topography, adhesion and stiffness images of the cross grating. Here, we intentionally chose a part of the sample with a central defect to demonstrate that we always studied exactly the same area and that the images are created from unfiltered raw data. These three images reveal a strong correlation between mechanical properties and topography of the cross grating. Cross-sections taken from the PFM images confirm the findings that were made by measuring force–distance curves locally: at the hills the SRG is stiffer and is not as adhesive as in the valleys.

To summarize, both methods – measurements of force–distance curves and PFM – directly confirm the theoretical predictions that the film density changes under optically induced material flow and that this change strongly correlates with the topography grating (Saphiannikova *et al.*, 2004a,b). At present, we can only speculate on the reason for the periodic adhesion variations. The most promising candidate is again the orientational distribution of chromophores, which results from competition between the light-induced and flow-induced orientations (Geue *et al.*, 1997; Lagugne-Labarthet *et al.*, 1998). Depending on the preferential orientation at the particular local position, highly anisotropic azobenzene moieties can impose different attractive interactions onto the cantilever tip.

Inscription of nanostructures with an optical pen (the SNOM cantilever)

Nanostructures smaller than the optical wavelength can be produced using near-field optical techniques (Karageorgiev *et al.*, 2000; Landraud *et al.*, 2001; H'dhili *et al.*, 2001; Stiller *et al.*, 2003). In our experiments convex linear nanostructures

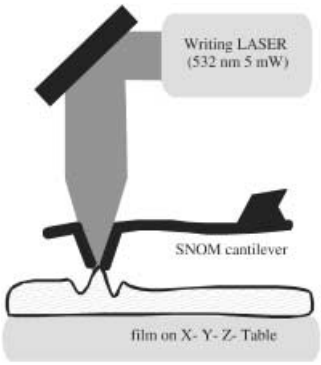

Fig. 6. Schema of the SNOM set-up used for inscription of the nanostructures shown in Figs 7 and 8.

were inscribed onto an azobenzene polymer film surface using the SNOM set-up (Fig. 6). The laser beam ($\lambda = 532$ nm) was focused in the SNOM cantilever to generate a highly localized optical near-field at the apex of the cantilever tip. The diameter of the near-field is similar to the aperture of the SNOM cantilever and is in the range of 100 nm. When the SNOM tip is moved along the sample surface, its optical near-field induces the movement of azobenzene polymer molecules into the centre of the field, i.e. in the direction of the light intensity gradient. This results in 10–20-nm-high reliefs on the sample surface. Thus, we can use the SNOM cantilever as an optical pen for inscription of different nanostructures. Recently, the same pDR1M film was irradiated with the laser beam focused by a lens, and it was also observed that the polymer chains had moved to the beam focus (Stiller *et al.*, 2004). Therefore, in both cases, pDR1M molecules were transported by an as yet unknown force in the direction of the light intensity gradient.

After switching the laser off, the SNOM cantilever can be used as an AFM tip to inspect inscribed structures, without manipulating the sample. Some examples of inscribed nanostructures visualized by the SNOM tip are presented in Figs 7 and 8. The first structure (Fig. 7) represents a 2D cross

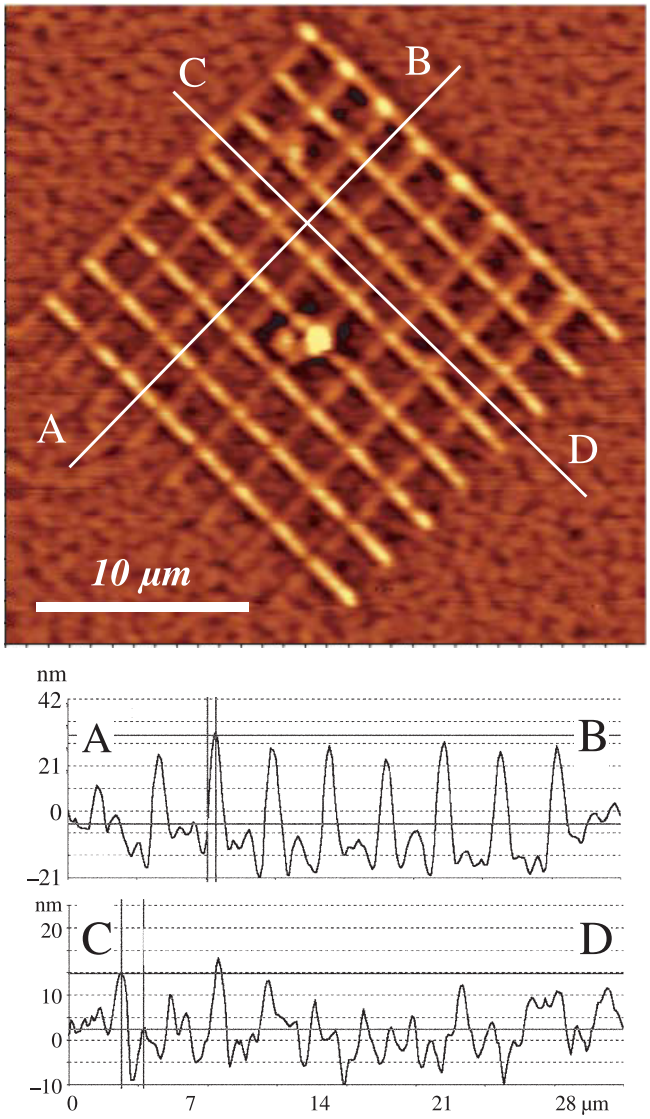

Fig. 7. Example of a regular nanostructure produced and investigated by a SNOM tip. It represents the two-dimensional cross grating built from two sets of eight 20-mm-long lines. The measured height of lines in the A–B direction is ~26 nm and in the C–D direction ~11 nm. The apparent line width is about 350 nm.

grating, which was produced by positioning the optical pen at equal distances of 2.5 µm along the *x*-direction and then moving the pen along the *y*-direction by about 20 µm. After inscribing eight lines, the procedure was repeated in the perpendicular direction. The apparent line width measured by the SNOM tip was found to be about 350 nm. However, it is well known that for all scanning probe microscopes the real width of a single structure is considerably smaller than the measured one, because the width is broadened by the tip radius (about 100 nm for the SNOM cantilever used in this study). Therefore, the real line width is expected to be in the

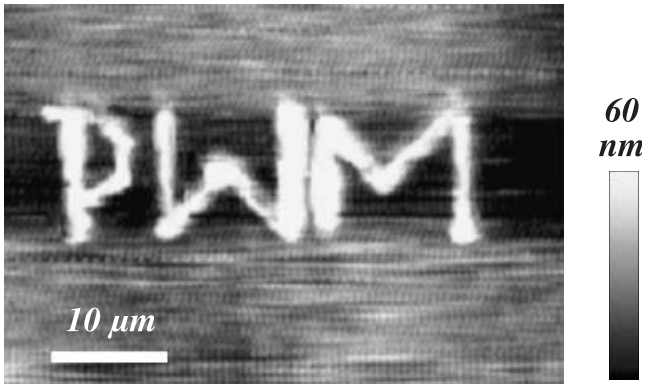

Fig. 8. Example of a non-regular nanostructure in surface topography – PWM (abbreviation from 'Physik Weicher Materie') – produced by an illuminated and investigated by a non-illuminated SNOM tip.

range of 100 nm and the structures inscribed with the help of the SNOM cantilever can indeed be termed nanostructures.

Interestingly, and as is clearly seen in Fig. 7, the first inscription step, when lines of about 25 nm height were produced along the direction C–D, is twice as effective as the second step made along the direction A–B (the lines were only 10 nm high). Such a noticeable decrease in the inscription efficiency at the second step can be explained by the anisotropy of the optically induced material transport, which depends not only on the intensity gradient but also on the polarization of the light (Kumar *et al.*, 1998). It is well known that the optical near-field at an illuminated SNOM tip is preferentially linearly polarized. Therefore, the efficiency of material transport should depend on the relation between the direction of light polarization and the direction of tip movement.

Another example of the nanostructures inscribed by an illuminated SNOM tip used as an optical pen can be seen on Fig. 8. Here, a non-regular relief pattern was produced by a manual motion of the SNOM cantilever in a manner chosen by the device operator. The three letters 'PWM', an abbreviation of our working group, were made by manipulation of the *x*–*y* table of the SNOM. Similarly, one can produce, for example, automatically or manually generated encoded technical figures for product protection or any user-defined nanostructure at an azobenzene-containing surface.

Conclusions

We have shown that scanning probe microscopy is a very powerful technique for the study of light-induced material transport in azobenzene polymer films. With this technique, we have found that molecules of pDR1M used in this study had moved into the centre of the light and that the inscription efficiency strongly depends on the light polarization, i.e. on the preferential chromophore orientation. The latter finding, from our point of view, strongly supports the orientational theories

proposed in the literature (Geue *et al.*, 1997; Pedersen *et al.*, 1998; Bublitz *et al.*, 2001).

A change in mechanical and elastic properties of the polymer material was detected on the surface of 1D and 2D relief gratings. Stiffness and adhesion were measured with a high lateral resolution using force–distance curves and pulse force mode of the AFM. Both measurements indicated that polymer material is stiffer at the SRG hills and more adhesive at the valleys. Higher stiffness at the hills could be explained in terms of higher density, which is in agreement with recent theoretical predictions made by our group (Saphiannikova *et al.*, 2004a,b).

We also have shown that the molecular transport can be easily generated at the subwavelength level using a SNOM set-up. The SNOM cantilever can be used as an optical pen for inscription of both regular and non-regular nanostructures. These structures (with typical sizes five times smaller than the wavelength of the excitation laser beam) are totally invisible in the optical region, which opens vast application possibilities, especially in product protection.

Acknowledgements

This work was supported by the 'Deutsche Forschungsgemeinschaft' and the 'Ministry of Science, Research and Culture', Brandenburg.

References

Baldus, O., Leopold, A., Hagen, R., Bieringer, T. & Zilker, S.J. (2001) Surface relief gratings generated by pulsed holography: a simple way to polymer nanostructures without isomerizing side-chains. *J. Chem. Phys.* **114**, 1344–1349.

Barrett, C.J., Rochon, P.L. & Natansohn, A.L. (1998) Model of laser-driven mass transport in thin films of dye-functionalized polymers. *J. Chem. Phys.* **109**, 1505–1516.

Bublitz, D., Fleck, B. & Wenke, L. (2001) A model for surface-relief formation in azobenzene polymers. *Appl. Phys. B*, **72**, 931–936.

Dumont, M. & Osman, A.E. (1999) On spontaneous and photoinduced orientational mobility of dye molecules in polymers. *Chem. Phys.* **245**, 437–462.

Geue, T., Saphiannikova, M., Henneberg, O., Pietsch, U., Rochon, P. & Natansohn, A. (2002) Formation mechanism and dynamics in polymer surface gratings. *Phys. Rev. E*, **65**, 052801, 1–4.

Geue, Th, Ziegler, A. & Stumpe, J. (1997) Light induced orientation phenomena in ultrathin photochromic polymer films. *Macromolecules*, **30**, 5729.

H'dhili, F., Bachelot, R., Lerondel, G. & Barchisi, D. (2001) Near-field optics: direct observation of field enhancement below an appertureless probe using a photosensitive polymer. *Appl. Phys. Lett.* **79**, 4019–4021.

Ikawa, T., Mitsuoka, T., Hasegawa, M., Tsuchimori, M., Watanabe, O., Kawata, Y., Egami, C., Sugihara, O. & Okamoto, N. (2000) Optical near field induced change in viscoelasticity on an azobenzene-containing polymer surface. *J. Phys. Chem. B*, **104**, 9055–9058.

Karageorgiev, P., Stiller, B., Prescher, D., Dietzel, B., Schulz, B. & Brehmer, L. (2000) Modification of the surface potential of azobenzene-containing Langmuir–Blodgett films in the near field of a scanning Kelvin microscope tip by irradiation. *Langmuir*, **16**, no. 13, S5515–5518.

Keum, C.-D., Ikawa, T., Tsuchimori, M. & Watanabe, O. (2003) Photodeformation behavior of photodynamic polymers bearing azobenzene moieties in their main and/or side chain. *Macromolecules*, **36**, 4916–4923.

Kumar, J., Li, L., Jiang, X.L., Kim, D.-Y., Lee, T.S. & Tripathy, S. (1998) Gradient force: the mechanism for surface relief grating formation in azobenzene functionalized polymers. *Appl. Phys. Lett.* **72**, 2096–2098.

Lagugne-Labarthet, F., Buffeteau, T. & Sourisseau, C. (1998) Molecular orientations in azopolymer holographic diffraction gratings as studied by Raman confocal microspectroscopy. *J. Phys. Chem. B*, **102**, 5754–5765.

Lagugne-Labarthet, F., Sourisseau, C., Schaller, R.D., Saykally, R.J. & Rochon, P. (2004) Chromophore orientations in a nonlinear azopolymer diffraction grating: even and odd parameters from far-field Raman and near-field second harmonic generation microscopes. *J. Phys. Chem. B*, **108**, 17509–17068.

Landraud, L., Peretti, J., Chaput, F., Lampel, G., Boilot, J.-P., Lahlil, K. & Safarov, I. (2001) Near-field optical pattering on azo-hybrid sol-gel films. *Appl. Phys. Lett.* **79**, 4562–4564.

Lefin, P., Fiorini, C. & Nunzi, J.-M. (1998) Anisotropy of the photo-induced translational diffusion of azobenzene dyes in polymer matrices. *Pure Appl. Opt.* **7**, 71–82.

Natansohn, A.L. & Rochon, P. (2002) Photoinduced motions in azo-containing polymers. *Chem. Rev.* **102**, 4139–4175.

Pedersen, T.G., Johansen, P.M., Holme, N.C.R., Ramanujam, P.S. & Hvilsted, S. (1998) Mean-field theory of photoinduced formation of surface relief in side-chain azobenzene polymers. *Phys. Rev. Lett.* **80**, 89–92.

Pietsch, U., Rochon, P. & Natansohn, A. (2000) Formation of a buried lateral density grating in azobenzene polymer films. *Adv. Mater.* **12**, 1129–1132.

Saphiannikova, M., Geue, T., Henneberg, O., Morawetz, K. & Pietsch, U. (2004a) Linear viscoelastic analysis of formation and relaxation of azobenzene polymer gratings. *J. Chem. Phys.* **120**, 4039–4045.

Saphiannikova, M., Henneberg, O., Geue, T., Pietsch, U. & Rochon, P. (2004b) Non-linear effects during inscription of azobenzene surface relief gratings. *J. Phys. Chem. B*, **108**, 15084–15089.

Stiller, B., Karageorgiev, P., Buchsteiner, A., Geue, T., Henneberg, O., Brehmer, L., Natansohn, A.L. & Hollrichter, O. (2003) Optically induced mass transport generated in near-fields. SPIE Proceedings. The International Society for Optical Engineering. *Advanced Organic Nonorganic Opt. Mater.* **5122**, 173–178.

Stiller, B., Karageorgiev, P., Geue, T., Morawetz, K., Saphiannikova, M., Mechau, N. & Neher, D. (2004) Optically induced mass transport studied by scanning near-field optical – and atomic force microscopy. *Physics Low-Dimensional Structures*, **1/2**, 129–138.

Stiller, B., Karageorgiev, P., Jüngling, T., Prescher, D., Zetzsche, T., Dietel, R., Knochenhauer, G. & Brehmer, L. (2001) Optically induced switching of azobenzene containing self assembling monolayers investigated by Kelvin probe and scanning force microscopy. *Mol. Cryst. Liq. Cryst.* **355**, 401–411.

Stiller, B., Karageorgiev, P., Perez-Enciso, E., Velez, M., Vieira, S., Reiche, J., Knochenhauer, G., Prescher, D. & Brehmer, L. (2000) Scanning Kelvin microscopy as a tool for visualization of optically induced molecular switching in azobenzene self assembling films. *Surf. Interface Anal.* **30**, 549–551.

Viswanathan, N.K., Kim, D.Y., Bian, S., Williams, J., Liu, W., Li, L., Samuelson, L., Kumar, J. & Tripathy, S.K. (1999) Surface relief structures on azo polymer films. *J. Mater. Chem.* **9**, 1941–1955.

Yager, K.G. & Barett, C.J. (2001) All-optical pattering of azo polymer films. *Curr. Opin. Solid State Mater. Sci.* **5**, 487–494.

Thermodynamic Theory of Light-Induced Material Transport in Amorphous Azobenzene Polymer Films

Marina Saphiannikova* and Dieter Neher*

Institute of Physics, University of Potsdam, Am Neuen Palais 10, 14469 Potsdam, Germany

Received: June 16, 2005; In Final Form: August 16, 2005

It was discovered 10 years ago that the exposure of an initially flat layer of an azobenzene-containing polymer to an inhomogeneous light pattern leads to the formation of surface relief structures, accompanied by a mass transport over several micrometers. However, the driving force of this process is still unclear. We propose a new thermodynamic approach that explains a number of experimental findings including the light-induced deformation of free-standing films and the formation of surface relief gratings for main inscription geometries. Our basic assumption is that under homogeneous illumination, an initially isotropic sample should stretch itself along the polarization direction to compensate the entropy decrease produced by the photoinduced reorientation of azobenzene chromophores. The magnitude of the elastic stress, estimated by taking the derivative of the free energy over the sample deformation, is shown to be sufficient to induce plastic deformation of the polymer film. Orientational distributions of chromophores predicted by our model are compared with those deduced from Raman intensity measurements.

Introduction

Incorporation of azobenzene chromophores into polymer systems via covalent bonding or even by blending gives rise to a number of unusual effects under visible and ultraviolet irradiation. The most astonishing effect is the inscription of surface relief gratings (SRGs) onto thin azobenzene polymer films.[1,2] Inscribing is usually performed by exposing the sample to a periodic intensity or polarization pattern resulting from the interference of two polarized laser beams. The absorption of light at a wavelength of about 480 nm induces material flow even at room temperature, several tens of kelvin below the glass transition temperature, T_G, of the polymers. The process of inscription is strongly dependent on the polarization state of the writing beams. Most groups report that two circular counterpolarized beams (circ−circ geometry) inscribe gratings of maximal diffraction efficiency, followed by two p−p polarized beams (p−p geometry), while two s−s polarized beams (s−s geometry) produce minimal surface changes.[3,4] However, on one particular functionalized copolymer system the p−p geometry is observed to be twice as efficient as the circ−circ geometry at a long time scale.[5]

Another interesting effect is the photoinduced deformation of azobenzene polymer films floating on a water surface.[6] It is shown that different types of azobenzene side-chain polyesters undergo opposite changes of shape under illumination with linear polarized light. Amorphous polyesters elongate along the direction of the electric field vector, while liquid-crystalline (LC) polyesters contract in the same direction. This result is in agreement with the observation that the phase of the SRGs, relative to that of the optical grating, strongly depends on the chemical architecture of the particular azobenzene polymer.[3]

A number of theories have been proposed to explain the material transport in SRGs on the molecular level.[7−11] Barret et al.[7] suggested the light-induced formation of a pressure gradient that depends on the light intensity and the polarization pattern produced by the writing beams. This pressure gradient develops from the increase of cis-population in the illuminated areas, due to the larger free volume requirement of the cis-isomers. However, the interference pattern of two circularly counterpolarized beams has nearly constant intensity and ellipticity along the grating vector,[10] and thus, this theory cannot explain the formation of SRGs in this inscription geometry. In contrast, the optical gradient theory of Tripathy and co-workers[8] describes satisfactorily all the important aspects of the experimental findings. Unfortunately, the force density estimated for conventional illumination conditions is 2 orders of magnitude smaller than that of the gravitational force (10^4 N/m^3)[12] and thus is far too small to be of influential importance. Lefin et al.[9] considered an anisotropic wormlike diffusion of azobenzene chromophores parallel to the orientation of their long axis just before photoisomerization takes place. Additionally, when a chromophore comes to a certain grating position, the authors assume that its orientation instantaneously relaxes to the average orientational distribution at this position. Thus, this scenario contradicts to a well-established "angular-hole-burning" mechanism:[13] The chromophores illuminated by linearly polarized light are gradually reoriented perpendicular to the polarization direction due to rotation during the isomerization cycle.

In the models discussed above, to explain the large-scale material transport at room temperature, it is necessary to assume a considerable degree of photoinduced plasticization, at least comparable with that at the glass transition. Therefore, in a linear viscoelastic modeling of SRG formation it was postulated that, as a result of the illumination with visible light, Young's modulus of the azobenzene polymer film is reduced by 3 orders of magnitude.[12,14] However, only very weak plasticization has been found in mechanical experiments performed recently in our group.[15,16] At room temperature, a less than 10% increase of the plate compliance upon homogeneous illumination with actinic light was observed. This is far below the degree of "softening" induced by heating the same layer above T_G. These

* To whom correspondence should be addressed. E-mail: mary@gadir.physik.uni-potsdam.de; neher@rz.uni-potsdam.de.

10.1021/jp053249h CCC: $30.25
Published on Web 09/21/2005

results suggest that illumination of an azobenzene polymer layer with actinic light must lead to a force that is strong enough to induce an observable material transport without significant light-induced plasticization of the film.

This force can originate from the light-induced orientation of azobenzene moieties. The probability that a chromophore, oriented at an angle θ with respect to the polarization direction, will be excited by the polarized light is proportional to $\cos^2\theta$. Therefore, starting from a sample with an isotropic angular distribution of the chromophores, multiple trans−cis−trans photoizomerization with linearly polarized light will result in a preferential orientation of the long axis of the chromophores.[13] After some time, a dynamic steady state will be established which is characterized by a rather small fraction of chromophores pointing in the polarization direction and thus a small photoizomerization rate. With respect to the following discussion, two things are important. First, even in the steady state, chromophores undergo frequent light-induced trans−cis−trans photoisomerization cycles, resulting in a rotational diffusion toward and away from the polarization direction. Second, the photoinduced alignment of the azobenzene moieties is solely due to excitation statistics, and thus, the chromophores do not gain a potential energy upon reorientation, if intermolecular interactions are omitted.

On the basis of the light-induced reorientation, Pedersen et al.[10] were able to explain the grating inscription with the help of the Maier−Saupe theory, which is valid for nematic liquid crystals: Under illumination with linearly polarized light, the azobenzene chromophores will orient parallel to each other and, therefore, their mutual attraction will increase. Due to this attraction, the sample should contract in the illuminated regions and the peaks of the SRG are predicted to form in the bright areas. Indeed, this prediction is consistent with results obtained for LC azobenzene polymers.[3] In another approach proposed by Bublitz et al.,[11] it is simply postulated that the orientation of chromophores along the grating vector leads to a deformation of the polymer film in this direction. Without providing a detailed microscopic picture, the authors correctly explain the inscription of SRGs as well as the deformation of azobenezene polymer films floating on a water surface.[6]

With every year, more and more evidence appears that chromophore reorientation must be the primary source for the inscription of SRGs and the film deformation under homogeneous illumination. Here, we like to mention studies carried out recently in the groups of Finkelmann and Ikeda on liquid-crystalline elastomers, in which preferential orientation of liquid-crystalline moieties was imposed during a cross-linking process.[17] These samples exhibit a substantial thermally induced contraction upon the nematic−isotropic phase transition.[18,19] This effect was explained by the strong coupling between LC ordering and the elastic properties of the polymer network.[20,21] Moreover, a reversible elongation−contraction[22] as well as bending−unbending behavior[23,24] of similar LC systems containing azobenzene moieties was observed upon alternating illumination with ultraviolet and visible light. The driving force for the large shape changes is suggested to arise from a variation in alignment order of the liquid-crystalline groups, caused by the trans−cis photoisomerization of the azobenzene chromophores.[25]

Following the spirit of these studies, we propose a new approach based on free energy and symmetry considerations for amorphous azobenzene polymer films. This approach readily explains uniaxial elongation of free-standing amorphous films as well as bending of the films on a flexible substrate under homogeneous illumination. Moreover, our model can correctly predict the formation of SRGs for the main inscription geometries (s−s, p−p, and circ−circ) as well as the orientational distribution of chromophores at any grating position. Last but not least, this approach allows us to estimate the light-induced elastic stress imposed by the light-induced reorientation of chromophores within the polymer matrix.

Light-Induced Reorientation of Chromophores. From a steric point of view, the azobenzene moiety can be considered as a rigid rod of length ∼15 Å and width ∼5 Å. The axis of one rod is labeled by the unit vector **e**, and the rod is assumed to have complete cylindrical symmetry about **e**. Starting from an isotropic sample, homogeneous illumination with polarized light leads to the reorientation of the chromophores. Following Onsager's approach,[26] this new orientational state can be described by the orientational distribution function

$$f(\theta_{\mathbf{E}}) = \text{norma}\cosh(\alpha \sin\theta_{\mathbf{E}}) \tag{1}$$

where α is the strength of the light-induced alignment and $\theta_{\mathbf{E}}$ is the angle between **e** and the electric field vector **E**. The normalization constant norma is given by

$$\text{norma} = [\int\int f(\theta_{\mathbf{E}})\, d\Omega]^{-1} \tag{2}$$

where $d\Omega = \sin\theta_{\mathbf{E}}\, d\theta_{\mathbf{E}}\, d\varphi$ with $0 \le \theta_{\mathbf{E}} \le \pi$ and $0 \le \varphi \le 2\pi$. Here, φ describes the angle of rotation of the unit vector around **E**. For $\alpha > 0$, this function has a peak at $\theta_{\mathbf{E}} = 90°$ (Figure 1a), that is, azobenzenes align preferentially perpendicular to **E**. With the increase of α, the order parameter

$$S_2 = \int\int \left[\frac{3}{2}\cos^2(\theta_{\mathbf{E}}) - \frac{1}{2}\right] f(\theta_{\mathbf{E}})\, d\Omega \tag{3}$$

decreases from 0 to −0.5. The latter value corresponds to the extreme case, when all azobenzene moieties lay in the same plane perpendicular to **E**. Thus, the electric field vector plays the role of the planar director in an ensemble of reoriented chromophores.

The entropy decrease per one azobenzene due to the preferential reorientation of chromophores is given by

$$S_{\text{azo}} = -k_{\text{B}} \int\int f(\theta_{\mathbf{E}}) \ln[4\pi f(\theta_{\mathbf{E}})]\, d\Omega \tag{4}$$

where k_{B} is Boltzmann's constant. Further, we shall assume that anisotropic interactions between azobenzene moieties can be neglected in the case of amorphous polymers because of the high steric hindrance imposed on the chromophores by a short spacer connecting the azobenzenes to the polymer backbone. Another factor that will be neglected in our approach is the change of the main chain entropy under illumination. With these two simplifications, the free energy per one azobenzene has only the entropy term $F_{\text{azo}} = -TS_{\text{azo}}$ where T is the absolute temperature. As it can be seen from Figure 1b, a relatively weak reorientation with $|S_2| \approx 0.25$ ($\alpha = 4$) already increases the free energy per one azobenzene by about 0.2 $k_{\text{B}}T$, whereas at stronger reorientations, $|S_2| > 0.4$ ($\alpha > 15$), the free energy increase becomes comparable with $k_{\text{B}}T$.

To minimize the free energy, the system under consideration needs to maximize its orientational entropy. In the case of free-standing films, this can be achieved if the sample stretches itself along the direction of the electric field vector, that is, along the planar director. This is observed experimentally in the case of amorphous polymers.[6] If one assumes affine deformation and incompressibility of the sample (see Appendix, part 1), then it

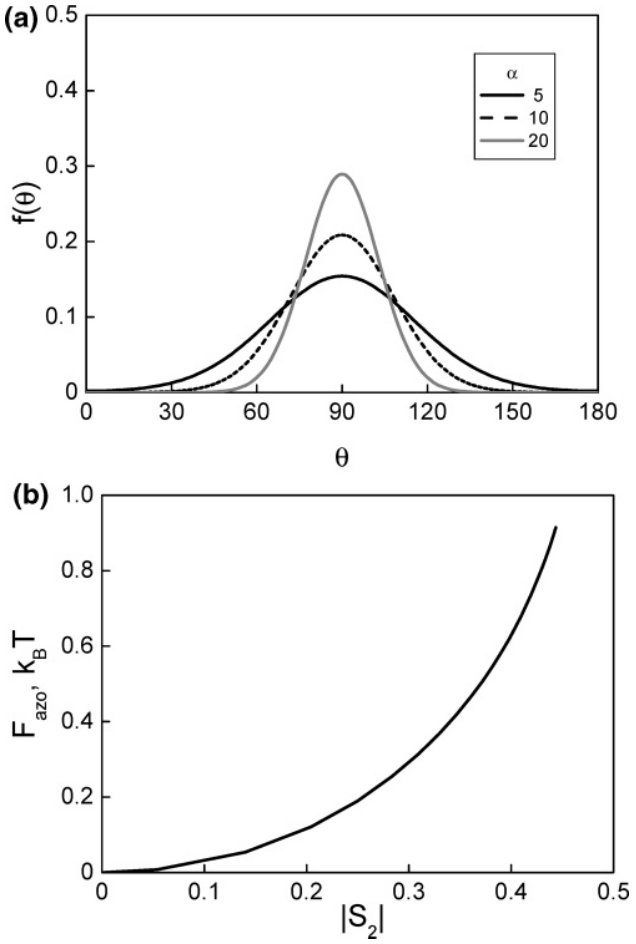

Figure 1. (a) Orientational distribution function $f(\theta)$ at different strengths of light-induced alignment: $\alpha = 5$, 10, and 20. (b) Dependence of the free energy increase per one azobenzene on the order parameter S_2.

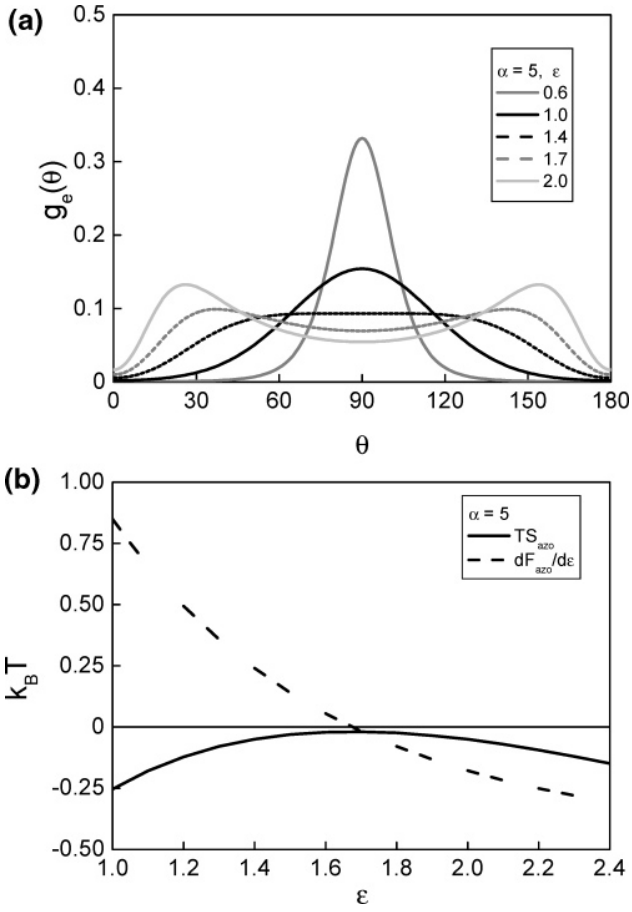

Figure 2. (a) Orientational distribution function at different strains: $\varepsilon = 0.6$, 1.0, 1.4, 1.7, and 2.0. The initial strength of light-induced alignment was $\alpha = 5$. (b) Dependence of the orientational entropy per one azobenzene on the elongation for $\alpha = 5$.

is possible to calculate a new orientational distribution function, $g(\varepsilon,\theta_1)$, for particular values of strain ε (Figure 2a). With the increase in strain, the peak around 90° gradually disappears, $g(\varepsilon,\theta_1)$ flattens, and two new peaks at 30° and 150° start to grow. At higher deformations, these peaks sharpen and shift toward 0° and 180°, that is, azobenzenes are reoriented by the elongation field and most of them are now aligned along the direction of the electric field vector. Correspondingly, with the increase in strain, the orientational entropy per one azobenzene goes through a maximum (Figure 2b). Hence, our approach predicts that after reaching this turning point, $\varepsilon_{max}(\alpha)$, the film should not furthermore change its shape. In reality, because the polarized light constantly reorients the chromophores back, perpendicular to **E**, higher deformation than ε_{max} should be possible.

The magnitude of elastic stress can be estimated by taking the derivative of the free energy over deformation[27]

$$\sigma(\varepsilon) = n\frac{\partial F(\varepsilon)}{\partial \varepsilon} \tag{5}$$

where n is the number density of chromophores. For relatively weak reorientation with $\alpha = 5$, we receive $(\partial F(\varepsilon)/\partial\varepsilon)|_{\varepsilon=1} = 0.85\ k_BT$ (Figure 2b); with n of about 1.5×10^{21} cm^{-3},[15,28] the elastic stress should be about 5 MPa at the beginning of deformation. This value is comparable with the magnitude of elastic stress which should be applied to unsoftened polymer films (elastic modulus of 1 GPa) in finite element simulations in order to mimic the inscription of SRGs.[12]

For further understanding, it is important to consider the changes in an initially isotropic sample under uniaxial deformation. Such a situation corresponds to the elongation (compression) in the nonilluminated areas of the SRG. It is clear that the initially flat orientational distribution should transform into a peaked function: If the sample contracts ($\varepsilon < 1$), then the maximum of $g(\varepsilon,\theta_1)$ grows at 90°; if the sample elongates ($\varepsilon > 1$), then the two maxima grow at 0° and 180° (Figure 3a). In both cases, an entropy decrease leads to the appearance of a restoring elastic force (the elongational branch of solution is shown in Figure 3b).

Surface Relief Gratings. To describe different inscription geometries, one needs to calculate $\theta_{\mathbf{E}}$ in the laboratory frame. Let us take the direction of the grating vector as the x-axis, the direction along the grating grooves (in the sample plane) as the y-axis, and the direction perpendicular to the substrate as the z-axis. In this frame, $\mathbf{e} = (e_x,e_y,e_z)$ with $e_x = \cos\theta_0$, $e_y = \sin\theta_0 \cos\varphi_0$, and $e_z = \sin\theta_0 \sin\varphi_0$. Here, θ_0 is the angle between **e** and the x-axis, and φ_0 is the angle between **e** and the y-axis. Further, $\cos\theta_{\mathbf{E}} = ((\mathbf{E}\cdot\mathbf{e})/|\mathbf{E}|\cdot|\mathbf{e}|)$.

For a grating with period D ($D = \lambda/2 \sin\Theta$, where λ is the wavelength of incident light and Θ is the incidence angle between the laser beams), the electric field vector, the light

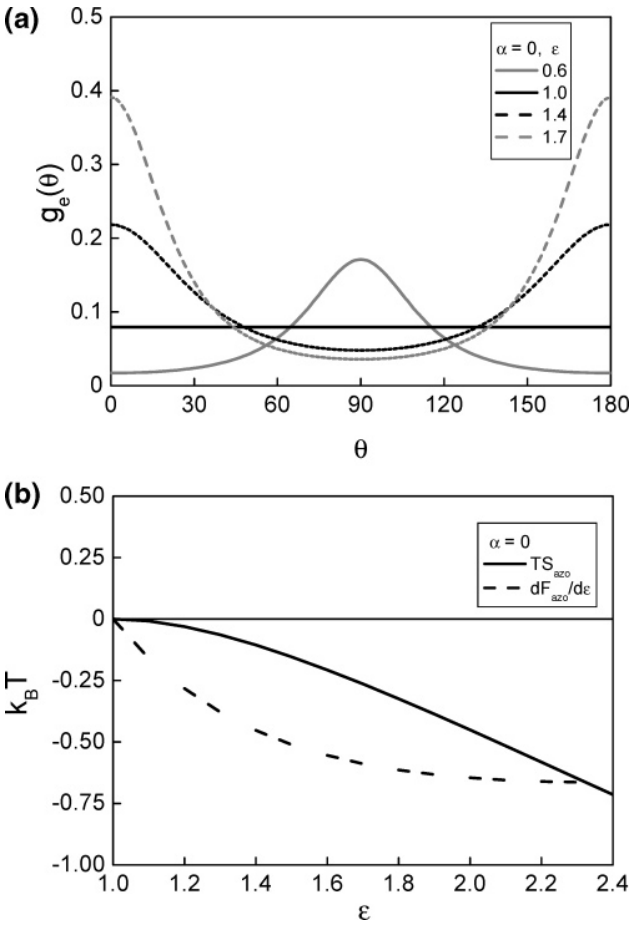

Figure 3. (a) Orientational distribution function at different strains: $\varepsilon = 0.6$, 1.0, 1.4, and 1.7 for $\alpha = 0$. (b) Dependence of the orientational entropy per one azobenzene on the elongation for $\alpha = 0$.

intensity, I, and the angle $\theta_{\mathbf{E}}$ are given by the following functions of x for p−p geometry

$$\mathbf{E} = E_0 \cos\left(\frac{\pi x}{D}\right) \mathbf{i}$$

$$I(x) = I_0 \cos^2\left(\frac{\pi x}{D}\right)$$

$$\sin\theta_{\mathbf{E}} = (1 - e_x^2)^{0.5}$$

for s−s geometry

$$\mathbf{E} = E_0 \sin\left(\frac{\pi x}{D}\right) \mathbf{j}$$

$$I(x) = I_0 \sin^2\left(\frac{\pi x}{D}\right)$$

$$\sin\theta_{\mathbf{E}} = (1 - e_y^2)^{0.5} \tag{6}$$

for circ−circ geometry

$$\mathbf{E} = E_0 \cos\left(\frac{\pi x}{D}\right) \mathbf{i} + E_0 \sin\left(\frac{\pi x}{D}\right) \mathbf{j}$$

$$I(x) = I_0$$

$$\sin\theta_{\mathbf{E}} = \left[1 - \left(\cos\left(\frac{\pi x}{D}\right) e_x + \sin\left(\frac{\pi x}{D}\right) e_y\right)^2\right]^{0.5}$$

In the above formulas, the term $\cos\Theta$ is omitted being close to unity at small incidence angles. To make a comparison with the experimental results discussed later, we have chosen in eq 6 the same assignment as in the series of papers written by Lagugne-Labarthet et al.[29,30] The strength of alignment should be proportional to the intensity of light, therefore, we have introduced for p−p geometry

$$\alpha(x) = \alpha_0 \cos^2\left(\frac{\pi x}{D}\right)$$

for s−s geometry

$$\alpha(x) = \alpha_0 \sin^2\left(\frac{\pi x}{D}\right) \tag{7}$$

for circ−circ geometry

$$\alpha(x) = \alpha_0$$

This, finally, leads to three orientational distribution functions for p−p geometry

$$f(\theta_0,x) = \text{norma}\cdot\cosh\left\{\alpha_0 \cos^2\left(\frac{\pi x}{D}\right)(1 - e_x^2)^{0.5}\right\}$$

for s−s geometry

$$f(\theta_0,\varphi_0,x) = \text{norma}\cdot\cosh\left\{\alpha_0 \sin^2\left(\frac{\pi x}{D}\right)(1 - e_y^2)^{0.5}\right\} \tag{8}$$

for circ−circ geometry

$$f(\theta_0,\varphi_0,x) = \text{norma}\cdot\cosh\left\{\alpha_0\left[1 - \left(\cos\left(\frac{\pi x}{D}\right) e_x + \sin\left(\frac{\pi x}{D}\right) e_y\right)^2\right]^{0.5}\right\}$$

Using these functions, the orientational entropy per one azobenzene at the position x along the grating vector can be calculated as

$$S_{\text{azo}}(x) = -k_B \int\int f(\theta_0,\varphi_0,x) \ln[4\pi f(\theta_0,\varphi_0,x)]\, d\Omega \tag{9}$$

and, hence, the drop of orientational entropy per one grating period D due to the preferential reorientation of chromophores can be expressed as

$$S_0 = -k_B n h_0 D \int_0^D S_{\text{azo}}(x)\, dx \tag{10}$$

where h_0 is the thickness of the active layer. Here, for simplicity, the sample width along the y-axis is taken to be D. Further, a dimensionless quantity

$$\hat{S}_0 = \frac{S_0}{2k_B n h_0 D^2} = \int_0^{1/2} S_{\text{azo}}(\hat{x})\, d\hat{x} \tag{11}$$

with $\hat{x} = x/D$

will be considered. Due to symmetry of solution, the dimensionless entropy $\hat{S}_0$ is calculated for a half of grating period.

To maximize its orientational entropy, the film can undergo an appropriate deformation $\varepsilon(x)$ at every position along the grating vector. Due to translational symmetry along the y-axis, the sample can only deform itself in two other directions. Again, if we assume an incompressible material, elongation (contraction) along the grating vector has to be accompanied by contraction (elongation) in the direction perpendicular to the

sample surface. Further, since the polarization pattern is a sinusoidal function with periodicity D, it is meaningful to assume $\varepsilon(x)$ to be of the same form

$$\varepsilon(x) = 1 + \varepsilon_0 \cos(2\pi x/D + \phi). \quad (12)$$

Here, ϕ is the phase of the surface relief grating: $\phi = 0$ (case I) corresponds to the mass transport into nonilluminated regions for the p−p geometry, while $\phi = \pi$ (case II) describes the mass transport into nonilluminated regions for the s−s geometry. Further, we shall consider only these two cases as other phases lead to asymmetrical solutions.

At small deformations, $\varepsilon_0 < 0.2$, the deformation law given by eq 12 results in a nearly sinusoidal grating. At higher deformations, the grating deviates from a sinusoidal one because the finite element with the initial coordinate x_0 shifts toward

$$x(x_0) = \int_0^{x_0} \varepsilon(x)\, dx = x_0 \pm \varepsilon_0 \frac{D}{2\pi} \sin(2\pi x_0/D) \quad (13)$$

where the sign "−" corresponds to case I and the sign "+" to case II. However, the grating period is preserved: $D^{-1} \int_0^D \varepsilon(x)\, dx = 1$. The grating relief height at coordinate x is defined by $h(x) = h_0/\varepsilon(x_0(x))$, which ensures the incompressibility of the sample: $D^{-1} \int_0^D h(x)\, dx = h_0$.

If we again assume affine deformation and take into account that the film is confined along the y-axis, then it is possible to calculate a new orientational distribution function, $g(\varepsilon,\theta_1,\varphi_1)$, at any position x for the value of strain $\varepsilon(x)$ (see Appendix, part 2). The dimensionless entropy per half of a grating period after deformation is given by

$$\hat{S}(\varepsilon_0) = \frac{1}{2k_B n h_0 D^2} \int_0^{1/2} \frac{S_{azo}(\varepsilon(\hat{x}))}{\varepsilon(\hat{x}_0(\hat{x}))}\, d\hat{x} \quad (14)$$

where

$$S_{azo}(\varepsilon) = -k_B \int\int g(\varepsilon,\theta_0,\varphi_0) \ln[4\pi g(\varepsilon,\theta_0,\varphi_0)]\, d\Omega \quad (15)$$

and the absolute change of dimensionless entropy per half of a grating period is equal to $\Delta\hat{S} = \hat{S}(\varepsilon_0) - \hat{S}_0$.

Results

I. p−p Geometry. Following the assignment of Lagugne-Labarthet et al.,[29] we have used $I(x) = I_0 \cos^2(\pi x/D)$, whereby the intensity maxima appear at $x = 0$ or $x = D$ and the intensity minimum at $x = D/2$. Elongation in the region of low intensity, case II, results in the further decrease of entropy, and thus, we should rule out this possibility. Contrary, as it can be seen from Figure 4a, elongation in the region of high intensity, case I, effectively increases the entropy. Thus, our model predicts that polymer chains move from the regions with high light intensity into the nonilluminated regions. This is indeed observed experimentally for most amorphous polymers. Different maximal deformations are predicted depending on the strength of light-induced alignment: from 0.15 for $\alpha = 5$ until 0.25 for $\alpha = 20$. If one considers a 500 nm thick polymer layer, then the height of SRG will be in the range of 150−250 nm.

Our approach allows us further to calculate the orientational distribution function at any position of SRG. Figure 4b represents this function for case I at the valleys (intensity maximum, $x = 0$ or $x = D$) and at the peak (intensity minimum, $x = D/2$) before and after deformation. Due to elongation, chromophores situated at the valleys of the SRG become less oriented. Therefore, local entropy is considerably increased upon

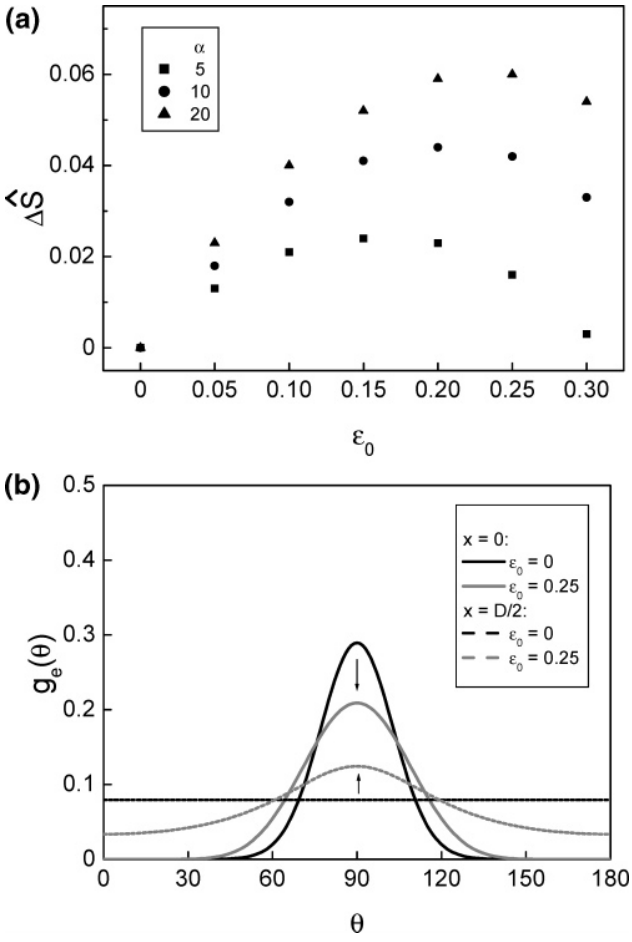

Figure 4. p−p geometry, case I. (a) Dependence of the absolute change of the dimensionless entropy on the strain for different strengths of the initial light-induced alignment: $\alpha = 5$, 10, and 20. (b) Orientational distribution function at different positions of the grating for $\varepsilon_0 = 0.25$: solid, $x = 0$ or $x = D$; dashed, $x = D/2$; black, before stretching; gray, after stretching. The initial strength of light-induced alignment was $\alpha = 20$. Black arrows show the direction of transformation of the distribution function.

deformation. Due to the compressive deformation at the peak (situated in the dark area), the initially randomly oriented chromophores align perpendicular to the grating vector. This leads to a slight decrease of the local entropy, the value of which nevertheless stays higher than that at the valley. On the whole, the total entropy, integrated over one grating period, is effectively increased due to favorable redistribution of mass: polymer chains move in the direction of local entropy increase.

We note here that orientational distribution functions calculated from Raman intensity measurements were shown to be bimodal at the peak of SRG ($x = D/2$) and broad asymmetric at the valleys (Figure 11 from ref 29), with maxima around $\theta = 60°$ and 120°. The shape of these functions point to high deformations reached in the real experiment. Indeed, SRGs with the height of at least 200 nm were inscribed on 400 nm thick pDR1M layers. This corresponds to an average deformation of about 1.3; however, one expects a much higher degree of deformation in the upper layer of the SRG due to the strong absorption of light. In fact, using $\alpha = 5$ and $\varepsilon_0 = 0.7$, our calculations also predict a broad asymmetric function at the valleys, with maxima around $\theta = 40°$ and 140°. To make the comparison with the experimental results easier, we have used the same normalization as in Figure 11 in ref 29 and presented the function as a polar plot (Figure 5a, the black curve). Quite

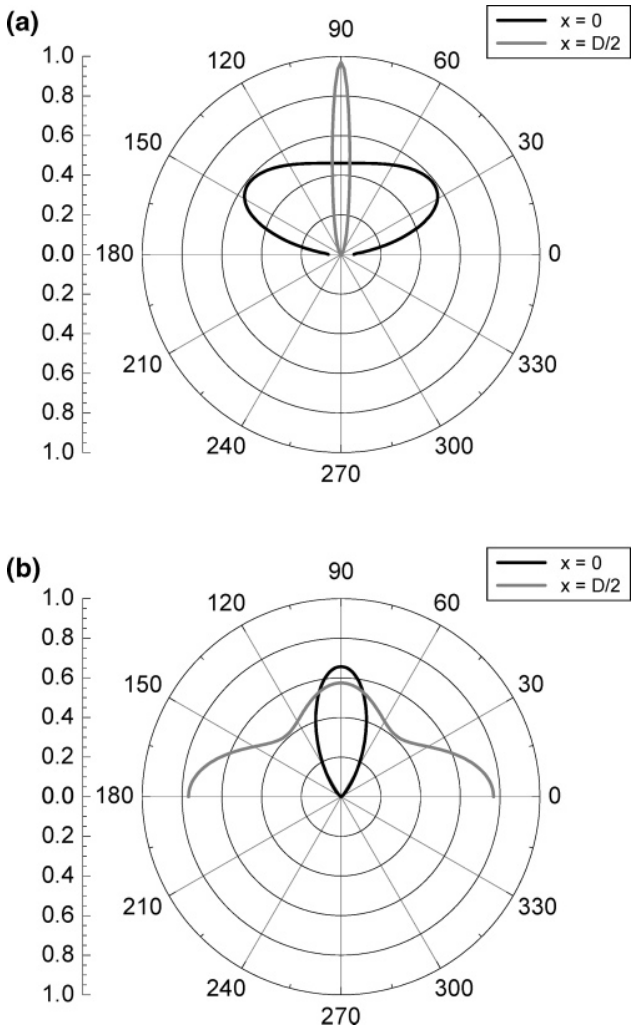

Figure 5. Polar diagrams of the orientational distribution function at different positions of the grating: black, $x = 0$ or $x = D$; gray, $x = D/2$. (a) p−p geometry, case I, normalization as in ref 29; $\alpha = 5$ and $\varepsilon_0 = 0.7$. $g_e(\theta)$ is divided by 4 at $x = D/2$. (b) circ−circ geometry, case I, normalization as in ref 30; $\alpha = 20$ and $\varepsilon_0 = 0.25$. $g_e(\theta)$ is divided by 2 at $x = 0$.

surprising is the appearance of a bimodal distribution function in the Raman intensity measurements at the peaks of the SRG. In this region of high compression (low light intensity), our approach predicts that the initially isotropic orientational distribution transforms into a unimodal function with the maximum at $\theta = 90°$ (Figure 5a, the gray curve).

II. s−s Geometry. We have chosen the assignment $I(x) = I_0 \sin^2(\pi x/D)$, whereby the intensity minima appear at $x = 0$ or $x = D$ and the intensity maximum at $x = D/2$. Elongation in the region of low intensity, case I, results in the further decrease of entropy, and thus, we rule out this possibility. On the contrary, as it can be seen from Figure 6a, weak elongation in the region of high intensity, case II, increases the entropy. Thus, our model predicts that polymer chains move from the regions with high light intensity into nonilluminated regions, as in the p−p geometry, and this is also observed experimentally. Different maximal deformations are predicted depending on the strength of the initial light-induced aligment: from 0.05 at $\alpha = 5$ until 0.15 at $\alpha = 20$. Hence, in agreement with experiment, the s−s geometry leads to only shallow gratings.

Figure 6b represents the orientational distribution function for case II before and after deformation at the valley ($x = D/2$, intensity maximum) and at the peaks ($x = 0$ or $x = D$, intensity minimum). Due to compressive deformation at the peaks of the SRG, the initially randomly oriented chromophores align perpendicular to the grating vector, which leads to a slight decrease of the local entropy. Due to elongation at the valley (situated in the bright area), the double-peaked function becomes more pronounced and, hence, the local entropy in this region also decreases. However, the total entropy, integrated over one grating period, is slightly increased because the polymer material moves in the direction of the local entropy increase.

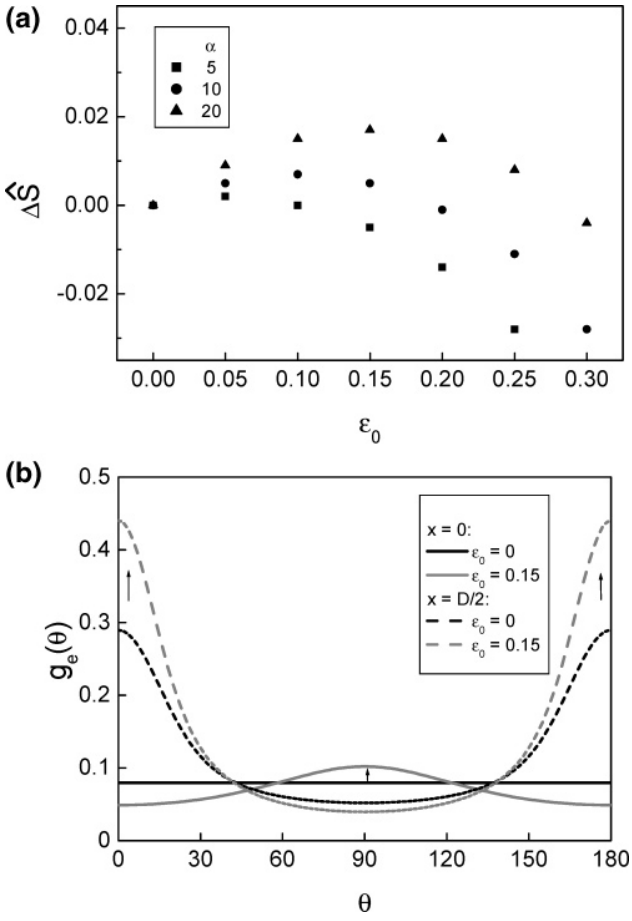

Figure 6. s−s geometry, case II. (a) Dependence of the absolute change of the dimensionless entropy on the strain for different strengths of light-induced alignment: $\alpha = 5$, 10, and 20. (b) Orientational distribution function at different positions of the grating: solid, $x = 0$ or $x = D$; dotted, $x = D/2$; black, before stretching; gray, after stretching; $\alpha = 20$ and $\varepsilon_0 = 0.15$.

III. circ−circ Geometry. Following the assignment of Lagugne-Labarthet et al.,[29] we have chosen $\mathbf{E} = E_0 \cos(\pi x/D)\mathbf{i} + E_0 \sin(\pi x/D)\mathbf{j}$ whereby $I(x) = \text{const}$. Elongation at $x = 0$ or $x = D$, case I, effectively increases the entropy (Figure 7a). Thus, our model predicts that polymer chains move from the regions where **E** is parallel to the grating vector into the regions where **E** is perpendicular to the grating vector. Similar to the p−p geometry, the valleys appear at $x = 0$ or $x = D$ and peaks at $x = D/2$. Different maximal deformations are predicted depending on the strength of light-induced alignment: from 0.10 at $\alpha = 5$ until 0.15 at $\alpha = 20$. Comparison with the values for maximal deformation obtained for the two other geometries reveals that the circ−circ geometry appears to be more effective for inscription of SRGs than the s−s geometry (especially at low values of α) but less effective than the p−p geometry. However, it is found experimentally that the circ−circ geometry

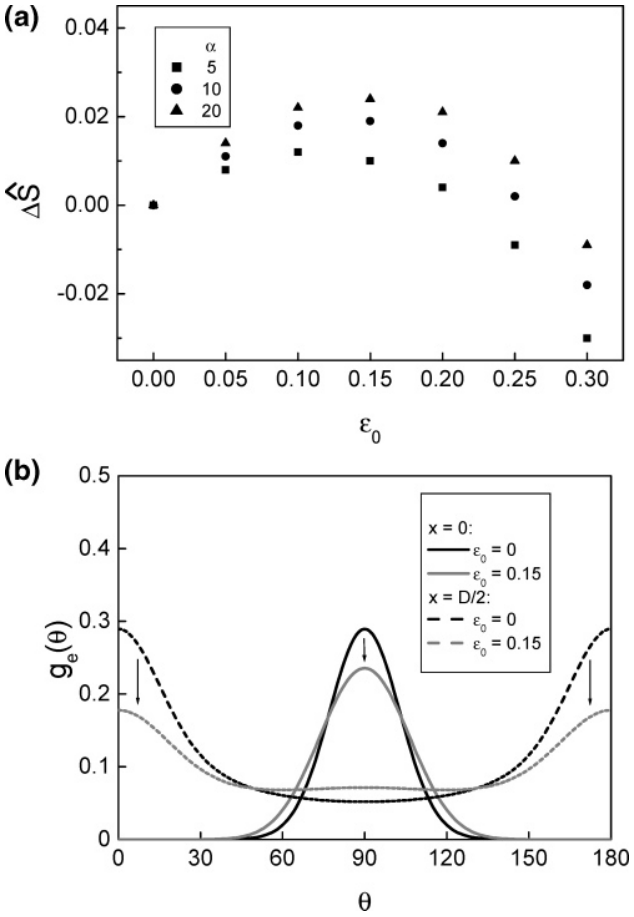

Figure 7. circ−circ geometry, case I. (a) Dependence of the absolute change of the dimensionless entropy on the strain for different strengths of light-induced alignment: $\alpha = 5$, 10, and 20. (b) Orientational distribution function at different positions of the grating: solid, $x = 0$ or $x = D$; dotted, $x = D/2$; black, before stretching; gray, after stretching; $\alpha = 20$ and $\varepsilon_0 = 0.15$.

is most effective, concerning the rate of grating formation and the resulting grating heights.[3,4] A possible reason for the discrepancy between the model prediction and experimental results will be discussed later.

The electric field in the circ−circ geometry is a linear superposition of the electric fields in the p−p and in the s−s geometries. Since the p−p geometry induces a stronger force, it is not surprising that our calculations predict chain transport to occur in the same direction as in the p−p geometry and that the predicted effectiveness of the circ−circ geometry is between that of the s−s and p−p geometries. Bublitz et al.[11] obtain the same result, although the superposition principle is not fulfilled in their paper. These authors predicted that in the case of s−s inscription, polymer chains move from the nonilluminated regions into the regions with high light intensity, that is, in the same direction as for the p−p geometry. Thus, one would expect that in the model of Bublitz et al.[11] the circ−circ geometry is shown to be the most effective one, which is not the case. Also, the theory of Pedersen et al.[10] (for LC polymers) predicts that material transport for the p−p and circ−circ geometries occurs in the same direction.

Figure 7b represents the orientational distribution function after circ−circ inscription for case I, before and after deformation, at the valleys ($x = 0$ or $x = D$, **E** is parallel to the grating vector) and at the peaks ($x = D/2$, **E** is perpendicular to the grating vector). Due to elongation, chromophores situated at the valleys of SRG become less oriented, and the local entropy is considerably increased. Due to the compressive deformation at the peaks, the chromophores initially oriented along the grating vector will be reoriented perpendicular to it, which also leads to a slight increase of the local entropy. Here, the orientational distribution functions have a particular feature—at higher deformations a small peak situated at $\theta = 90°$ starts to grow. Orientational distribution functions obtained from Raman intensity measurements were shown to be bimodal at $x = 0$ or $x = D$ and have three maxima around $\theta = 0°$, 90°, and 180° at $x = D/2$ (Figure 9 from ref 30). Using $\alpha = 20$ and $\varepsilon_0 = 0.25$, we can also obtain this three-peaked function at $x = D/2$, but contrary to ref 30, it is found at the SRG peaks. To make comparison with the experiment easier, we have used the same normalization as in Figure 9 of ref 30 and presented the three-peaked function as a polar plot (Figure 5b, the gray curve). At $x = 0$ or $x = D$, a unimodal function with the maximum at $\theta = 90°$ (Figure 5b, the black curve) is predicted for $\alpha = 20$ and $\varepsilon_0 = 0.25$.

The discrepancy in the shape of the orientational distribution functions determined from Raman spectrometry results and of those obtained here can be explained by the following reasons: On one hand, the mass transport of polymer chains can disturb the theoretically predicted distributions, as pointed out in ref 30; on the other hand, the experimentally determined functions are reconstructed from the P2 and P4 order parameters values which may lead to some uncertainties.

Discussion and Conclusions

The thermodynamic approach proposed in this paper allows us to explain a number of experimental findings, among them are the light-induced deformation of free-standing films and the inscription of SRGs in three main geometries. We have shown that under homogeneous illumination the sample should stretch itself along the polarization direction to compensate for the entropy decrease produced by photoinduced reorientation of the chromophores. A value for the elongational tension can be estimated by taking the derivative of the free energy over the sample deformation. This tension is shown to be sufficient to induce plastic deformation of the polymer film.

In agreement with experimental findings, we predict that polymer chains should move into the nonilluminated regions in the case of the s−s and p−p inscription geometries. For the circ−circ geometry, we expect the same direction of the chain transport as for the p−p geometry (from the regions where **E** is parallel to the grating vector), similar to prediction by Bublitz et al.[11] and contrary to the experimental reports.[30,31] Presently, we cannot propose any reason during inscription with two circularly polarized beams that the chains should move in the direction opposite to that found for the p−p geometry. Therefore, the question arises of how the position of grating peaks relative to the direction of an electric field vector is defined in the experiments with periodic polarization pattern, where there is no intensity modulation along the grating period.

Another problem is that our calculations predict an intermediate efficiency for the circ−circ geometry in comparison to the s−s and p−p geometries. Only one functionalized copolymer system has so far been reported to exhibit the highest surface grating efficiency in the p−p inscription geometry,[5] whereas a number of the other experiments[3,4] unambiguously show that the circ−circ geometry is the most effective one. We suppose that a possible reason for the discrepancy between most experimental studies and our prediction is a slight light-induced softening of the polymer film. Obviously, this softening is

expected to be less pronounced in the p−p and s−s geometries due to the presence of nonilluminated regions. On the other hand, if one assumes a considerable plasticization under illumination, then it becomes difficult to understand how a sinusoidal grating can be inscribed, for example, by two p−p polarized interfering beams. Let us consider a sinusoidal stress in the direction of the grating vector and assume a linear relationship between the stress and the strain. Let us further assume that Young's modulus decreases many orders of magnitude at the intensity maxima while at the intensity minima it stays unaffected. Then, elongation in the region of high light intensity will not be accompanied by a contraction of similar magnitude in the region of low light intensity. As a consequence, two peaks will grow on both sides of the illuminated region. This is not observed experimentally. Also, it seems plausible that considerable modulation of the sample compliance should result in a strongly unsinusoidal thickness modulation with two peaks per period of the illumination grating.

It should be noted that presently we do not consider the dynamic reorientation of chromophores that takes place in the cis−cis geometry when polymer material is moving between two grating positions with slightly different polarization directions. One may expect that this reorientation can be also responsible for the higher effectiveness of the cis−cis geometry in comparison with the p−p geometry.

In our approach, we do not take into account the sample compressibility which is shown to lead to the formation of a buried density grating in azobenzene polymer films.[32,33] We believe that this simplification will not affect the outcome of our approach qualitatively as the predicted density changes do not exceed 5%.[12] Further, we neglect any intermolecular interactions between azobenzene chromophores, although these interactions may play a role at high laser intensities. With the increase of light intensity, the strength of chromophore reorientation increases which in its turn should lead to an increase of attractive side−side interactions between chromophores. If the attractive contribution to the free energy overcomes the entropy term, then the mass transport will change its direction, as is found in ref 34. The same is true in the case of liquid-crystalline systems which have nonnegligible intermolecular interactions between the chromophores.[3]

Another interesting prediction of our theory is that an azobenzene polymer film coated on a flexible substrate should bend when illuminated homogeneously with polarized light. The bending will be again caused by the coupling between chromophore orientation and the elastic deformation of the amorphous polymer film. The sample coated on a flexible substrate cannot be directly stretched, but it can be slightly bent which will lead to chromophore disorientation and thus to an increase of the orientational entropy (decrease in the free energy).

Acknowledgment. M.S. would like to acknowledge Prof. Ullrich Pietsch (University of Potsdam) and his "azobenzene" group—Dr. Thomas Geue (Paul Scherrer Institute, Zurich), Dr. Oliver Henneberg, and Dr. Knut Morawetz—for many years of fruitful collaboration without which this work could not be done. Further, we acknowledge Norman Mechau for fruitful discussions. This work was financially supported by the DFG under Grants NE410/6-2 and NE410/8-1.

Appendix. Affine transformation under uniaxial tension

1. Free-Standing Film. Let us consider a free-standing film subjected to a uniaxial tension, ε, along the x-axis. Polymer material is assumed to be incompressible and isotropic. Due to cylindrical symmetry it is convenient to define the unit vector as $\mathbf{e} = (e_x,e_r)$ with $e_x = \cos\theta_0$ and $e_r = \sin\theta_0$, where θ_0 is the angle between $\mathbf{e}$ and the x-axis.

Under affine deformation the unit vector $\mathbf{e}$ transforms into $\mathbf{e}'(\varepsilon) = (\varepsilon e_x,\varepsilon^{-1/2}e_r)$ which has to be normalized to a new unit vector $\mathbf{e}(\varepsilon) = (\mathbf{e}'(\varepsilon)/|\mathbf{e}'(\varepsilon)|)$. The direction of $\mathbf{e}(\varepsilon)$ is described by a new angle θ_1

$$\cos\theta_1 = \frac{\cos\theta_0}{[\cos^2\theta_0 + \varepsilon^{-3}\sin^2\theta_0]^{0.5}} \tag{A1.1}$$

A new orientational distribution function, $g(\varepsilon,\theta_1)$, can be determined using the following relation

$$\int\int g(\varepsilon,\theta_1)\,\mathrm{d}\Omega_1 = \int\int f(\theta_0)\,\mathrm{d}\Omega_0 \tag{A1.2}$$

which leads to

$$g(\varepsilon,\theta_1) = f(\theta_0)\frac{\mathrm{d}\cos\theta_0}{\mathrm{d}\cos\theta_1} \tag{A1.3}$$

Using eqs A1.1 and A1.3, the new distribution function is determined to be

$$g(\varepsilon,\theta_1) = f(\theta_0)\varepsilon^3[\cos^2\theta_1 + \varepsilon^3\sin^2\theta_1]^{-3/2} \tag{A1.4}$$

In this formula, the old angle θ_0 should be expressed through the new angle θ_1 using the following transformation

$$\cos\theta_0 = \frac{\cos\theta_1}{[\cos^2\theta_1 + \varepsilon^3\sin^2\theta_1]^{0.5}} \tag{A1.5}$$

2. Film Confined in One Direction. Let us consider a similar situation, but now the film is confined along the y-axis. The unit vector is defined as $\mathbf{e} = (e_x,e_y,e_z)$ with $e_x = \cos\theta_0$, $e_y = \sin\theta_0\cos\varphi_0$, and $e_z = \sin\theta_0\sin\varphi_0$. Here, θ_0 is the angle between $\mathbf{e}$ and the x-axis, and φ_0 is the angle between $\mathbf{e}$ and the y-axis.

Under affine deformation the unit vector $\mathbf{e}$ transforms into $\mathbf{e}'(\varepsilon) = (\varepsilon e_x,e_y,\varepsilon^{-1}e_z)$ which is further normalized to a new unit vector defined by

$$\cos\theta_1 = \frac{\cos\theta_0}{[\cos^2\theta_0 + \varepsilon^{-2}\sin^2\theta_0(\cos^2\varphi_0 + \varepsilon^{-2}\sin^2\varphi_0)]^{0.5}} \tag{A2.1}$$

$$\cos\varphi_1 = \frac{\cos\varphi_0}{(\cos^2\varphi_0 + \varepsilon^{-2}\sin^2\varphi_0)^{0.5}}$$

Using the following relation

$$\int\int g(\varepsilon,\theta_1,\varphi_1)\,\mathrm{d}\Omega_1 = \int\int f(\theta_0,\varphi_0)\,\mathrm{d}\Omega_0 \tag{A2.2}$$

one can show that the new distribution function, $g(\varepsilon,\theta_1,\varphi_1)$, is given by

$$g(\varepsilon,\theta_1,\varphi_1) = f(\theta_0,\varphi_0)\frac{\mathrm{d}\cos\theta_0}{\mathrm{d}\cos\theta_1}\frac{\mathrm{d}\varphi_0}{\mathrm{d}\varphi_1} \tag{A2.3}$$

After simple rearrangement, one arrives to the following expression

$$g(\varepsilon,\theta_1,\varphi_1) = f(\theta_0,\varphi_0)\varepsilon^3[\cos^2\theta_1 + \varepsilon^2\sin^2\theta_1(\cos^2\varphi_1 + \varepsilon^2\sin^2\varphi_1)]^{-3/2} \quad \text{(A2.4)}$$

in which the old angles θ_0 and φ_0 should be expressed through the new angles θ_1 and φ_1

$$\cos\theta_0 = \frac{\cos\theta_1}{[\cos^2\theta_1 + \varepsilon^2\sin^2\theta_1(\cos^2\varphi_1 + \varepsilon^2\sin^2\varphi_1)]^{0.5}} \quad \text{(A2.5)}$$

$$\cos\varphi_0 = \frac{\cos\varphi_1}{(\cos^2\varphi_1 + \varepsilon^2\sin^2\varphi_1)^{0.5}}$$

References and Notes

(1) Rochon, P.; Batalla, E.; Natansohn, A. *Appl. Phys. Lett.* **1995**, *66*, 136.

(2) Kim, D. Y.; Li, L.; Jiang, X. L.; Shivshankar, V.; Kumar, J.; Tripathy, S. K. *Macromolecules* **1995**, *28*, 8835.

(3) Viswanathan, N. K.; Kim, D. Y.; Bian, S.; Williams, J.; Liu, W.; Li, L.; Samuelson, L.; Kumar, J.; Tripathy, S. K. *J. Mater. Chem.* **1999**, *9*, 1941.

(4) Henneberg, O.; Panzner, T.; Pietsch, U.; Geue, T.; Saphiannikova, M.; Rochon, P.; Finkelstein, K. *Z. Kristallogr.* **2004**, *219*, 218.

(5) Lagugne-Labarthet, F.; Buffeteau, T.; Sourisseau, C. *J. Phys. Chem. B* **1999**, *103*, 6690.

(6) Bublitz, D.; Helgert, M.; Fleck, B.; Wenke, L.; Hvilstedt, S.; Ramanujam, P. S. *Appl. Phys. B* **2000**, *70*, 863.

(7) Barrett, C. J.; Rochon, P. L.; Natansohn, A. L. *J. Chem. Phys.* **1998**, *109*, 1505.

(8) Kumar, J.; Li, L.; Jiang, X. L.; Kim, D.-Y.; Lee, T. S.; Tripathy, S. *Appl. Phys. Lett.* **1998**, *72*, 2096.

(9) Lefin, P.; Fiorini, C.; Nunzi, J.-M. *Pure Appl. Opt.* **1968**, *7*, 71.

(10) Pedersen, T. G.; Johansen, P. M.; Holme, N. C. R.; Ramanujam, P. S.; Hvilsted, S. *Phys. Rev. Lett.* **1998**, *80*, 89.

(11) Bublitz, D.; Fleck, B.; Wenke, L. *Appl. Phys. B* **2001**, *72*, 931.

(12) Saphiannikova, M.; Geue, T. M.; Henneberg, O.; Morawetz, K.; Pietsch, U. *J. Chem. Phys.* **2004**, *120*, 4039.

(13) Dumont, M.; Osman, A. E. *Chem. Phys.* **1999**, *245*, 437.

(14) Geue, T.; Saphiannikova, M.; Henneberg, O.; Pietsch, U.; Rochon, P.; Natansohn, A. *Phys. Rev. E* **2002**, *65*, 052801.

(15) Mechau, N.; Neher, D.; Börger, V.; Menzel, H.; Urajama, K. *Appl. Phys. Lett.* **2002**, *81*, 4715.

(16) Mechau, N.; Saphiannikova, M.; Neher, D. *Macromolecules* **2005**, *38*, 3894.

(17) Küpfer, J.; Finkelmann, H. *Makromol. Chem., Rapid Commun.* **1991**, *12*, 717.

(18) Wermter, H.; Finkelmann, H. *e−Polym.* **2001**, *013*, 1.

(19) Clarke, S. M.; Hotta, A.; Tajbakhsh, A. R.; Terentjev, E. M. *Phys. Rev. E* **2001**, *64*, 061702.

(20) de Gennes, P. G.; Hebert, M.; Kant, R. *Macromol. Symp.* **1997**, *113*, 39.

(21) Warner, M.; Terentjev, E. M. *Liquid Crystal Elastomers*; Clarendon: Oxford, U.K., 2003.

(22) Finkelmann, H.; Nishikawa, E.; Pereira, G. G.; Warner, M. *Phys. Rev. Lett.* **2001**, *87*, 015501.

(23) Camacho-Lopez, M.; Finkelmann, H.; Palffy-Muhoray, P.; Shelly, M. *Nat. Mater.* **2004**, *3*, 307.

(24) Yu, Y.; Nakano, M.; Shishido, A.; Shiono, T.; Ikeda, T. *Chem. Mater.* **2004**, *16*, 1637.

(25) Sung, J.-H.; Hirano, S.; Tsutsumi, O.; Kanazawa, A.; Shiono, T.; Ikeda, T. *Chem. Mater.* **2002**, *14*, 385.

(26) de Gennes, P. G.; Prost, J. *The Physics of Liquid Crystals*, 2nd ed.; Clarendon Press: Oxford, U.K., 1995.

(27) Landau, L. D.; Lifshitz, E. M. *Theory of Elasticity*, 2nd ed.; Elsevier Science Ltd.: Oxford, U.K., 1981.

(28) Henneberg, O. *In-situ Untersuchungen zur Entstehung von Oberflächengittern in Polymeren*; Potsdam University: Potsdam, Germany, 2004.

(29) Lagugne-Labarthet, F.; Bruneel, J. L.; Rodriguez, V.; Sourisseau, C. *J. Phys. Chem. B* **2004**, *108*, 1267.

(30) Lagugne-Labarthet, F.; Buffeteau, T.; Sourisseau, C. *J. Phys. Chem. B* **1998**, *102*, 5754.

(31) Barrett, C.; Rochon, P.; Natansohn, A. *J. Phys. Chem.* **1996**, *100*, 8836.

(32) Pietsch, U.; Rochon, P.; Natansohn, A. *Adv. Mater.* **2000**, *12*, 1129.

(33) Geue, T.; Saphiannikova, M.; Henneberg, O.; Pietsch, U.; Rochon, P.; Natansohn, A. *J. Appl. Phys.* **2003**, *93*.

(34) Bian, S.; Williams, J. M.; Kim, D. Y.; Li, L.; Balasubramanian, S.; Kumar, J.; Tripathy, S. *J. Appl. Phys.* **1999**, *86*, 4498.

Condensed Matter Physics 2006, Vol. 9, No 1(45), pp. 87–94

CONDENSED MATTER PHYSICS

Photo-induced deformations in azobenzene-containing side-chain polymers: molecular dynamics study

J.Ilnytskyi*[1,3], M.Saphiannikova[2], D.Neher[1]

[1] Institute for Physics, University of Potsdam,
Am Neuen Palais 10, 14469 Potsdam, Germany

[2] Leibniz Institute of Polymer Research,
Hohe Str. 6, 01069 Dresden, Germany

[3] Institute for Condensed Matter Physics,
National Academy of Sciences of Ukraine,
1 Svientsitskii Str., 79011 Lviv, Ukraine

Received August 28, 2005, in final form January 23, 2006

We perform molecular dynamics simulations of azobenzene containing side-chain liquid crystalline polymer subject to an external model field that mimicks the reorientations of the azobenzenes upon irradiation with polarized light. The smectic phase of the polymer is studied with the field applied parallel to the nematic director, forcing the $trans$ isomers to reorient perpendicularly to the field (the direction of which can be assosiated with the light polarization). The coupling between the reorientation of azobenzenes and mechanical deformation of the sample is found to depend on the field strength. In a weak field the original smectic order is melted gradually with no apparent change in the simulation box shape, whereas in a strong field two regimes are observed. During the first one a rapid melting of the liquid crystalline order is accompanied by the contraction of the polymer along the field direction (the effect similar to the one observed experimentally in azobenzene containing elastomers). During the slower second regime, the smectic layers are rebuilt to accomodate the preferential direction of chromophores perperdicular to the field.

Key words: *liquid crystals, azobenzene, polymers, molecular dynamics*

PACS: *31.15.Qg, 64.70.Md, 64.70.Nd*

1. Introduction

Azobenzene-containing polymer materials (here and further on we will use the term "azo-polymers") possess unique attractive features due to the *trans-cis* photoisomerization of the chromophores. On absorbing a photon the planar *trans* isomer transforms into the bent and twisted *cis* form, the latter undergoing reverse transformation either by the same mechanism or by thermally induced back isomerization [1], see figure 1. The absorption bands for both photoisomerization processes depend on the chemical nature of the substituents R, R'. If both bands overlap then the cyclic *trans-cis-trans* photoisomerization can take place during illumination with single wavelength.

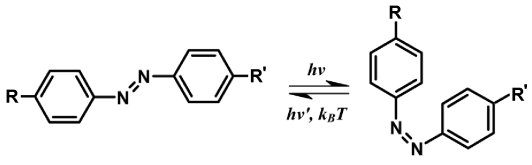

Figure 1. The photoisomerization cycle for azobenzene.

*E-mail: iln@icmp.lviv.ua

Unsubstituted *trans*-azobenzene is a crystalline powder at room conditions with the melting point at $T_{\mathrm{M}} = 68 - 69°\mathrm{C}$ (some computer simulations relevant to its crystallisation can be found in [2]). Its derivatives have been mostly studied either in solution (acting as dyes) or being dispersed or attached to a polymer framework of various architecture (main-chain, side-chain, elastomeric, dendritic). In the latter case the azobenzene groups act as typical mesogens and induce liquid crystalline (LC) phases [3]. It has further been used as a photo-switchable component in block copolymer system or as a dye dopant combined with other mesogens, e.g. $5CB$, see [4,5].

Let us concentrate on two particular polymeric architectures, namely LC elastomers and LC side-chain polymers. LC elastomers are rubbers with covalently attached mesogenic units. As the result, there is a strong coupling between nematic order and mechanical stress of the underlying polymeric framework [6]. This leads, for instance, to the remarkable property of nematic elastomers to change their shape reversibly by up to 400% in the vicinity of their nematic-isotropic (NI) transition [7]. The theory of nematic networks is now well established [8,9]. In chromophore containing LC elastomers the orientational order can be also affected by the light. A large mechanical deformation has been observed experimentally on azobenzene containing LC elastomers with both covalently attached and dissolved azo dyes in response to the non-uniform illumination [10–12].

Unlike LC elastomers, the chains of LC side-chain polymers are not cross-linked and, therefore, are more free to move. One of the new applications of side-chain azo-polymers is the fabrication of sinusoidally modulated surface structures, known as surface relief gratings (SRG). These are produced on thin polymer films using optical setups with various interference patterns similar to the ones used for holographic recordings [13]. The process is all-optical and the SRG films can be applied as diffractive elements and in optical storage media (see, reviews [14,15] and references therein). The main peculiarity of this process is the nature of the force behind this photo-induced large scale mass-transport that takes place in the amorphous state of a polymer. A number of theories have been developed, namely, thermal gradients, diffusive mechanisms, pressure gradients resulting from the isomerization, the superposition of the interactions between the azo dipoles and the electric field of the light interference pattern, and a recent entropic theory (for more detail, see review [15] and [16]). However, none of these is able to describe equally well all the combinations of optical setups and different polymers being used. In fact, a clear microscopical picture of both photo-induced reversible and irreversible changes in azo-polymers is still missing.

The aim of this study is not to perform an in-scale modelling of the photo-induced effects in azo-polymers but rather to take a look at some possible microscopic mechanisms behind these. The idea is to simulate the azo-polymer in "dark" and "light" areas and to analyse the mechanical response of the system to the light. To this end we use molecular dynamics simulation with NPT ensemble and anisotropic pressure control. This allows the simulation box to fluctuate independently in all three dimensions while keeping the total pressure equal to the atmospheric one. The change in the shape of the box reflects (with some limitations given below) that of the macroscopic sample and can be seen as an indication of the mechanical response of the system to an external perturbation. The simulations are performed on a side-chain architecture but we expect many similarities to the elastomer system, particularly on a short time scale. The details of the model are presented in the next section.

2. Model

Atomic-level modelling of the photo-induced deformations in azo-polymers faces a number of difficulties. For instance, a length scale of the material deformation in SRG is of the order of microns (typical film thickness is about 1μm, the grating periodicity is $1 - 5\mu$m) and the recording time ranges from seconds to tens of minutes. This length and time scale is clearly beyond the current capabilities of atomistic molecular dynamics simulations, therefore one needs to find ways to speed up the effect being considered. Another issue is the level of required chemical detailization which also influences the speed of the simulations to a great extent. The SRGs are known to be successfully recorded on a great variety of azobenzene containing chemical structures, which can be seen as an indication that the molecular model is not needed to be chemically exact.

Most types of azo-polymers used for SRG inscription can be split into two groups: the amorphous and LC systems. The terminology evidently originates from the phase in which a particular polymer can be found at moderate temperatures, $T < 100°\mathrm{C}$. Typical amorphous systems have a short spacer (typically, of 1–4 CH_2 groups) which links the azobenzene to the polymer backbone, and, sometimes, a stiffer backbone. The glass transition temperatures T_g are normally above 100°C. The LC systems, on the contrary, have a relatively long spacer (often of 10 or more CH_2 groups) and, as a result, lower T_g. At the temperature interval $T = 20° - 100°\mathrm{C}$ these are usually found in the smectic phase.

The photo-induced effects are known to occur on much shorter time-scales in LC azo-polymers. In particular, recordings of SRG within 0.5 s have been reported [5], as compared to tens of minutes for amorphous systems. For this reason we have chosen this particular architecture for our simulations. The smectic phases inherent to LC azo-polymers may also shed some light on the importance of the aggregation of azobenzenes [17–19], since the rearrangement of these aggregates is expected to be on much shorter time scale in LC azo-polymers. We empolyed the semi-atomistic modelling, in which the CH_n groups of the alkyl chains are represented as united-atom Lennard-Jones monomers and the azobenzene groups (including possible substituents) are considered to be anisometric units interacting via the Gay-Berne potential [20] with the following parametrisation, $\mu = 1$, $\nu = 2$, $\kappa = 3$, $\kappa' = 5$. The bonded interactions include bond stretch, bond bending and torsional terms (for more details, see [21]) with the force field developed for branched alkanes [22]. Each polymer consists of a backbone of 39 monomer with 10 side-chains attached to it. Each side-chain has a flexible spacer of 10 monomers terminated by the azo model unit (see, figure 2).

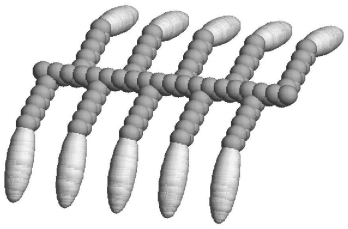

Figure 2. A single side-chain of azo-polymer.

The detailed study of the photoisomerization of azobenzene is beyond the scope of this paper, therefore we employed a simplified statistical description of this effect. It is assumed that the material contains azobenzene with substituents so that rapid cyclic *trans*-*cis* isomerization occurs and the photostationary state is quickly established. The *trans*-*cis* photoisomerization rate is known to be proportional to $\cos^2(\theta)$ (θ is the angle between the long axis of the isomer and the light polarization) therefore *trans* isomers are to be found predominantly perpendicular to the light polarization (where the probability for the photoisomerization is the lowest). This effect can be modelled via an external model field, the energy of each i-th *trans* isomer in a field is

$$U_\mathrm{i}^\mathrm{field} = F \cdot P_2(\cos(\theta_\mathrm{i})). \tag{1}$$

Here the field strength is $F > 0$, θ_i is the angle between the long axis of the i-th *trans* azobenzene and the prescribed direction (here and thereafter referred as the field direction), and $P_2(x) = 1/2(3x^2 - 1)$ is the second Legendre polynomial. Unlike the electric or magnetic fields which align the mesogens parallel to a given direction, the field defined via equation 1 forces *trans* azobenzenes to be confined in the planes perpendicular to the field direction. The angular derivative of $U_\mathrm{i}^\mathrm{field}$ with respect to θ_i is related to the torque applied to each azobenzene. The *cis* isomers are not included in our model explicitly.

One should mention that our model lacks some important aspects of photoisomerization, particularly, the existence of *cis* isomers and the dynamical nature of the photostationary state. The only effect taken into account is the reorientation of the *trans* isomers of the azobenzenes.

3. Results

At first, our model side-chain LC polymer has been examined with respect to the formation of LC phases. The initial configuration was built by packing 64 side chains (see, figure 2) into the simulation box in some regular layered way (see, figure 3, on the left, here and thereafter we show the snapshots of the polymer contained in one periodic box only). To avoid artificial splitting-up of the polymer at the box edges along X axis, the backbones were positioned to interdigitate throughout the box boundaries and the periodic boundary conditions have been employed (see, figure 3, in the middle).

Figure 3. Initial geometrically packed configuration (on the left), backbones interdigitation along the X axis (in the middle) and equlibrated configuration after simulation for 4 ns at atmospheric pressure $P = P_{\mathrm{atm}} = 1\,\mathrm{atm}$ at $T = 500\,\mathrm{K}$ (on the right).

This initial configuration was equilibrated then for the times of up to 4 ns at atmospheric pressure $P = P_{\mathrm{atm}} = 1\,\mathrm{atm}$ and at different temperatures T ranging from 200 K to 600 K. The molecular dynamics was performed with the aid of the parallel program GBMOLDD [21,23] in an anisotropic NPT ensemble with the timestep ranging from 1 fs to 1.5 fs. The Hoover barostat has been used to fix the tensile stress at $P_{\mathrm{xx}} = P_{\mathrm{yy}} = P_{\mathrm{zz}} = P_{\mathrm{atm}}/3 = 1/3\,\mathrm{atm}$, and the temperature has been controlled by means of the Nose-Hoover thermostat. The ensemble chosen allows independent fluctuations for each box dimension and proved to be especially useful to simulate smectic and crystal phases to avoid the incommesurability of the box dimensions with the characteristic pitch of the phase.

The model system revealed crystalline, smectic and isotropic phases with the transition temperature from the smectic to the isotropic phase at T_{SI} just above 500 K. At $T = 500\,\mathrm{K}$ the system still has weak smectic order (see,figure 3, on the right), but the proximity to T_{SI} allows us to easily perturb the delicate balance of internal interactions. This particular configuration equilibrated at $T = 500\,\mathrm{K}$ and P_{atm} (the corresponding mass density is $\rho = M/V = 0.63\,\mathrm{g/cm^3}$) was chosen to study the response of the system on an external model field defined via equation 1 with various strengths F. The field direction has been chosen to coinside with the nematic director of the original smectic configuration (see figure 3, on the right) to maximize the reorientation effect.

The simulational setup described above has much in common with the experiments of Finkelmann's group on the photoresponse of nematic elastomers [12] except the fact that our system is built of non-crosslinked chains. However, on a short time scale the effect of chains diffusion can be neglected and the model system can be affinely deformed. In this case splitting of the macroscopic sample into a grid of adjacent cells will map the shape of each cell onto that of the whole sample. One can consider the simulation box (which is able to fluctuate freely in shape) as one of such cells. On a larger time scale, however, this does not hold due to chain diffusion.

To study the coupling of the sample shape with the LC order of the chromophores, we have monitored the scaled box dimensions, $s_{\mathrm{x}} = L_{\mathrm{x}}/V^{1/3}$, $s_{\mathrm{y}} = L_{\mathrm{y}}/V^{1/3}$, $s_{\mathrm{z}} = L_{\mathrm{z}}/V^{1/3}$ and the nematic order parameter $S_2 = \langle P_2(\theta_{\mathrm{i}})\rangle$ and analysed the snapshots of the systems in a course of the simulations. Here, $L_{\mathrm{x}}, L_{\mathrm{y}}, L_{\mathrm{z}}$ are the box dimensions, $V = L_{\mathrm{x}}L_{\mathrm{y}}L_{\mathrm{z}}$ is the volume of the box, θ_{i} is

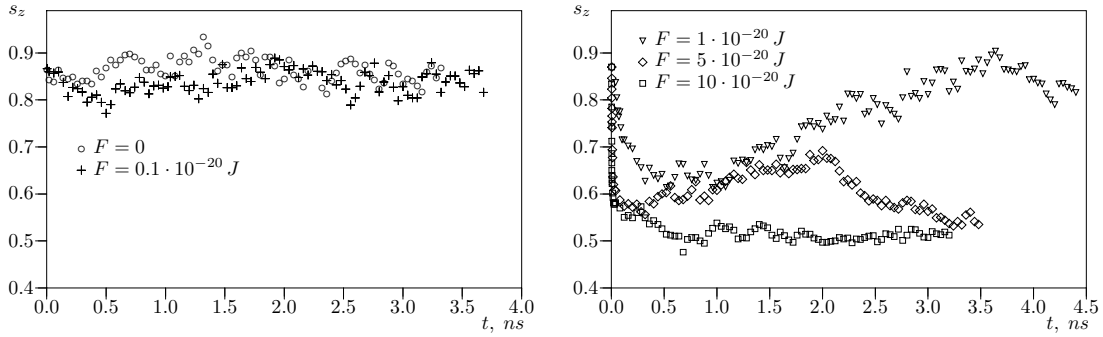

Figure 4. Box shape parameter s_z along the direction of the external model field *vs* time, weak fields (left graph) and strong fields (right graph).

the angle between the long axis of the i-th chromophore with the nematic director and $P_2(x)$ is the second Legendre polynomial. One should mention that in the presence of an external field one can measure the nematic order either in respect to the field direction or in respect to the instantaneous director of the chromophores. For our simulational setup, the former will only confirm that the chromophores are indeed perpendicular to the field (the order parameter defined in this way will be equal to $-1/2$), whereas the latter will also provide the level for chromophores self-organizations (if any) in other directions. The usual procedure for the calculation of the order parameter is as follows. At each time t the instantaneous order parameter tensor is evaluated first, then it is diagonalised so that the maximum eigenvalue provides the value for the scalar order parameter S_2. All the simulations were performed at fixed temperature $T = 500\,\mathrm{K}$ and atmospheric pressure P_{atm} while the box shape was allowed to fluctuate. The Z axis was chosen along the nematic director of the original smectic phase. The model field has been applied in the same direction.

For a weak field strength, $F = 0.1 \cdot 10^{-20}\,\mathrm{J}$, no changes of the box shape were observed at all times studied (up to 4ns, see figure 4, on the left). On the contrary, the case of stronger field strengths, $F \geqslant 1 \cdot 10^{-20}\,\mathrm{J}$, reveals an analogy with the experiments on nematic elastomers. Here a quick initial contraction of the box was observed along the field direction (see, figure 4, on the right).

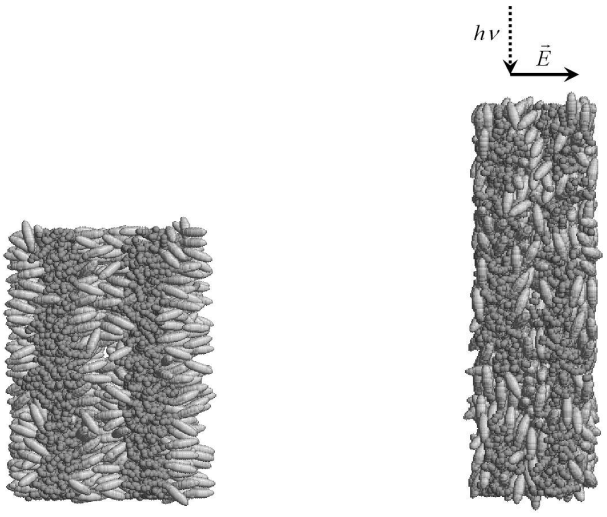

Figure 5. Snapshots of the model system at times $t = 0$ (left image) and $t = 10\,\mathrm{ps}$ (right image) at a temperature $T = 500\,\mathrm{K}$, the light propagation is shown by a dotted arrow whereas the field direction is designated as $\vec{E}$, the field strength parameter is $F = 5 \cdot 10^{-20}\,\mathrm{J}$.

This contraction was accompanied by the extension of the box in the other two dimensions, so that no apparent change in the average material density has been observed. The side-by-side comparison of the snapshots of the system at time $t = 0$ and that at $t = 10\,\text{ps}$ in a strong field $F = 5 \cdot 10^{-20}\,\text{J}$ (see, figure 5) suggests that the contraction of the sample has its origin in steric interactions. At time $t = 0$, in the smectic phase, the long axes of the azobenzenes are aligned preferentially along the Z axis. After applying the external field in the same direction, this order melts within *ca.* $t = 10\,\text{ps}$ as being energetically unfavourable and a new orientational order with the azobenzenes perpendicular to the Z axis is started to be induced. This quick reorientation happens on a time scale far less than that of the chains diffusion, so that, the voids emerging around the azobenzenes cannot be filled. As a result, the material contracts rapidly along the Z axis. One can conclude that the material demonstrates an elastic response to a strong external field, similar to the elastomer system, on a short time scale.

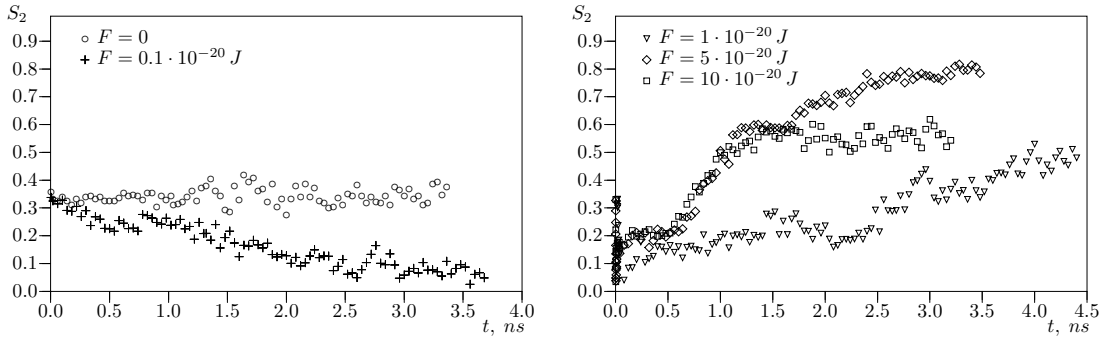

Figure 6. The orientational order parameter S_2 for the chromophores *vs* time, weak fields (left graph) and strong fields (right graph).

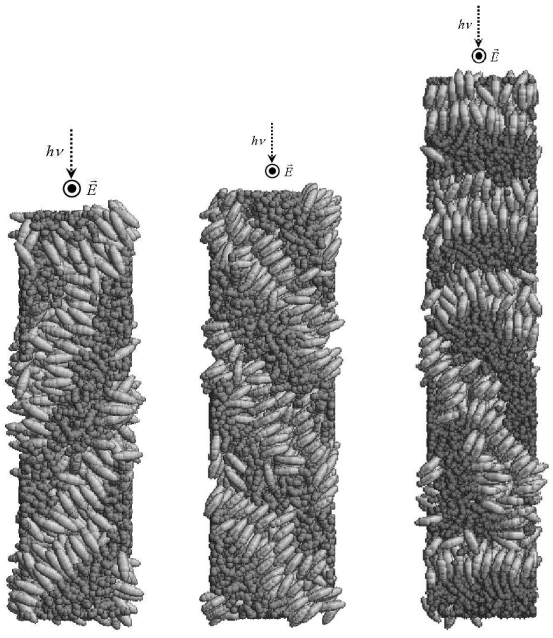

Figure 7. Self-organised smectic layers in planes perpendicular to the field direction $\vec{E}$ (directed towards the observer) after the time $t = 4\,\text{ns}$ and field strength $F = 1 \cdot 10^{-20}\,\text{J}$ (left image), $F = 5 \cdot 10^{-20}\,\text{J}$ (middle image) and $F = 10 \cdot 10^{-20}\,\text{J}$ (right image), the light propagation is shown by a dotted arrow.

The shape of the simulation box on a longer time scale is of lesser interest as far as chain diffusion smears out its resemblance to the shape of the macroscopic sample. However, the dynamics of the orientational order parameter S_2 is of interest. One should mention that the behaviour of the order parameter in a weak field reveals only slow "melting" of the initial smectic phase (see, figure 6, on the left). The time scale of this process is comparable with the chains diffusion kinetics and neither changes of the box shape nor regrowing of new phases have been observed up to times of 4 ns (see, figure 4, 6 on the left).

In the case of a stronger field, after an initial quick fall-down, the order parameter S_2 grows until it reaches a final new value, for instance $S_2 \sim 0.8$ for $F = 5 \cdot 10^{-20}$ J (see, figure 6). During this process, all the chromophores reorient preferably perpendicularly to the field direction, and self-organize into new smectic layers (see, figure 7).

One should mention that in a very strong field, $F > 10 \cdot 10^{-20}$ J, the structure of the ordered phase is a polysmectic with many possible defects, as a result of quick formation of smectic clusters with rather high interfacial energy.

To summarize the results, our simulations of a side-chain azo-polymer subjected to a external model field, reproduce some of the features of real photo-active polymers observed previously in experiment. In weak fields, only a photo-chemical smectic-isotropic transition is observed [24] with no apperent change of the polymer shape. In stronger fields, on a short time scale, photo-induced contraction of the sample in the direction of light polarization is observed (the effect similar to the one in nematic elastomers [12]), whereas on a longer time scale the reorganisation of smectic layers is observed (for more details, see. [25]).

4. Conclusions

This study considers molecular dynamics simulations of a model side-chain azo-polymer subject to an external model field which approximates some aspects of the photoisomerization of *trans* azobenzenes. In weak fields a photo-chemical smectic-isotropic transition is reproduced, while in stronger fields, the short time scale behaviour is similar to the photoresponse of azobenzene-containing elastomers. On longer time scale, reorganisation of smectic layers in strong fields is observed.

The results obtained in this study confirm that the chromophore reorientation may play a significant role in photo-induced effects in azo-polymers. In particular, both effects of reversible contraction/extension of LC elastomers and SRG formation in LC side-chain polymers might be of the same microscopic origin, as was already suggested before [16]. More detailed modelling is needed to describe other aspects of photoisomerization which will be subject of subsequent studies.

5. Acknowledgements

The authors acknowledge the financial support under DFG Grant NE410/8–1 and computer time offered by Computing Cluster of the Institute for Condensed Matter Physics, Lviv, Ukraine.

References

1. Ho C.H., Yang K.N., Lee S.N., J. Polym. Sci. A, 2001, **39**, 2296.
2. Saphiannikova M. et al., J. Chem. Phys., 2003, **118**, 9007–9014.
3. Goodby J.W. et al., J. Mater. Chem., 2001, **11**, 2631.
4. Wu Y. et al., Macromol., 1998, **31**, 1104; *ibid.*, 1998, **31**, 4457.
5. Ubukata T., Seki T., Ichimura K., Adv. Mater., 2000, **12**, 1675.
6. de Gennes P.G., Phys. Let. A, 1969, **28**, 725; Acad. Sci. Ser. B, 1975, **281**, 101.
7. Finkelmann H., Wermter H., Abstr. Pap. Am. Chem. Soc., 2000, **219**, 189.
8. Warner M., Gelling K.P., Vilgis T.A., J. Chem. Phys., 1988, **88**, 4008.
9. Warnew M., Terentjev E.M. Liquid Crystal Elastomers. Clarendon, Oxford, 2003.
10. Cviklinski J., Tajbakhsh A.R., Terentjev E.M., Eur. Phys. J. E, 2002, **9**, 427.
11. Yu Y., Nakano M., Ikeda T., Nature, 2003, **425**, 145.

12. Camacho-Lopez M. et al., Nature Materials, 2004, **3**, 310.
13. Rochon P., Batalla E., Natansohn A., Appl. Phys. Lett., 1995, **66**, 136; Kim D., Tripathy S., Lian L., Kumar J., Appl. Phys. Lett., 1995, **66**, 1166.
14. Viswanathan N.K. et al., J. Mater. Chem., 1999, **9**, 1941.
15. Yager K.G., Barrett C.G., Curr. Op. Sol. St. Mat. Sci., 2001, **5**, 487.
16. Saphiannikova M., Neher D., J. Phys. Chem. B, 2005, **109**, 19428.
17. Kasha M. Spectroscopy of the Excited State. Plenum, New York, p. 337, 1976.
18. Lagugne Labarthet F. et al., Macromol., 2000, **33**, 6815.
19. Kim B.J., Park S.Y., Choi D.H., Bull. Korean Chem. Soc., 2001, **22**, 271.
20. Gay J.G., Berne B.J., J. Chem. Phys., 1981, **74**, 3316.
21. Ilnytskyi J.M., Wilson M.R., Comp. Phys. Comm., 2001, **134**, 23.
22. Martin M.G., Siepmann J.I., J. Phys. Chem. B, 1999, **103**, 4508.
23. Ilnytskyi J.M., Wilson M.R., Comp. Phys. Comm., 2002, **148**, 43.
24. Ikeda T. et al., Macromol., 1990, **23**, 36.
25. Natansohn A., Rochon P., Can. J. Chem./Rev. Can. Chim., 2001, **79**, 1093.

Фото-індуковані деформації азобензинових полімерних гребінців: моделювання за допомогою молекулярної динаміки

Я.Ільницький[1,3], М.Саф'яннікова[2], Д.Неєр[1]

[1] Інститут фізики, Потсдамський університет,
ам Ноєс Пале 10, 14469 Потсдам, Німеччина
[2] Інститут полімерних досліджень ім. Ляйбніца,
вул. Гое 6, 01069 Дрезден, Німеччина
[3] Інститут фізики конденсованих систем НАН України,
вул. Свєнціцького 1, 79011 Львів, Україна

Отримано 28 серпня 2005 р., в остаточному вигляді – 23 січня 2006 р.

За допомогою методу молекулярної динаміки вивчається поведінка рідкокристалічних азобензинових полімерних гребінців в модельному зовнішньому полі, яке моделює переорієнтування азобензинових груп (хромофор) при опроміненні поляризованим світлом. Зокрема, у смектичній фазі полімеру, при умові співпадіння напрямку зовнішнього поля із напрямком нематичного директора хромофор, відбувається переорієнтація хромофор перпендикулярно до напрямку прикладеного поля (який може бути асоційований із поляризацією світлового пучка). Знайдено, що взаємозв'язок між переорієнтацією хромофор та механічними деформаціями зразка суттєво залежить від величини прикладеного поля. В слабкому полі смектичний порядок повільно розмивається без зміни форми виділеного фрагменту зразка, в сильному ж полі спостережено два режими. Під час першого із них швидке руйнування смектичної фази супроводжується скороченням фрагменту полімера вздовж напрямку поля (ефект, аналогічний до експериментально спостережуваного ефекту скорочення нематичного фото-еластомера при опроміненні). Під час же другого, повільнішого, режиму смектичний порядок поступово перебудовується в такий спосіб, що хромофори тепер розташовані перепендикулярно до прикладеного поля.

Ключові слова: *рідкі кристали, азобензин, полімери, молекулярна динаміка*

PACS: *31.15.Qg, 64.70.Md, 64.70.Nd*

Molecular tracer diffusion in thin azobenzene polymer layers

N. Mechau
Institute of Physics, University of Potsdam, Am Neuen Palais 10, 14469 Potsdam, Germany

M. Saphiannikova
Institute of Physics, University of Potsdam, Am Neuen Palais 10, 14469 Potsdam, Germany and Leibniz-Institut für Polymerforschung, Hohe Straße 6, 01069 Dresden, Germany

D. Neher[a)]
Institute of Physics, University of Potsdam, Am Neuen Palais 10, 14469 Potsdam, Germany

(Received 11 October 2006; accepted 12 November 2006; published online 18 December 2006)

Translational diffusion of fluorescent tracer molecules in azobenzene polymer layers is studied at different temperatures and under illumination using the method of fluorescence recovery after photobleaching. Diffusion is clearly observed in the dark above the glass transition temperature, while homogeneous illumination at 488 nm and 100 mW/cm^2 does not cause any detectable diffusion of the dye molecules within azobenzene layers. This implies that the viscosity of azobenzene layers remains nearly unchanged under illumination with visible light in the absence of internal or external forces. © *2006 American Institute of Physics*. [DOI: 10.1063/1.2405853]

The illumination of azobenzene containing polymer layers with a periodic intensity or polarization pattern can cause a long-range light-induced material transport which results in the formation of so-called surface relief gratings (SRGs). The first inscription of SRGs onto azobenzene layers was independently reported by two research groups in 1995.[1,2] Though the evolution of the SRG can be modeled precisely using a fluid mechanics approach or linear viscoelastic analysis,[3,4] the nature of the driving force for mass transport at the micrometer range is still discussed controversially.[5,6] Nearly all models require the viscosity of the azobenzene polymer under illumination to be comparable to that in the melt. Therefore, various authors have proposed a light-induced softening of azobenzene layers based on additional free volume which is created by the cyclic *trans-cis-trans* photoisomerization of the azobenzene chromophores.[7–9]

Kumar *et al.* were the first to report the softening of an azobenzene polymer film by measuring the indentation of an atomic force microscope (AFM) tip before and after homogeneous illumination. However, no quantitative results have been presented.[10] Later Srikhirin *et al.* have observed a slight increase of 1% in the elastic compliance of a polymer layer doped with azobenzene chromophores under illumination with visible and UV light.[11] A change of 10% in the mechanical compressibility of azobenzene layers under illumination has been found experimentally in electromechanical and dielectric measurements performed (at 5 kHz) in our group.[12,13] Furthermore, we have found a decrease of the elastic modulus by 50% using the pulse-force mode of the AFM and nanoindentation.[14] Recently, a significant light-induced decrease in the viscosity has been reported by Karageorgiev *et al.*[15] The analysis of the experimental compression curve under constant load yielded a light-induced viscosity of $\eta=4.1$ GPa s, which is far below the typical viscosity in the glassy state ($\eta>10^{12}$ Pa s). The authors interpreted this result on the basis of increased segmental diffusivity of the polymer chains under illumination. However, note that these experiments were performed in the presence of a mechanical force imposed on the sample by the AFM tip, and thus, the viscosity change was determined during polymer yielding caused by the tip.

In this study, we used fluorescence recovery after photobleaching (FRAP) to follow changes in the viscosity of azobenzene layers by measuring the translational diffusion of small dye-tracer molecules at different temperatures and under illumination. According to the well-accepted reptation theory, there is a direct relation between the translational diffusion of segments and the viscosity of a polymer sample.[16] Even minor increases in the free volume ($<5\%$),[17] such as induced by an increase in temperature above the glass transition temperature (T_g), are known to cause significant changes in both viscosity and diffusivity. Therefore, performing FRAP experiments below T_g under illumination should provide clear evidence of the proposed light-induced softening. The present study clearly shows that a translational diffusion of dye-tracer molecules is only observable at temperatures above the glass transition temperature, while illumination does not cause any detectable diffusion of the dye molecules. This implies that light-induced translational diffusion is nearly negligible in homogeneous samples in the absence of external or internal forces.

The material investigated is an amorphous azobenzene side-chain polymer, poly(2-hydroxyethyl)methacrylate-(co-(2-(4-(4-cyanophenylazo)phenoxy)acetyl)methacrylate) with a molecular weight of 86 000 g mol^{-1}, an azobenzene content of 62%, and $T_g=90$ °C. As the tracer molecules we used a commercial red fluorescent dye (D10000) from "Molecular Probes." This dye exhibits an absorption maximum at 632 nm, well beyond the absorption of the azobenzene film. The emission of the dye in the polymer matrix is at 650 nm. The chemical structure of the used dye is shown in the inset of Fig. 1. A mixture of the azobenzene polymer and the red dye (0.01 wt % relative to the polymer mass) was dissolved in tetrahydrofurane. This solution was spun onto a glass substrate at 1000 rpm to obtain layers of ~200 nm thickness, as measured with a Dektak profilometer. We found that the fluorescence intensity of the dye in azobenzene containing layer was more than two times lower than in an inert polymer matrix such as poly(methylmethacrylate) (PMMA). Investigations on solutions containing both the dye and the

[a)]Electronic mail: neher@rz.uni-potsdam.de

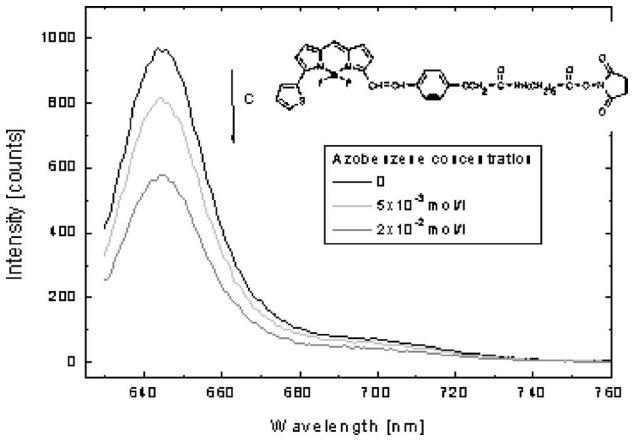

FIG. 1. Fluorescence spectra of the dye-tracer molecule (D10000) dissolved in tetrahydrofuran at different concentrations of the azobenzene polymer. The inset shows the chemical structure of the used dye-tracer molecule D10000.

azobenzene polymer at different concentrations showed a strong decrease in the fluorescence with azobenzene concentration (Fig. 1). This indicates that the fluorescence quenching is due to an energy or charge transfer to the azobenzene, as has been observed for other dye-doped azobenzene layers.[18]

The translational diffusion of the dye molecules within the azobenzene layers was measured by the FRAP technique. An initial "writing" step with high intensity light, of a focused HeNe laser ($\sim 10^8$ mW/cm^2), creates a spatial variation of the fluorescent dye concentration in the layer by local photobleaching. A second "reading" cycle creates a fluorescence intensity image by scanning the sample with an attenuated reading intensity of the same HeNe laser, at a reduced intensity of $\sim 10^4$ mW/cm^2, across an area of $\sim 40 \times 40$ μm^2. The scanning and the fluorescence detection was done with a modified confocal Raman spectrometer (Dilor).

Figure 2 shows successive line scans of the fluorescence across the bleached region at temperatures below and above T_g. While at room temperature (23 °C), ~70 °C below T_g, the spatial fluorescence intensity of the bleached area did not change within hours [Fig. 2(a)], the diffusion of the dye molecules could be well observed at a temperature of 110 °C, 20 °C above T_g [Fig. 2(b)]. These results become comprehensible in the framework of the free volume theory. From these results, the diffusion coefficient D can be calculated in the two-dimensional case by using the Einstein relation: $D = a^2/(4\tau)$, where a^2 is the area of the bleached region and τ is the time constant of the fluorescence recovery of the bleached region. With $\tau \approx 100$ min at 110 °C and a diameter of the bleached area of 4 μm, the diffusion coefficient was calculated to be 7×10^{-11} cm^2/s. This compares well with values for the diffusion coefficient of small tracer molecules in a PMMA matrix above the glass transition temperature.[19]

To test if tracer diffusion can be caused by light well below T_g, similar experiments were performed while illuminating a large area of the layer, including the photobleached spot, with circularly polarized light of an Ar$^+$ laser at a wavelength of 488 nm and a moderate intensity of 100 mW/cm^2. These parameters are usually used for the inscription of SRGs. Consequently, if an active light-induced change in the viscosity takes place at room temperature, it should be detectable by the initiation of the diffusion. However, the data

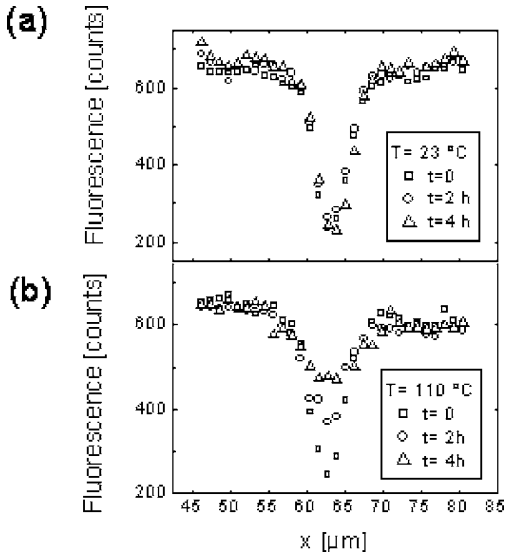

FIG. 2. Line scans of the fluorescence intensity across the bleached region in FRAP experiments at several times after the bleaching at high intensities. The delay time between two successive scans was chosen to be 2 h which is much longer than duration of the line scan (1 min). Measurements were performed at different temperatures of the azobenzene layer: (a) at room temperature (23 °C), ~70 K below the glass transition temperature, and (b) ~20 K above the glass transition temperature.

in Fig. 3(a) clearly show that light-induced diffusion of the dye molecules within the polymer layer is absent under the above mentioned conditions. Additionally, we found that illumination with linear polarized light did not lead to any demonstrable dye diffusion in any particular direction.

Interestingly, we observed a distinct reduction of the fluorescence intensity when the homogeneous illumination of the Ar$^+$ laser at 488 nm wavelength is switched on [Fig. 3(a)]. We presume that this reduction is caused by an addi-

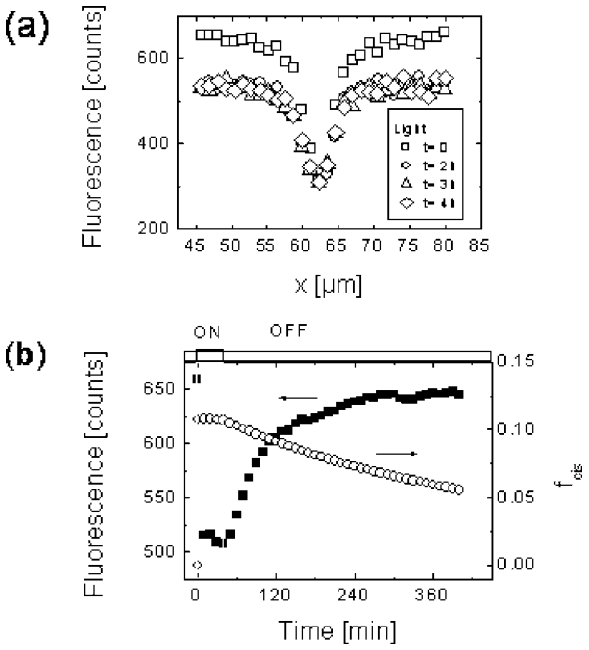

FIG. 3. (a) Fluorescence intensity profile measured across the bleached region at several times after the bleaching process. Between the scans (delay time=1 h), the layer was illuminated by the light of an Ar$^+$ laser at 488 nm and at a moderate intensity of 100 mW/cm^2. (b) The time dependence of the fluorescence intensity and the *cis* fraction measured during and after illuminating the sample at 488 nm with an intensity of 100 mW/cm^2.

tional fluorescence quenching in the presence of *cis* isomer of the azobenzene dye, which forms upon photoisomerization. As can be seen in Fig. 3(b), the fluorescence intensity starts to decrease rapidly with the increase of the *cis* fraction after the light is switched on. When the light is switched off again, the *cis* fraction decreases due to thermal back relaxation and, correspondingly, the fluorescence intensity increases back to the initial level before illumination. Because the relative fluorescence intensity decreases with increasing *cis* concentration in a highly nonlinear fashion, we presume that quenching is due to short-range interactions, probably electron transfer.[18] For a constant *cis* fraction during the illumination at 488 nm, the measured spatial fluorescence intensity remains constant [Fig. 3(a)]. The absence of appreciable changes in fluorescence intensity in the subsequent scanning cycles in Fig. 3(a) provides strong evidence that illumination with moderate intensities of 488 nm wavelength does not induce any dye diffusion within the azobenzene layers.

This main result of our study is in contradiction to the concept of photoinduced translational diffusion as proposed by Lefin *et al.*[20] and of anisotropic photofluidity as proposed later by Karageorgiev *et al.*[15] Based on the observation that the width of a scratch in an azobenzene layer was gradually reduced only when the light polarization was perpendicular to the scratch, the latter authors concluded that an azobenzene layer under illumination behaves like a fluid in the direction perpendicular to the light polarization and like a solid in the parallel direction. Because illumination with polarized light induces orientational order among the azobenzene units, the anisotropic fluidity was attributed to the anisotropic angular distribution of photoinduced motion. Our results, however, show that no appreciable light-induced dye diffusion takes place if a homogeneous azobenzene layer is illuminated with uniform light. Apparently, the long-range mass transport during SRG writing is not directly related to light-induced molecular motion on the molecular level.

We have recently proposed that illumination of an azobenzene layer results in an anisotropic stress related to the reorientation of the azobenzene chromophores.[21,22] Under typical SRG writing conditions, this stress was predicted to be in the range of several megapascals. At present, we do not have information about the yield stress of our azobenzene polymer, but we like to point out that PMMA, which forms the backbone of a number of azobenzene polymers, including the one studied here, has a yield stress of about 50 MPa at a deformation rate of 10^{-5} s^{-1} (this rate is comparable to the rate of grating inscription).[23] Thus, the stress predicted in our studies shall not be sufficient to induce mass flow in glassy polymer samples well below T_g. However, Karageorgiev *et al.* reported a significant lowering of the yield stress of an azobenzene layer under illumination, which, in combination with a light-induced force, might indeed lead to macroscopic mass transport as observed during SRG-formation experiments.[15]

In conclusion, we showed that photoisomerization of azobenzene at light intensities typically used for the SRG writing does not cause segmental diffusion in the polymer layers. This leads us to the conclusion that anisotropic light-induced stress above the yield point of the azobenzene polymer is needed to cause the macroscopic transport during SRG formation.

The authors would like to thank V. Börger and H. Menzel from the Braunschweig Technical University for supplying the polymer. H. Weigt is greatly acknowledged for his aid by realizing the fluorescence experiments. The authors thank C. Kollwitz for the helpful assistance. This work was financially supported by the DFG under Grant No. NE410/6-2 and NE410/8-1.

[1] D. Y. Kim, L. Li, X. L. Jiang, V. Shivshankar, J. Kumar, and S. K. Tripathy, Macromolecules **28**, 8835 (1995).
[2] P. Rochon, E. Batalla, and A. Natansohn, Appl. Phys. Lett. **66**, 136 (1995).
[3] K. Sumaru, T. Yamanaka, T. Fukuda, and H. Matsuda, Appl. Phys. Lett. **75**, 1878 (1999).
[4] M. Saphiannikova, Th. M. Geue, O. Henneberg, K. Morawetz, and U. Pietsch, J. Chem. Phys. **120**, 4039 (2004).
[5] K. G. Yager and C. J. Barrett, Curr. Opin. Solid State Mater. Sci. **5**, 487 (2001).
[6] N. K. Viswanathan, D. Y. Kim, Sh. Bian, J. Williams, W. Liu, L. Li, L. Samuelson, J. Kumar, and S. K. Tripathy, J. Mater. Chem. **9**, 1941 (1999).
[7] C. Barrett, P. Rochon, and A. Natansohn, J. Chem. Phys. **109**, 1505 (1998).
[8] S. Bian, J. M. Williams, D. Y. Kim, L. Li, S. Balasubramanian, J. Kumar, and S. Tripathy, J. Appl. Phys. **86**, 4498 (1999).
[9] O. Henneberg, T. M. Geue, M. Saphiannikova, U. Pietsch, L. F. Chien, P. Rochon, and A. Natansohn, Appl. Phys. Lett. **79**, 2357 (2001).
[10] J. Kumar, L. Li, X. L. Jiang, D.-Y. Kim, T. S. Lee, and S. Tripathy, Appl. Phys. Lett. **72**, 2096 (1998).
[11] T. Srikhirin, A. Laschitsch, D. Neher, and D. Johannsmann, Appl. Phys. Lett. **77**, 963 (2000).
[12] N. Mechau, D. Neher, V. Börger, H. Menzel, and K. Urajama, Appl. Phys. Lett. **81**, 4715 (2002).
[13] N. Mechau, M. Saphiannikova, and D. Neher, Macromolecules **38**, 3894 (2005).
[14] B. Stiller (unpublished).
[15] P. Karageorgiev, D. Neher, B. Schulz, B. Stiller, U. Pietsch, M. Giersing, and L. Brehmer, Nat. Mater. **4**, 699 (2005).
[16] G. Strobl, *The Physics of Polymers* (Springer, Berlin, 1997).
[17] L. H. Sperling, *Introduction to Physical Polymer Science*, 3rd ed. (Wiley-Interscience, New York, 2001).
[18] R. Gimenez, M. Millaruelo, M. Pinol, J. L. Serrano, A. Vinuales, R. Rosenhauer, T. Fischer, and J. Stumpe, Polymer **46**, 9230 (2005).
[19] J. Haley and T. P. Lodge, J. Chem. Phys. **122**, 234914 (2005).
[20] P. Lefin, C. Fiorini, and J.-M. Nunzi, Pure Appl. Opt. **7**, 71 (1998).
[21] M. Saphiannikova and D. Neher, J. Phys. Chem. B **109**, 19428 (2005).
[22] N. Mechau, dissertation, Potsdam University, Germany, 2005.
[23] R. P. M. Janssen, L. C. A. van Breemen, C. P. Pelletier, L. E. Govaert, and H. E. H. Meijer, Proceedings of the 13th International Conference on Deformation, Yield and Fracture of Polymers, April 10-13, (Rolduc Abbey, Kerkrade, Netherlands, 2006), pp. 303–306.